Title: **Evaluation of H-EPLM STM TB/TV Test Results**

CI-No: 120 000

Prepared by:	Thermal Team A. Hauser	Date:	28.06.06
Checked by:	J. Kroeker J. Kroeker		28.06.2006
Product Assurance:	R. Stritter		28.6.06
Configuration Control:	W. Wietbrock W. Wietbrock		03.07.06
Project Management:	Dr. W. Fricke		03/07/06

Distribution: See Distribution List (last page)

Issue	Date	Sheet	Description of Change	Release
1	21.04.06	All	First Issue	
1.1	28.06.06		Sect. 3.4 Venting paths during TP5 and TP7 added in Fig. 3.4-3. Sect. 3.5 Typos in titles of Fig. 3.5-9 and 3.5-10 corrected. Sect. 5.3 (RID18100 TP-03 Disposition implemented): Implementation of HACS power dissipation data during TB1 and TB2. Calculated heat load to the LOU Support Plate added. TB2 temperatures in Fig. 5.3-1 added. ANNEX Attachment instructions how to calculate HACS power dissipation from HACS recording files in ANNEX 2 **Note:** Changes w.r.t. Issue 1 are written in red colour. For new introduced sections, figures or tables only the headings/titles are written in red colour.	

Table of Content

Table of Figures

List of Tables

1 Scope

This technical report describes the evaluation of the measurement results obtained from the H-EPLM STM TB/TV qualification test performed in the LSS chamber at ESTEC. The performance evaluation described in this report is based on the measured data reported in RD 01. It contains the test evaluations which don't rely on the TMM, but serves as input for the test correlation activities to obtain and updated and refined H-EPLM TMM.

2 Reference Documents and Abbreviations

2.1 Reference Documents

RD 01 H-EPLM STM TB/TV Test Report, Doc.No.: HP-2-ASED-TR-0110, dated 17.01.2006

RD 02 Evaluation of Instrument Thermal Interface Test Results, Doc.No.: HP-2-ASED-RP-0180, Issue 1, dated 10.03.06

RD 03 LSS ESARAD simplified models from P. Poinas, YCT - ESTEC - ESA, delivered for XMM

RD 04 H-EPLM Thermal Model and Analysis, Doc.No.: HP-2-ASED-RP-0011, Issue 4, dated 15.04.04

RD 05 Integrated Test Procedure for H-EPLM STM TB/TV Test, Doc.No.: HP-2-ASED-TP-0056, Issue 1.1, dated 07.10.2005

RD 06 List of Acronyms, HP-1-ASPI-LI-0077, Issue 2, dated 12.07.2004

RD 07 Evaluation of Thermal Property Tests for the H-EPLM TMM, Doc.No.: HP-2-ASED-RP-0095, Issue 1, dated 15.04.2004

RD 08 HOT Evacuation Test, HP-2-ASED-SD-0052

RD 09 PPS Functional Check (via nozzles, without tilting), HP-2-ASED-SD-0054

RD 10 TRR for HOT Evacuation Test, HP-2-ASED-MN-1065

RD 11 TRR for the PPS functional test, HP-2-ASED-MN-1070

RD 12 Delta TRR for PPS Performance and Ventline Pressure Drop Test In Combination With HOT Evacuation Test II, HP-2-ASED-MN-1072

RD 13 PTR for HOT evacuation test, HP-2-ASED-MN-1069

RD 14 2nd HOT evacuation PTR, HP-2-ASED-MN-1077

RD 15 PTR for PPS functional test (w/o tilting SD-0055), HP-2-ASED-MN-1071

RD 16 PPS 2nd Vent line Pressure Test PTR, HP-2-ASED-MN-1078

RD 17 NRB on the PPS 2 Vent Line Pressure Test (HP-2-ASED-SD-0060), HP-2-ASED-MN-1076

RD 18 Pierre Jamotton: Thermal and Mechanical Properties Measurement Bench at Low Temperature, ESA SP-467, August 2001 and ESA SP-400, August 1997

RD 19 Mesure d'emissivité à basse Température – Rapport de stage CNES, Département Thermique CNES / juin 1997, William Roumagnac

RD 20 ASED assessment of thermal & mechanical properties of black anodised surfaces, HP-2-ASED-TN-0091, dated 26.03.2004

RD 21 C. Fabron: IASI PV Mesures emissivities a basses temperatures, ALCATEL ref. DIVT 3525, dated 04.02.1999

RD 22 Determination of the Emittance of three black anodized samples, Report ZAE 2 – 0804-08, dated 06.10.2004

RD 23 Emissivity Measurements at LEEE on Herschel Coatings – Summary Report, Doc.No.: HP-3-CSAG-TR-0013, dated 15.09.2005

RD 24 Inspection of thermo-optical properties of black paint Aeroglaze Z306 in LSS, ESTEC Materials Report No 4054, dated 18.08.2004

RD 25 VDI Wärmeatlas, 7. Auflage 1994, Kapitel Ka 5

RD 26 Procurement specification for the HIFI Alignment Camera System, HP-2-ASED-PS-0040, Issue 4, dated 03.12.2004

RD 27 HACS Thermal – Mechanical Performance Analysis Report, HP-2-TNO-RP-0002, Issue 2, dated 22.11.2004

2.2 Abbreviations

CVSE	Cryo Vacuum Service Equipment
DLCM	Direct Liquid Content Measurement
HOT	Helium One Tank
HTT	Helium Two Tank
IAD	InterADapter
PPS	Passive Phase Separator
TB	Thermal Balance
TP	Test Phase
TTAP	Thermal Test Adapter Payload
TTAS	Thermal Test Adapter Spacecraft
TV	Thermal Vacuum

Further Abbreviations are listed in RD 06.

3 CVV Internal Performance

3.1 Instrument Interface Performance

The test results measured at the instrument interfaces and the corresponding evaluation is described in detail in RD 02. During evaluation of the thermal performance of the instrument interfaces additional findings have been derived which are interesting for the overall system thermal performance. The most important ones are summarized again here:

- Temperature gradients within HTT wall lead to parasitic heat to the L0 I/Fs especially in horizontal CVV position (outside LSS).
- To measure helium gas outlet temperature the distance of L1 temperature sensors from flexible strap I/F should be >> 150 mm even for 4.7 mg/s helium mass flow rate.
- Temperature fluctuations occur when helium mass flow is routed via valve V104 and not via PPS, see section 3.4.
- Heat input via the JFET harness bundles to L3 is much smaller than expected; i.e. thermal coupling to OBP is much better or heat is rejected from the bundles by radiation.

The heat load to the HTT in case of no MTD electrical power is evaluated for the test phases TB1 and TB 2 in the **Table 3.1-1** compiling the temperature gradients between MTD L0 interface and helium temperature (average of DLCM sensors T101, T102, T104 and T105). In TB1 those gradients are negative indicating that there must be small offset in some of the measured temperatures. However, one can conclude that the heat load to the Helium via the L0 interfaces is rather negligible for TB1. Except for the PACS Blue Detector the corresponding gradients in TB2 are about 6 mK higher compared to TB1 (see sixth column in **Table 3.1-1**) leading in total to a heat load to the helium that is 4.63 mW higher in TB2 compared to TB1 (last column in **Table 3.1-1**).

L0 Interface	dT to LHe (TB1)	dT to LHe (TB2)	L0 con-ductance*	Q HTT (TB2)	dT to LHe (TB2-TB1)	Q HTT (TB2-TB1)
PACS Red Detect. (T221)	-10.8 mK	-4.4 mK	24.5 mW/K	~ 0	6.5 mK	0.158 mW
PACS Cooler Evap. (T222)	-10.6 mK	-3.8 mK	55 mW/K	~ 0	6.8 mK	0.376 mW
PACS Cooler Pump (T223)	-1.2 mK	4.4 mK	18 mW/K	0.08 mW	5.7 mK	0.102 mW
PACS Blue Detect. (T224)	-2.5 mK	152.8 mK	18.5 mW/K	2.827mW**	155.4 mK	2.874 mW
SPIRE Detector (T225)	-10.1 mK	-4.1 mK	42 mW/K	~ 0	6.1 mK	0.256 mW
SPIRE Pump (T226)	-9.8 mK	-3.4 mK	45.6 mW/K	~ 0	6.5 mK	0.296 mW
SPIRE Evaporator (T227)	-6.5 mK	0.0 mK	63 mW/K	~ 0	6.5 mK	0.412 mW
HIFI (T228)	-1.1 mK	4.0 mK	30.6 mW/K	0.124 mW	5.2 mK	0.159 mW
In total:				**3.03 mW**		**4.63 mW**

*) conductance values taken from Sect. 3 of RD 02

**) parasitic heat from warmer part of HTT upper bulkhead in tilted configuration, see also Sect. 3.2 of RD 02

Table 3.1-1: HTT Heat Load via MTD L0 Interfaces during TB1 and TB2

3.2 Verification of DLCM Measurement

The Direct Liquid Content Measurement (DLCM) device was operated during the STM campaign as listed in **Table 3.2-1**. As reference values, the HTT helium contents is shown in as calculated from the integrated (CVSE_004) mass flow measurements in comparison with liquid level probe measurements. Note that with a total offset correction of 0.8 kg over the complete test duration with a total He consumption of 33.9 kg, the integrated mass flow measurement and the liquid level probe readings match very well.

For the evaluation of the DLCM measurements, the average of the 4 DLCM temperature sensors T101, T102, T104 and T105 is used. The temperature values before and after the measurements are calculated from piecewise linear regressions of this average and the timestamp of the start or end of the measurement. As an example, the linear regressions are shown in **Figure 3.2-1**. The HTT temperature drifts before and after the measurement is evaluated from these regressions. For the heating duration Δt, the setting in the automatic script is used since the time resolution in the recording file is only about 3 seconds, while the duration of the heating phase is reliably 200 seconds (when operated from the script). The heater power P is calculated from the SCOE measured current and voltage values (4-wire technique). The evaluation is based on the difference of the internal energies u before and after the heater operation, where a correction of the start temperature by the existing HTT temperature drift (average of drift before and after the measurement) is performed:

$$m_{He} = \frac{\Delta t \cdot P}{u(T_{after}) - u(T_{before} + \Delta t \cdot {dT_{HTT,av}}/{dt})}$$

The Helium mass calculated with this approach is compared to the Liquid Level Probe measurements in **Table 3.2-1**. Note that for measurement Ref2, the DLCM heating power is assumed to be equal to the set point of 20 W since no measurements of the heater current and voltage is available for this measurement due to a SCOE failure. For the measurement Ref4, the temperature at the end of the measurement is subject to increased measurement error since only very few temperature measurements are recorded after the DLCM operation, again due to a SCOE failure which caused a complete data loss during this time (see **Figure 3.2-1**).

The Helium masses determined with the DLCM operation compare very well with the level probe measurements; the deviation is below 4% for all four cases. Note that the correlation between DLCM measurement and level probe read-out is excellent even for a very short heating time of only 20 s.

Ref	Timestamp	Phase	HTT temperature				DLCM heating		DLCM results		Level Probe Filling level %	dev
			before		after		duration	Power	He contents			
			value [K]	drift [K/d]	value [K]	drift [K/d]	[s]	[W]	[kg]	[%]		
1	28.09.2005 14:51:31	Pre-TBTV	1.8490	0.06653	1.8515	0.05170	200	10.08	256.2	74.14	75.75	-2.2%
2	23.10.2005 10:35:00	TP4	1.7384	0.01466	1.7438	0.01339	200	20	301.73	87.37	89.76	-2.7%
3	31.10.2005 20:21:00	TP6	1.7862	0.00344	1.7866	0.00176	20	20.23	309.94	89.73	89	0.81%
4	31.10.2005 20:53:00	TP6	1.7866	0.00176	1.7911	0.00311	200	20.23	318.17	92.11	89	3.4%

Table 3.2-1: DLCM measurements overview

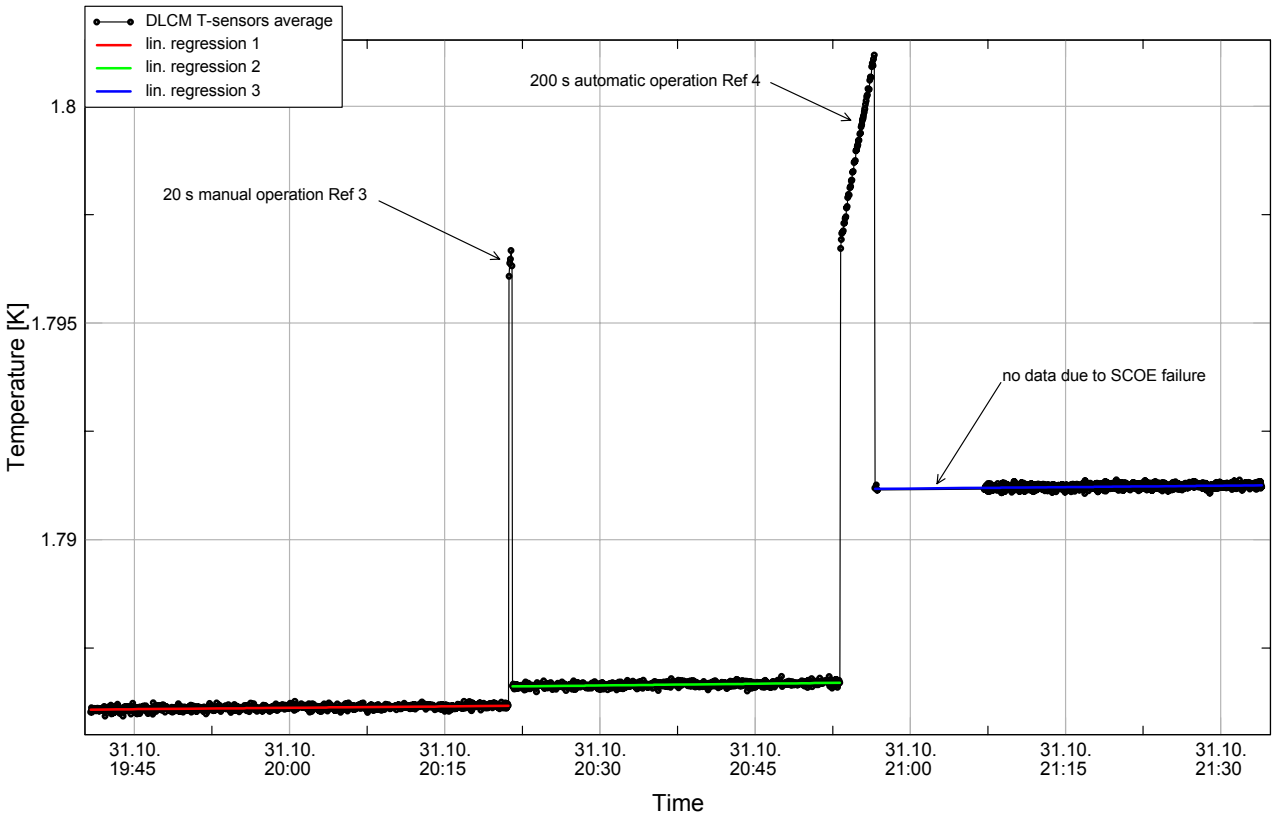

Figure 3.2-1: HTT temperature during DLCM operation in TP6

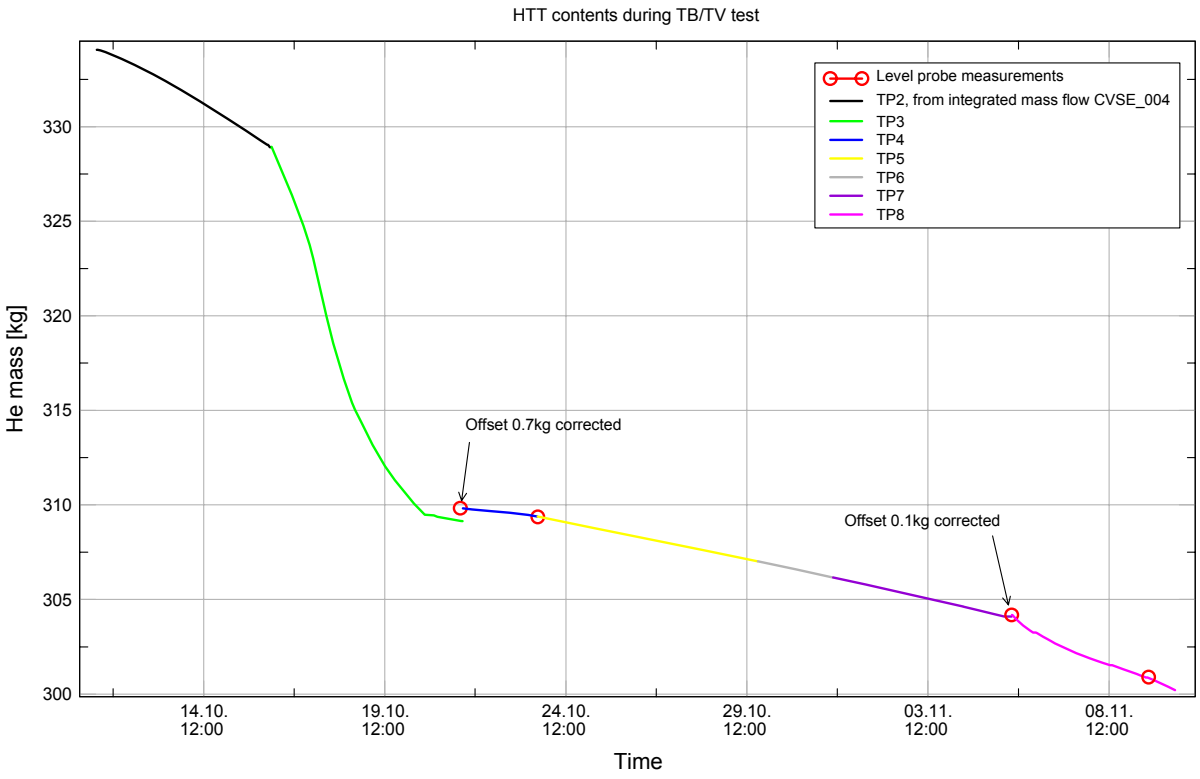

Figure 3.2-2: HTT He contents during the STM TB/TV test

3.3 Temperature Gradients and Absorbed Heat within OBA

The L1 and OBP (L2) temperature evolution during TP4 is shown in **Figure 3.3-1** and the maximum measured gradient within the OBP as well as the gradient between HIFI MTD and OBP is shown in **Figure 3.3-2**. The gradient within OBP includes also the sensors located on the Optical Bench Shield (OBS) and is with about 0.65 K highest during JFET operation. The gradient between HIFI MTD and OBP is only about 0.15 K.
The heat absorbed by the gaseous helium along the three different OBA ventline sections (L1, L2, L3) is shown in **Figure 3.3-3** together with the ventline section from the HTT outlet to the L1 inlet (T232 taken for L1 inlet, because T231 was not available during TP4). As HTT outlet the mean value of the DLCM sensor readings (T101, T102, T104 and T105) is taken. After PACS L1 switch off the heat absorbed between HTT and sensor T232 is about 6-8 mW. Except during JFET operation the heat absorbed by the L3 ventline is about 2 mW which is much lower than expected.

The corresponding evaluation has been performed for TP5 that is the first thermal balance test phase TB1 (**Figure 3.3-4**, **Figure 3.3-5** and **Figure 3.3-6**), for TP6 (**Figure 3.3-7**, **Figure 3.3-8** and **Figure 3.3-9**) and for TP7 that is the second thermal balance phase TB2 (**Figure 3.3-10**, **Figure 3.3-11** and **Figure 3.3-12**). The basic results are summarized in **Table 3.3-1** and **Table 3.3-2**.

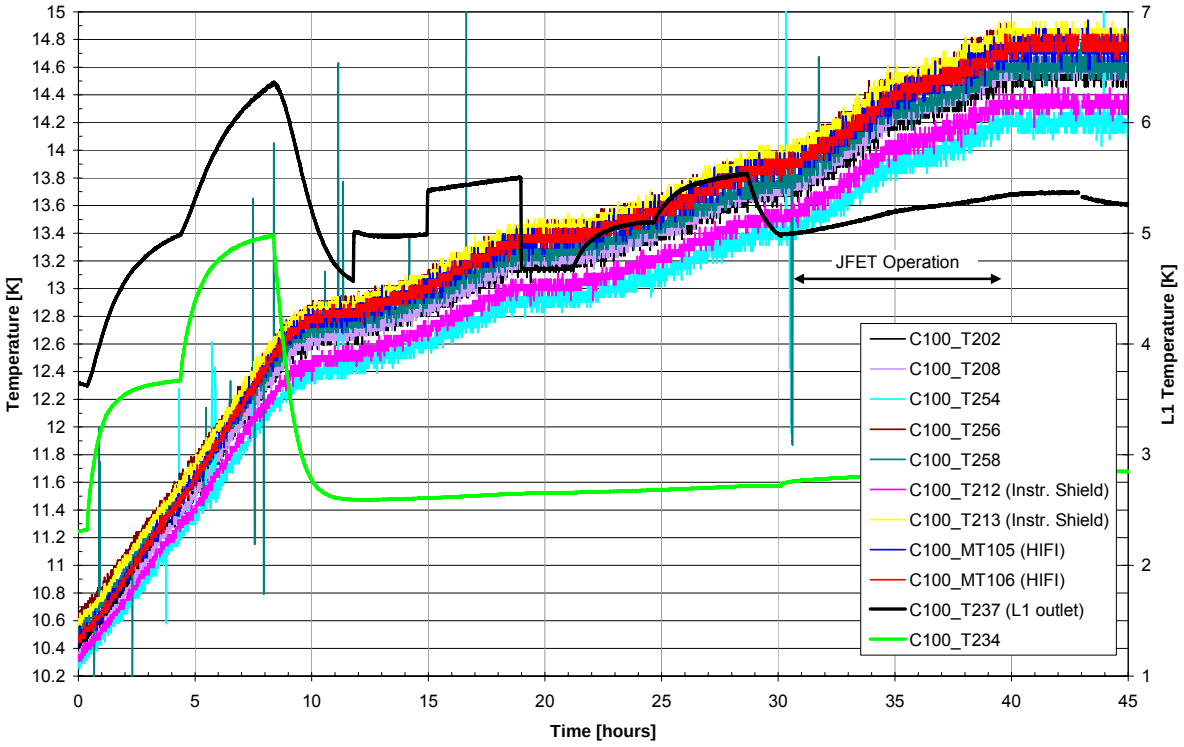

Figure 3.3-1: OBP Temperature Evolution during TP4

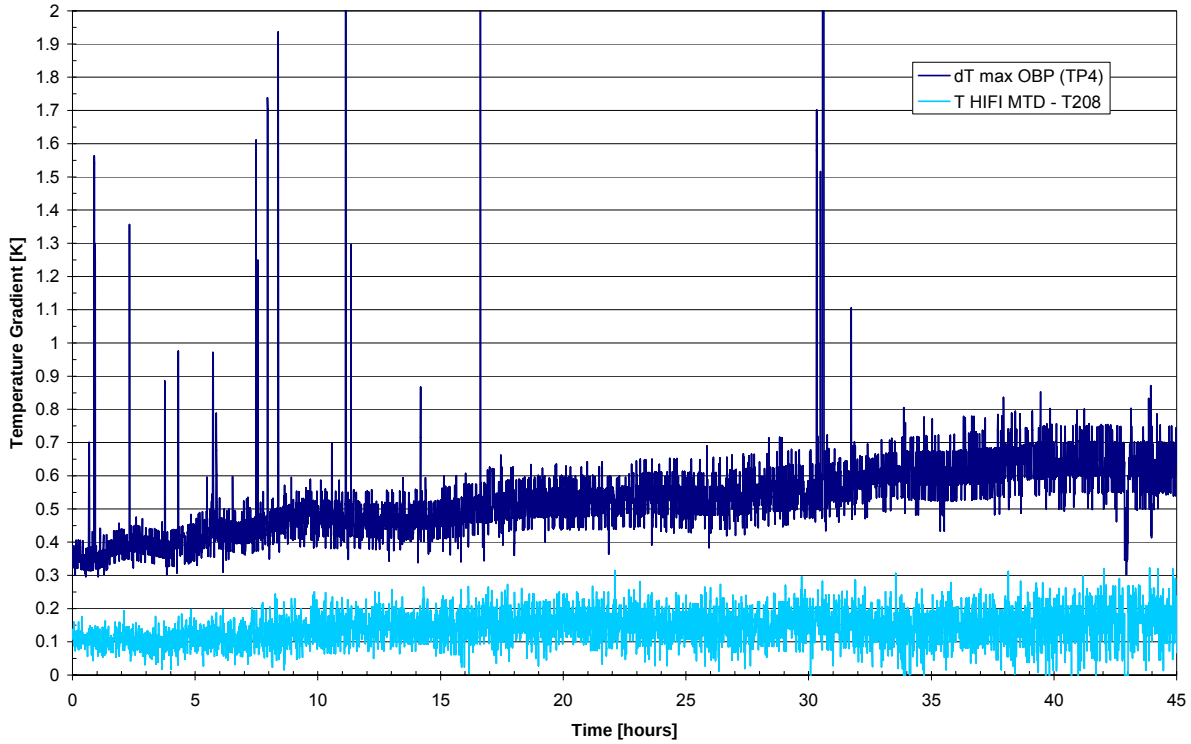

Figure 3.3-2: OBP Temperature Gradients during TP4

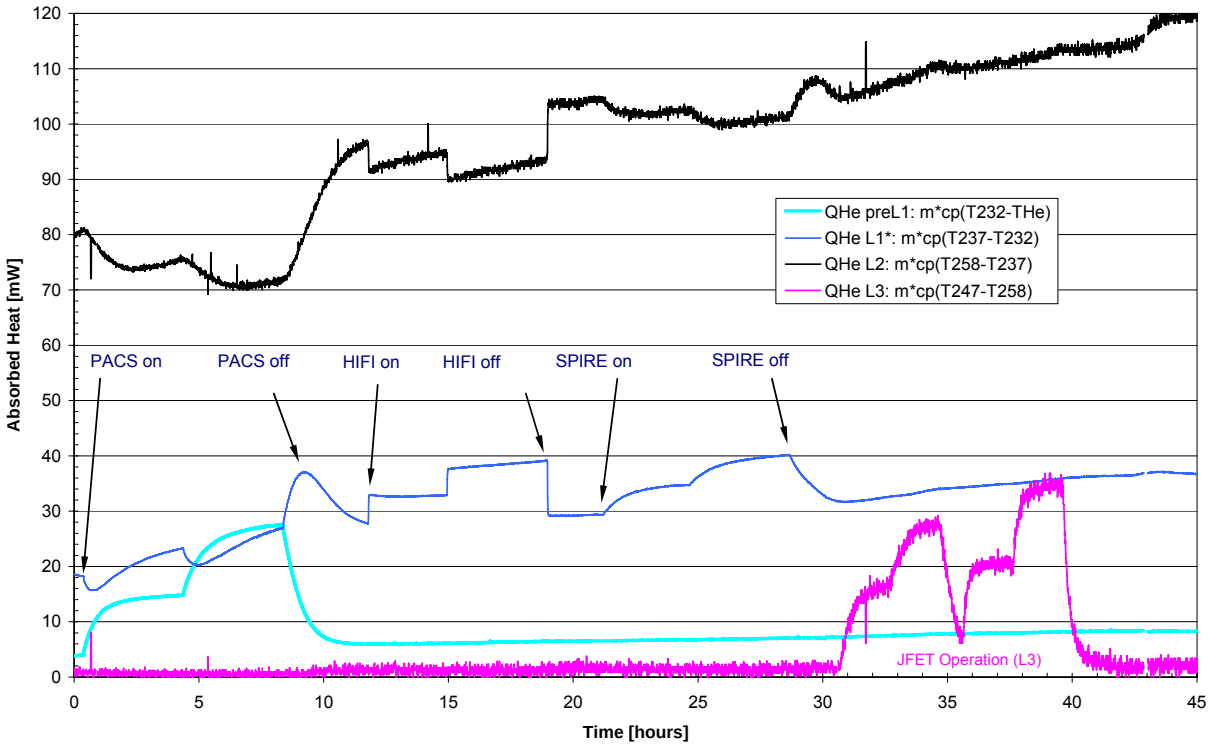

Figure 3.3-3: Absorbed Heat by OBA Ventline during TP4

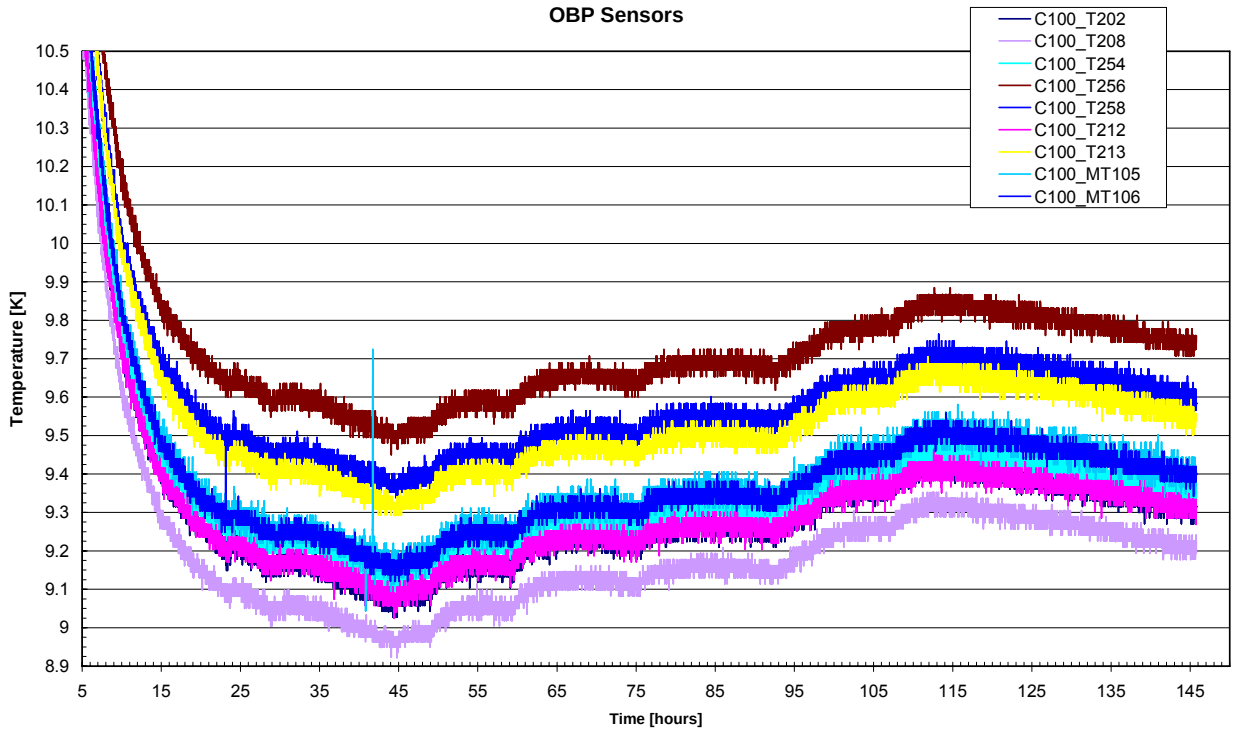

Figure 3.3-4: OBP Temperature Evolution during TP5 (TB1)

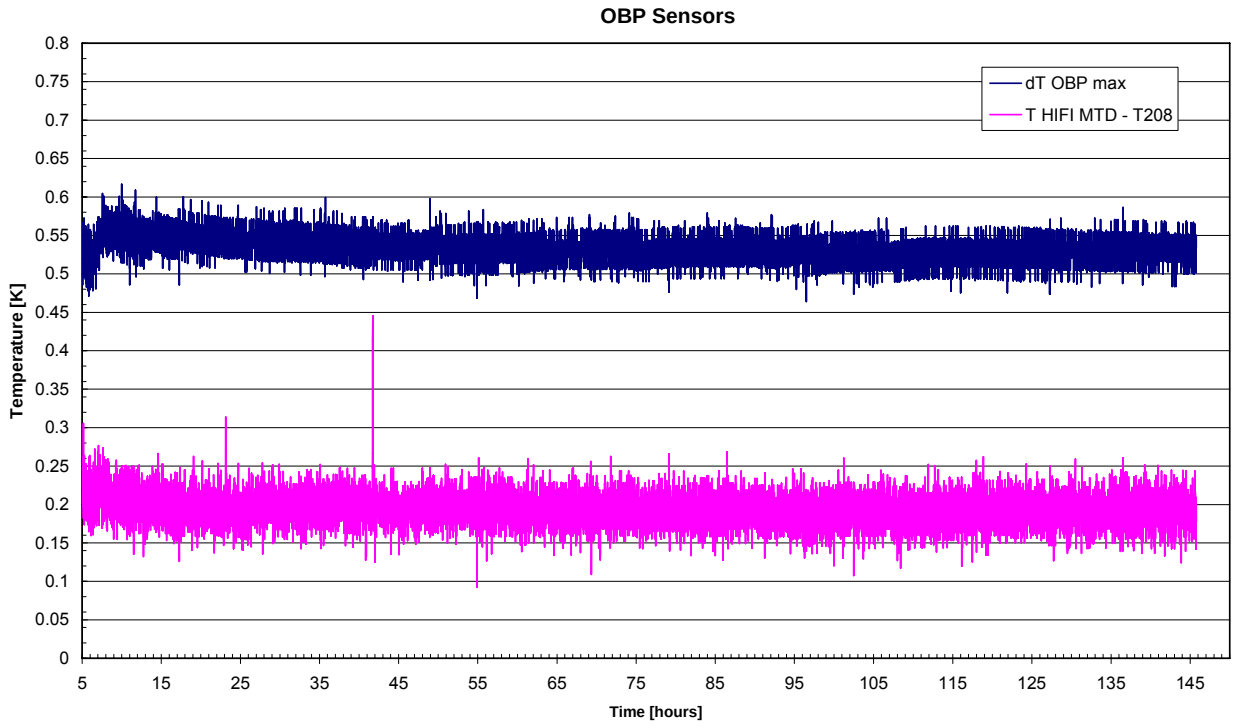

Figure 3.3-5: OBP Temperature Gradients during TP5 (TB1)

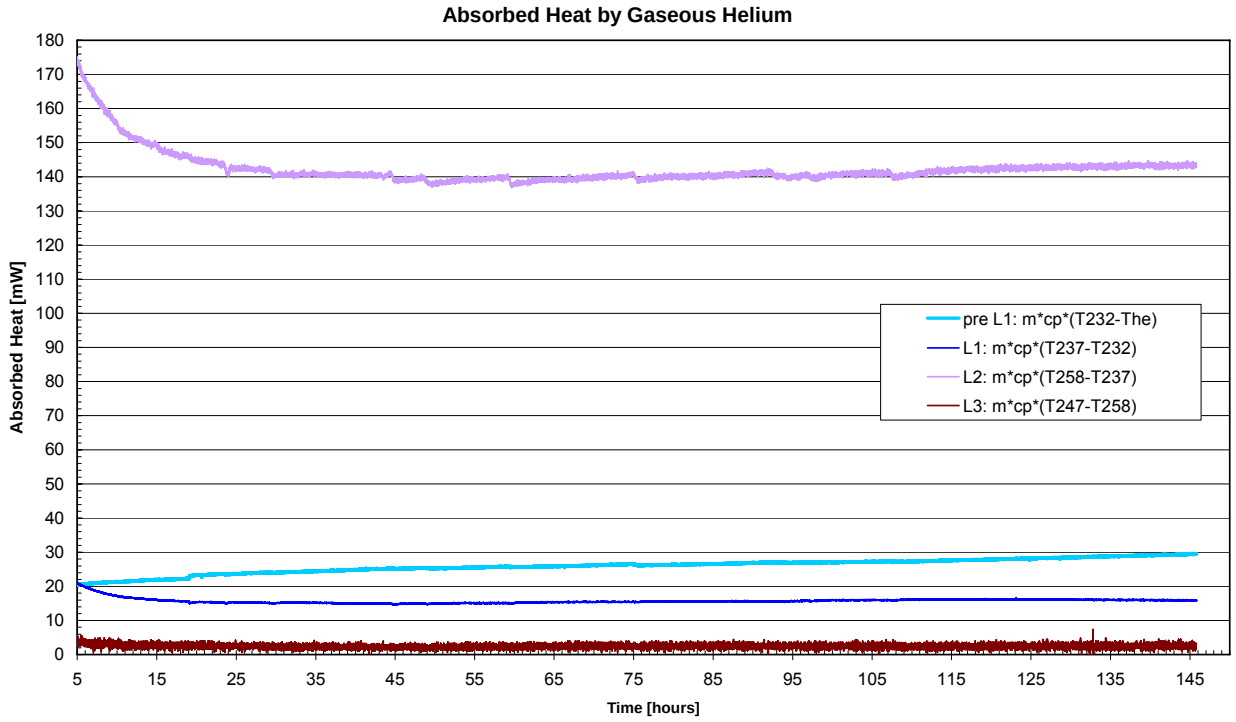

Figure 3.3-6: Absorbed Heat by OBA Ventline during TP5 (TB1)

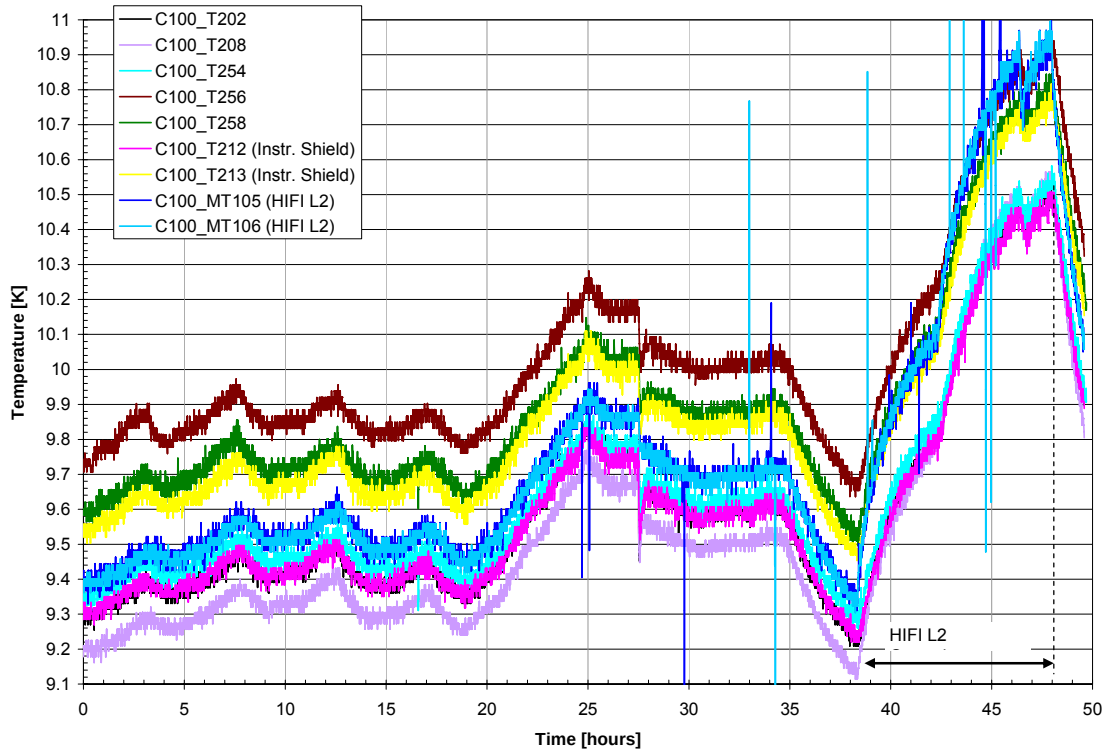

Figure 3.3-7: OBP Temperature Evolution during TP6

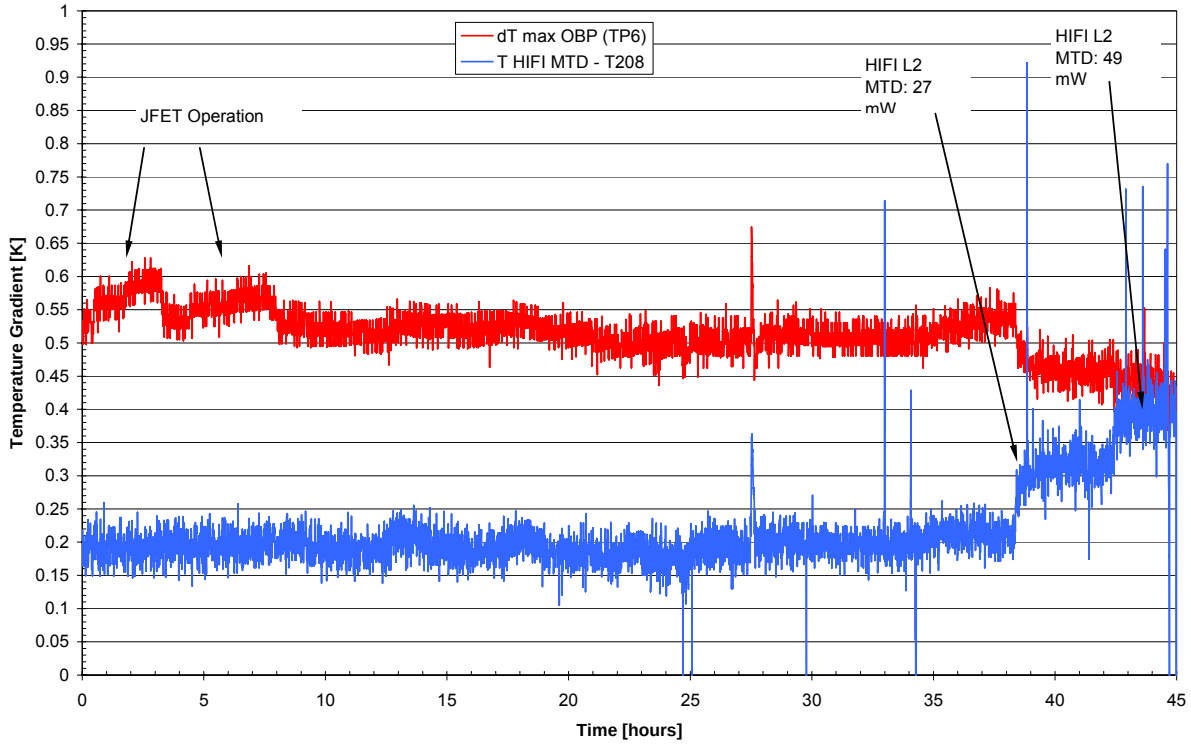

Figure 3.3-8: OBP Temperature Gradients during TP6

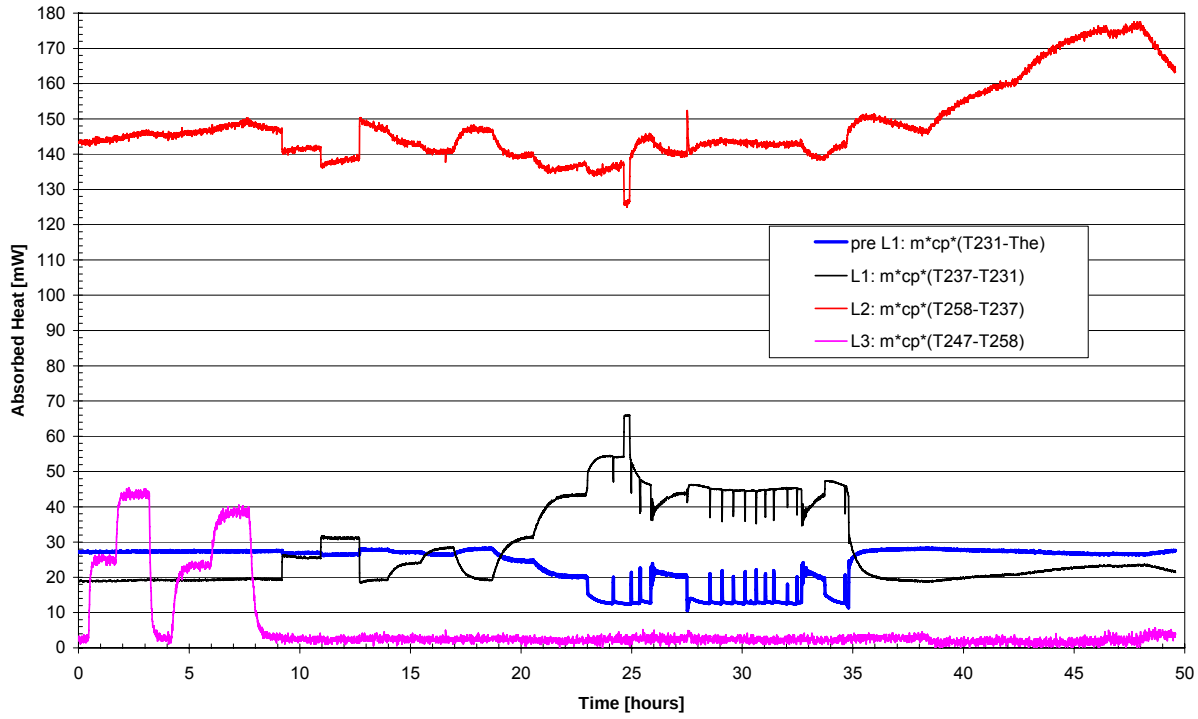

Figure 3.3-9: Absorbed Heat by OBA Ventline during TP6

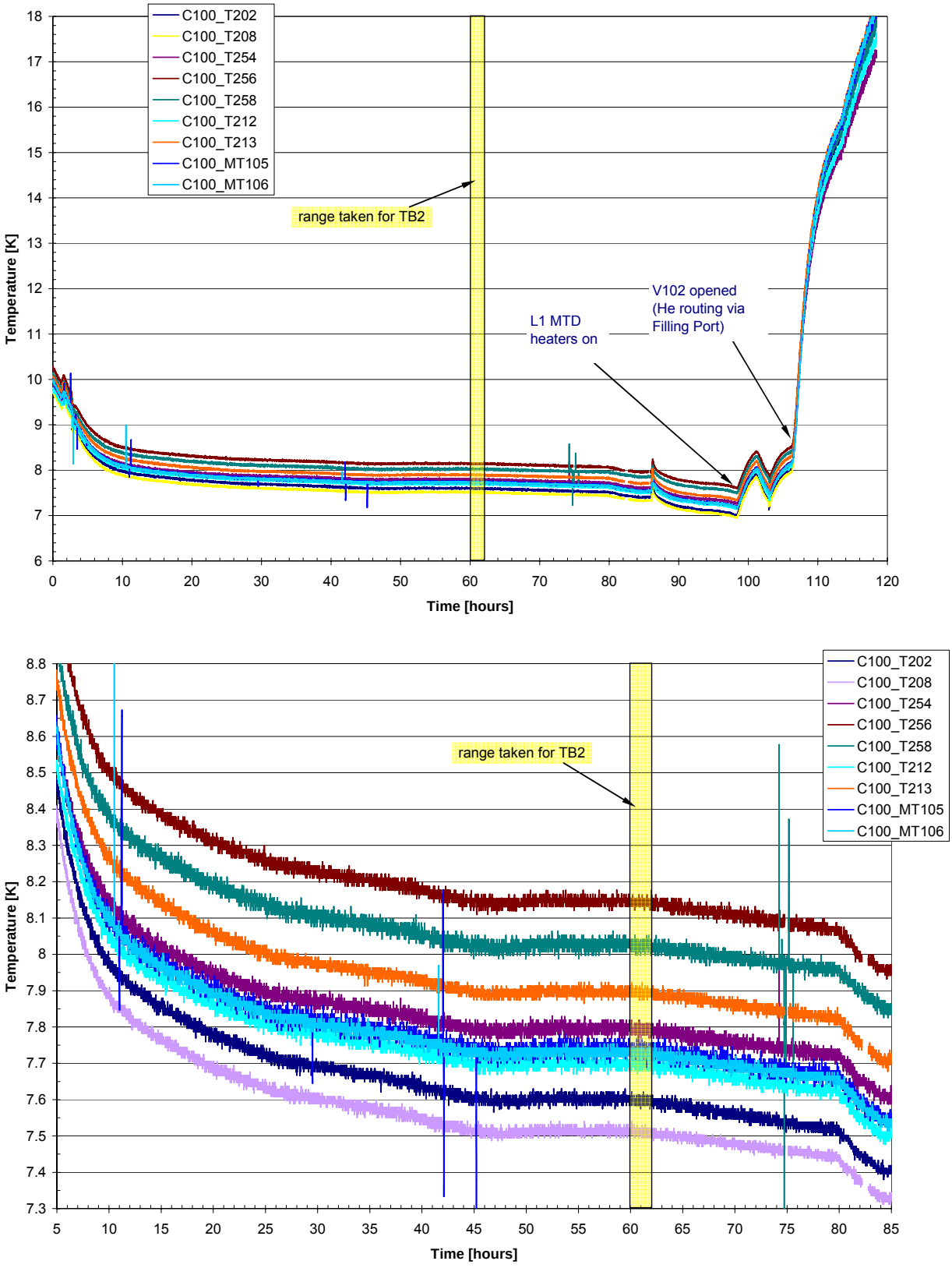

Figure 3.3-10: OBP Temperature Evolution during TP7 (TB2)

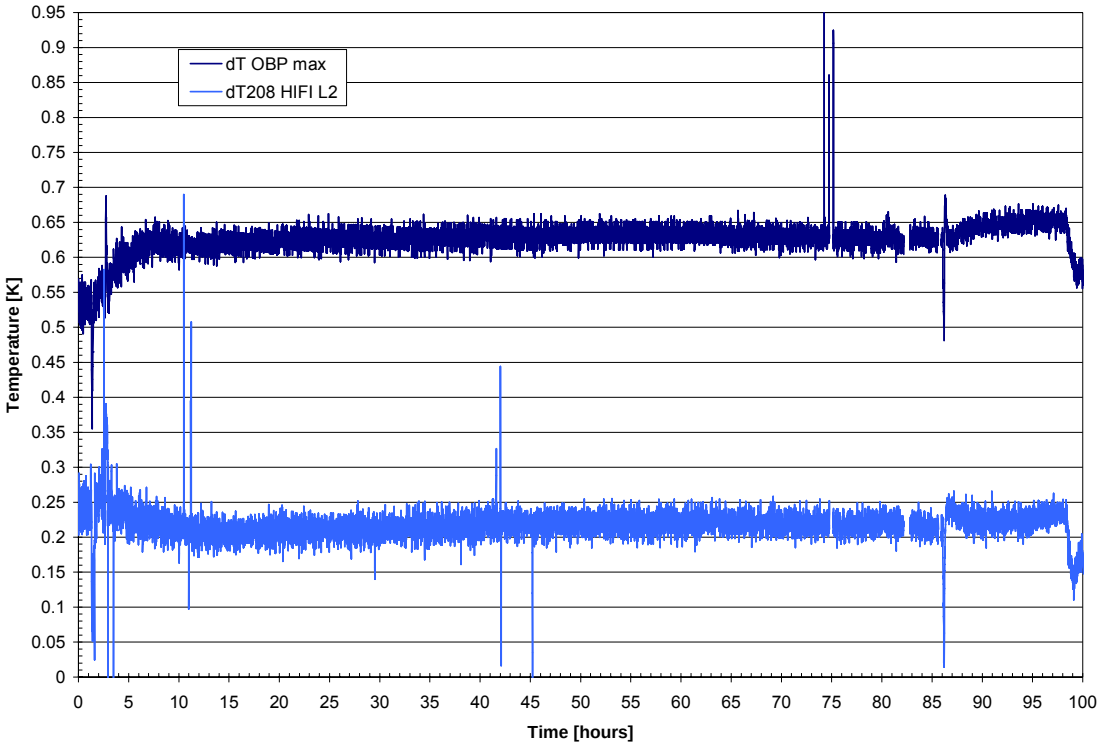

Figure 3.3-11: OBP Temperature Gradients during TP7 (TB2)

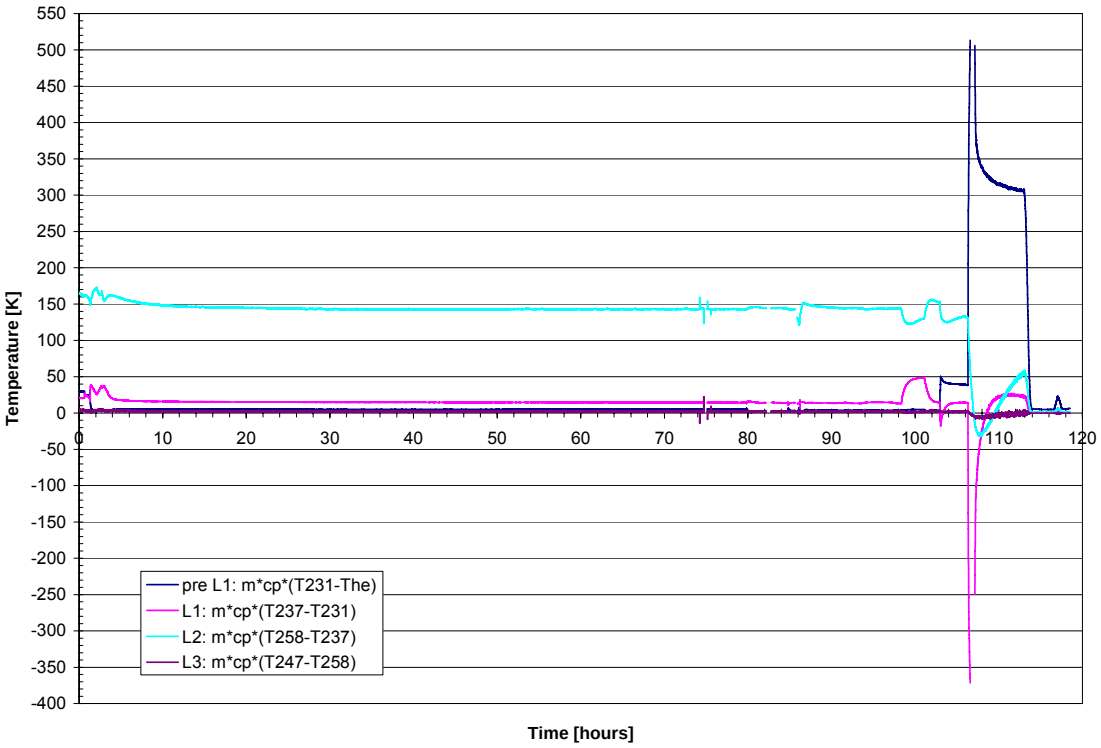

Figure 3.3-12: Absorbed Heat by OBA Ventline during TP7 (TB2)

Test Phase	Mass flow	He venting	S/C Tilt	OBP avg.	dT max OBP incl. OBS	dT HIFI-OBP	Remark
TP4 (MTD op.)	2.30 mg/s	via PPS	14°	14.5K	0.65 K	0.15 K	at end of TP4
TP5 (TB1)	4.64 mg/s	via V104	0°	9.4 K	0.53 K	0.20 K	
TP6 (MTD op.)	4.75 mg/s	via V104	0°	10 K	0.55 K	0.20 K	
TP7 (TB2)	5.03 mg/s	via PPS	16°	7.8 K	0.63 K	0.22 K	

Table 3.3-1: OBP Temperatures and Gradients

Test Phase	Mass flow	He venting	pre L1 $m \cdot cp \cdot (T231-T_{He})$	L1 $m \cdot cp \cdot (T237-T231)$	L2 $m \cdot cp \cdot (T258-T237)$	L3 $m \cdot cp \cdot (T247-T258)$
TP4 [a]	2.46 mg/s	via PPS	8.3 mW [c] [d]	37 mW [c]	119 mW	2.0 mW
TP5 (TB1)	4.64 mg/s	via V104	30 mW [c] [d] 27mW [d]	37 mW [c] 19 mW	143 mW	2.5 mW
TP6 [b]	4.65mg/s	via V104	27mW [d]	19 mW	144 mW	3.0 mW
TP7 (TB2)	5.03 mg/s	via PPS	5.3 mW [d]	15 mW	143 mW	2.2 mW

a) at end of test phase (MTD's off)
b) at begin of test phase (MTD's off)
c) T232 used instead of T231
d) 5.355 kJ/(kg K) taken for helium capacity instead of 5.2 kJ/(kg K). T_{He} is the average of all DLCM sensors

Table 3.3-2: Absorbed Heat on OBA Ventline

Conclusions:

- In all investigated test phases the temperature gradient within the OBP (L2) is less than 0.65 K.
- The gradient between OBS and OBP is negligible compared to the gradient within the OBP.
- The gradient between HIFI MTD and OBP is less than 0.22 K when HIFI MTD is off.
- When the JFETs are off the gradient between JFETs and OBP is less than 0.4 K.
- About 5 mW are absorbed from ventline between HTT and L1 inlet when helium routing is via PPS; 27 mW (i.e. a factor of 5 more) when routed via V104
- Heat absorbed by L3 ventline is (2-3) mW only meaning that most of the conductive heat via the JFET harness bundles is either absorbed via the Vespel standoffs by the OBP or/and rejected by radiation before reaching the JFET boxes

3.4 Temperature Fluctuations on L1 Ventline

Unexpected temperature fluctuations and peaks on the L1 ventline have been measured during TP5 (TB1) and TP6 when the venting helium is routed via the valve V104, see **Figure 3.4-1**. During TP4 and TP7 (TB2) when the helium is routed via the PPS no such fluctuations or peaks have been observed, see **Figure 3.4-2**. Temperature readings of the sensor T232 during TP6 in comparison to TP4 are shown also in **Figure 3.4-8** and **Figure 3.4-9**; the readings during TP4 are regarded as usual noise. The venting paths for the different test phases are shown in **Figure 3.4-3**.

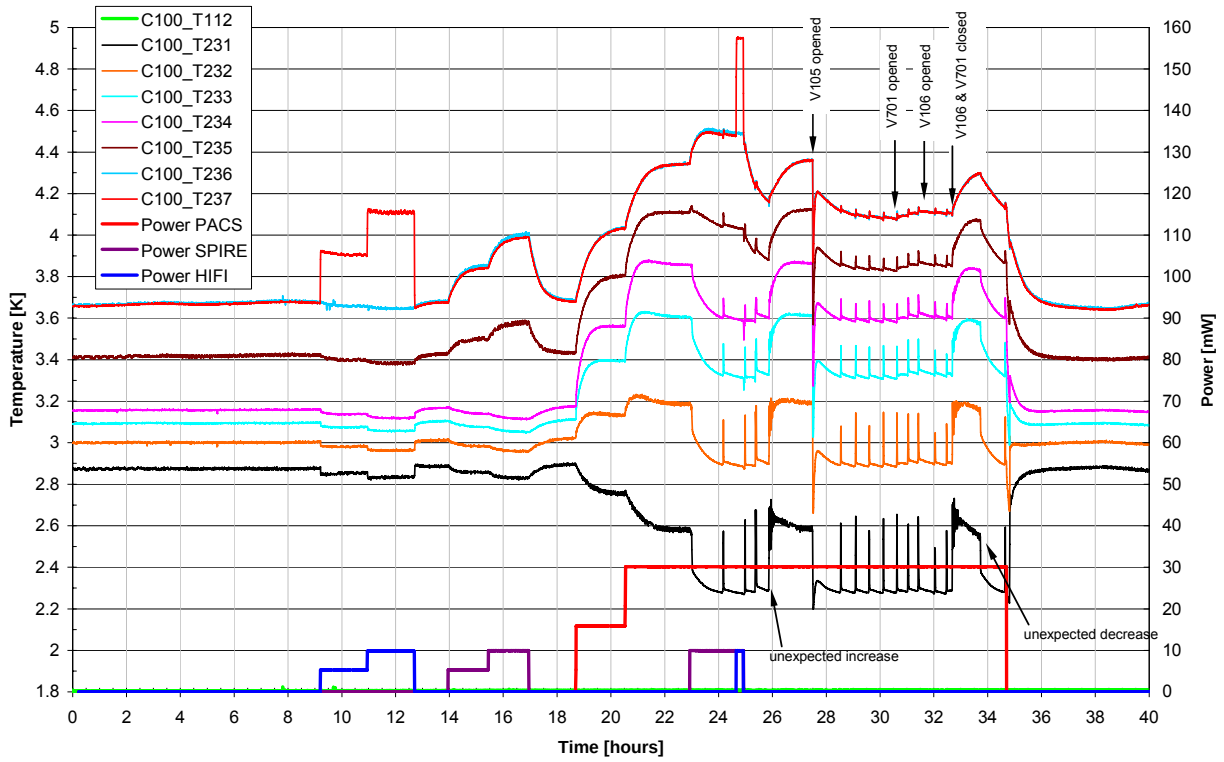

Figure 3.4-1: Temperature and Power Evolution of L1 Ventline during TP6

To quantify the temperature peaks and fluctuations during TP6 in more detail extractions out of **Figure 3.4-1** are presented in

- **Figure 3.4-4** showing single peaks up to 0.4 K (~2 minutes duration per peak) in intervals of about 30 minutes during PACS heating.
- **Figure 3.4-5** showing ±10 mK fluctuations with ~3 minutes interval during PACS heating and a rapid temperature drop of 0.2 K at additionally SPIRE switch on.
- **Figure 3.4-6** showing ±10 mK fluctuations with ~4 minutes interval before V105 opening and a rapid temperature drop of about 0.4 K after V105 opening.
- **Figure 3.4-7** showing decreasing fluctuations after closure of V106 and V107.

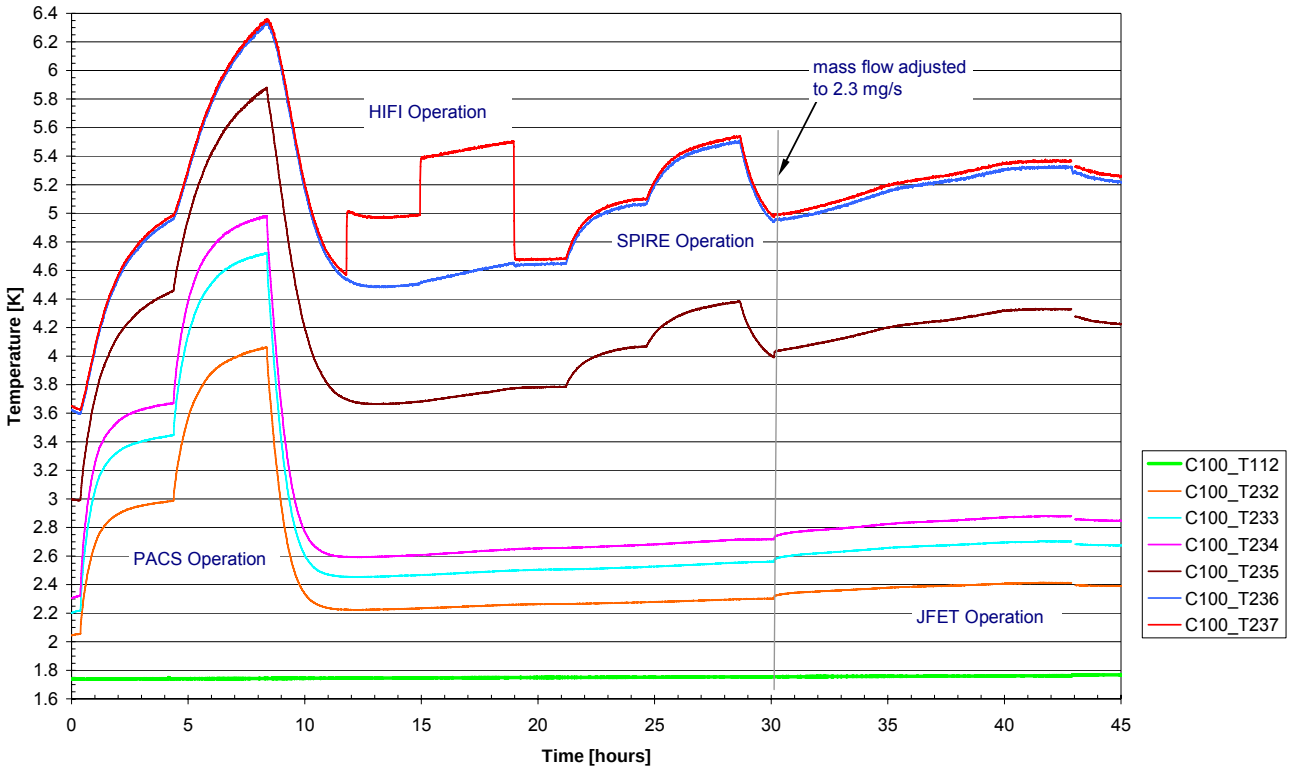

Figure 3.4-2: Temperature Evolution of L1 Ventline during TP4

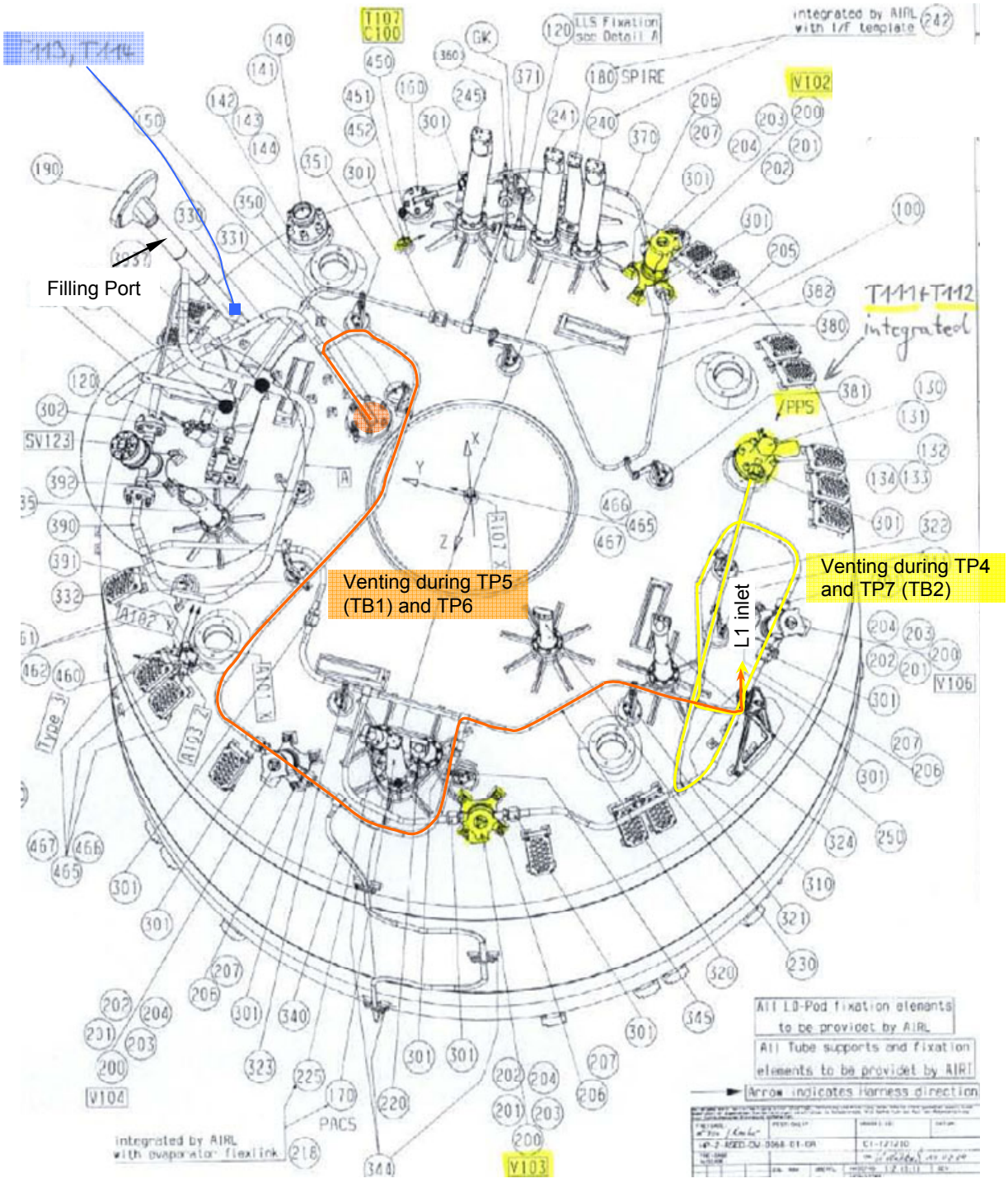

Figure 3.4-3: Helium Venting Paths during Test Phases TP4,TP5,TP6 and TP7

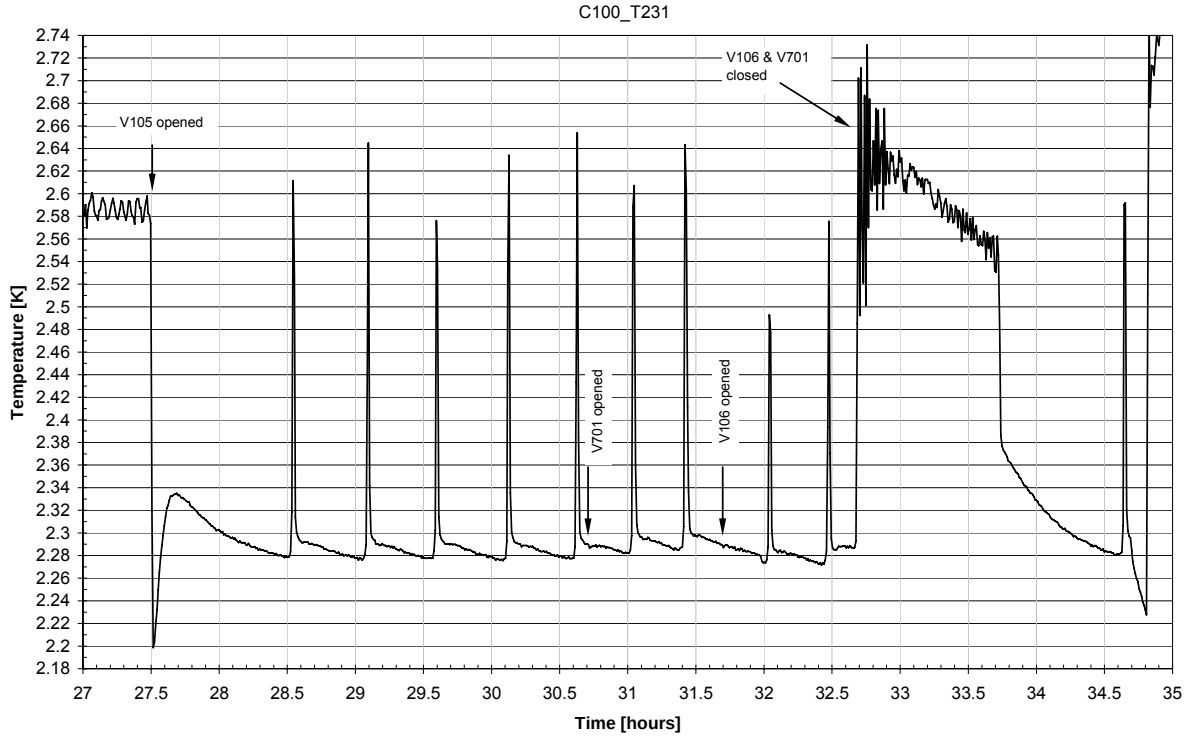

Figure 3.4-4: T231 Temperature Fluctuations and Peaks during PACS L1 Heating (TP6)

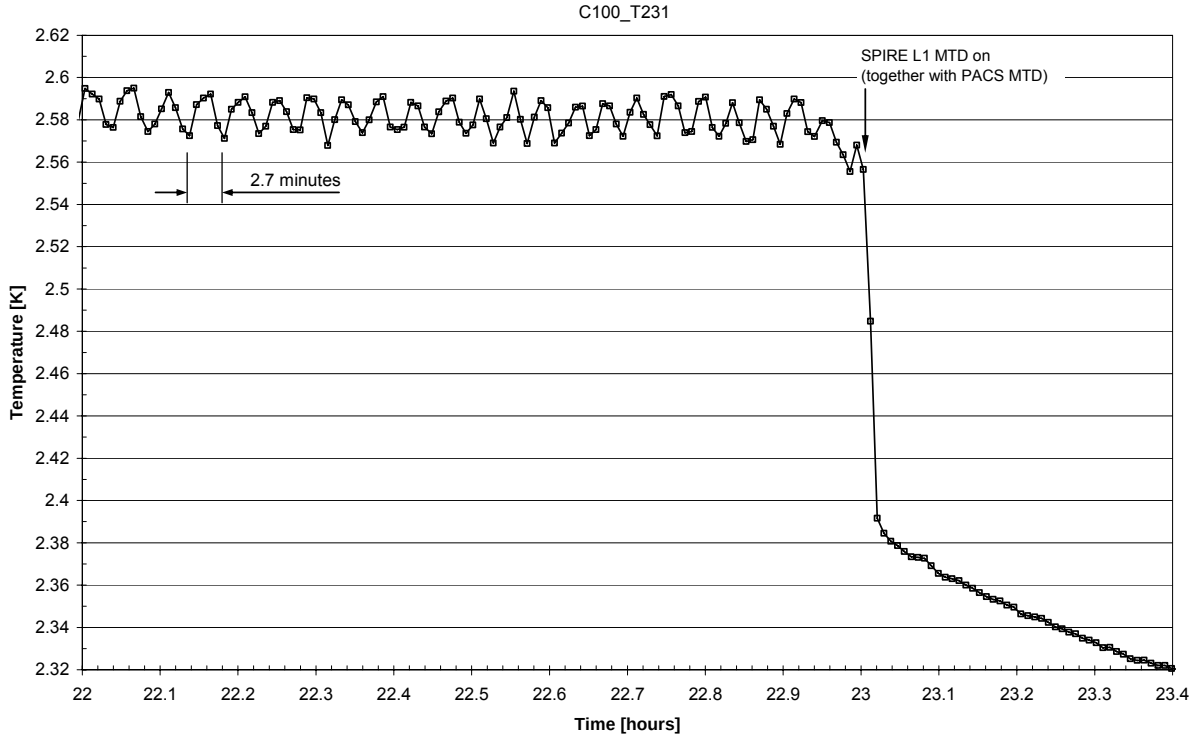

Figure 3.4-5: T231 Temperature Fluctuations during PACE Heating before SPIRE Heating (TP6)

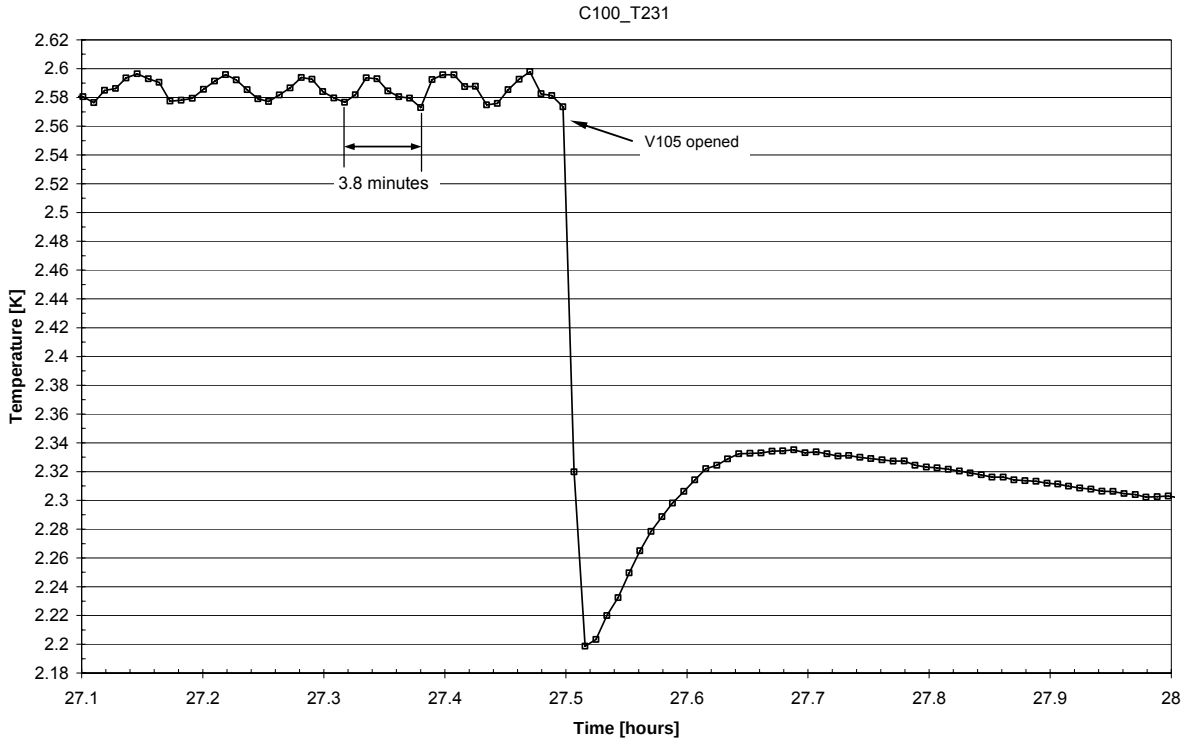

Figure 3.4-6: T231 Temperature Fluctuations before V105 Opening (TP6)

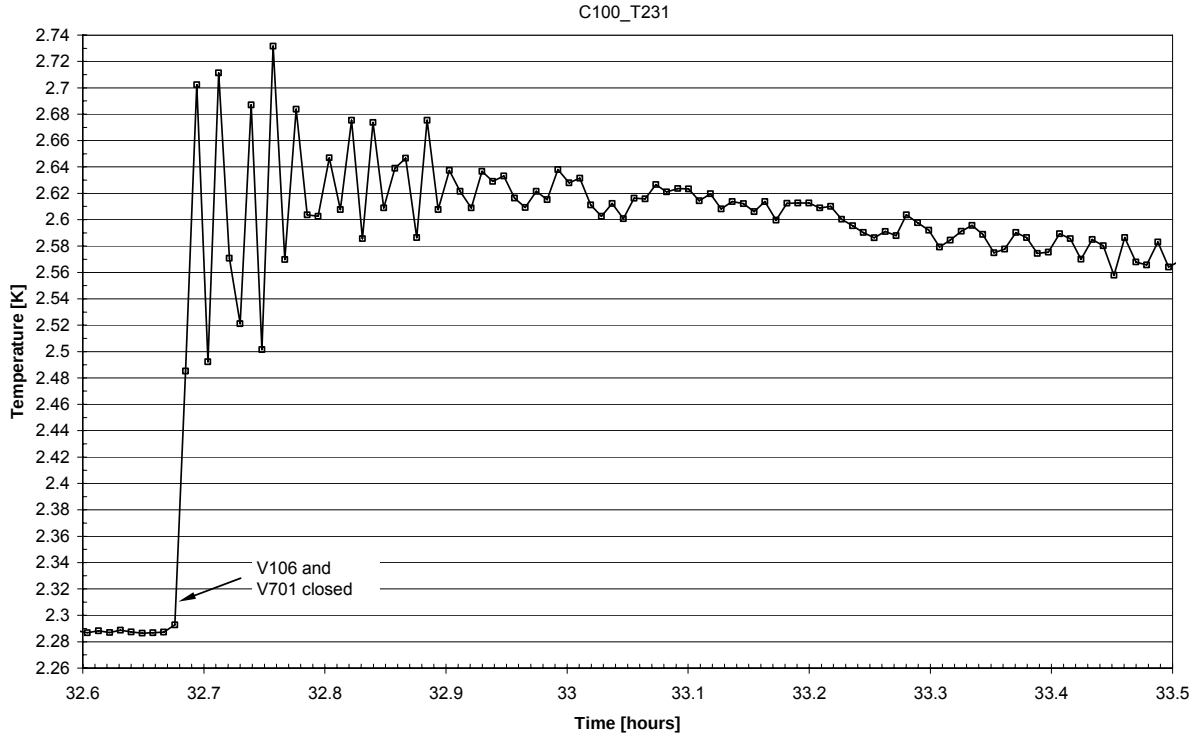

Figure 3.4-7: T231 Temperature Fluctuations after V106 and V701 Closure (TP6)

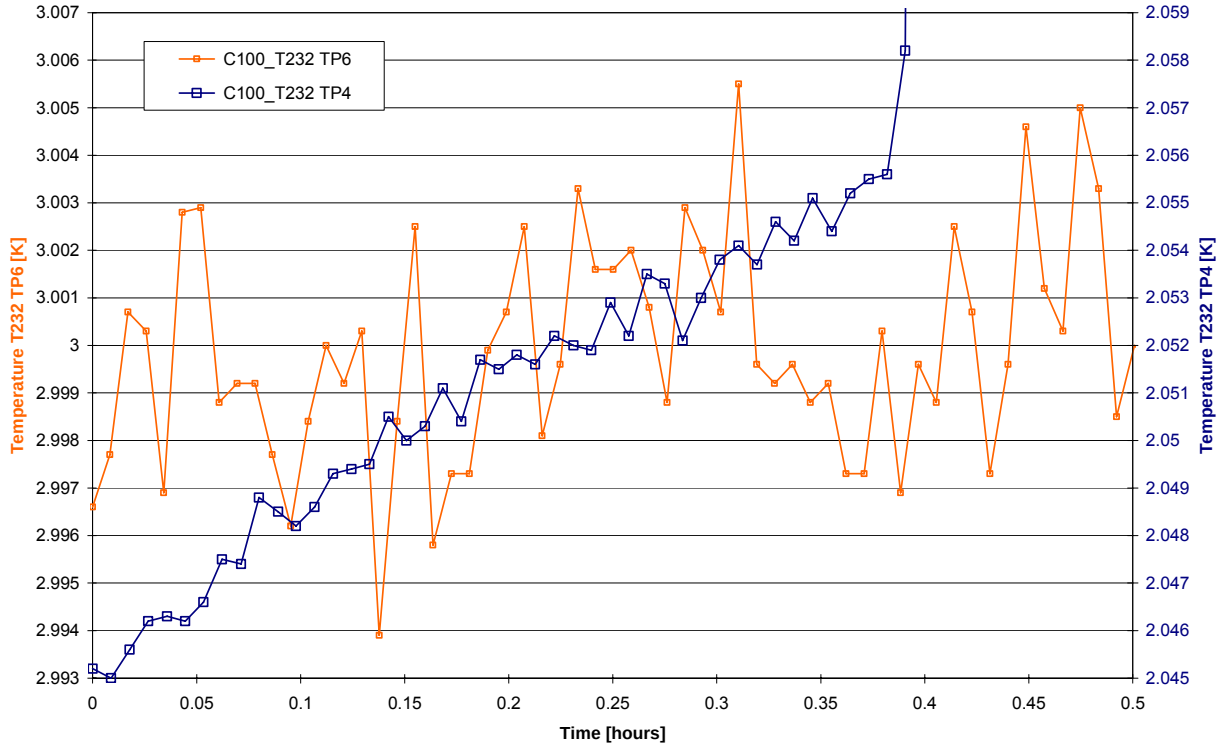

Figure 3.4-8: T232 Temperature Fluctuations at Begin of TP6 and Begin of TP4

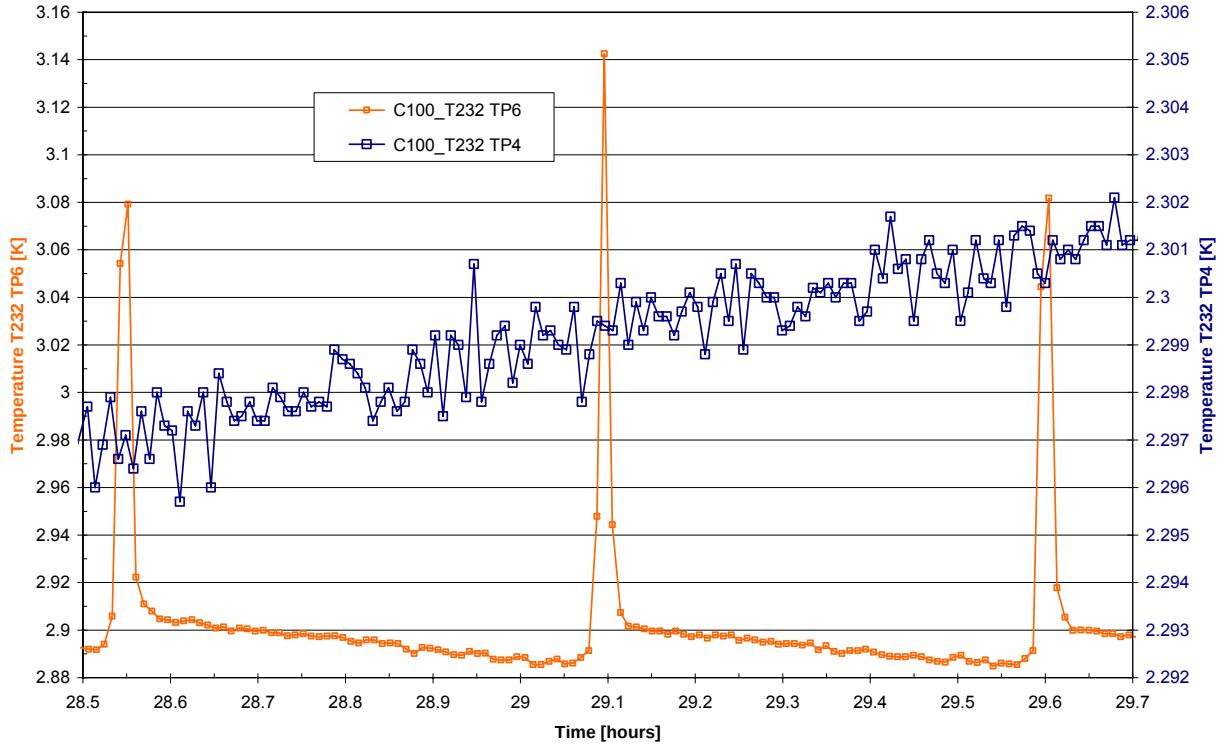

Figure 3.4-9: T232 Temperature Fluctuations of TP6 (PACS op.) and TP4 after 29 hours

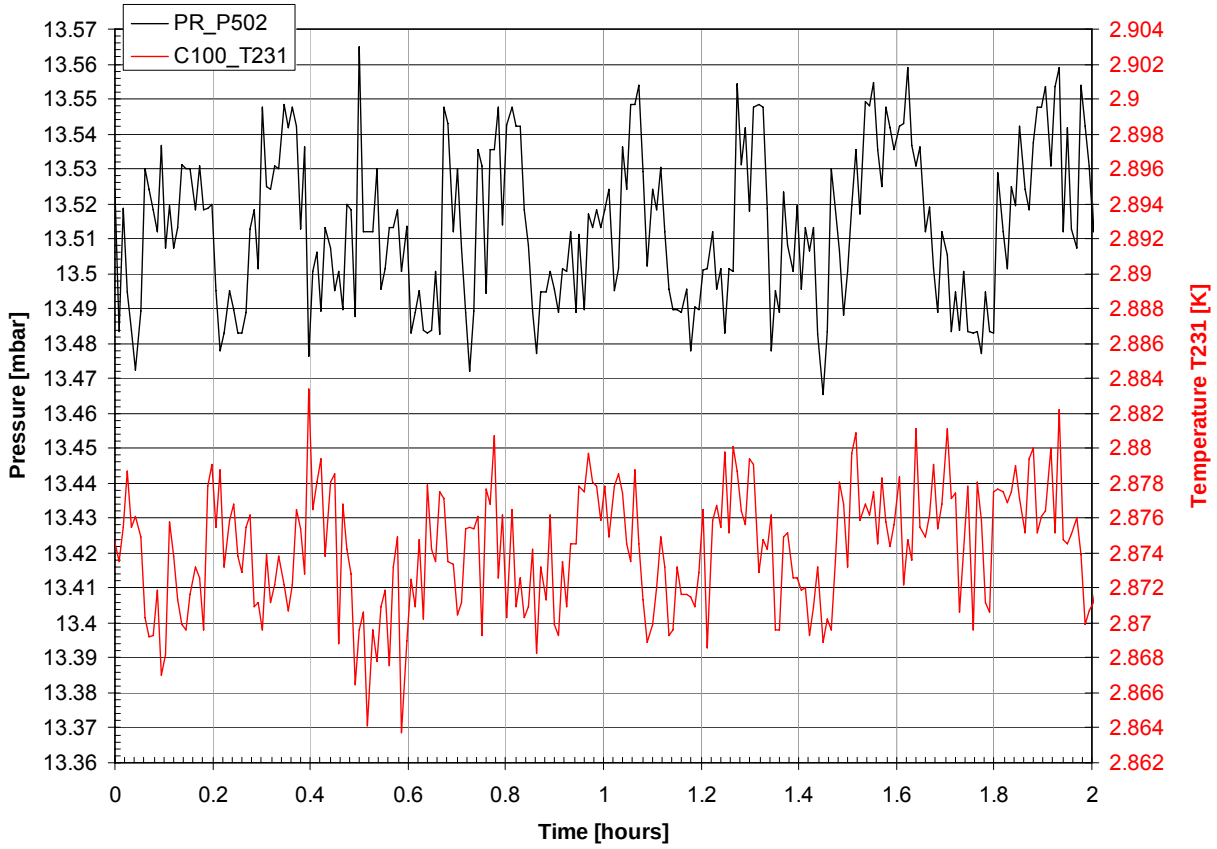

Figure 3.4-10: T231 Temperature and P502 Pressure Fluctuations at Begin of TP6

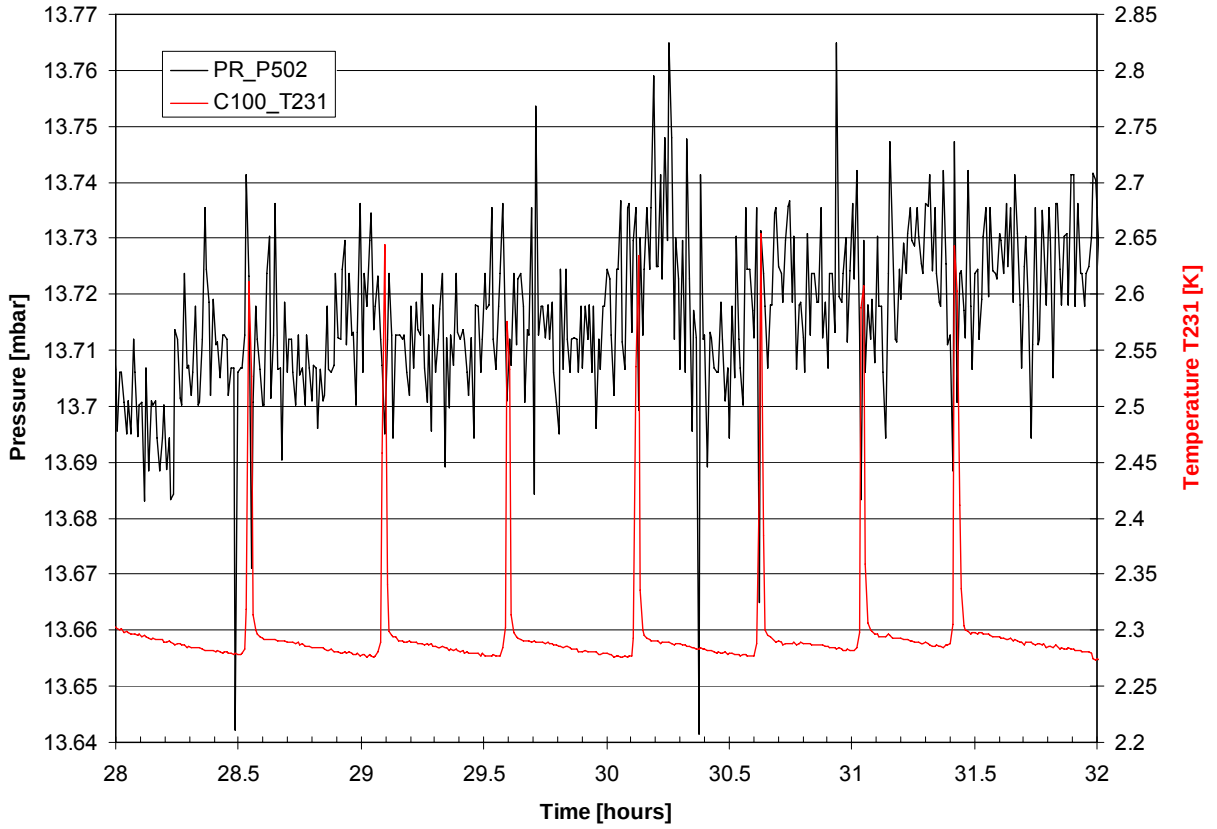

Figure 3.4-11: T231 Temperature and P502 Pressure Fluctuations during PACS Operation (TP6)

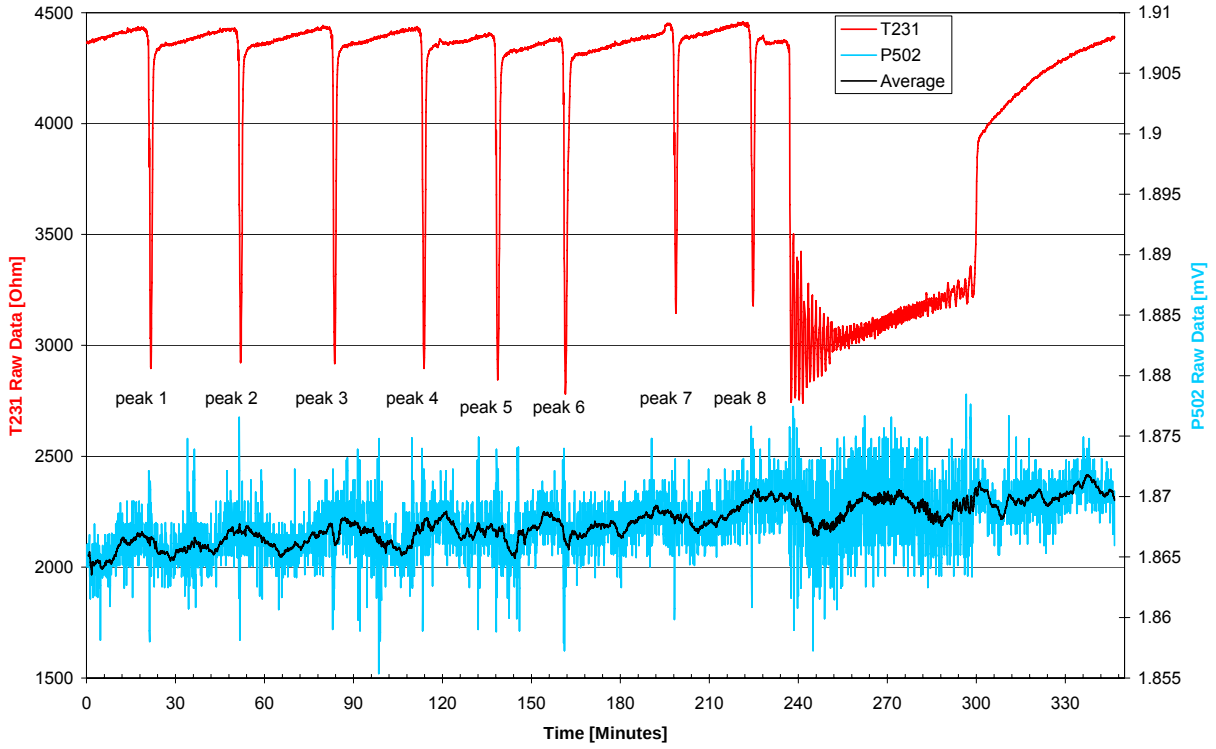

Figure 3.4-12: T231 Peaks and P502 Fluctuations of Raw Data during TP6 PACS Operation

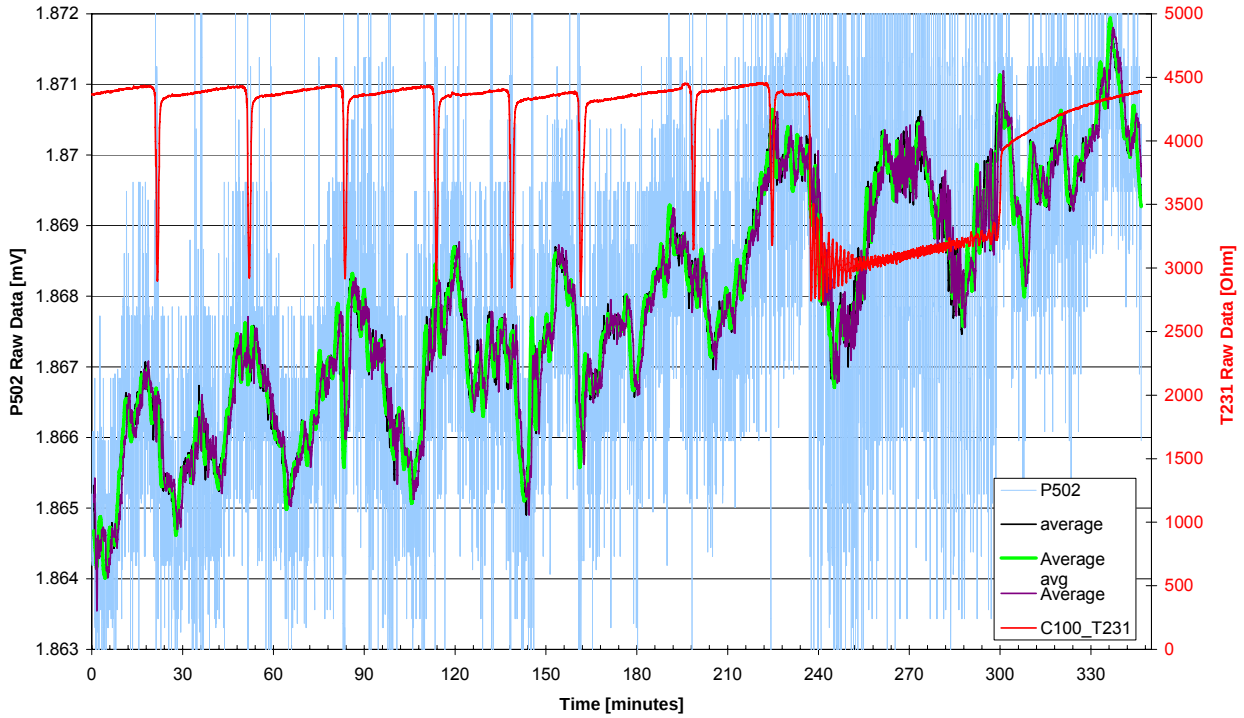

Figure 3.4-13: T231 Peaks and averaged P502 Fluctuations of Raw Data during TP6 PACS Operation

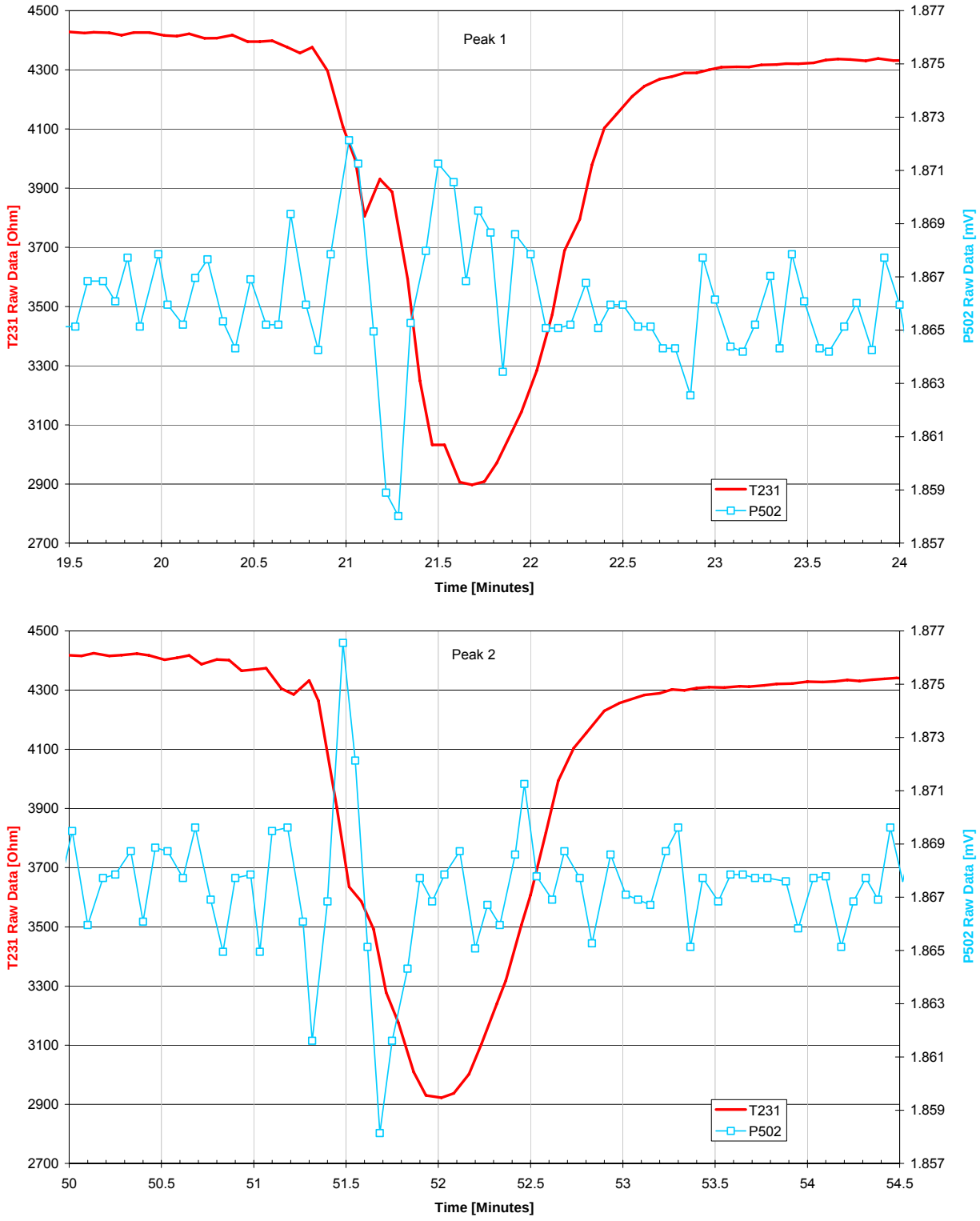

Figure 3.4-14: T231 Peak 1 and Peak 2 versus P502 Fluctuations during TP6 (Raw Data)

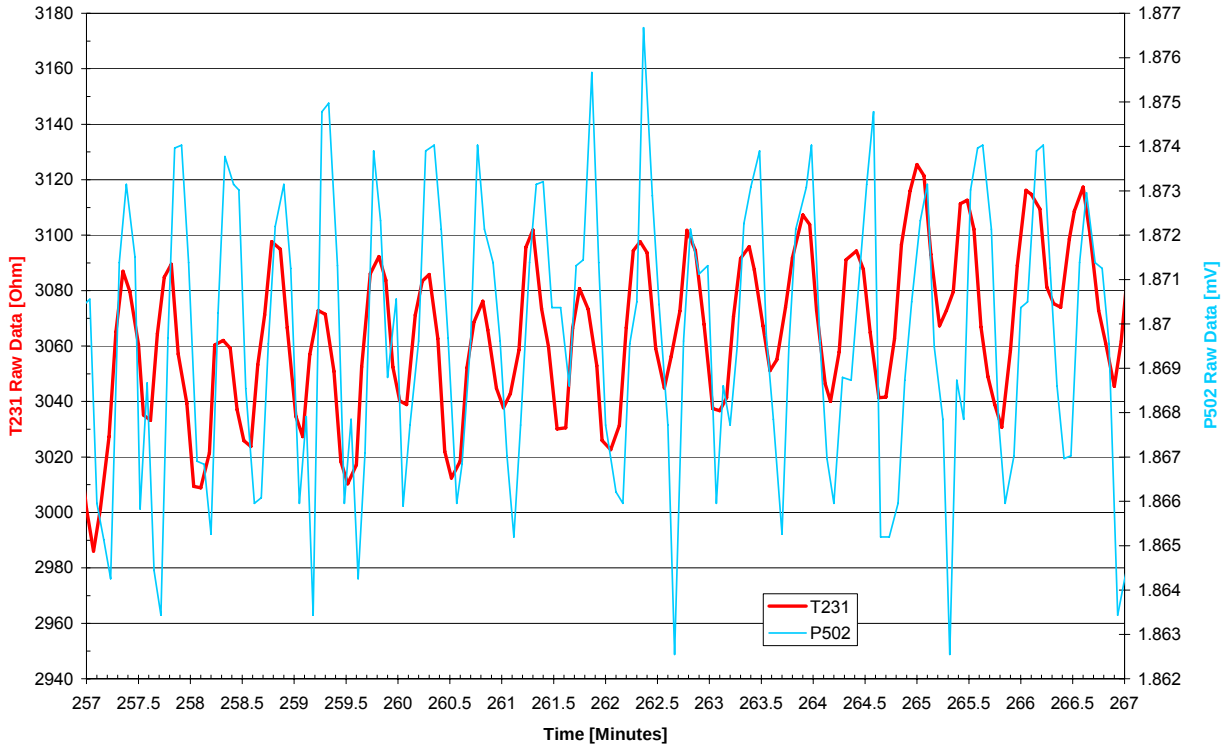

Figure 3.4-15: T231 versus P502 Fluctuations during TP6 after Closure of V106 and V701 (Raw Data)

To check whether the temperature fluctuations correspond with pressure fluctuations, the data of P502 are shown together with the T231 data in **Figure 3.4-10** and **Figure 3.4-11**. Since in a first view not a clear relation can be seen the raw data of both sensors (P502 and T231) are shown in **Figure 3.4-12** to **Figure 3.4-15**. The raw data measurements are available in steps of about 3 seconds whereas the time steps of the engineering data are 30 seconds. Taking the average values for the raw pressure data makes a relation between T231 temperature peaks and P502 pressure fluctuations visible, see **Figure 3.4-13**. It seems that peaks in the pressure coincident with peaks in the temperature (note: ohm values are reciprocal to temperature in K; mV values are equivalent to pressure in mbar). A further zoom of the first two T231 peaks is given in **Figure 3.4-14**, however no further information can be gained here. Finally a zoom directly after closure of V106 and V701 is shown in **Figure 3.4-15** showing a clear correspondence between pressure and temperature fluctuation. In this case however it seems that a peak in the pressure coincident with a dell in temperature.

A summary of all relevant data is compiled in **Table 3.4-1**. Here also the raw data of the C100 sensors T113 and T114 located on the Filling Port are noted. Evaluation of those raw data reveals that in TP6 the Filling Port temperature is at roughly 55 K and about 1 K colder in the phase when the PACS MTDs are switched on. Since the data of T231 are not available for TP4 the T232 data are also listed for both test cases.

	Begin TP6	TP6 after 30 hours (PACS op)	Begin TP4	TP4 after 30 hours (before JFET op)
	29.10.05 19:15	31.10.05 01:18	21.10.05 15:00	22.10.05 21:00
Valve 104	open	open	closed	closed
Valve 106	closed	closed	open	open
S/C tilt	0°	0°	14°	14°
Mass flow	4.65 mg/s	4.75 mg/s	2.23 mg/s	2.30 mg/s
CVV (T906)	101 K	101 K	99 K	100 K
TS1 (T421)	35 K	35 K	27 K	37 K
T114 raw value	137 ohm	138 ohm	140 ohm	138.6 ohm
T113 raw value	135 ohm	136 ohm	138 ohm	136.6 ohm
T113 temp.	55.3 K ± 10K	54.1 K ± 10K	51.8 K ± 10K	53.2 K ± 10K
T231 (absolute)	2.874 K	2.28 K	not available	not available
T231 fluctuation	± 0.01 K	up to 0.37 K peaks	not available	not available
T232 (absolute)	3.00 K	2.89 K	2.05 K	2.30 K
T232 fluctuation	± 0.005 K	up to 0.25 K peak	± 0.001 K	± 0.001 K
P502 (absolute)	13.51 mbar	13.71 mbar	11.15 mbar	11.75 mbar
P502 fluctuation	± 0.05 mbar	± 0.06 mbar	± 0.05 mbar	± 0.05 mbar

Table 3.4-1: Measured and Derived Data for TP4 and TP6 Fluctuations

Conclusions:

- Temperature fluctuations and peaks on L1 ventline occurred when helium was routed via V104; no fluctuations were observed when the Helium was routed via PPS (V106).
- In dedicated test phases a relation between pressure fluctuation and temperature fluctuations can be seen using the raw data recordings with a higher time resolution. The reasons for the fluctuations and peaks are not fully understood yet.
- A Filling Port temperature around 50 K has been derived for the two test cases.

3.5 Thermal Shields Performance

The Thermal Shields temperature evolution during the first TB phase (TP5) is shown in **Figure 3.5-1** to **Figure 3.5-3**. The heat absorbed by the helium ventline routed along the shields is shown in **Figure 3.5-4** using the average mass flow rate as shown in **Figure 3.5-5**.

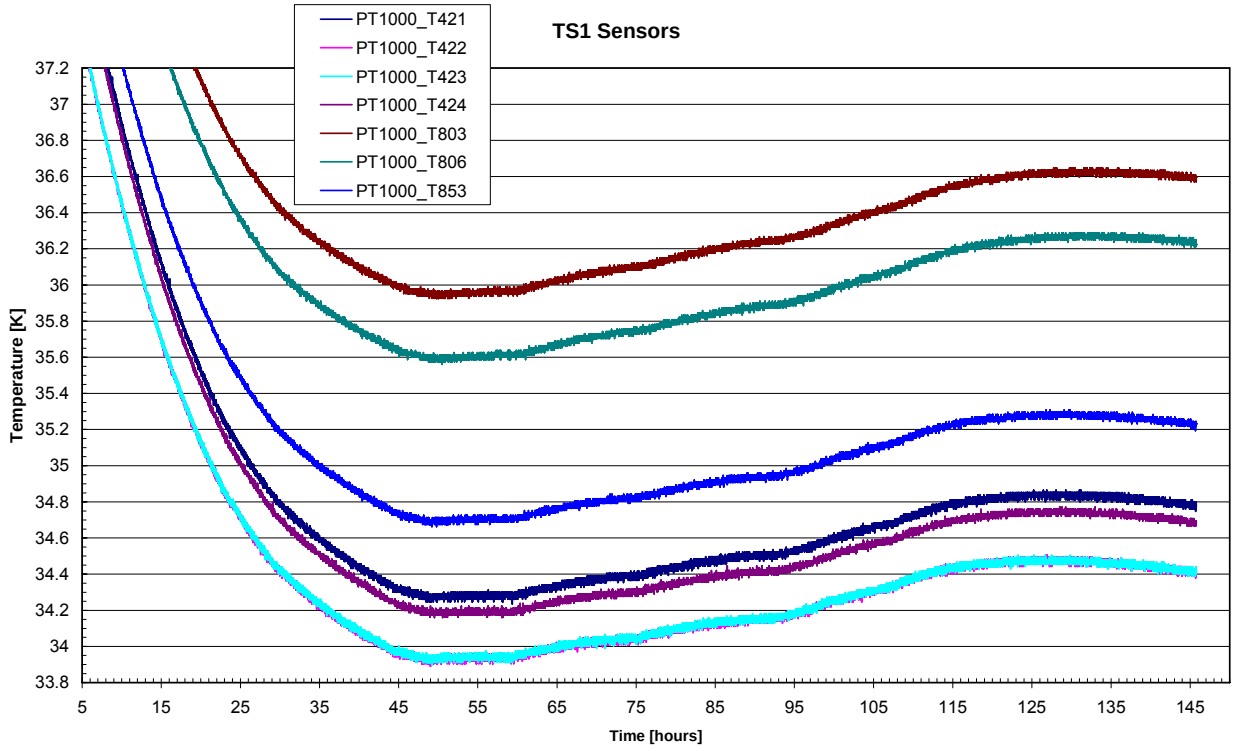

Figure 3.5-1: TS1 Temperature Evolution during TB1 Test Phase (TP5)

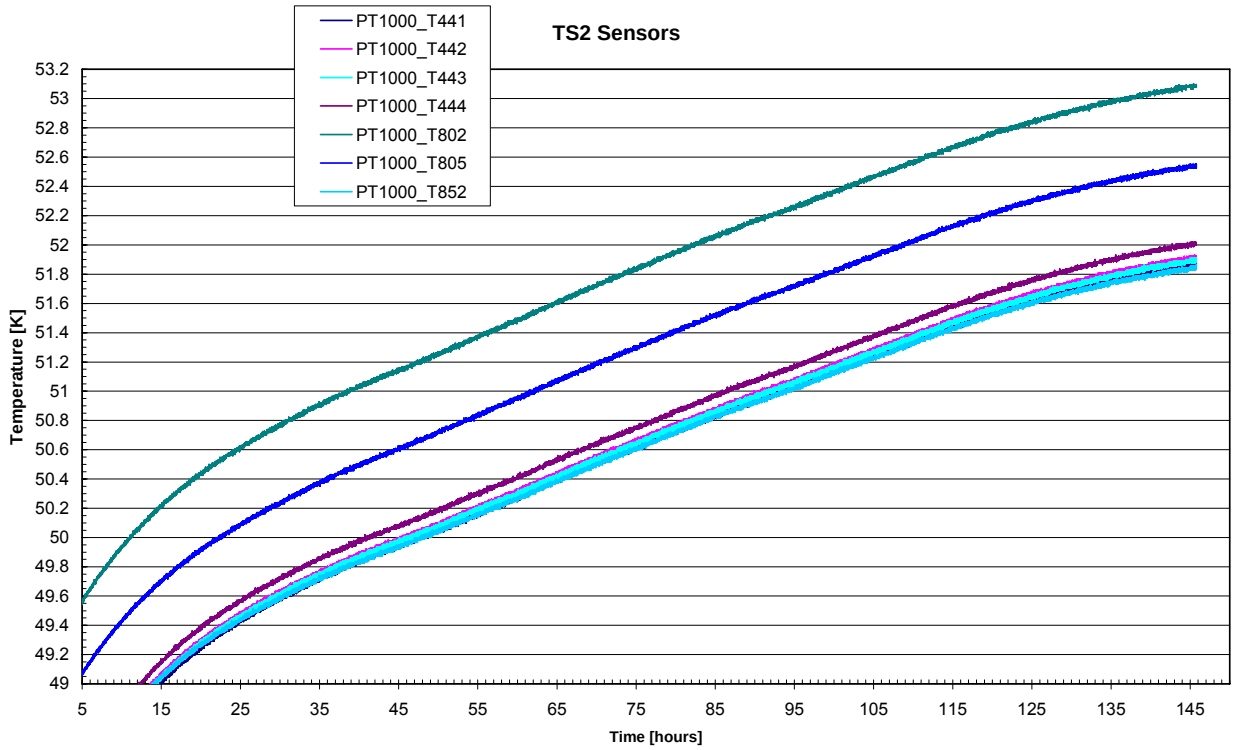

Figure 3.5-2: TS2 Temperature Evolution during TB1 Test Phase (TP5)

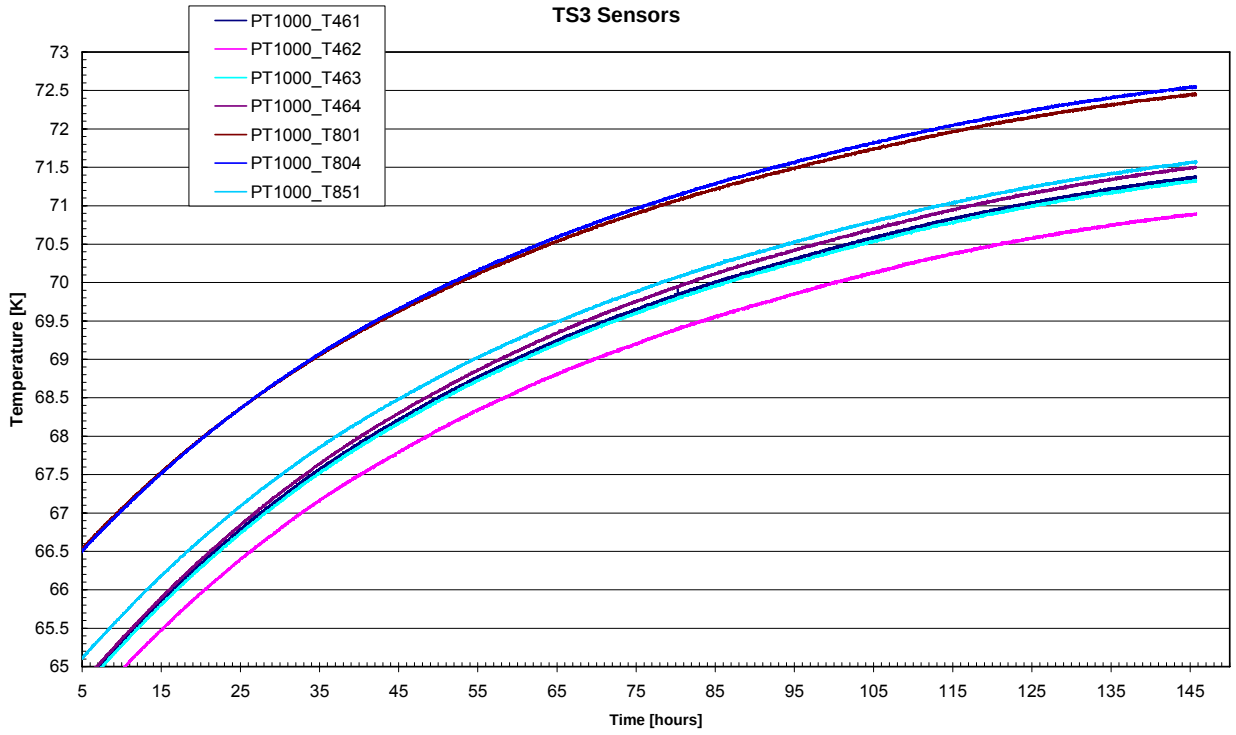

Figure 3.5-3: TS3 Temperature Evolution during TB1 Test Phase (TP5)

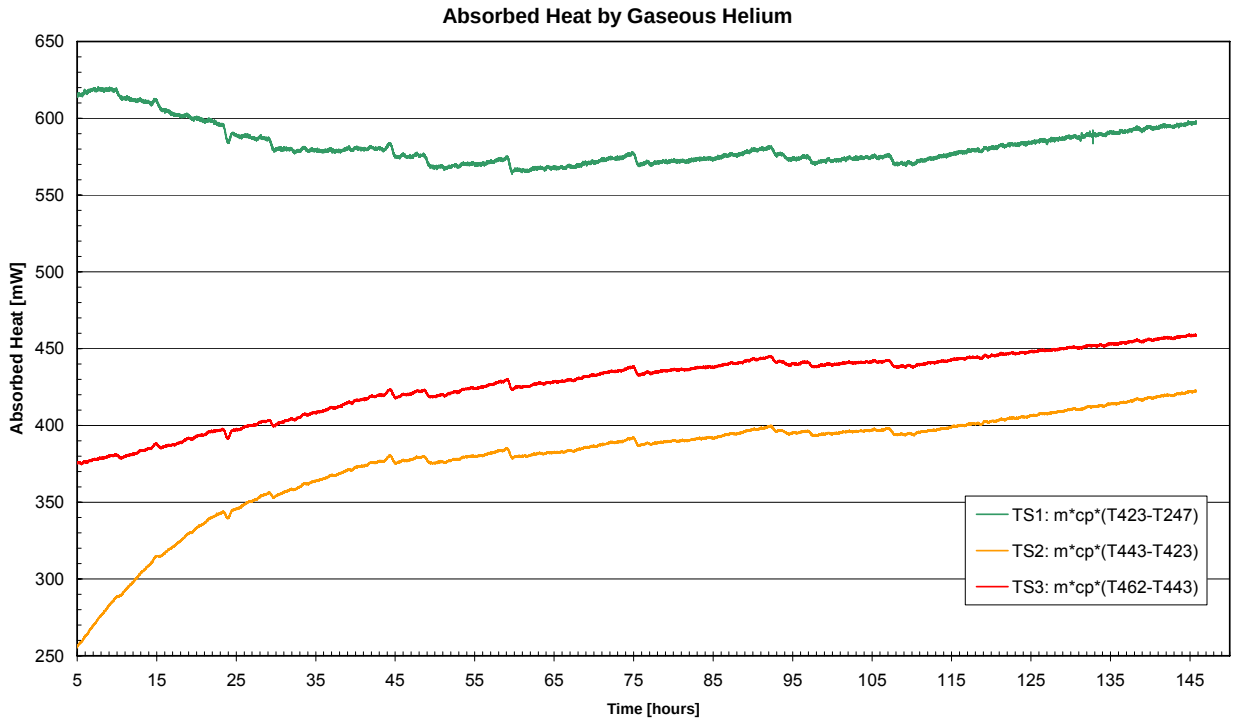

Figure 3.5-4: Absorbed Heat on Shields Ventline during TB1 Test Phase (TP5)

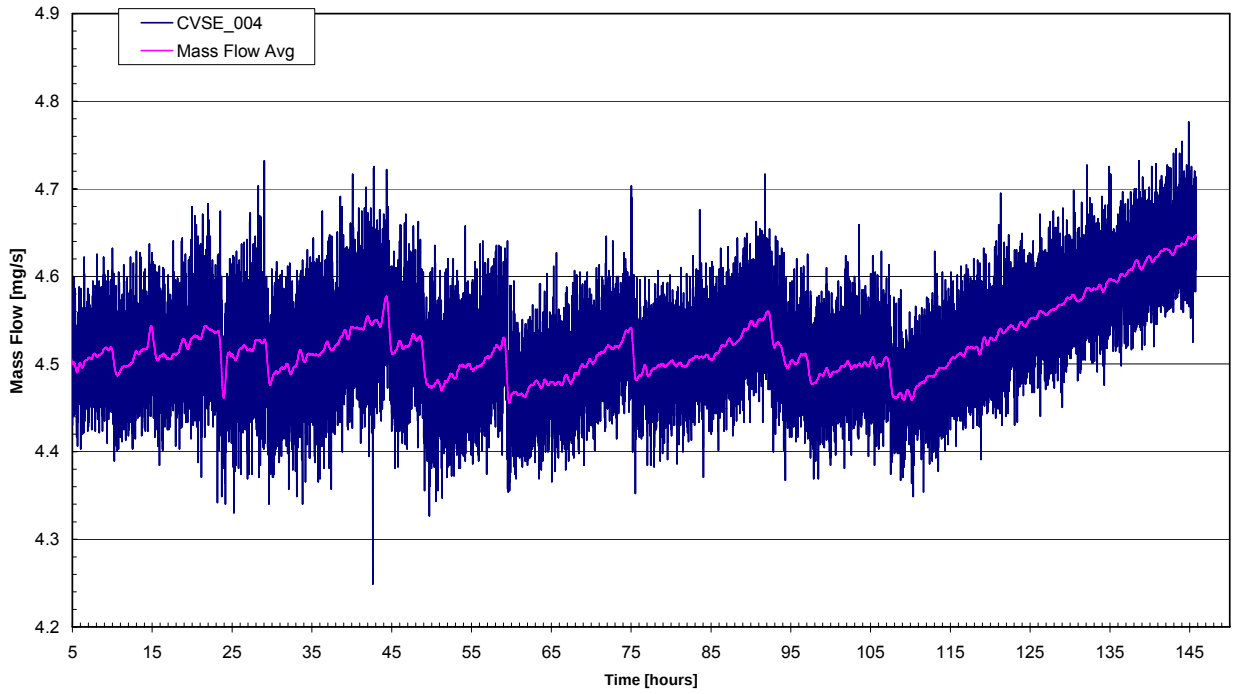

Figure 3.5-5: Helium Mass Flow Evolution during TB1 Test Phase (TP5)

The Thermal Shields temperature evolution during the first TB phase (TP5) is shown in **Figure 3.5-6** to **Figure 3.5-8** . The heat absorbed by the helium ventline routed along the shields is shown in **Figure 3.5-9** using the average mass flow rate as shown in **Figure 3.5-10**.

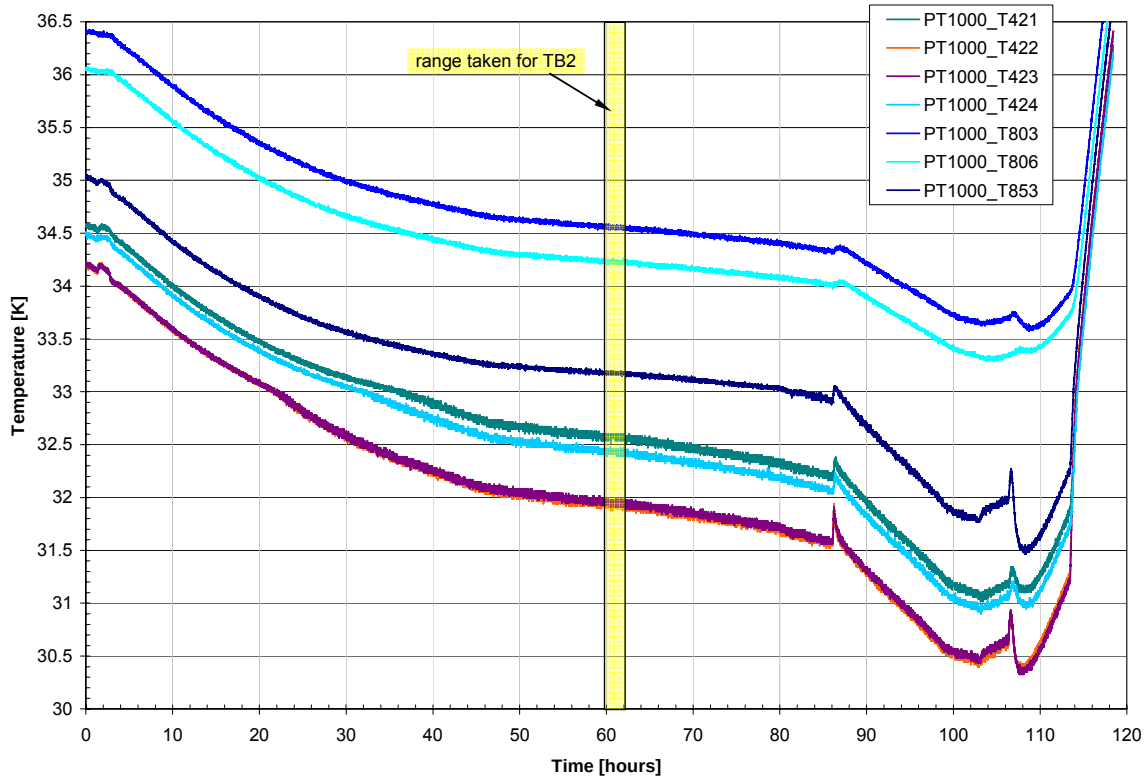

Figure 3.5-6: TS1 Temperature Evolution during TB2 Test Phase (TP7)

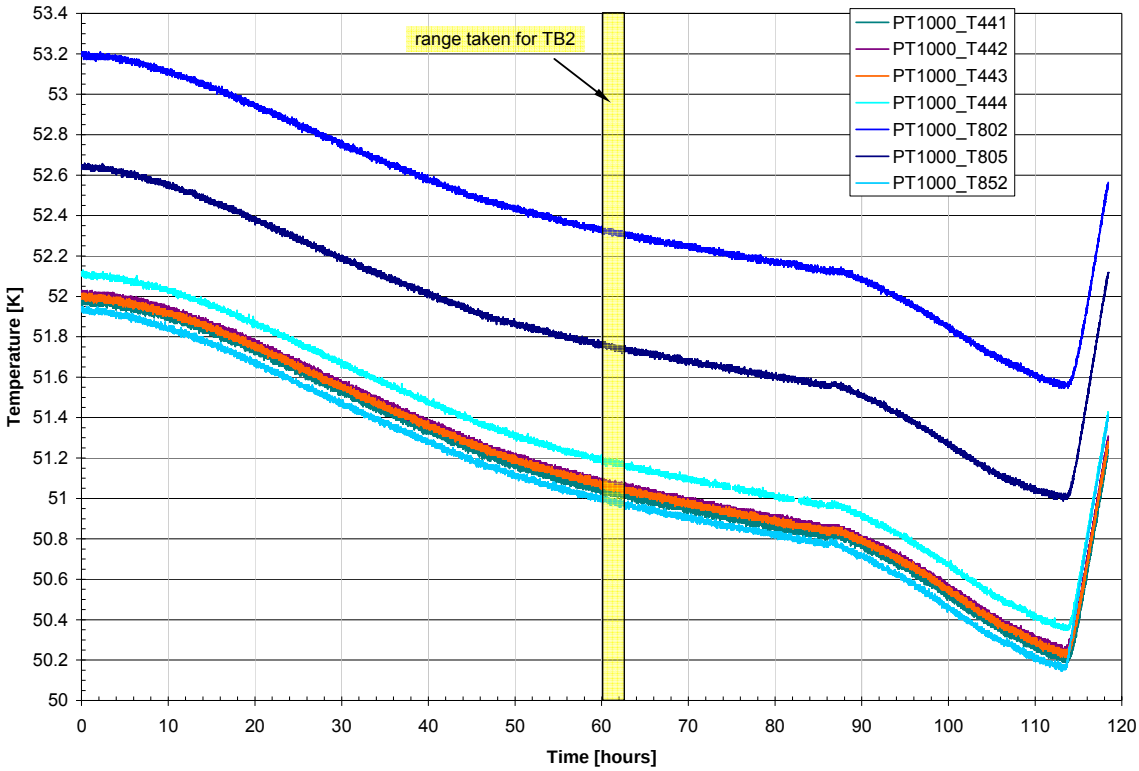

Figure 3.5-7: TS2 Temperature Evolution during TB2 Test Phase (TP7)

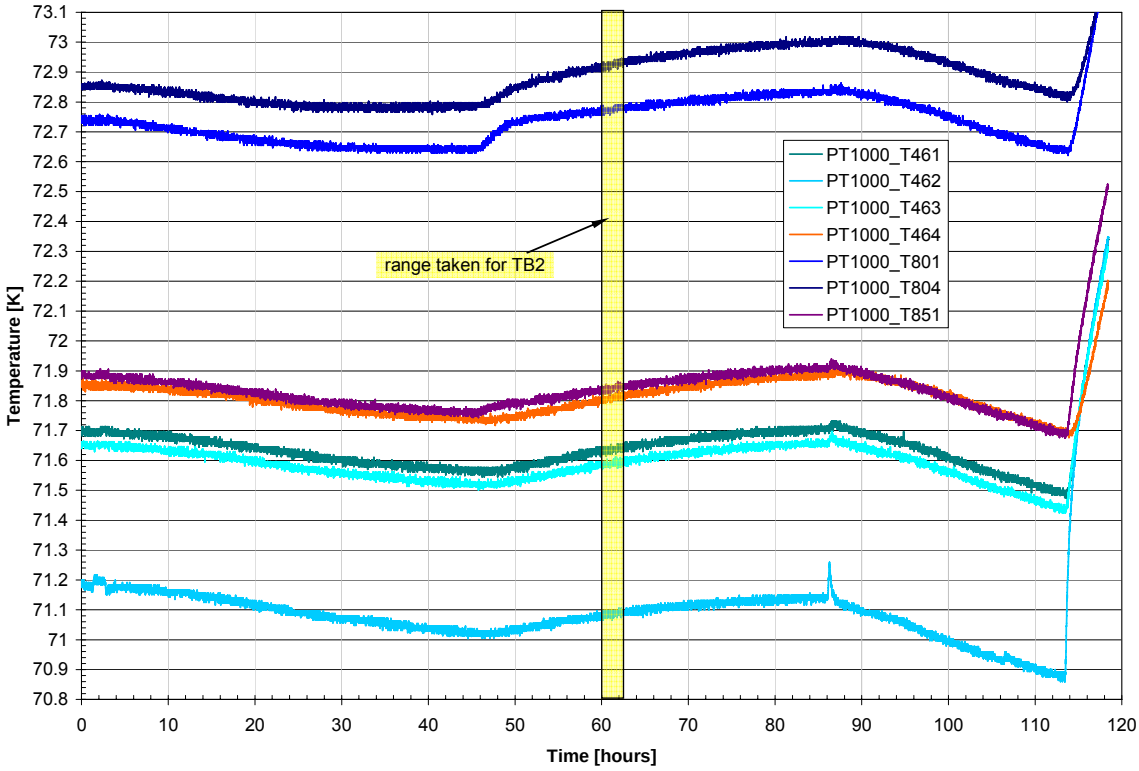

Figure 3.5-8: TS3 Temperature Evolution during TB2 Test Phase (TP7)

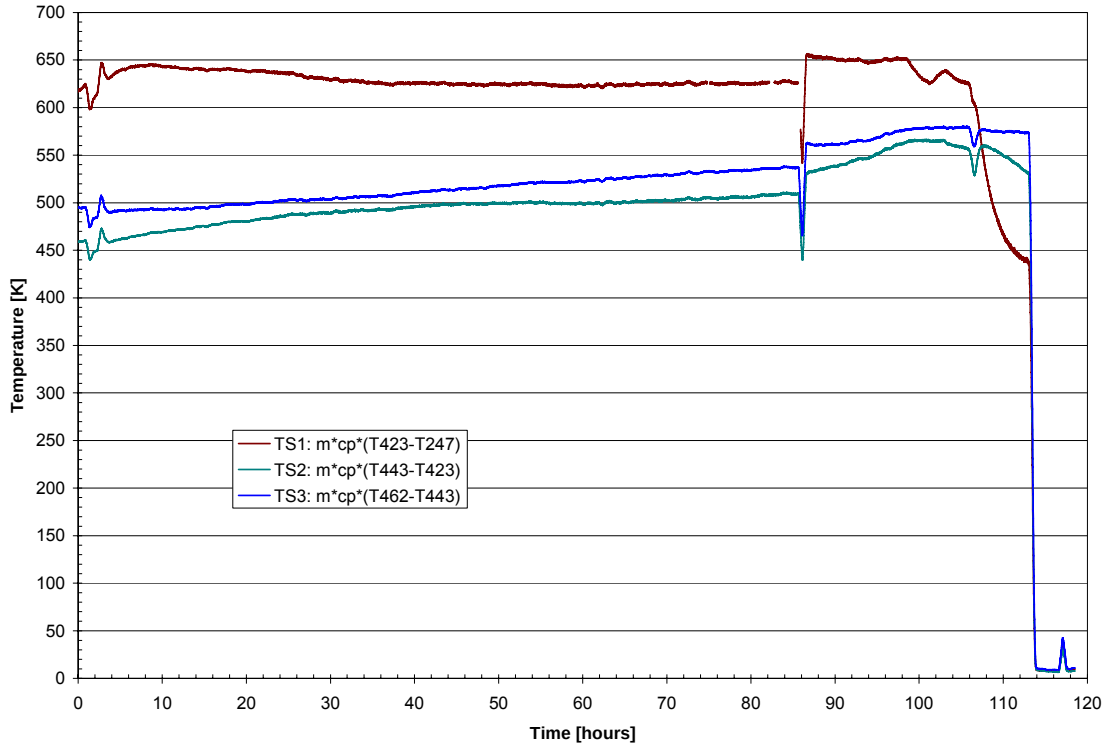

Figure 3.5-9: Absorbed Heat on Shields Ventline during TB2 Test Phase (TP7)

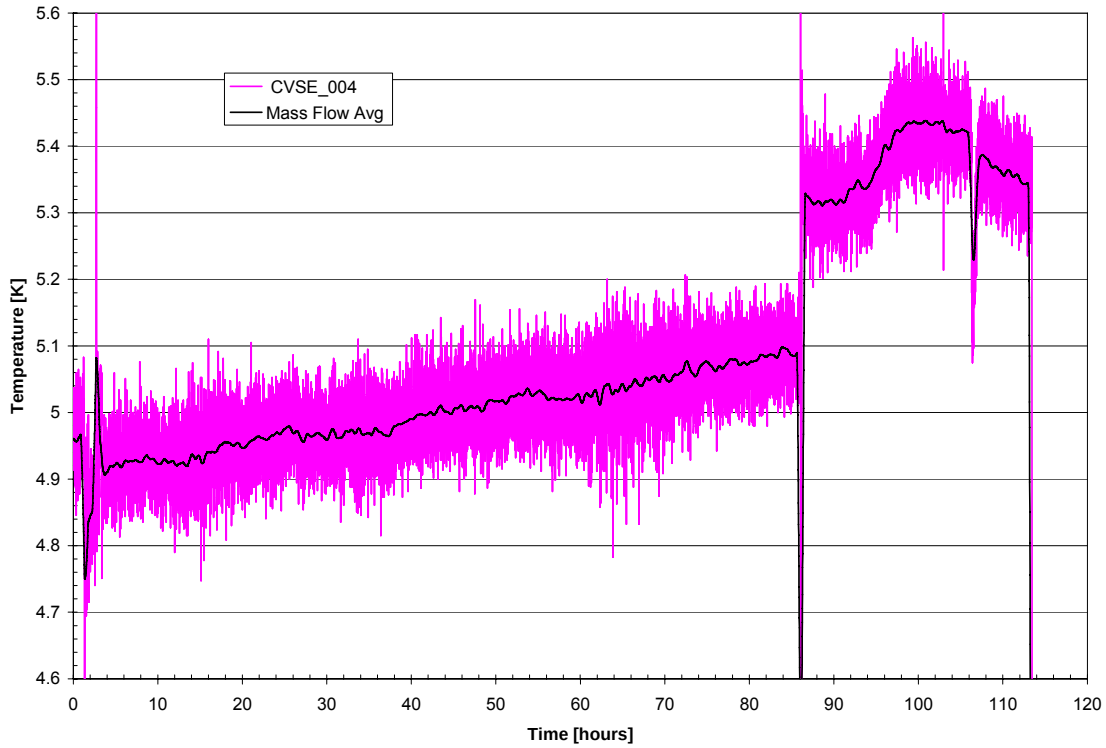

Figure 3.5-10: Helium Mass Flow Evolution during TB2 Test Phase (TP7)

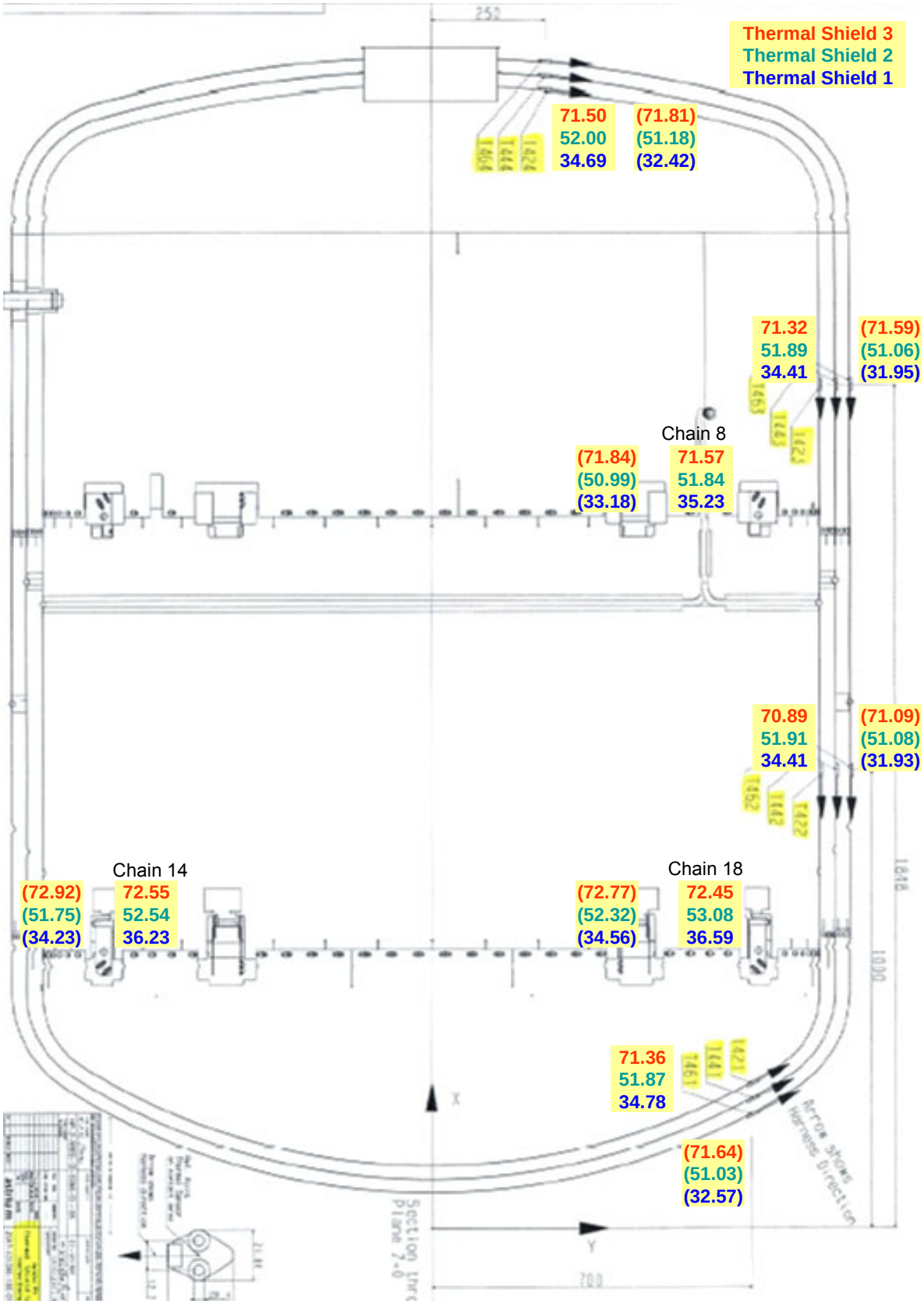

Figure 3.5-11: Thermal Shields Temperature Distribution during TB1 and (TB2)

	TB1	TB2	Remark
Helium routing	via V104	via PPS (V106)	
S/C tilt	0° (vertical)	16° around Z axis	
Mass Flow	4.64 mg/s	5.03 mg/s	CVSE_004
TS1 average	35.2 K -0.15 K/day	33.0 K -0.14 K/day	including chain sensors
TS1 max gradient	0.37 K (2.2 K)*	0.64 K (2.6 K)*	
Upp chain –TS1 (T853-T423)	0.82 K	1.23 K	Stiff CuBe bracket (chain 8)
Low chain –TS1 (T803-T422)	**2.18 K**	**2.63 K**	Soft CuBe bracket (chain 18)
Absorbed heat $m_{*}cp_{*}$(T423-T247)	596 mW	624 mW	
TS2 average	52.2 K +0.21 K/day	51.3 K -0.21 K/day	including chain sensors
TS2 max gradient	0.13 K (1.2 K)*	0.15 K (1.3 K)*	
Upp chain –TS2 (T852-T443)	-0.04 K	-0.07 K	Stiff CuBe bracket (chain 8)
Low chain –TS2 (T802-T442)	**1.17 K**	**1.24 K**	Soft CuBe bracket (chain 18)
Absorbed heat $m_{*}cp_{*}$(T443-T423)	422 mW	500 mW	
TS3 average	71.7 K +0.27 K/day	72.0 K +0.14 K/day	including chain sensors
TS3 max gradient	0.61 K (1.7 K)*	0.72 K (1.8 K)*	
Upp chain –TS3 (T851-T463)	0.25 K	0.25 K	Stiff CuBe bracket (chain 8)
Low chain –TS3 (T801-T462)	**1.56 K**	**1.68 K**	Soft CuBe bracket (chain 18)
Absorbed heat $m_{*}cp_{*}$(T462-T443)	458 mW	524 mW	

*) values in brackets include chain sensors

Table 3.5-1: Thermal Shields Temperatures, Gradients and Absorbed Heat

Conclusions:

- The measured temperature gradients within the Thermal Shields are less than 1 K (all shields)
- Gradient between chain bolts and shields is about (1.2-1.4) K higher on lower chains compared to the upper chains. This is because the conductance of the stiff CuBe bracket at the upper chain is about 8 times higher compared to the soft CuBe bracket at the lower chain.
- Gradient between chain bolts and TS1 is higher compared to the other shields because additional heat is introduced via the harness that is anchored on TS1. The gradient is around 1 K.

4 CVV External Performance

4.1 Thermal Balance Test Phases

Two thermal balance test cases were conducted in the LSS: one with the HSS Rig controlled at 173 K (TB1) and the second one with the HSS Rig controlled at 293 K (TB2). Except the LOU MTD heating no other parameter has been changed in TB2. The main results are compiled in **Table 4.1-1**.

For the Telescope Thermal Dummy no steady state was achieved at the end of TB1. The increase of the HSS Rig by 120 K led to an increase of the average CVV temperature of about 2.1 K.

Item	TB1		TB2		Remark
	T avg	dTmax	T avg	dTmax	
CVV	102.42 K	4.88 K	104.51 K	5.87 K	SCOE sensors not included
CVV –Z Radiator	101.19 K	1.5 K	102.65 K	1.5 K	SCOE sensors not included
CVV –Y Radiator	101.94 K	1.5 K	103.82 K	1.1 K	SCOE sensors not included
CVV +Y Radiator	102.16 K	1.6 K	104.28 K	2.5 K	SCOE sensors not included
CVV MLI UB & Baffle	109.8 K	0.3 K	136.8 K	1.6 K	4 sensors (incl. baffle MLI)
CVV MLI cylindrical part	114.6 K	14.1 K	143.1 K	25.7 K	5 sensors
CVV MLI lower bulkhead	134.4 K	14.8 K	154.4 K	3.3 K	3 sensors
SVM Thermal Shield	130.0 K	11.5 K	133.3 K	12.9 K	incl. strut sensors near shield
SVM Thermal Shield SLI	113.9 K	8.3 K	124.1 K	24.0 K	4 sensors
LOU Baseplate	110.1 K	2.32 K	139.6 K	1.56 K	6.2 W heating in TB2
LOU Radiator	109.2 K	2.2 K	127.3 K	6.4 K	6 sensors
TTAP	273.3 K	1.3 K	273.7 K	1.7 K	active controlled
TTAP SLI	198.6 K	17 K	202.4 K	21 K	7 sensors
HSS Rig	173.0 K	3 K	292.8 K	6 K	active controlled
HSS Rig MLI	140.5 K	7 K	174.7 K	13 K	12 sensors
Telescope TD	123.5 K	5.0 K	118.8 K	4.5 K	-1.7 K/day at end of TB1
Telescope MLI	117.7 K	11 K	125.1 K	26.7 K	-1 K/day at end of TB1

Table 4.1-1: Steady State Temperatures during the two TB Test Phases

4.2 Temperature Gradients within CVV Structure and Radiators

The temperature distribution at the end of TB1 within the CVV structure, the CVV radiators, Waveguides and CVV struts is shown in **Figure 4.2-1**, **Figure 4.2-2** and **Figure 4.2-4**.

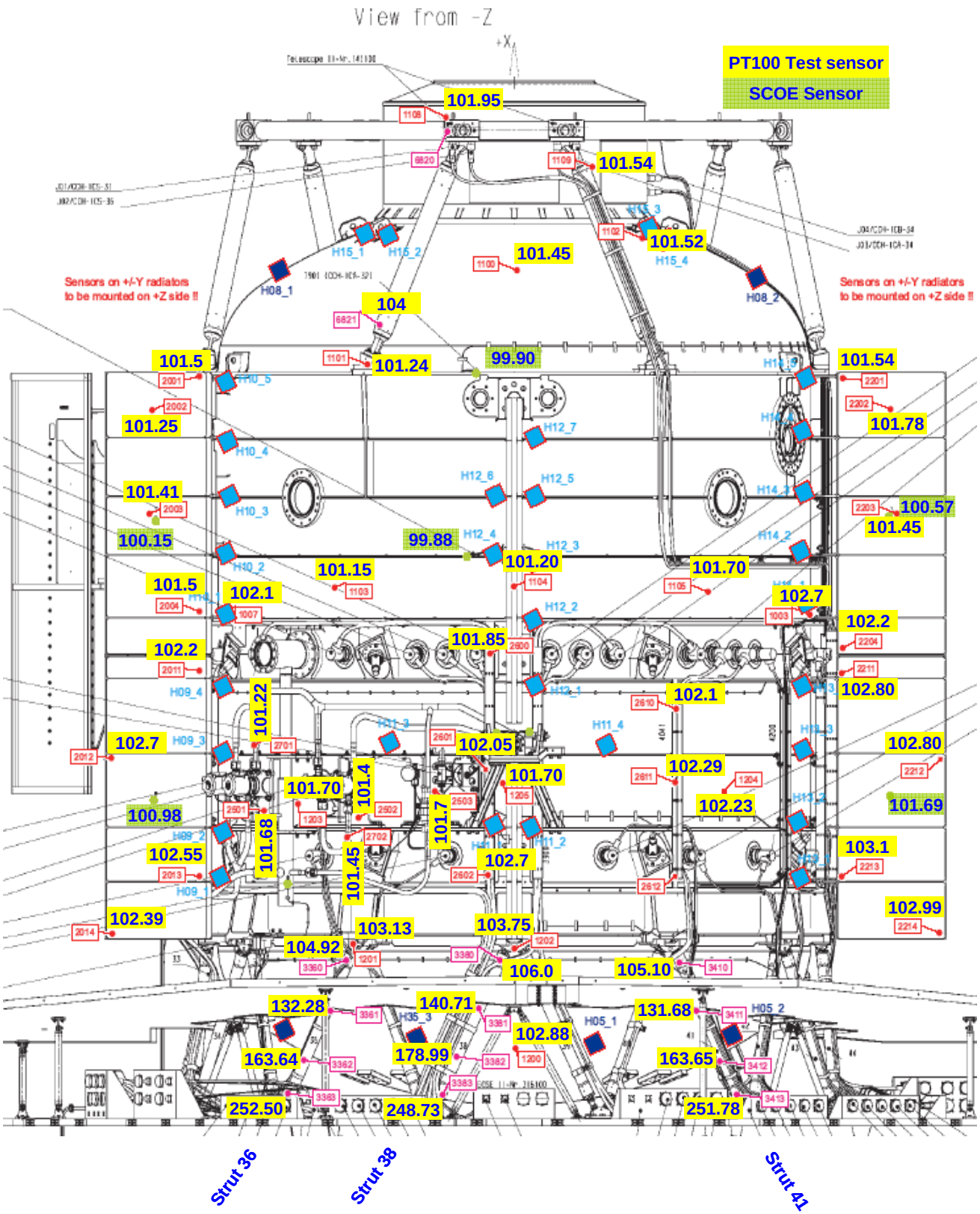

Figure 4.2-1: Temperature Distribution on CVV -Z Side during TB1 Test Phase

View from –Y

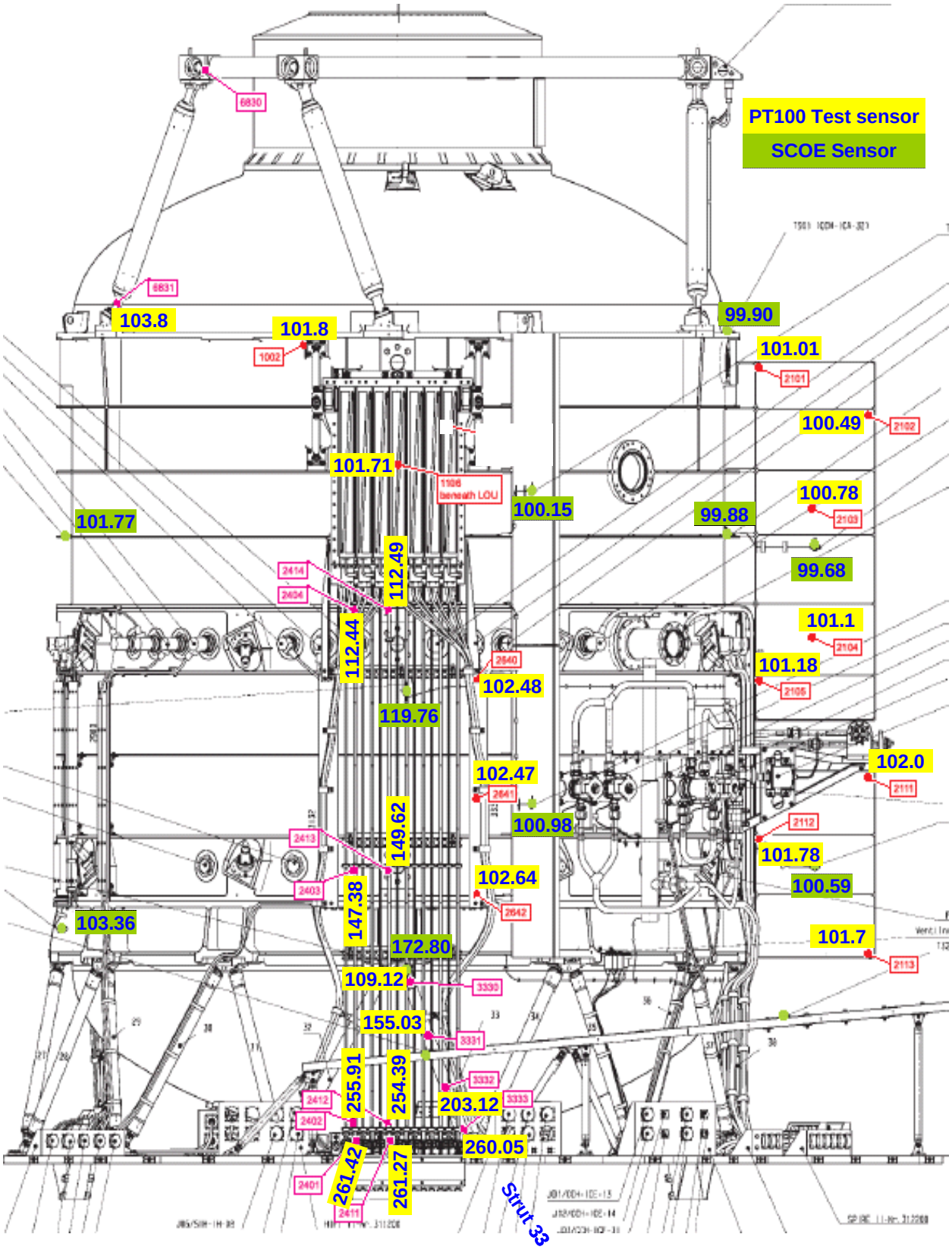

Figure 4.2-2: Temperature Distribution on CVV -Y Side during TB1 Test Phase

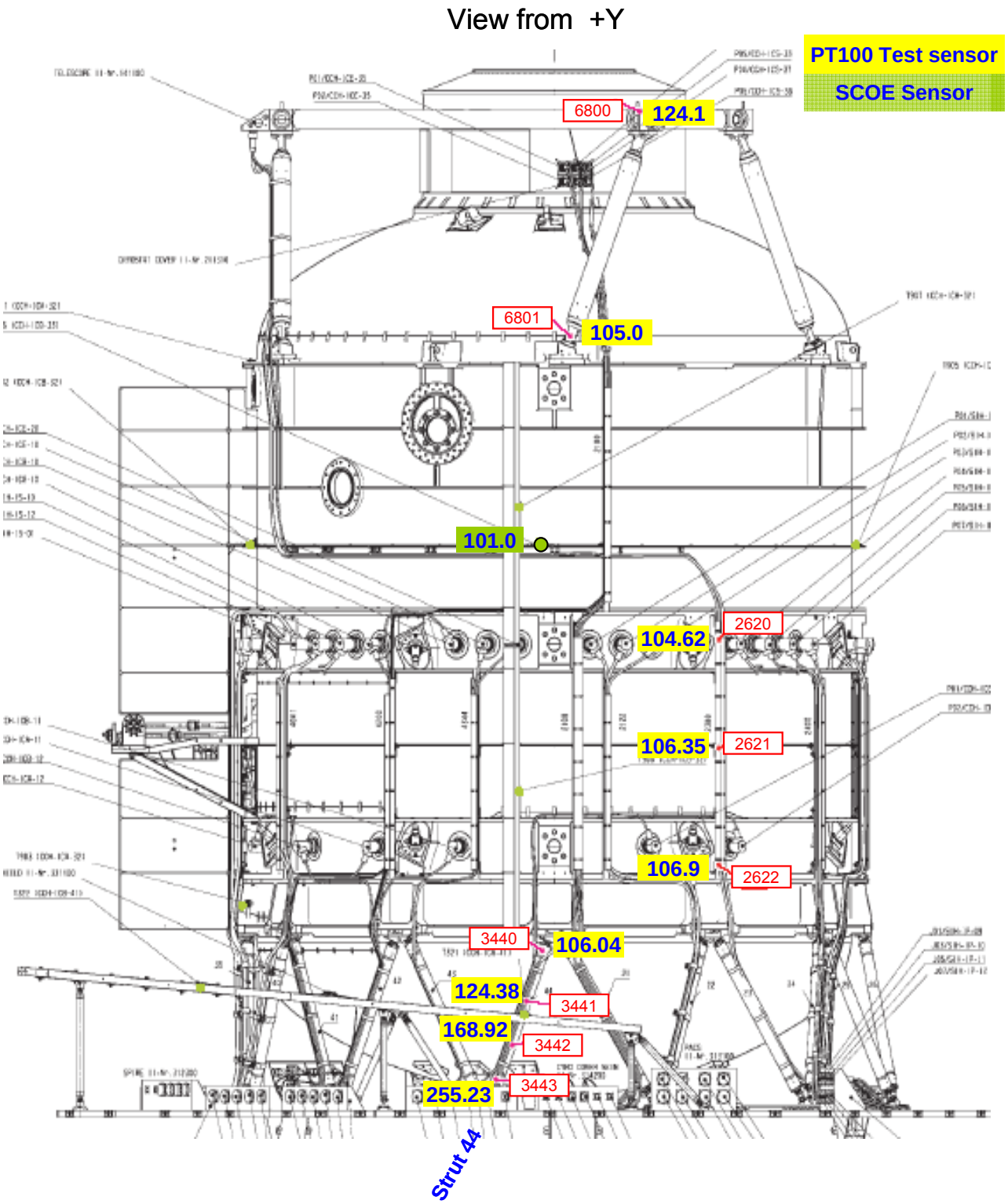

Figure 4.2-3: Temperature Distribution on CVV +Y Side during TB1 Test Phase

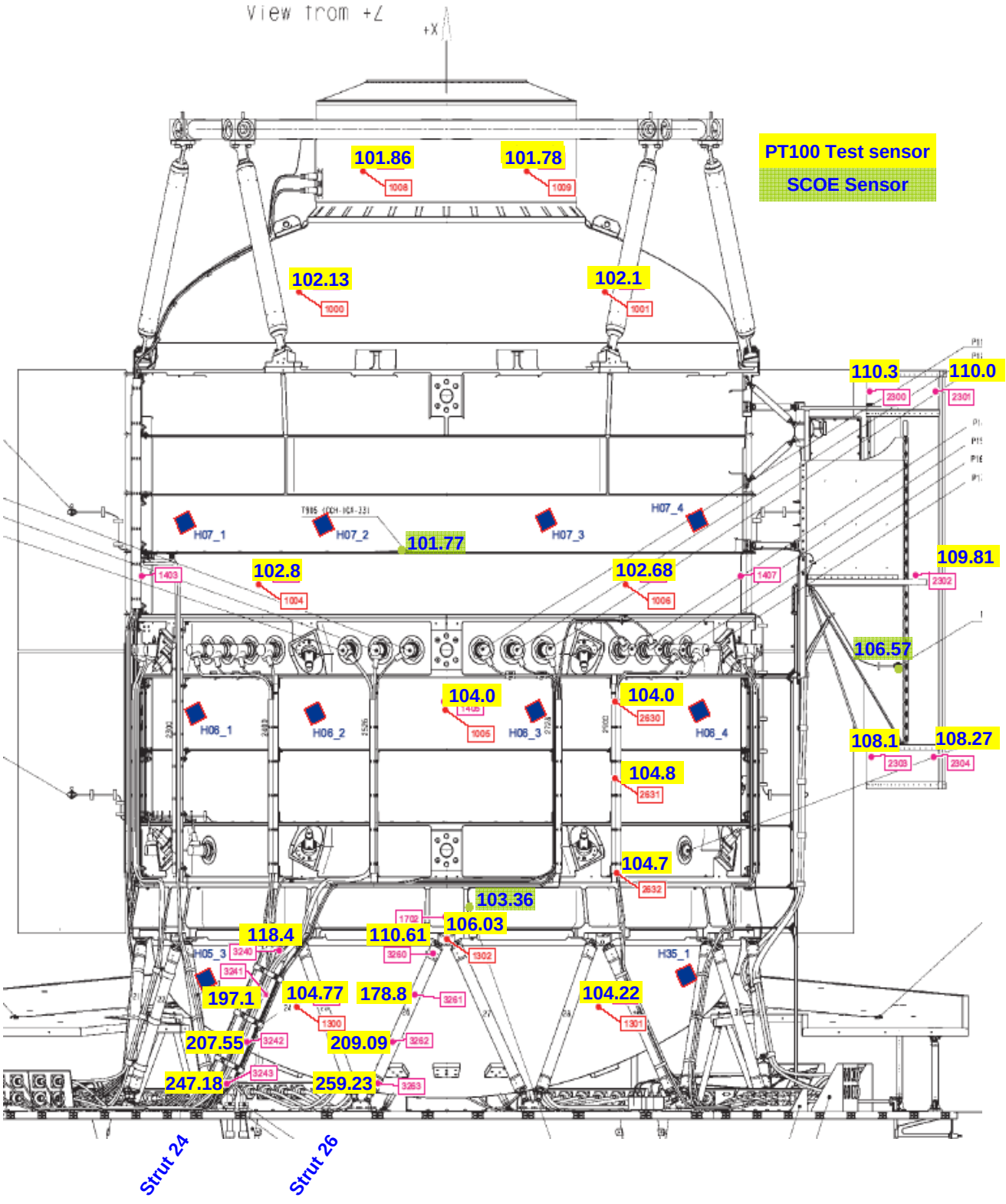

Figure 4.2-4: Temperature Distribution on CVV +Z Side during TB1 Test Phase

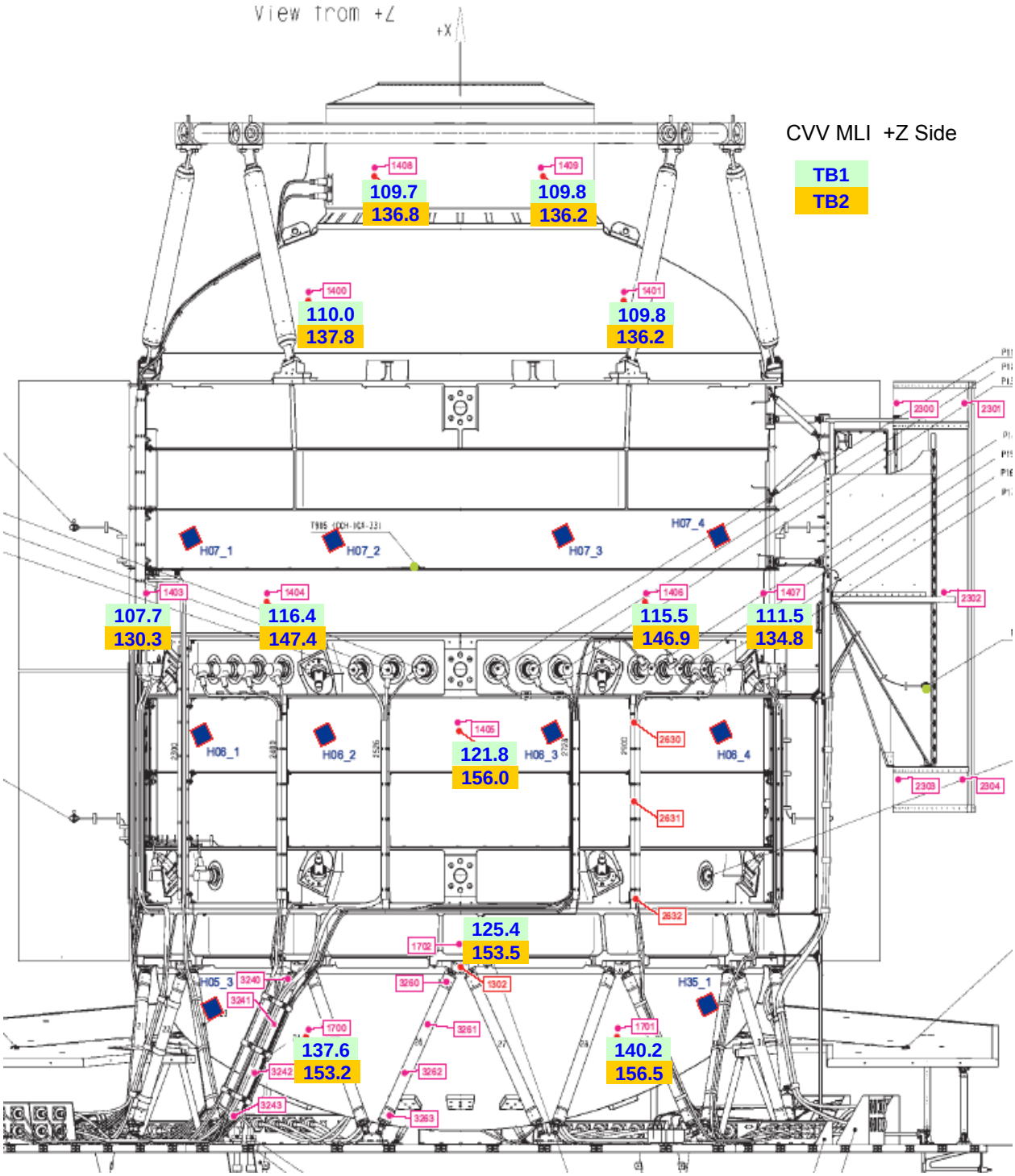

Figure 4.2-5: Temperature Distribution on CVV MLI +Z Side during TB1 and TB2 Test Phase

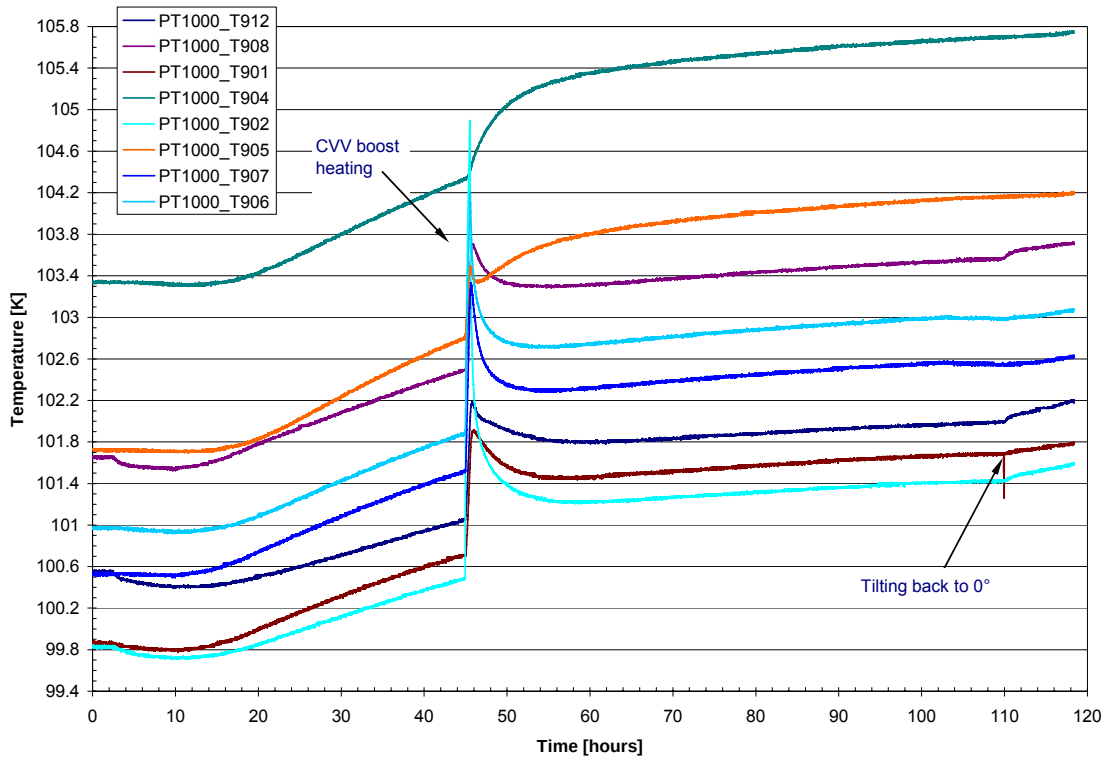

Figure 4.2-6: CVV Temperature Evolution during TB2 Test Phase (TP7)

Conclusions:

- The measured temperature gradient within the CVV main structure is about 5 K
- The gradient between CVV main structure and ±Y radiators is less than 1 K
- The gradient between CVV main structure and -Z radiator is less than 2 K
- Increase IR Rig temperature from 173 K to 293 K and switch on the LOU MTD with 6.2 W increases the CVV temperature by about 2.1 K
- The SCOE sensors (PT1000 with Al-housing) show about 1.2 K lower temperature than the corresponding PT100 test sensors
- Tilting of the S/C by 16° inside the LSS is affecting the CVV temperature due to variation of the view factors to the LSS walls; see **Figure 4.2-6** at 110 hours
- Increase IR Rig temperature from 173 K to 293 K and switch on the LOU MTD with 6.2 W increases the CVV MLI temperature by about 26 K, see **Figure 4.2-5**.

4.3 CVV Struts and Harness

The CVV strut temperatures during TB1 and TB2 are compiled in **Table 4.3-1** and shown as graphs in **Figure 4.3-1** and **Figure 4.3-2**. The temperatures along the harness profiles are listed in **Table 4.3-2**. Note that for TB1 the geographical temperature distribution is also shown in the figures of the previous section.

		Strut 24	Strut 26	Strut 33	Strut 36	Strut 38	Strut 41	Strut 44
Location /section		+Y/+Z	+Z	-Y	-Y/-Z	-Z	+Y/-Z	+Y
attached Harness		PACS	none	SPIRE	CCH	SPIRE	CCH	CCH
brass cross section:		3.81 mm²	0 mm²	0.61 mm²	2.56 mm²	6.19 mm²	0.42 mm²	0 mm²
steel cross section:		24.6 mm²	0 mm²	8.5 mm²	0.4 mm²	26.9 mm²	1.4 mm²	1.8 mm²
TB1	tube fitting CVV	118.4	110.6	109.1	104.9	106.0	105.1	106.0
	tube near CVV	197.1	178.8	155.0	132.3	140.7	131.7	124.4
	tube near TTAP	207.6	209.1	203.1	163.6	179.0	163.7	168.9
	tube fitting TTAP	247.2	259.2	260.1	252.5	248.7	251.8	255.2
TB2	tube fitting CVV	121.2	113.8	111.6	106.6	107.6	106.8	108.7
	tube near CVV	200.3	184.5	160.0	134.5	142.1	133.7	133.0
	tube near TTAP	210.3	213.3	206.1	165.1	179.9	165.3	172.6
	tube fitting TTAP	248.3	260.5	260.9	253.0	249.2	252.3	255.9

Table 4.3-1: CVV Strut Temperatures [K] during TB1 and TB2

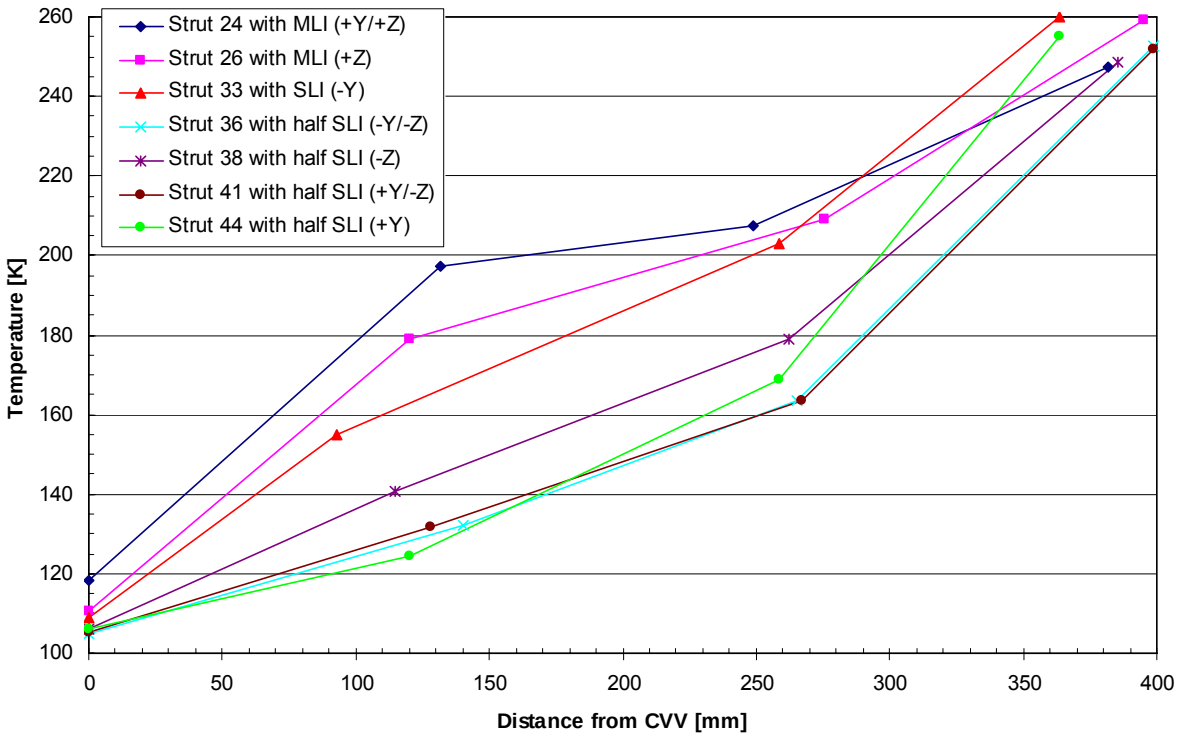

Figure 4.3-1: CVV Strut Temperatures TB1 Test Phase

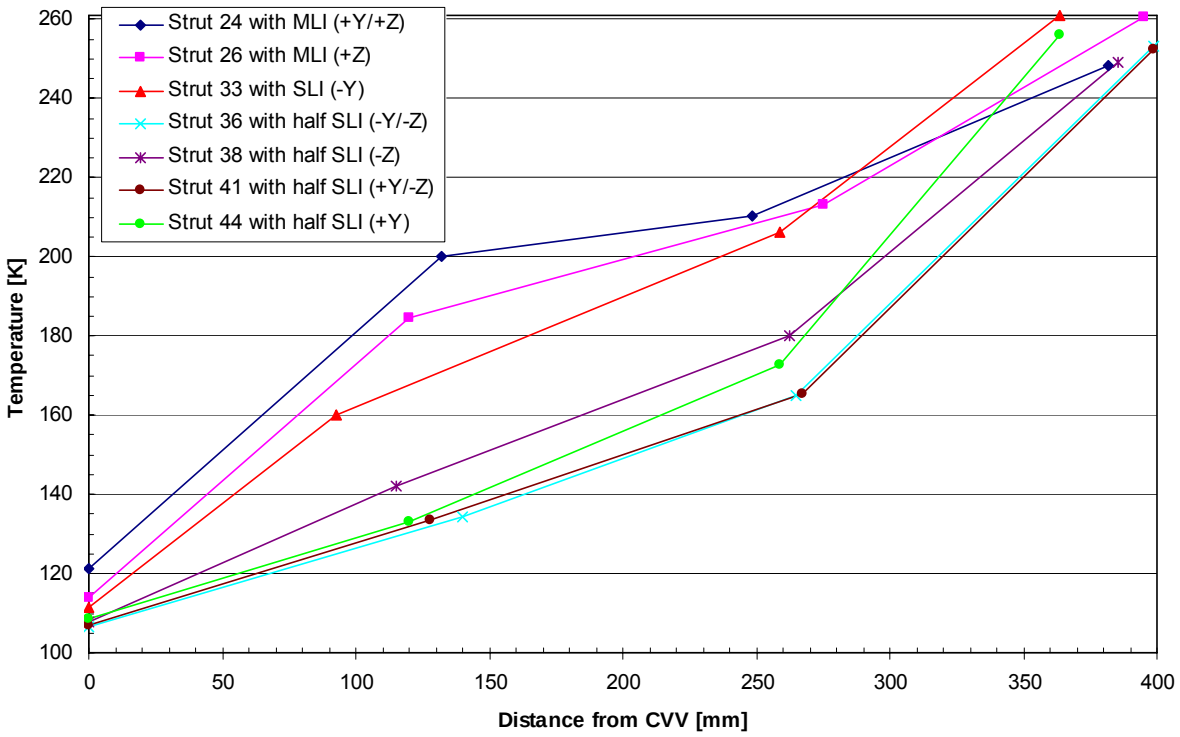

Figure 4.3-2: CVV Strut Temperatures TB2 Test Phase

		HP 3334	HP 2900	HP 3800	HP 4041	HP 2300
Location /section		-Y (from strut 33)	-Y/-Z	-Z	+Y/-Z	+Y/-Z
attached Harness		SPIRE	HIFI	SPIRE	SPIRE	Telescope
brass cross section:		0.61 mm²	1.98 mm²	2.33 mm²	2.98 mm²	**8 mm² Copper**
steel cross section:		8.5 mm²	4.3 mm²	20.4 mm²	7.5 mm²	0 mm²
TB1	CVV top	102.48	104.0	101.85	102.1	104.62
	CVV mid	102.47	104.8	102.05	102.29	106.35
	CVV bottom	102.64	104.7	102.7	no data	106.9
	dT bottom -top	0.16	0.7	0.85	n.a.	2.28
TB2	CVV top	104.57	106.54	103.23	103.7	106.99
	CVV mid	104.60	107.32	103.5	103.7	108.75
	CVV bottom	104.75	107.5	104.1	no data	109.39
	dT bottom -top	0.18	0.96	0.87	n.a.	2.4

Table 4.3-2: CVV Harness Profile Temperatures [K] during TB1 and TB2

Conclusions:

- attached harness bundles clearly affects the CVV strut temperature (e.g. Strut24 and Strut26)
- a high gradient is measured along the harness profile carrying the Telescope harness (8 mm² Cu)

4.4 Performance of LOU Radiator

The temperature distribution on the LOU Support plate and the LOU Radiator is shown in **Figure 4.4-1** and **Figure 4.4-3** for the two TB cases. The maximum gradient within the LOU Radiator is 6.4 K during TB2 when the LOU MTD is heated with 6.2 W.

The transient behaviour during TB2 is shown in **Figure 4.4-4**. During the test phase different MTD heaters were switched on with the same electrical power to investigate the corresponding temperature gradients. The MTD switching is shown in detail in **Figure 4.4-5**.

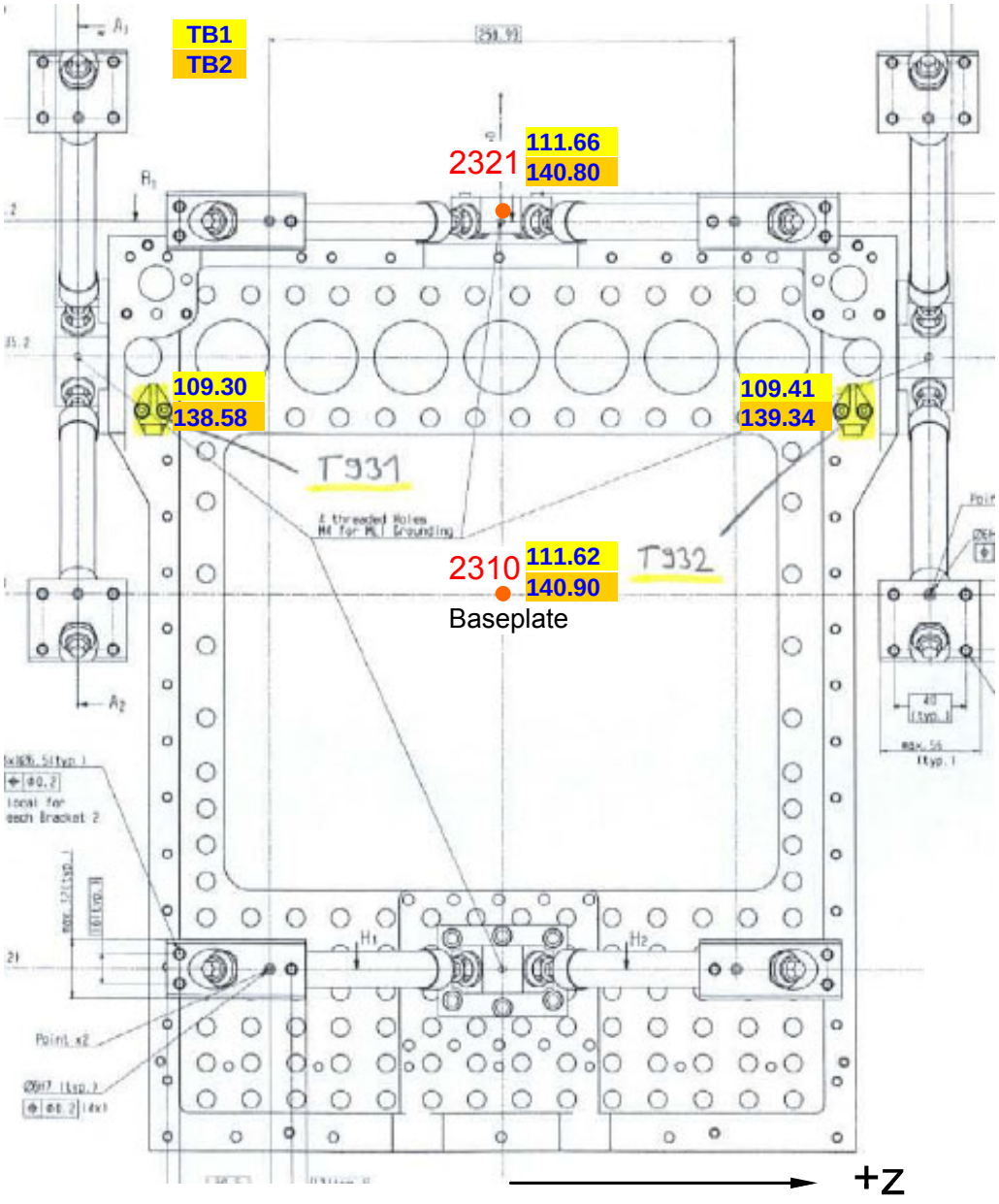

Figure 4.4-1: Temperature Distribution on LOU Support and Baseplate during TB1 and TB2

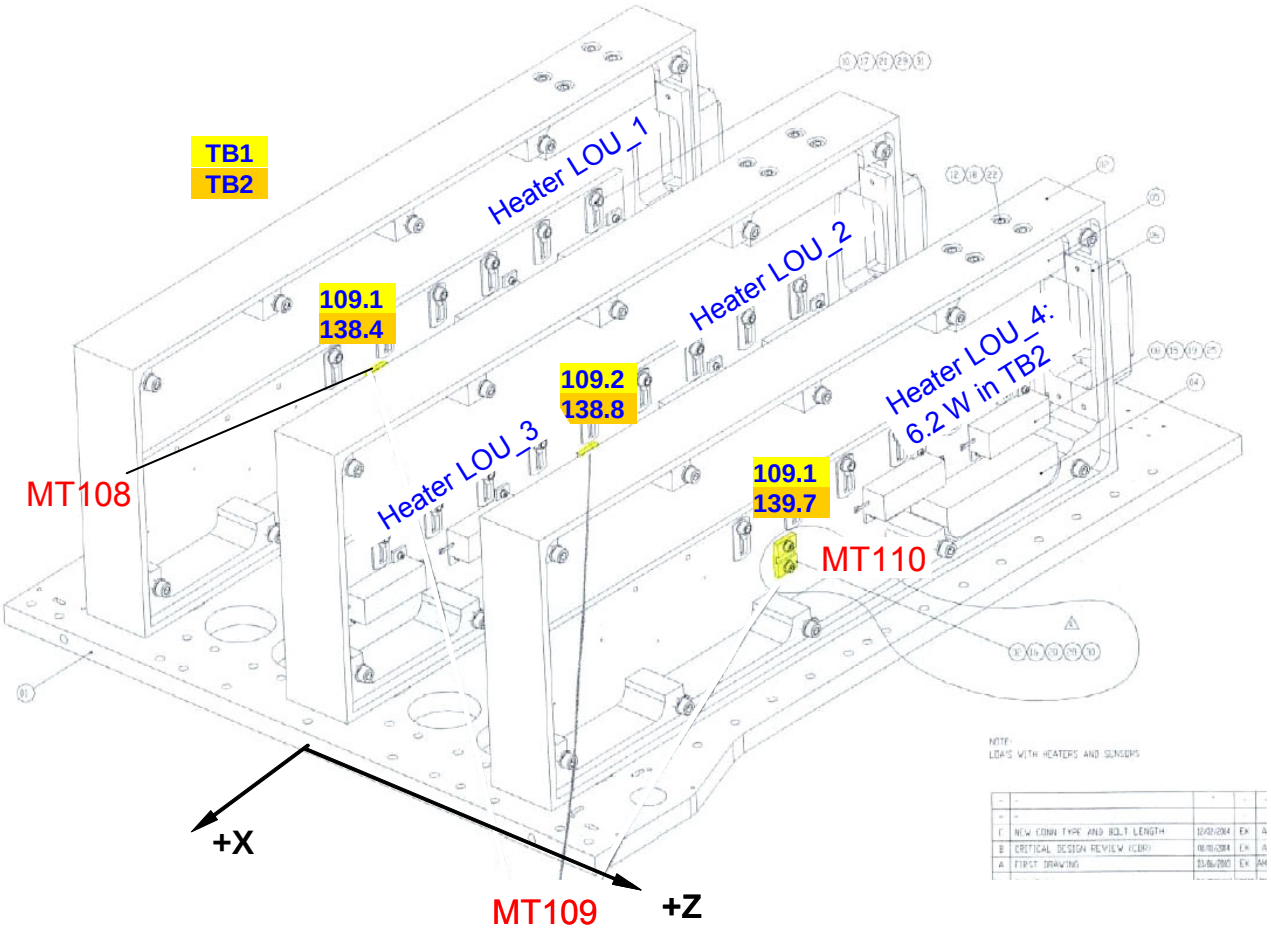

Figure 4.4-2: LOU MTD Heater and Sensor Location and TB1 & TB2 Temperatures

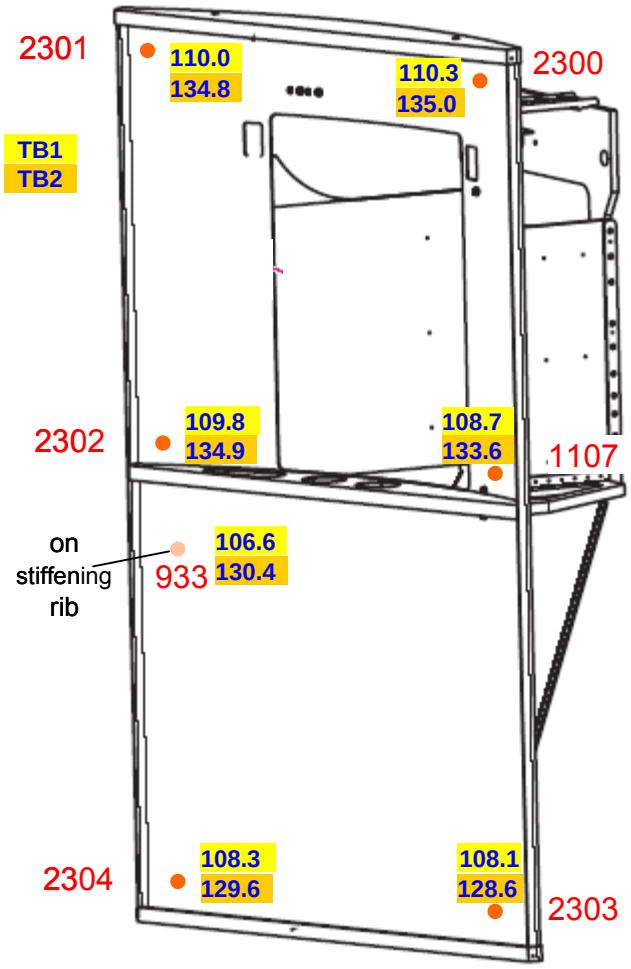

Figure 4.4-3: Temperature Distribution on LOU Radiator during TB1 and TB2

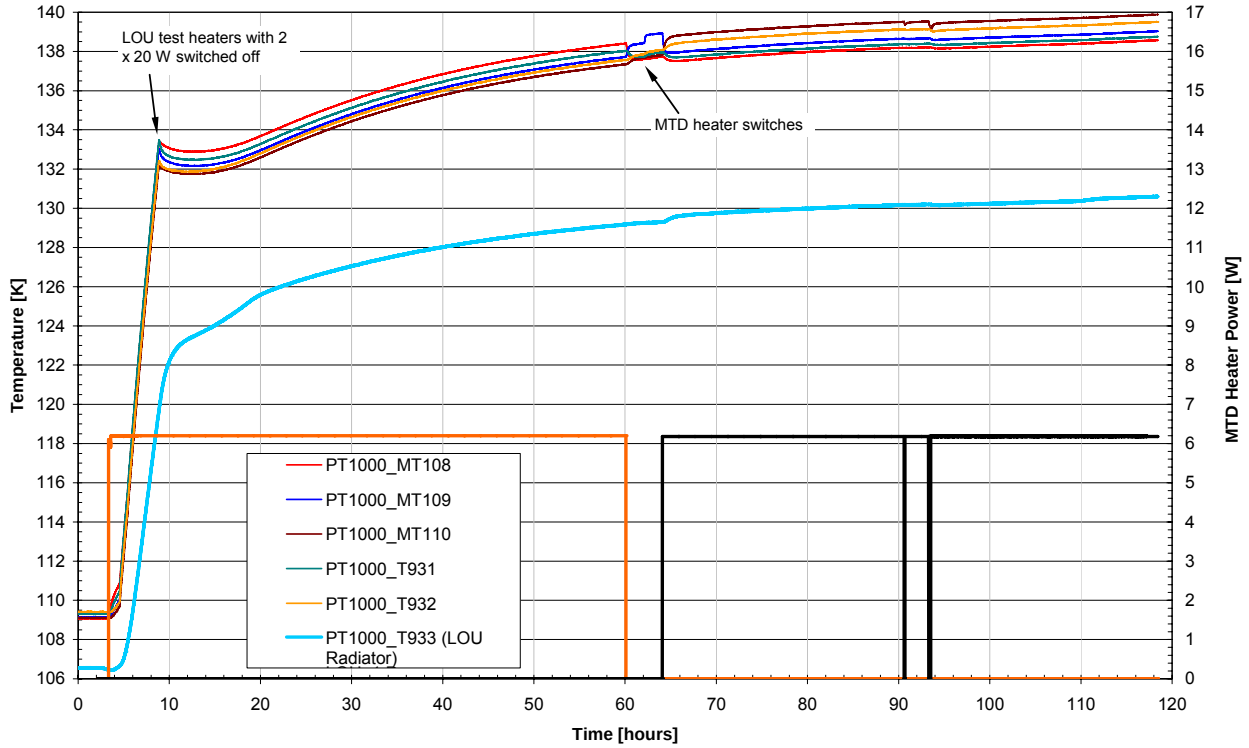

Figure 4.4-4: LOU Temperature Evolution during MTD Heating (TB2)

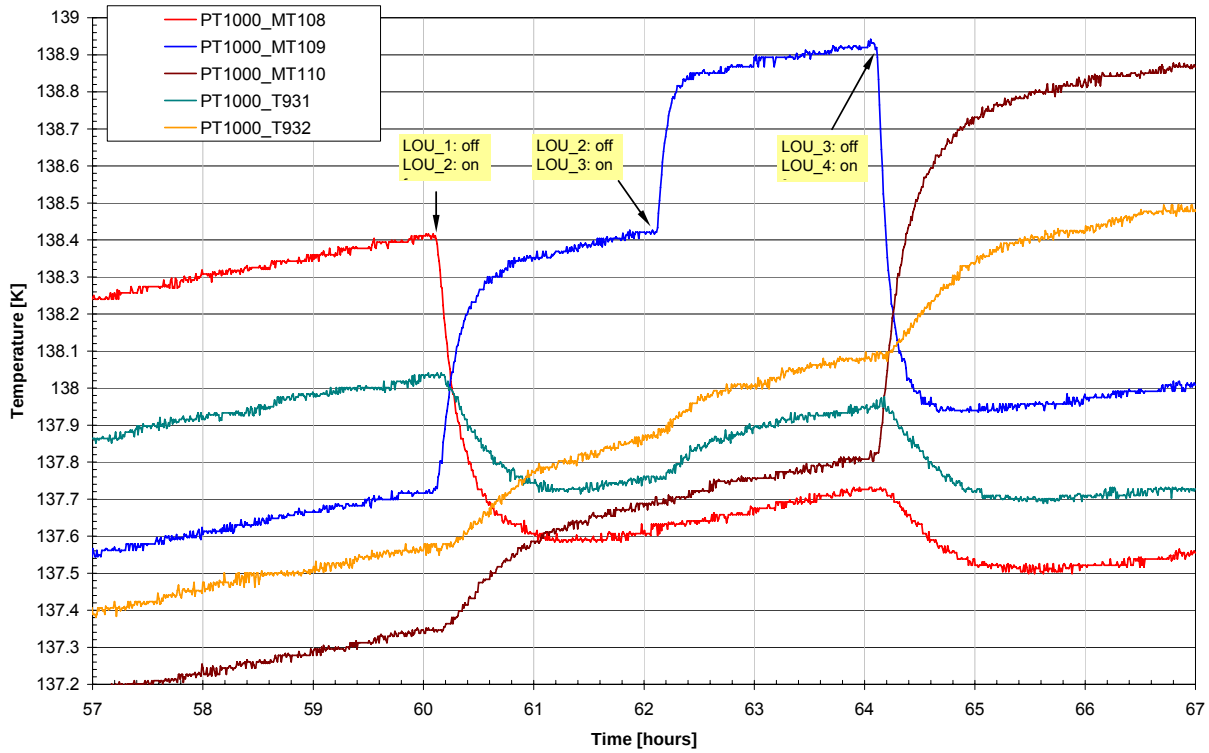

Figure 4.4-5: LOU Temperature Evolution during Switch of MTD Heaters (TB2)

Conclusions:

- The measured temperature gradient within the LOU Radiator is 6.4 K (TB2)
- Heating the LOU MTD with 6.2 W increases the LOU Baseplate temperature by about 30 K
- The gradient between LOU Baseplate and mean Radiator temperature is about 12 K at 6.2 W electrical heating power

4.5 Performance of SVM Thermal Shield

The temperature distribution on the SVM Thermal Shield and its SLI is shown in **Figure 4.5-1** for TB1 and in **Figure 4.5-2** for TB2.

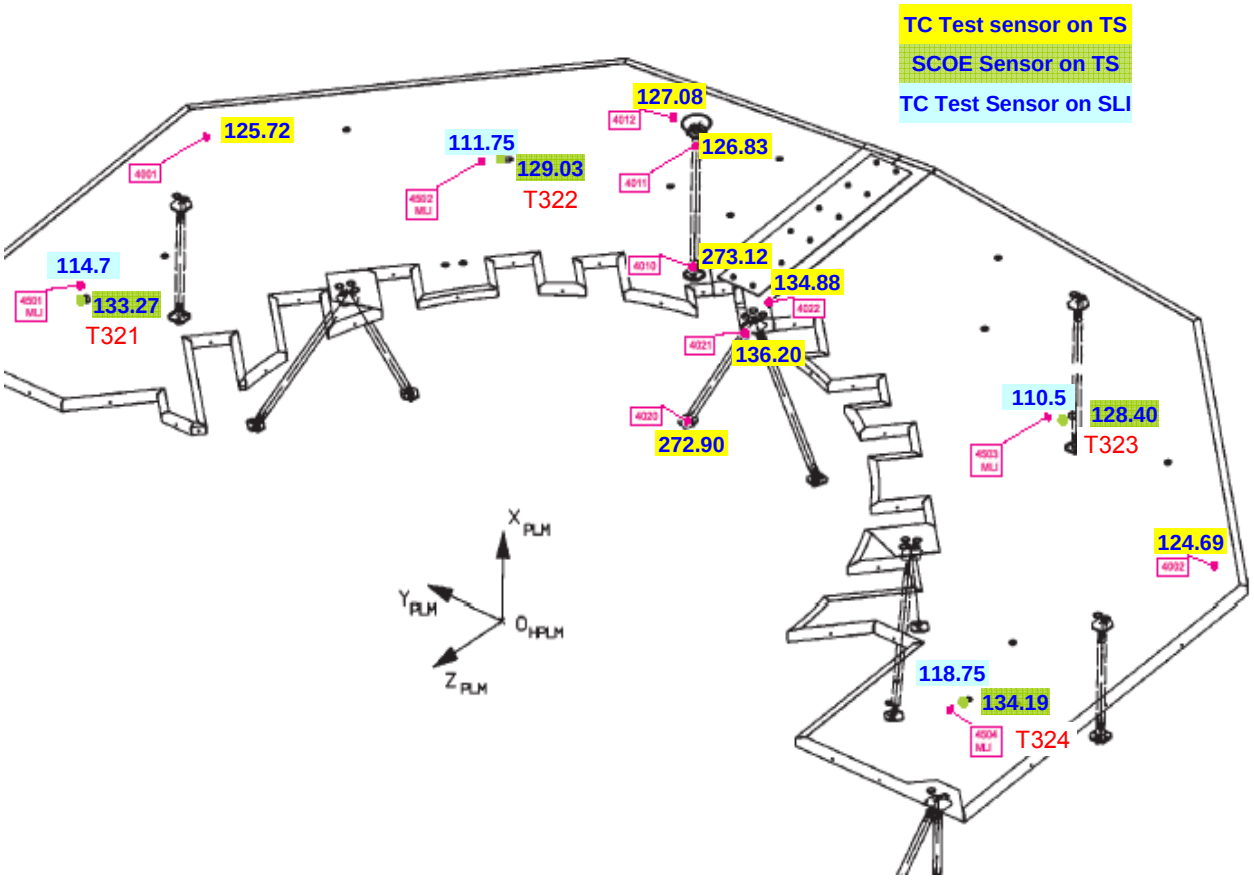

Figure 4.5-1: Temperature Distribution on SVM Thermal Shield with SLI during TB1 Test Phase

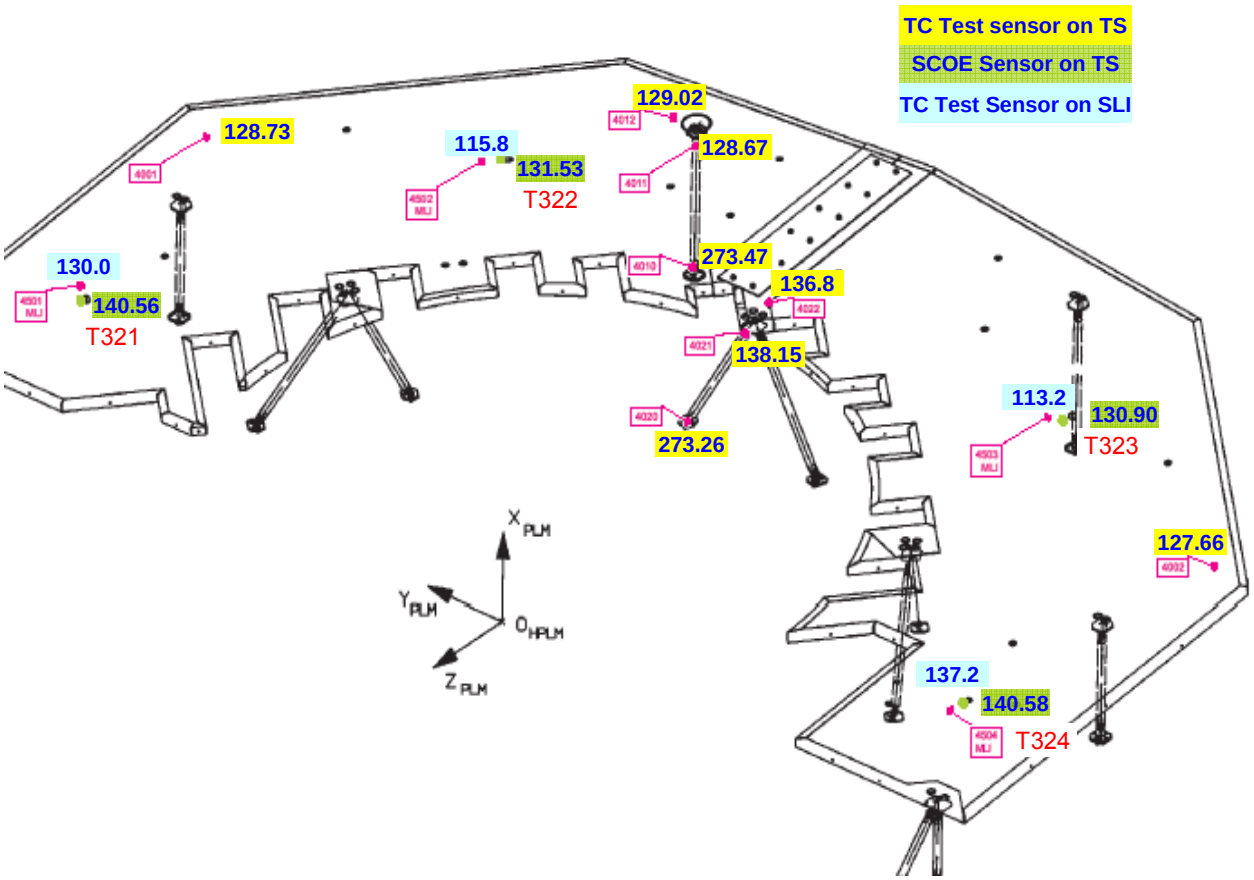

Figure 4.5-2: Temperature Distribution on SVM Thermal Shield with SLI during TB2 Test Phase

Conclusions:

- The measured temperature gradient within the SVM Thermal Shield is up to about 13 K
- The Shield temperature is about 3 K higher in TB2 due to the increased IR Rig temperature from 173 K to 293 K
- The Shield SLI temperature is about 10 K higher in TB2 due to the increased IR Rig temperature

4.6 Impact of Test Harness

The test harness for temperature sensors and test heaters routed to the CVV and to the LOU was thermally anchored at the LSS lower panel using STYCAST brackets. The harness was isolated from the TTAP by means of Delrin washers and wrapped with MLI. In total 16 heater circuits, 73 PT100 sensors and 30 thermocouples were directly routed to the CVV and attached at a CVV harness rail by means of lacing-cord. The heater circuit harness is composed of 9x2 AWG 20 wires and 7x2 AWG 16 wires made of copper. Each PT100 harness consists of 4 AWG 28 copper wires and each thermocouple harness consists of one AWG 28 copper and one AWG 28 constantan wire.

Thus, the harness cross section amounts to 53.8 mm² copper consisting of 27.7 mm² for the heater circuits and 23.7 mm² for the PT100 temperature sensors and 2.4 mm² for the thermocouples. For the thermocouples an additional cross-section of 2.4 mm² Constantan was present, which is considered to be negligible compared to total amount of copper.

In order to determine the heat load to the CVV via the test harness two Thermocouples were implemented in the harness bundle in a distance of 500 mm as shown in **Figure 4.6-1**. The corresponding heat flow to the CVV is listed in following **Table 4.6-1** and has to be considered for the TMM TB test correlation.

Test Phase	T9800	T9810	T9810-T9800	Copper Conductivity	Heat Flow
TB1 (29.10.05)	134.0 K	148.85 K	14.85 K	423 W/mK	676 mW
TB2 (05.11.05)	136.5 K	151.2 K	14.7 K	422 W/mK	668 mW

Table 4.6-1: Heat Input to CVV via Thermally Anchored Test Harness

Part of the above mentioned test harness is further routed from the CVV structure to the LOU MTD and the LOU Radiator:
3 heater circuits with 7.9 mm²,
16 thermocouples with 1.3 mm² and
1 PT100 with 0.3 mm² copper.
This amounts to a total copper cross section of 9.5 mm². The length of the LOU test harness is roughly estimated to 300 mm.

The test harness for CVV MLI, Telescope TD and warm parts of the HACS (electronics and radiator) was not thermally anchored at the LSS lower panel, but isolated from the TTAP by means of Delrin washers and wrapped with MLI. In total 40 thermocouples were routed in one bundle and fixed on CVV MLI stand-offs by means of lacing-cord to avoid direct thermal contact to the CVV structure. The effective copper harness cross section is about 3.4 mm² consisting of 3.24 mm² copper and 3.24 mm² Constantan with a thermal conductivity of about 5% of the copper conductivity.

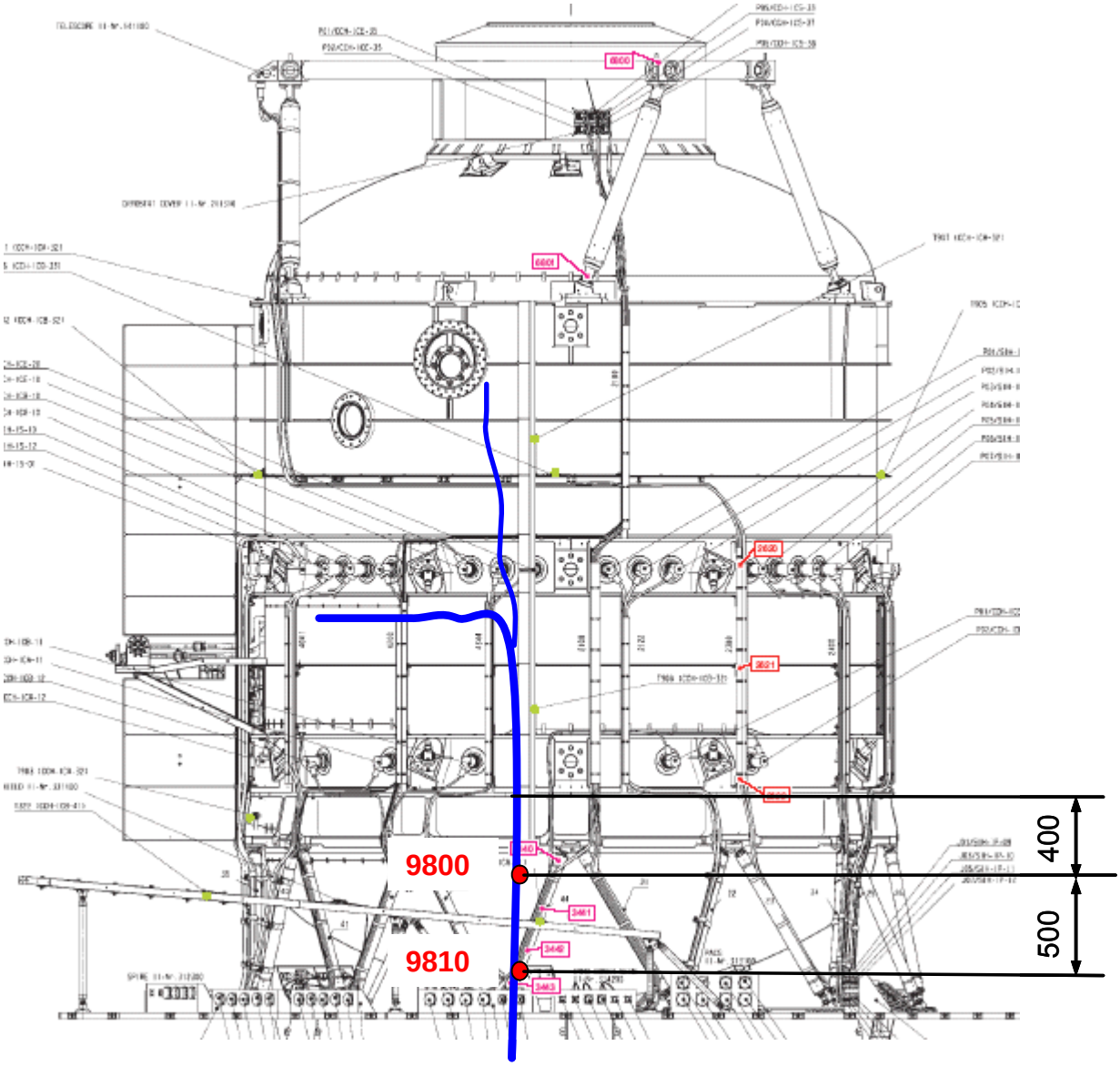

Figure 4.6-1: Thermally Anchored Test Harness for CVV at +Y Side

In order to determine the heat load via this test harness two thermocouples were implemented in the harness bundle in a distance of 300 mm as shown in **Figure 4.6-2**. The corresponding heat flow across the harness is listed in following **Table 4.6-2**.

Test Phase	T9811	T9801	T9811-T9801	Copper Conductivity	Heat Flow
TB1 (29.10.05)	248 K	160.05 K	88 K	407 W/mK	406 mW
TB2 (05.11.05)	250 K	169.5 K	80.5 K	407 W/mK	371 mW

Table 4.6-2: Heat Input to CVV MLI via Test Harness

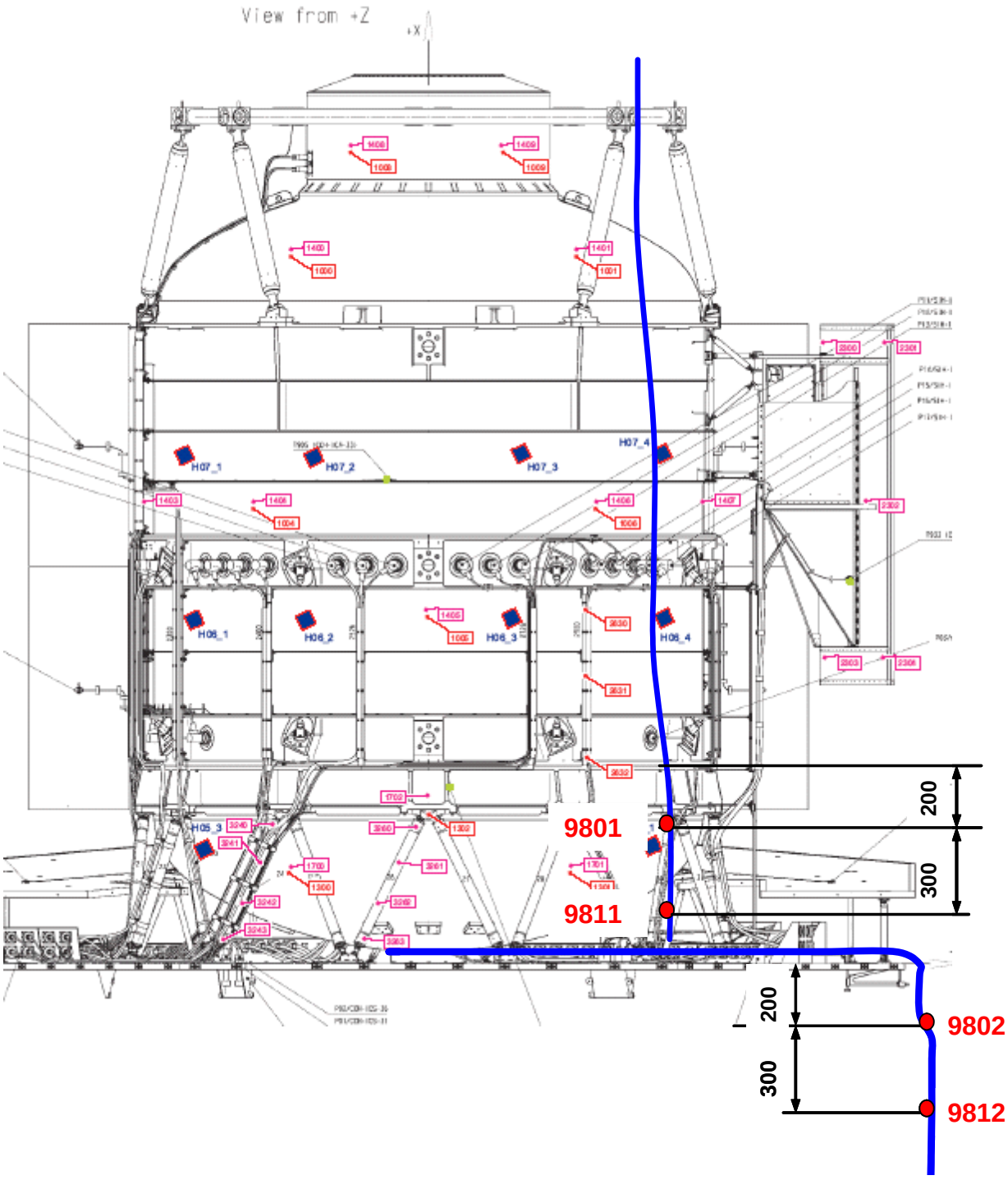

Figure 4.6-2: Test Harness for TTAP and Telescope TD at –Y Side

Conclusions:

- A conductive heat load via test harness to the CVV of 0.7 W shall be considered for TMM correlation for both TB cases
- During CVV warm-up (TP8) the test harness became too hot and the heater power needed to be limited such that the maximum allowable temperature was not exceeding 125°C. For the future part of the test harness bundle (e.g. side facing the LSS) should be not covered with MLI.

4.7 Telescope Dummy

The temperature evolution of the Telescope Dummy during the whole TB/TV test in presented in **Figure 4.7-1** showing that no steady state conditions are achieved at the end of TB1 (TP5). However at the end of TB2 (TP7) with increased IR Rig temperature is seems that for this Telescope environment quasi steady state is achieved. The reason for the very long time constant of the Telescope Dummy is that it is covered completely with MLI (-X) or SLI (+X) with low emissive surface. Furthermore the Telescope is thermally isolated from the CVV which is only 10-20 K colder.

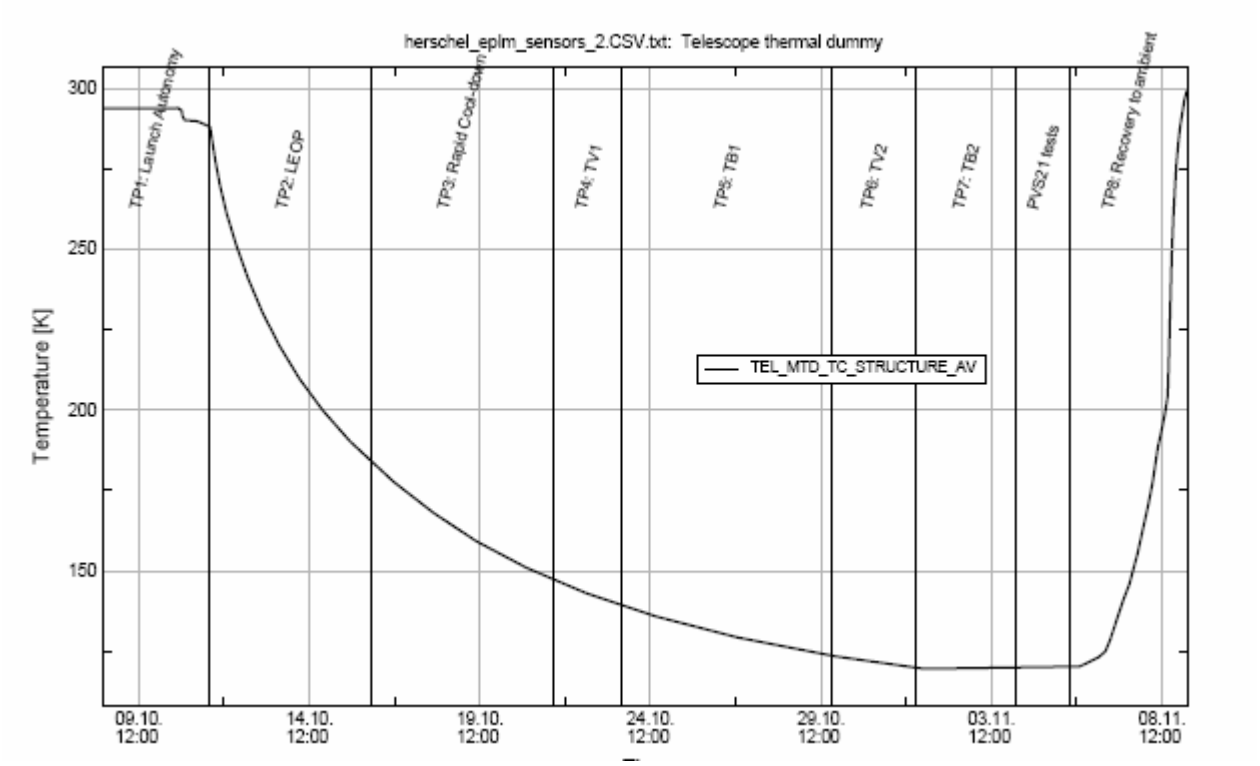

Figure 4.7-1: Telescope Thermal Dummy Average Temperature during all Test Phases

The temperature distribution within the Telescope Dummy and its MLI is shown in **Figure 4.7-2** for TB1 and in **Figure 4.7-3** for TB2.

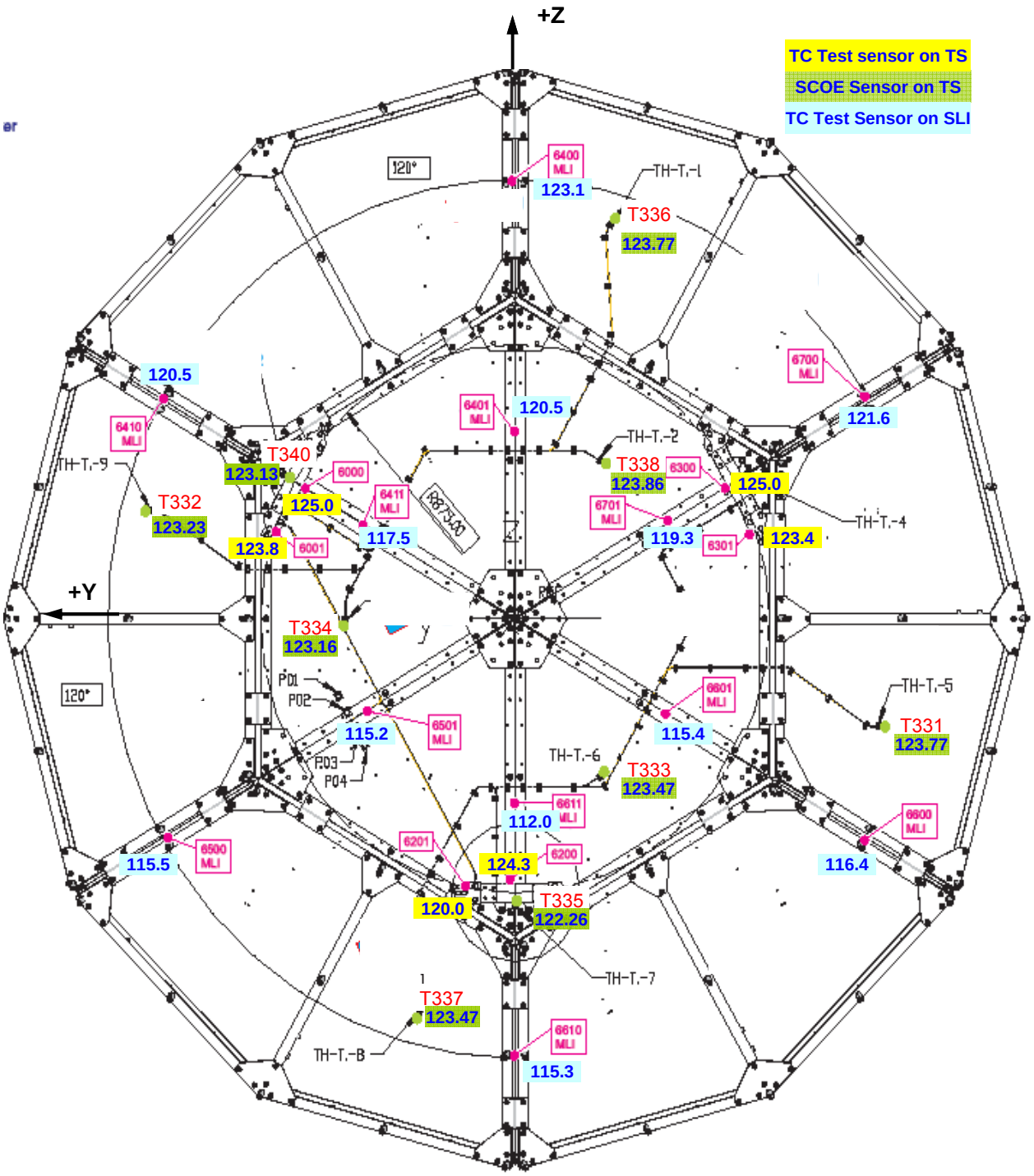

Figure 4.7-2: Temperature Distribution on Telescope Dummy with MLI during TB1

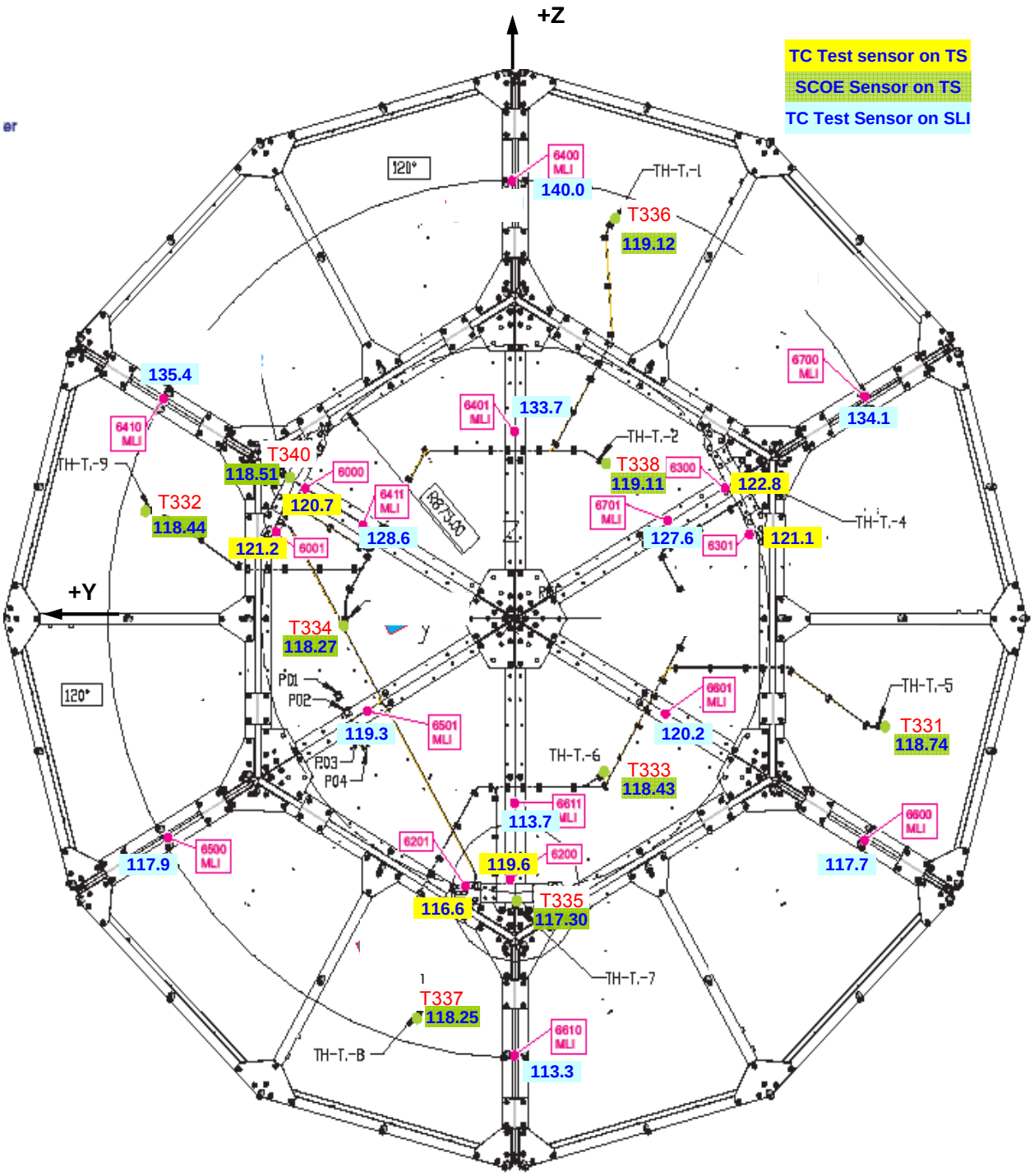

Figure 4.7-3: Temperature Distribution on Telescope Dummy with MLI during TB2

Conclusions:

- Steady state has been achieved in TB2 only (~119 K).
- The measured temperature gradient within the Telescope Dummy structure is about 5 K.
- SCOE sensors show about 2 K lower temperatures than PT100 test sensors

5 GSE and HACS

5.1 Temperature Behaviour of Thermal Test Adapter TTAP

The temperature distribution within the TTAP (yellow background) and the TTAP SLI (blue background) is given in **Figure 5.1-1**. The measured gradient within the TTAP is less than 2 K and within the SLI the maximum measured gradient is about 17 K. To keep the TTAP at 273 K it was necessary to switch on the redundant heater circuits in addition. The applied electrical power is shown in **Figure 5.1-1**, too.

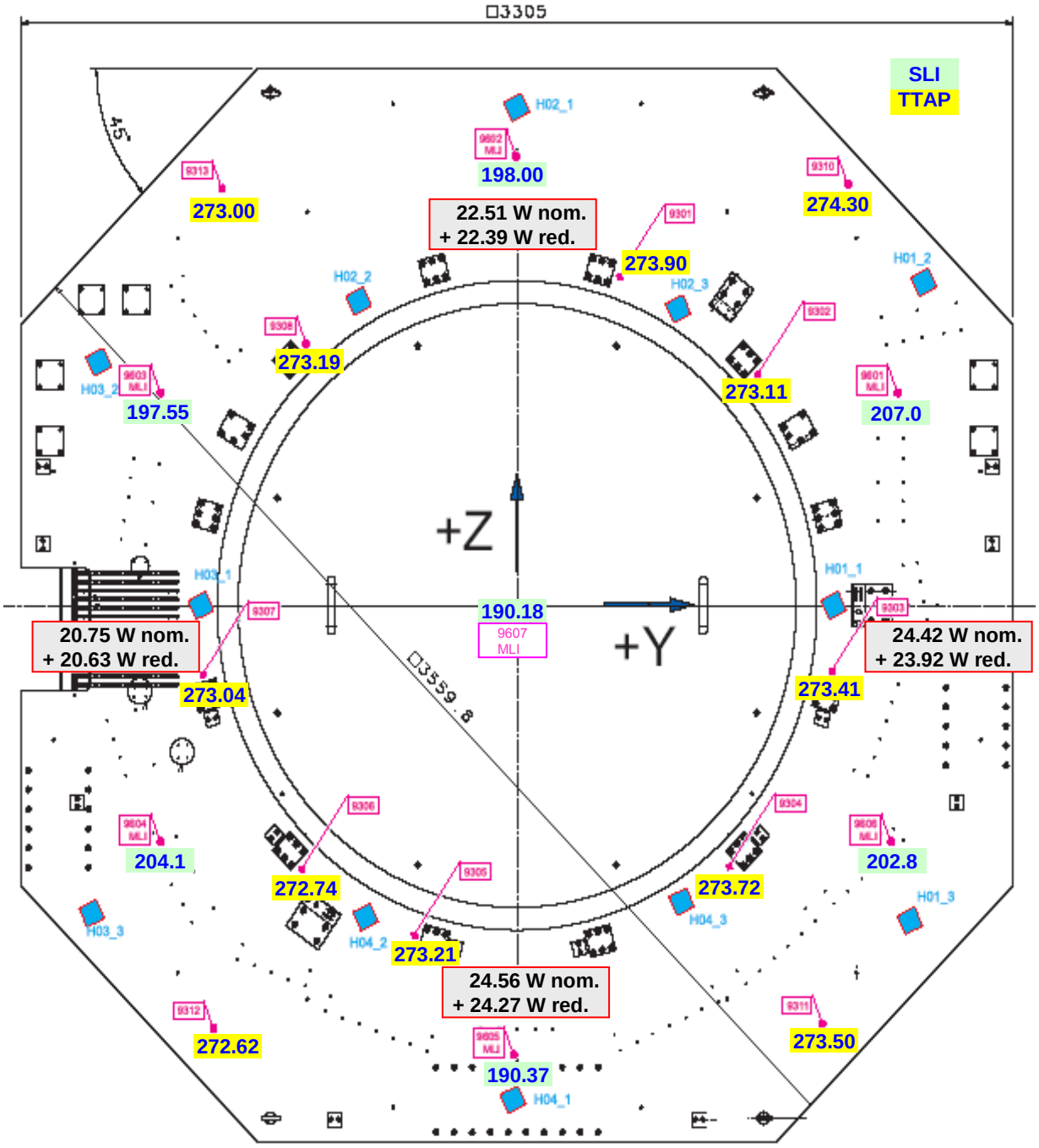

Figure 5.1-1: Temperature and Power Distribution on TTAP and TTAP SLI during TB1

TTAP Section	**+Y** (H01)	**+Z** (H02)	**-Y** (H03)	**-Z** (H04)	**Total**
Heater Power TB1	48.34 W	44.90 W	41.20 W	48.83 W	**183 W**
Harness Power TB1	5.63 W	4.91 W	4.27 W	6.59 W	21.4 W
Heater Power TB2	46.43 W	43.07 W	39.90 W	47.86 W	**177 W**
Harness Power TB2	5.44 W	4.74 W	4.15 W	6.36 W	20.7 W

Table 5.1-1: Power Distribution to keep TTAP at 273 K during TB1 and TB2

Conclusions:

- About 180 W heating power is needed at the TTAP to keep it at 273 K
- The temperature gradient within the TTAP is less than 2 K
- About 21 W are dissipated in the heater harness

5.2 Performance of IR Rig

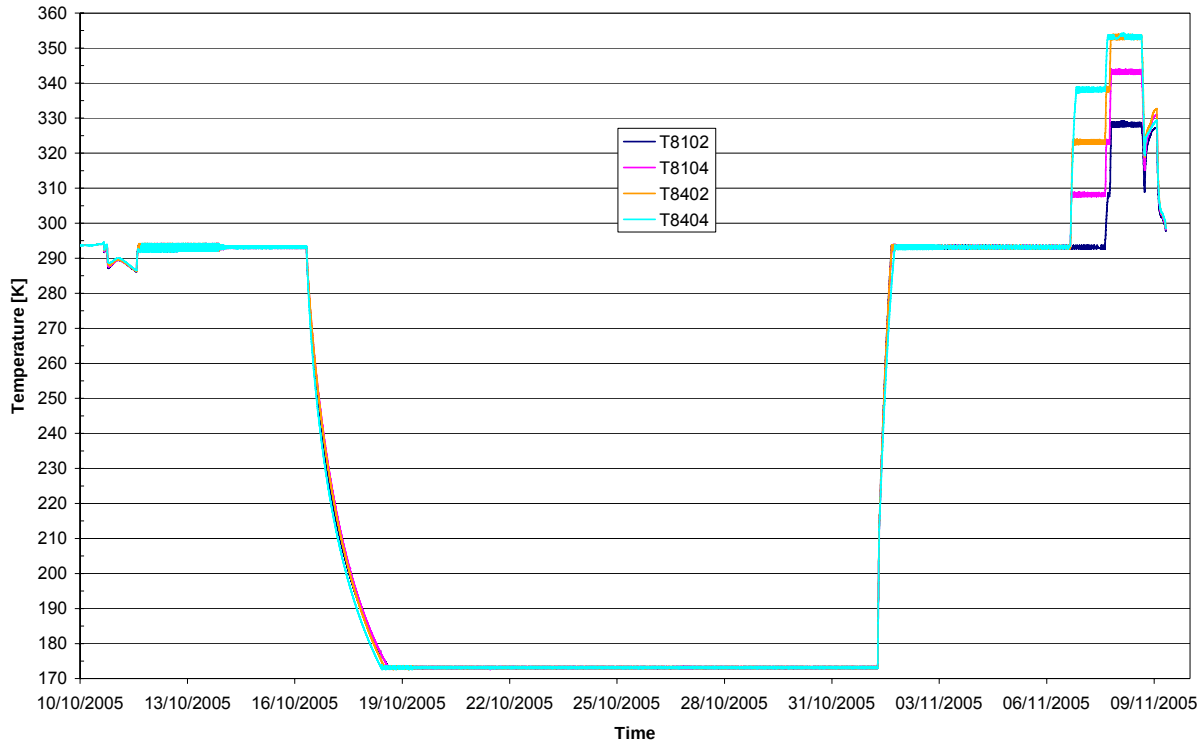

Figure 5.2-1: IR Rig Temperature Evolution during all Test Phases

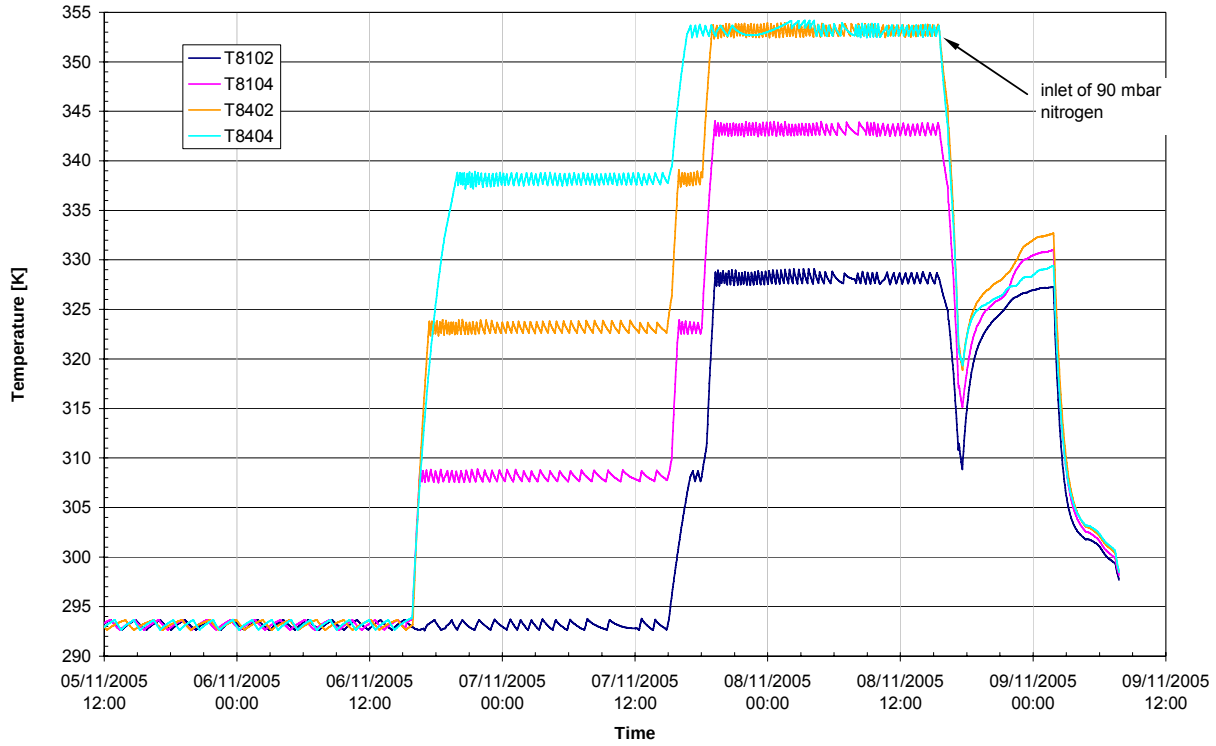

Figure 5.2-2: IR Rig Temperature Evolution during Warm-Up (TP8)

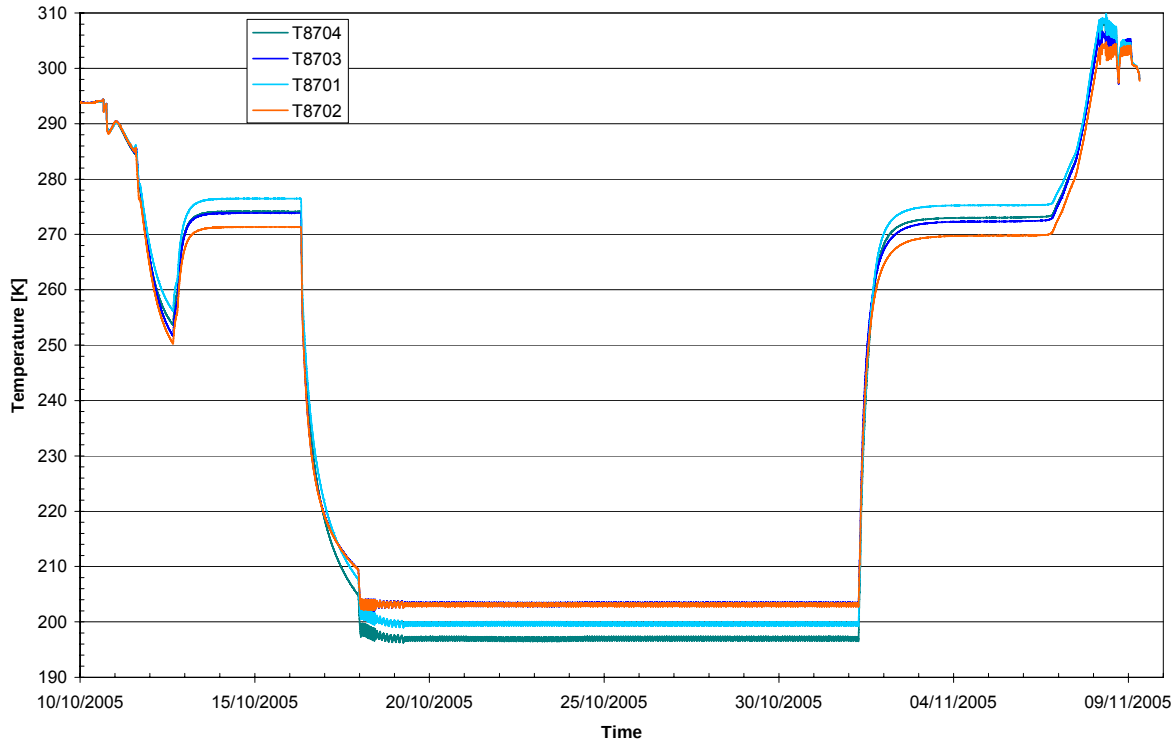

Figure 5.2-3: Temperature Evolution of IR Rig Support during all Test Phases

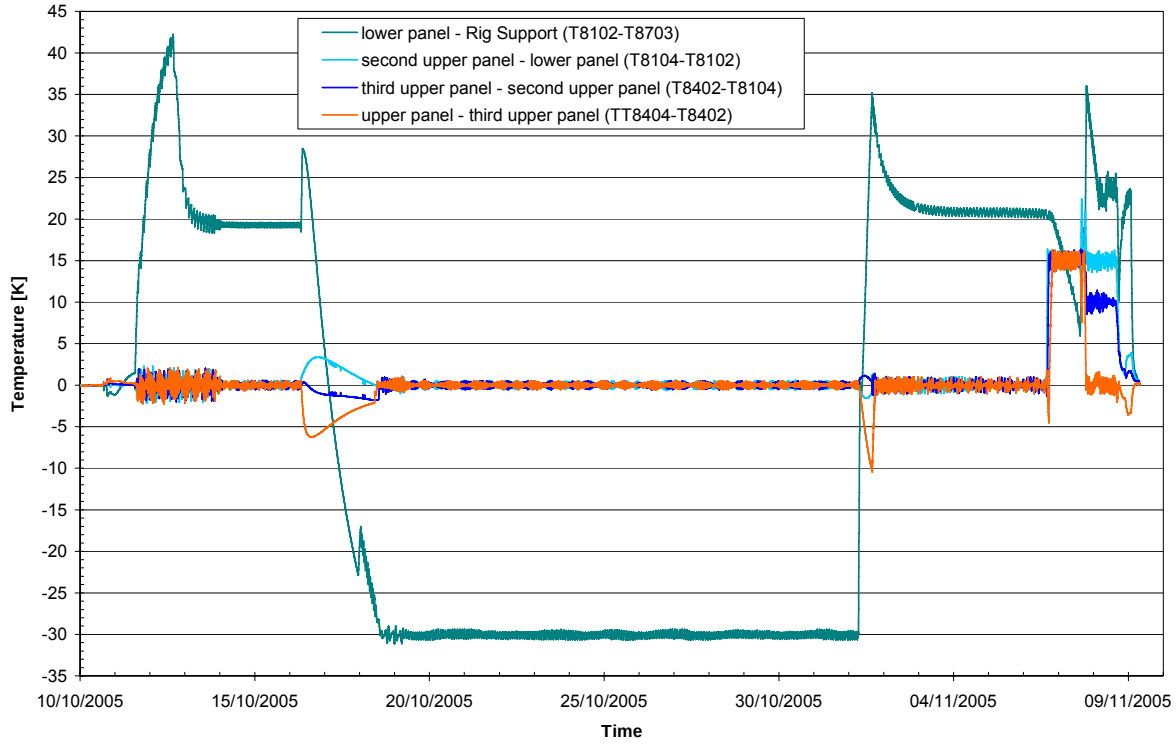

Figure 5.2-4: Temperature Gradients between IR Rig Panels and Support during all Test Phases

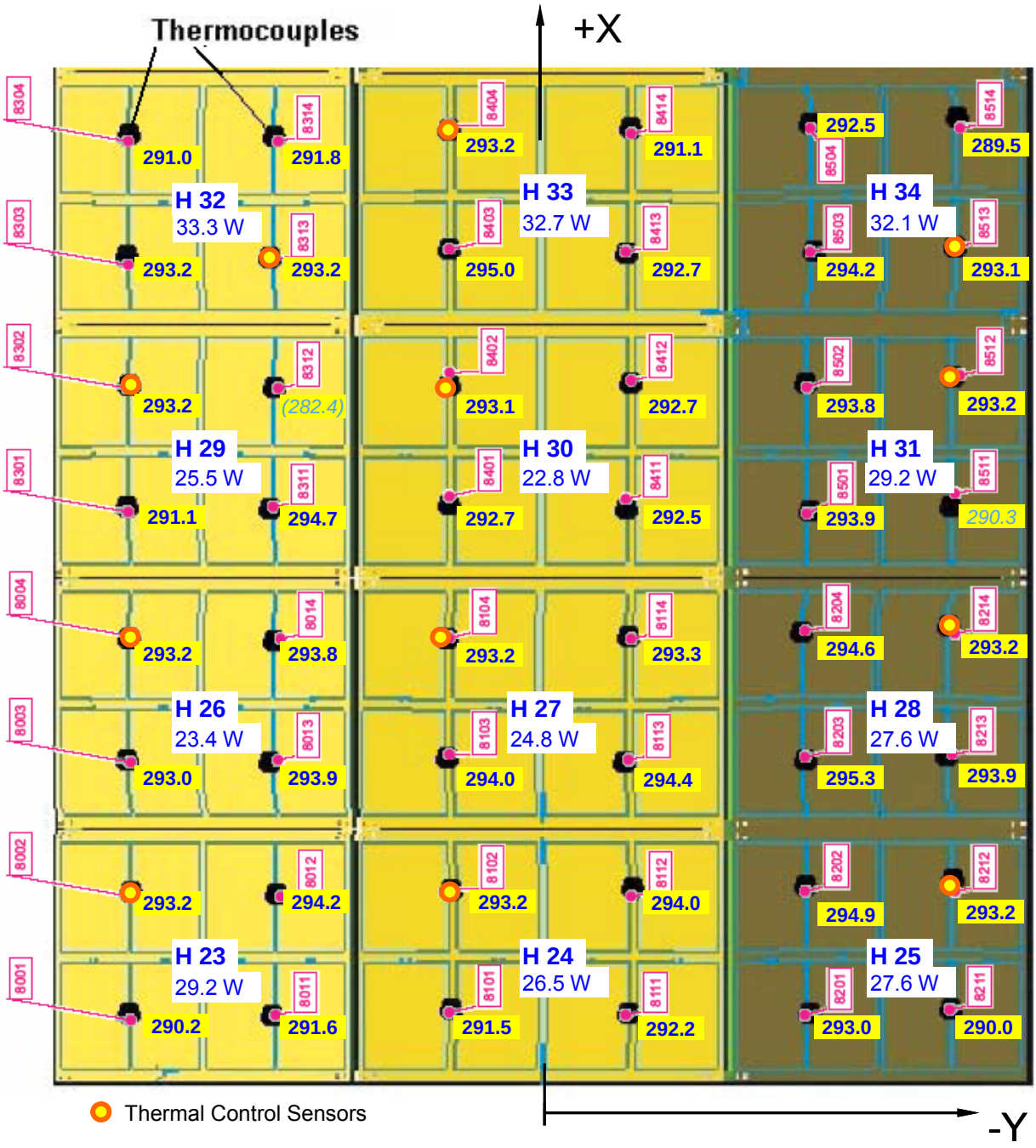

Figure 5.2-5: Temperature Distribution and Power Consumption on IR Rig during TB2

Test Phase	Rig Support	-X panel row H23,H24,H25	panel row H26;H27;H28	panel row H29;H30;H31	+X panel row H32;H33;H34	Remark
TP5 (TB1)	200 K *18.6 W*	173 K *1.5 W / panel*	173 K *2.2 W/panel*	173 K *2.4 W/panel*	173 K *3.1 W/panel*	
TP7 (TB2)	273 K *89.4 W*	293 K *27.8 W/panel*	293 K *25.3 W/panel*	293 K *25.8 W/panel*	293 K *32.7 W/panel*	
TP8 (07.11.05 00:00-15:00)	280 K *89.4 W*	293 K *19.2 W/panel*	308 K *26.2 W/panel*	323 K *33.3 W/panel*	338 K *58.7 W/panel*	ORS 66
TP8 (07.11.05 16:50-18:02)	290 K *89.4 W*	308 K *27.7 W/panel*	323 K *31.6 W/panel*	338 K *39.8 W/panel*	353 K *69.0 W/panel*	ORS 79
TP8, boost warm-up (08.11.05 00:00-15:30)	306 K *60.3 W*	328 K *19.7 W/panel*	343 K *29.7 W/panel*	353 K *39.2 W/panel*	353 K *45.9 W/panel*	ORS 81
TP8, 90 mbar N_2 (08.11.05 17:40-24:00)	304 K *38.3 W*	327K *89.3 W/panel*	331 K *89.2 W/panel*	332 K *89.0 W/panel*	329 K *89.0 W/panel*	ORS 89

Table 5.2-1: IR Rig Temperatures and Average Electrical Heater Power per Panel (Heater Circuit)

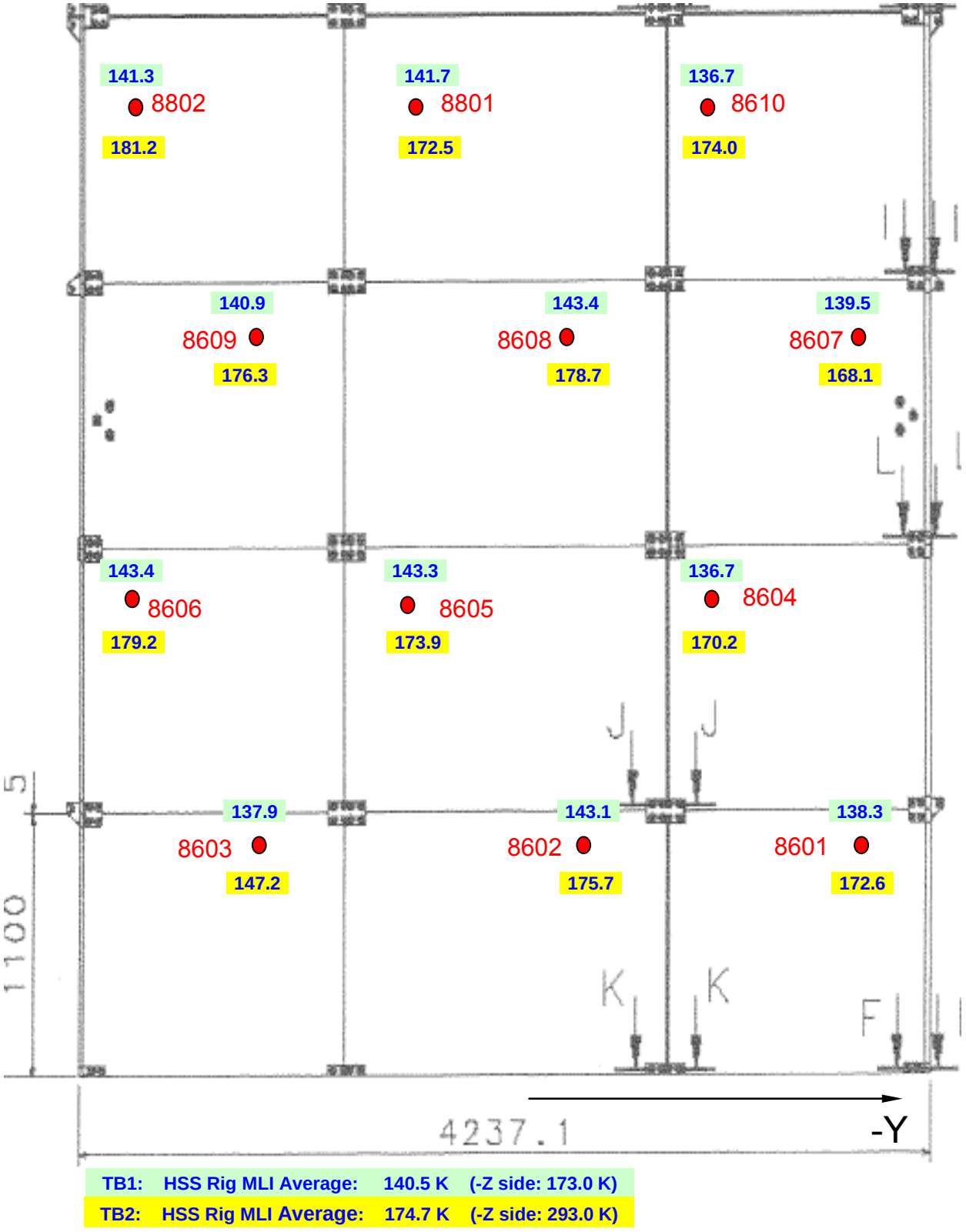

Figure 5.2-6: Temperature Distribution on IR Rig MLI during TB1 and TB2 Test Phase

Conclusions:

- Temperature control of individual IR Rig panels is verified by test
- Gradients between panels up to 20 K are verified by test

- Gradients between Rig Support and lower panels up to ±30 K are verified by test
- Temperature control to 80°C (353 K) can be achieved with 60 W per panel (~67% of max. power)
- In 90 mbar nitrogen atmosphere about 330 K can be achieved with max. power (~90 W per panel)

5.3 Thermal Behaviour of HACS

During the whole TB/TV test the Electronics Modules of the two HACS units were temperature controlled at 241 K by electrical heating. The average electrical power dissipation during TB1 and TB2 is calculated using the HACS recording files and the formulas provided by Peter Hoffmeyer, TERMA (see ANNEX-2). The results are compiled in **Table 5.3-1**. The measured temperature distribution for the +Z and –Z HACS unit is given in **Figure 5.3-1** showing that the temperature of the electronics modules is constant at 241 K and the temperature of the optics modules is 122-114 K.

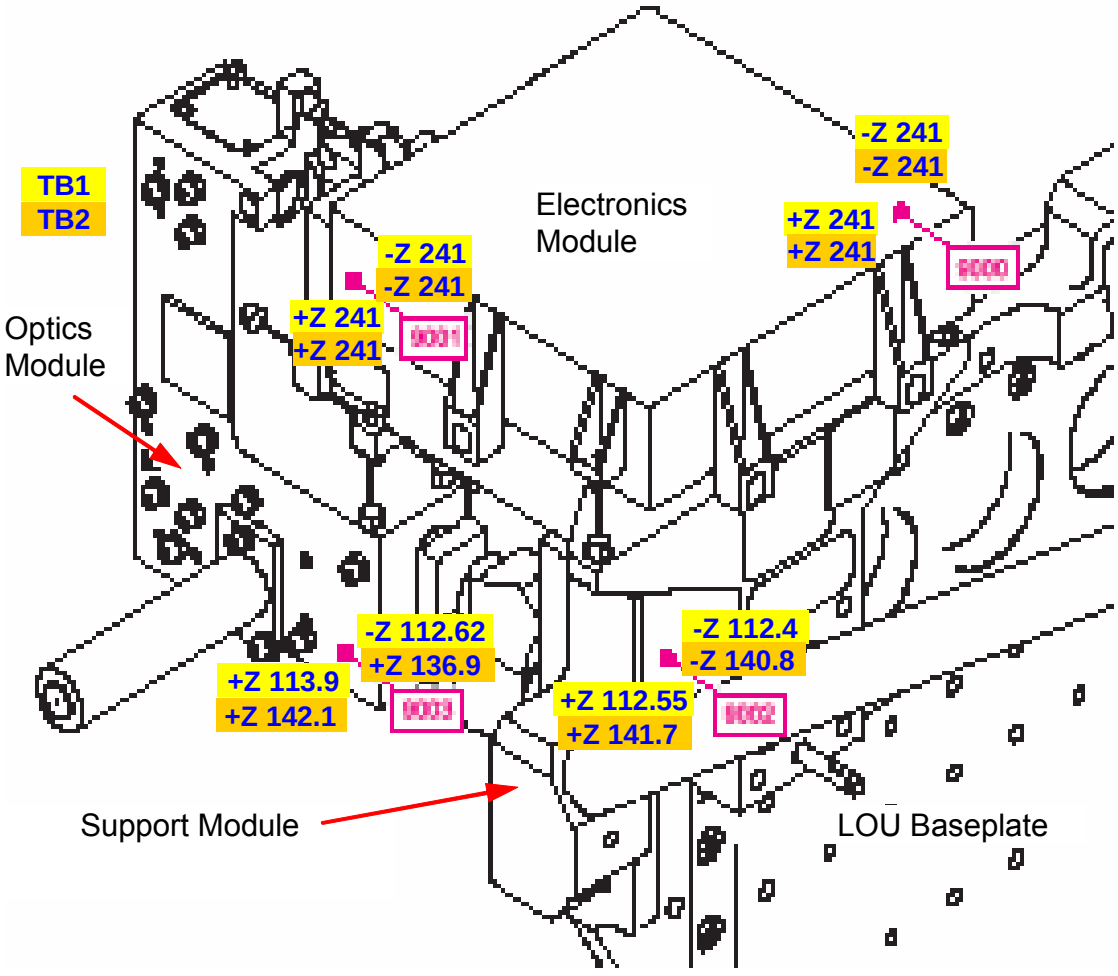

Figure 5.3-1: Temperature Distribution on HACS Units during TB1 and TB2 Test Phase

	TB1	TB2
IR Rig	173 K	293 K
LOU Baseplate	110 K	140 K
+Z Electronic power dissipation	1.411 W	1.407 W
+Z Heater duty cycle	50.0 %	42.2 %
+Z Heating power dissipation	1.28 W	1.08 W
Total +Z dissipation	**2.69 W**	**2.49 W**
-Z Electronic power dissipation	1.402 W	1.401 W
-Z Heater duty cycle	51.3 %	46.9 %
-Z Heating power dissipation	1.31 W	1.20 W
Total -Z dissipation	**2.71 W**	**2.60 W**

Table 5.3-1: HACS Average Power Dissipation in Electronics Modules during TB1 and TB2

To minimize the heat load transferred to the LOU Support Plate each Electronics Module is isolated from its Support Module by 6 Titanium struts of 0.9 mm diameter and 16 mm length [RD 27]. The thermal conductivity of Ti at 200 K with 5.8 W/mK leads to a conductance of 0.0014 W/K. Each HACS Support Module was attached to the LOU Support Plate by means of 4 M5 bolts and except the Radiator the whole HACS was wrapped with MLI. Therefore it can be assumed, that the heat transferred from the Electronics Module to the Support Module is further transferred to the LOU Support Structure. The calculated heat flows are compiled in **Table 5.3-2**.

		Electronic module	Support Module	Temperature gradient	Conductive heat flow	Radiative heat flow *	Total heat flow
TB1	**+Z**	241 K	112.6 K	128.4 K	0.18 W	0.08 W	**0.26 W**
	- Z	241 K	112.4 K	128.6 K	0.18 W	0.08 W	**0.26 W**
TB2	**+Z**	241 K	141.7 K	99.3 K	0.14 W	0.07 W	**0.21 W**
	- Z	241 K	140.8 K	100.2 K	0.14 W	0.07 W	**0.21 W**

*) assuming 0.0144 m² area and an emissivity of 0.3 (goldized Kapton) [RD 27]

Table 5.3-2: HACS heat flow from Electronics Module to Support Module during TB1 and TB2

Conclusions:

- Temperature control of the two HACS units performed very well
- Temperature difference of optics modules between +Z and –Z is about 2 K only
- Duty cycle of HACS heater between 42% and 51% demonstrates a proper thermal design
- Heat flow transferred to LOU Support Plate is less than 0.3 W per HACS unit. Thus the requirement of ≤ 0.5 W [RD 26] is met.

6 LSS Thermal Environment

6.1 TMM Used for Test Predictions

The LSS TMM/GMM used for TB test predictions is shown in Figure 6.1-1.

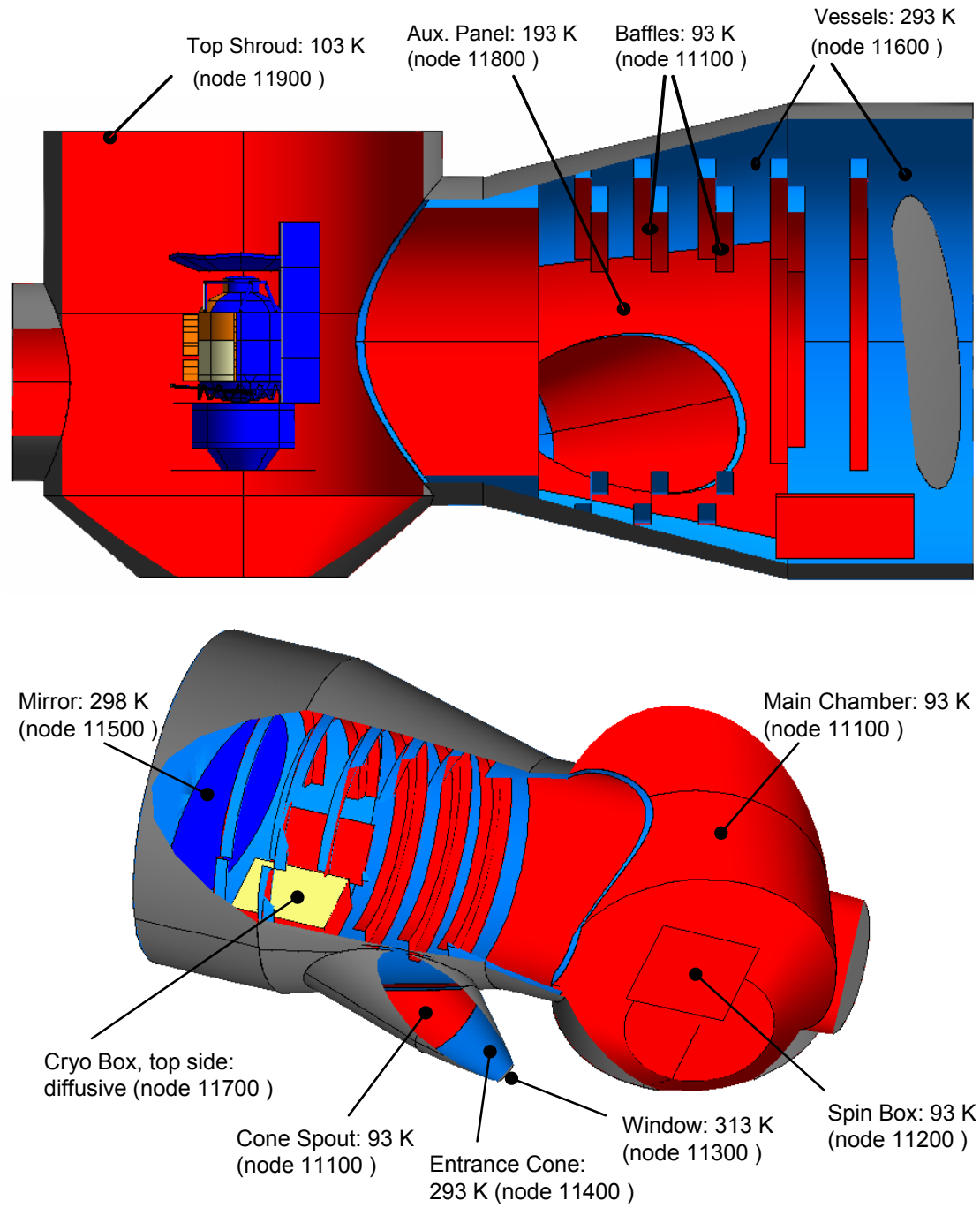

Figure 6.1-1: GMM and Temperature Distribution of LSS used for Prediction [RD 03]

6.2 LSS Temperature Distribution during H-EPLM STM TB Test

The LSS average temperatures based on measured temperatures during TB1 and TB2 are compiled in **Table 6.2-1**. For the LSS TMM the "4th power average temperatures without suspect sensors" are taken. The LSS TMM/GMM with refined nodal break-down is shown in **Figure 6.2-1**. The changes w.r.t. the previous version are marked in red.

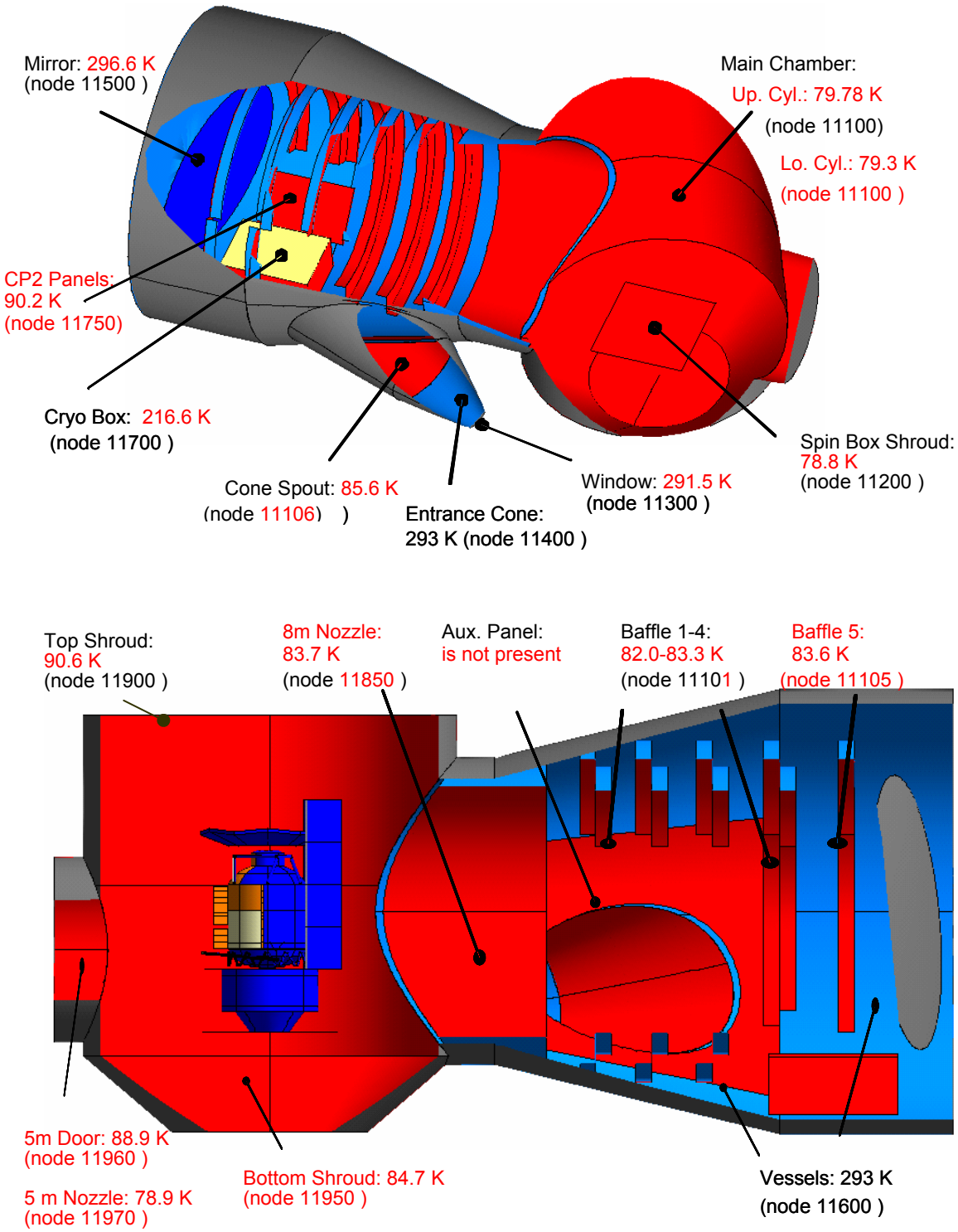

Figure 6.2-1: LSS GMM with "4th power average" Temperature Distribution

			TB1	TB2
5M DOOR	average	all sensors	90.7	90.7
	4th power average		91.5	91.5
	average	without suspect sensors	88.5	88.5
	4th power average		**88.9**	**88.9**
5m Nozzle	average	all sensors	78.9	78.8
	4th power average		**78.9**	**78.8**
TOP Shroud	average	all sensors	93.0	92.9
	4th power average		94.4	94.3
	average	without suspect sensors	90.1	90.0
	4th power average		**90.6**	**90.5**
BOT Shroud	average		96.3	96.2
	4th power average		102.5	102.4
	average	without suspect sensors	86.1	86.0
	4th power average		**84.7**	**84.6**
SHROUD 3	average	all sensors	78.8	78.7
	4th power average		**78.8**	**78.7**
Upper cylinder	average	all sensors	83.3	83.4
	4th power average		87.8	88.0
	average	without suspect sensors	79.7	79.6
	4th power average		**79.7**	**79.7**
Lower cylinder	average	all sensors	79.2	79.2
	4th power average		**79.2**	**79.2**
Spout	average	all sensors	100.7	100.7
	4th power average		124.5	124.7
	average	without suspect sensors	85.5	85.4
	4th power average		**85.6**	**85.5**
8m Nozzle	average	all sensors	83.4	83.4
	4th power average		**83.7**	**83.6**
BAF 1	average	all sensors	82.7	82.7
	4th power average		**83.1**	**83.0**
BAF 2	average		81.9	81.9
	4th power average		**82.0**	**81.9**
BAF 3	average		83.3	83.2
	4th power average		**83.3**	**83.2**
BAF 4	average		83.2	83.1
	4th power average		**83.3**	**83.3**
BAF 5	average	all sensors	88.4	88.3
	4th power average		89.7	89.6
	average	without suspect sensors	83.5	83.5
	4th power average		**83.6**	**83.5**
CP II	average	all sensors	98.4	98.3
	4th power average		103.9	103.8
	average	without suspect sensors	89.7	89.5
	4th power average		**90.2**	**90.0**
CPMP	average		216.6	216.7
	4th power average		**216.6**	**216.8**
MIR	average		296.4	296.4
	4th power average		**296.6**	**296.7**
Window	average		291.4	291.6
	4th power average		**291.5**	**291.8**

Table 6.2-1: Measured LSS Average Temperatures during TB1 and TB2

6.3 Discussion of IR Emissivity of LSS Surface

The GMM of the LSS used for the TB test predictions [RD 03] uses a hemispherical emissivity of the LSS walls of 0.9. Since the emissivity of LSS walls is a very important parameter for the CVV temperature which is almost at the same temperature level, this parameter is investigated in this section in more detail.

Measurements inside the LSS at 293 K revealed a normal emissivity of 0.90 [RD 24], however the hemispherical emissivity at LSS operational temperature of around 90 K is not (yet) known. To estimate the emissivity of the LSS at operational conditions measured temperature dependent emissivity data of similar black surfaces are compiled in **Table 6.3-1**. It shows that the emissivity at low temperature also depends on the thickness of the coating or paint. Unfortunately, the thickness of the Z306 painting in the LSS is not known which makes a comparison with other data difficult.

As a first step, the measured normal emissivity of 0.90 can be translated to a hemispherical emissivity using a relation factor of 0.95 as given in [RD 25]. This leads to a hemispherical emissivity of 0.855 at 293 K. For the time being extrapolation to 90 K can only be done using the data compiled in **Table 6.3-1**, e.g.:

- 0.76 interpolating the data of RD21 (too optimistic since emissivity at 293 K is 0.90 instead 0.855)
- 0.78 using the emissivity difference between 160 K and 90 K of RD 23
- 0.79 using a degradation factor for the emissivity between 160 K and 90 K of RD 23

Preliminary one can conclude that the hemispherical emissivity of the LSS wall at 90 K is very likely lower than 0.8.

Name	Thick-ness	Sub-strate	Total Hemispherical Emissivity at					Ref.
	[µm]		T_1 [K]	T_2 [K]	T_3 [K]	T_4 [K]	300K	
"OXAL" black anodi-zation for Herschel	50	Al 5083	20 K: **0.65**	40 K: **0.78**	65 K: **0.83**	100 K: **0.85**	**0.93**	RD 07
"OXAL" black anodization for Herschel (ZAE)	25-30	Al 5083	20 K: **0.60**	40 K: **0.72**	65 K: **0.80**	100 K: **0.84**	**0.89**	RD 22
	50	Al 5083	20 K: **0.60**	40 K: **0.76**	65 K: **0.82**	100 K: **0.85**	**0.90**	
	75	Al 5083	20 K: **0.72**	40 K: **0.80**	65 K: **0.84**	100 K: **0.86**	**0.91**	
"OXAL" black anodization for Herschel (LEEE)	25	Al 5083		40 K: **0.37**	70 K: **0.669**	100 K: **0.786**	**0.832** [1)]	RD 23
	50	Al 5083		40 K: **0.60**	70 K: **0.755**	100 K: **0.811**	**0.836** [1)]	
	75	Al 5083		40 K: **0.71**	70 K: **0.794**	100 K: **0.824**	**0.847** [1)]	
Black Paint Aeroglaze Z306	124	Al 2024	85 K: **0.71**	99 K: **0.81**	120 K: **0.86**	181 K: **0.89**	**0.90**	RD 21
Black Paint Chem-glaze Z 306 (Lords)	100	?	15 K: **0.811**	38 K: **0.797**	76 K: **0.802**	95 K: **0.817**	**0.917** [2)]	RD 18
Z 306 (LEEE)	?	?		40 K: **0.689**	70 K: **0.810**	90 K: **0.857**	**0.929** [1)]	RD 23
Z 306 (LSS)	?	Al				90 K: **??**	**<0.90** [3)]	RD 24
PU1 (MAP)	?	?	11 K: **0.877**	38 K: **0.869**	76 K: **0.848**	95 K: **0.825**	**0.89**	RD 18
PU1 (MAP)	100	Al 2024	131 K: **0.820**	194 K: **0.870**		225 K: **0.890**	**0.90**	RD 19
PUK	60	Al 5083	20 K: **0.75**	40 K: **0.80**	65 K: **0.84**	100 K: **0.87**	**0.93**	RD 20

1) at 160 K
2) at 153 K
3) normal emissivity measurement is 0.9, hemispherical emissivity is estimated to 0.855 at 300 K

Table 6.3-1: Compilation of Total Hemispherical Emissivity Data for Thermal Coatings

6.4 Post-Test Inspection of LSS

When the S/C had been removed from the LSS after the STM TB/TV test, the LSS was inspected again to identify possible additional heat sources. Pictures were taken which are discussed below. A summary of the inspection outcomes is given in **Table 6.4-1**.

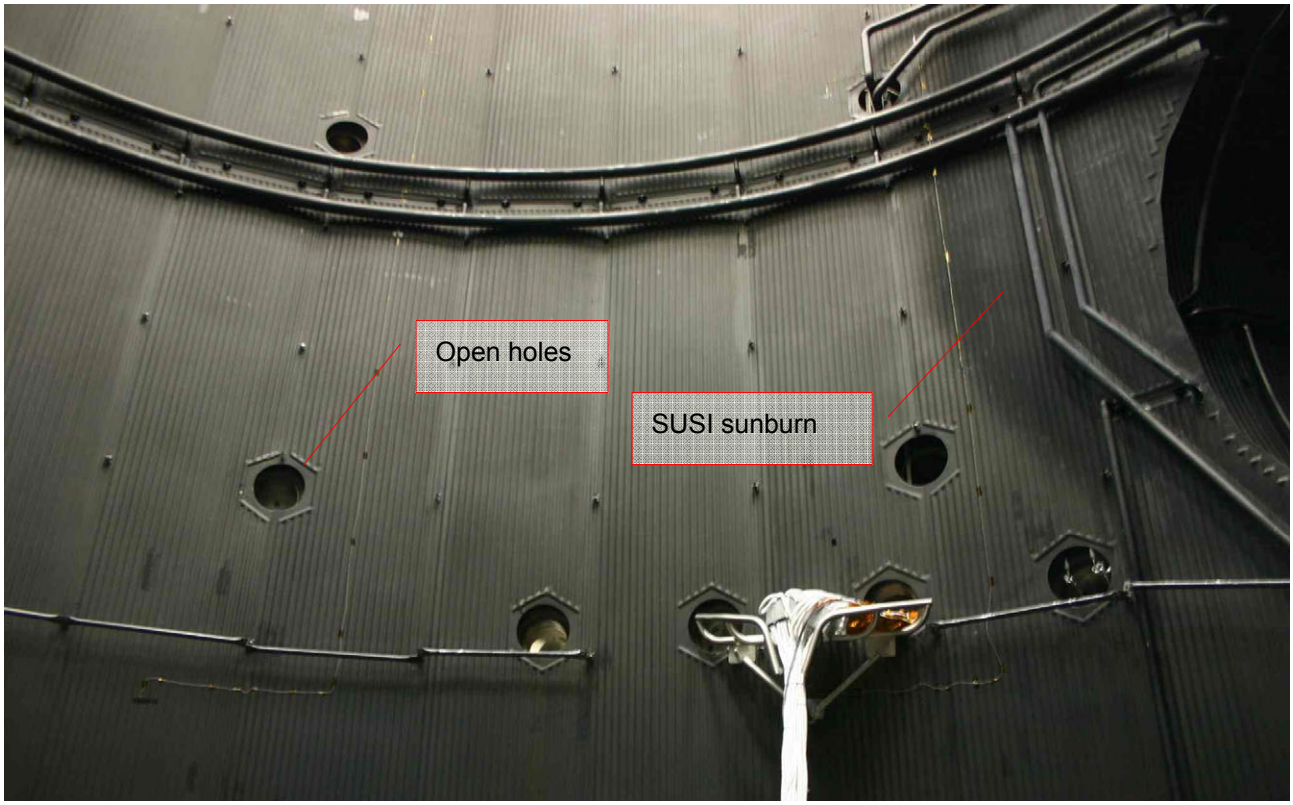

Figure 6.4-1: LSS feedthroughs

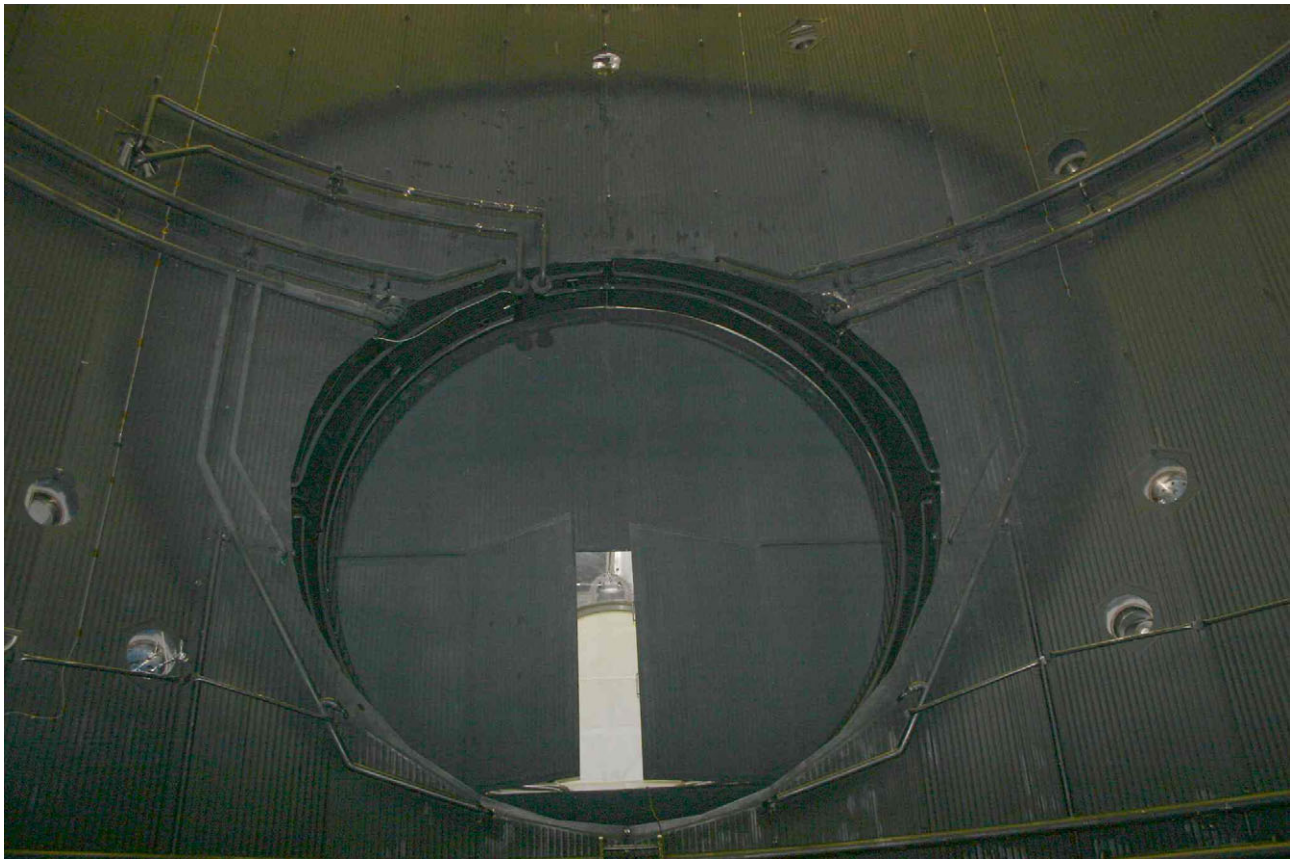

Figure 6.4-2: Sunburnt black surface of LSS back wall (SUSI switched off)

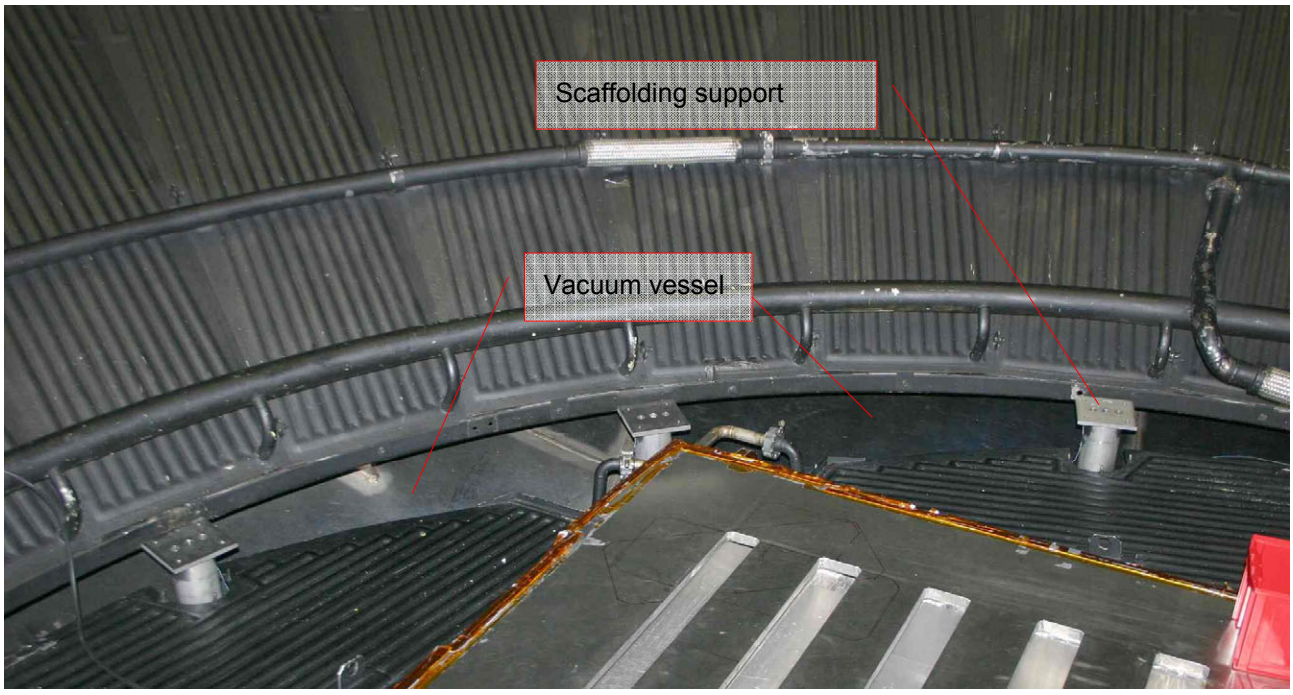

Figure 6.4-3: Scaffolding supports and view to vacuum vessel

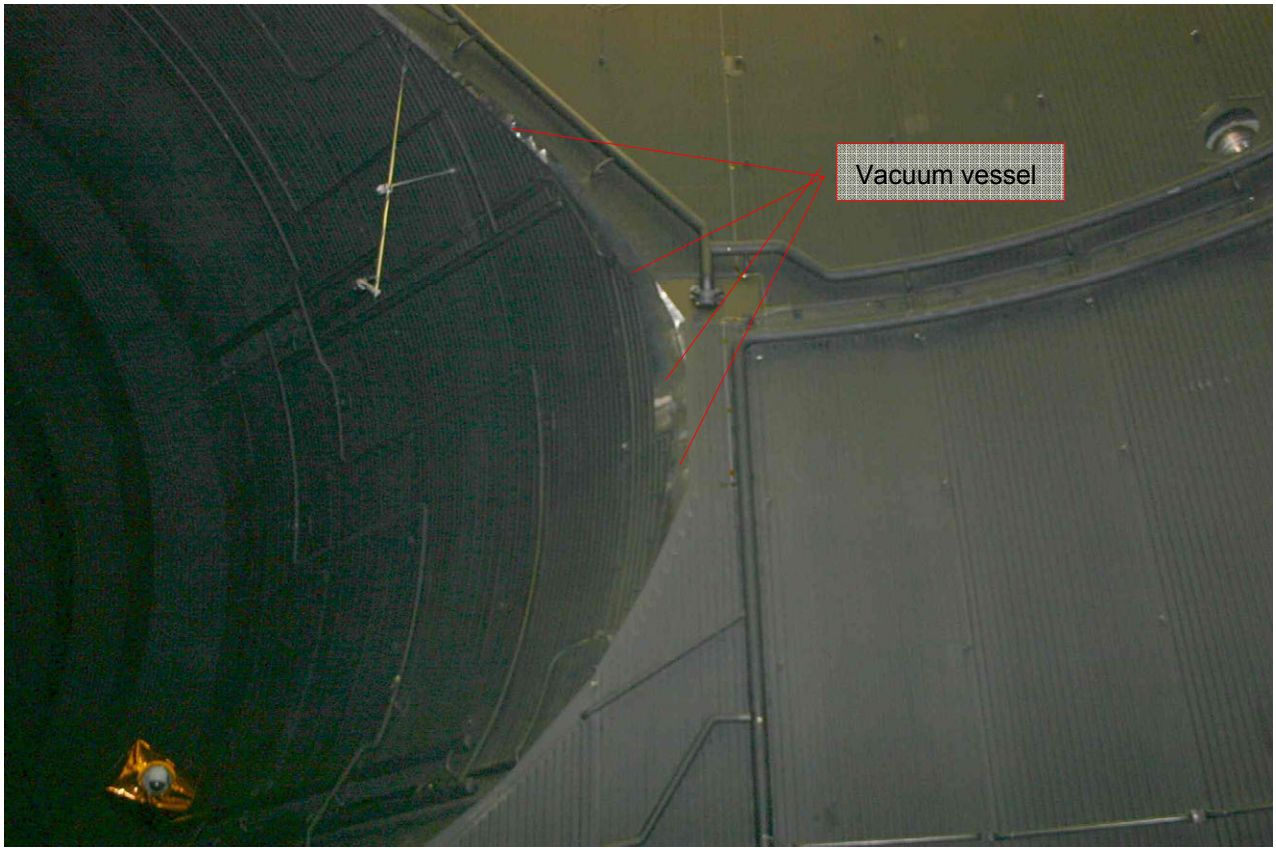

Figure 6.4-4: Shroud gaps in nozzle connection to cylinder

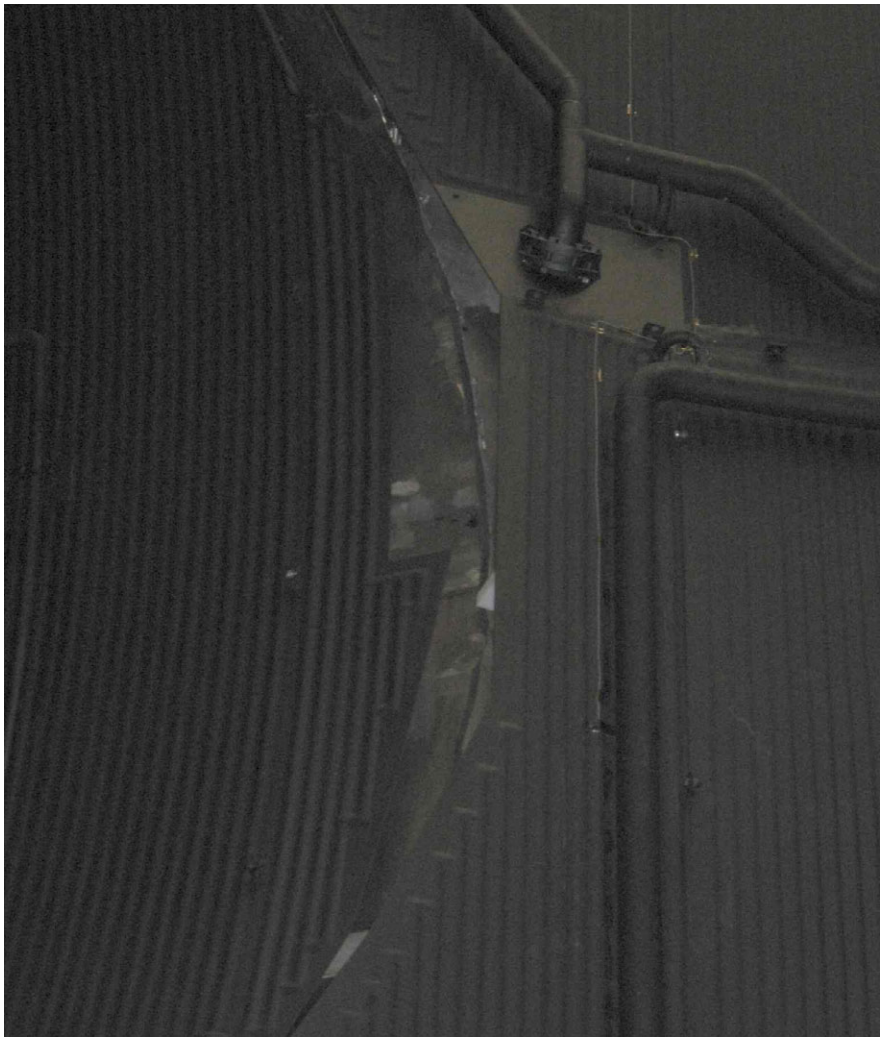

Figure 6.4-5: Shroud gaps in nozzle connection to cylinder (detail)

Figure 6.4-6: Circumferential gap in connection from nozzle to cylinder

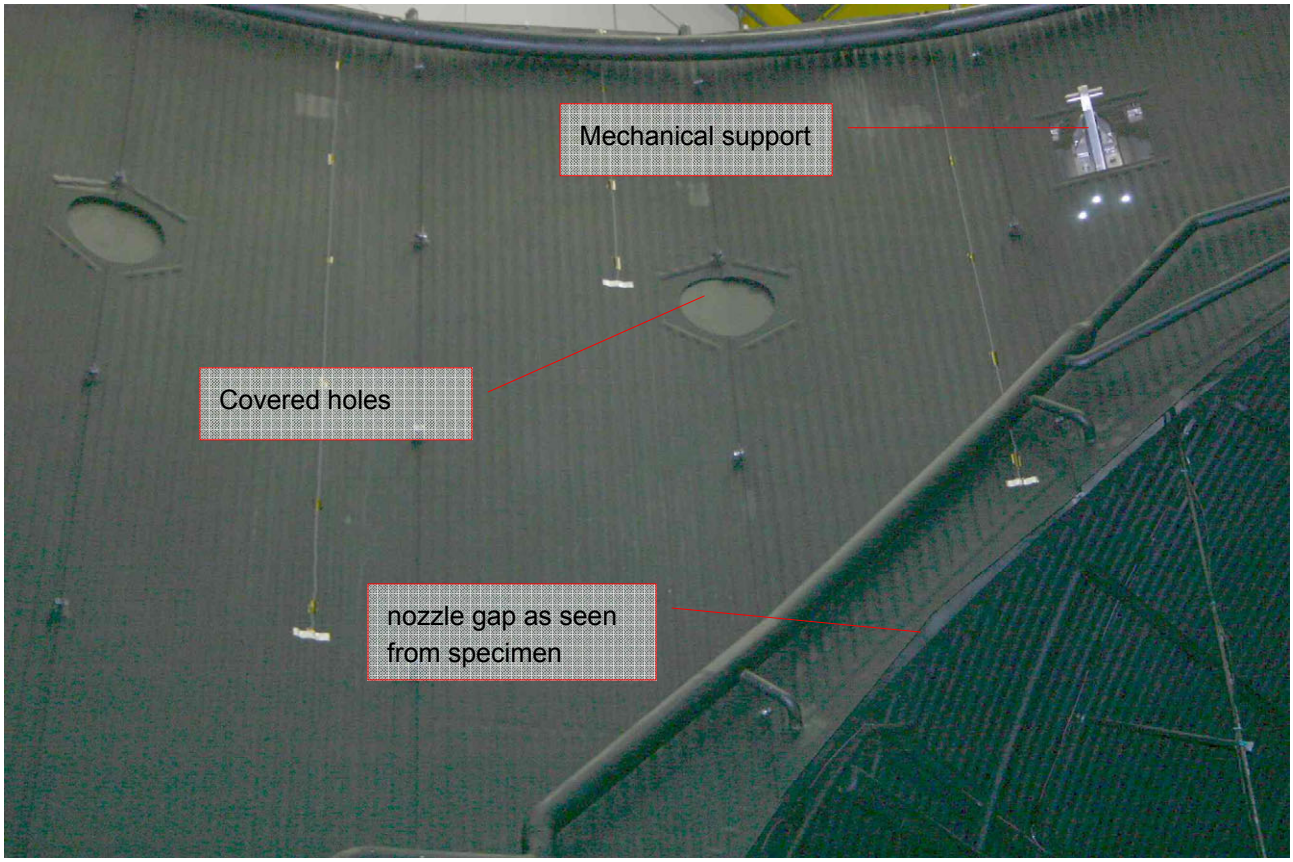

Figure 6.4-7: Mechanical support and nozzle gap

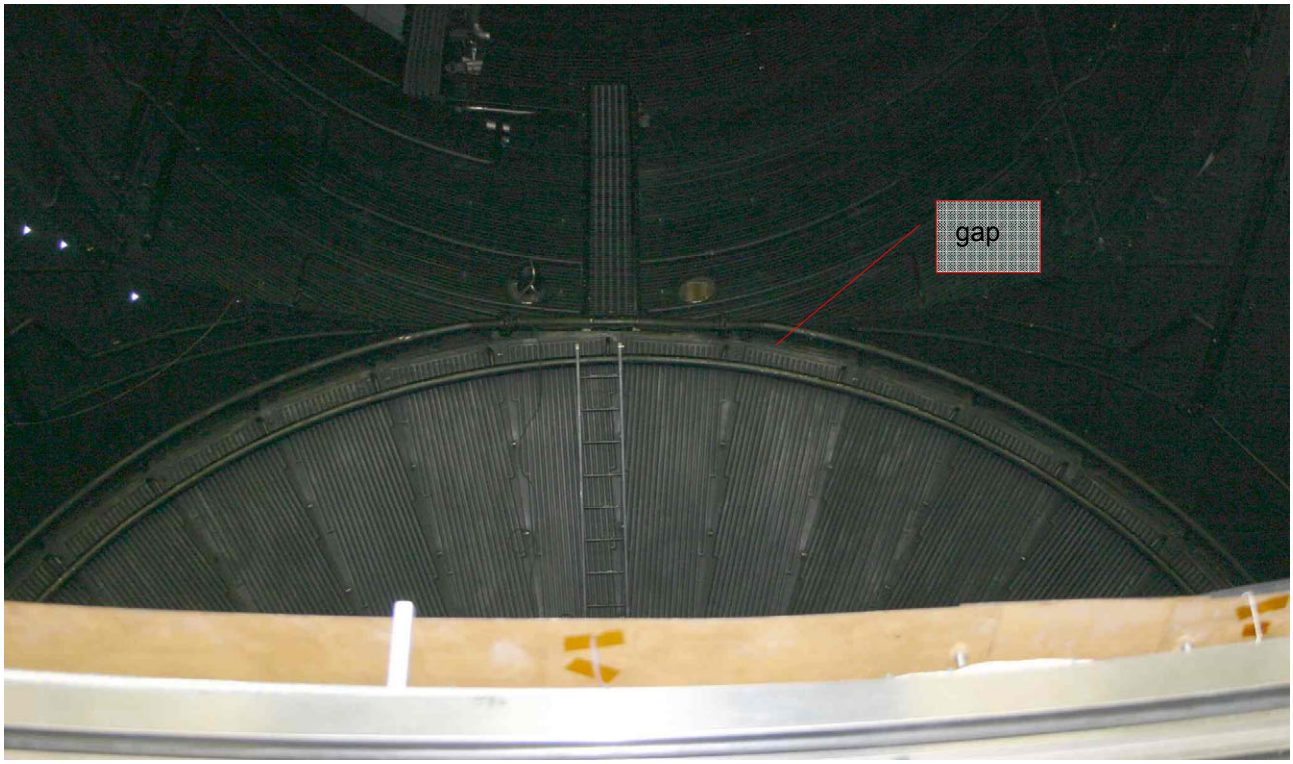

Figure 6.4-8: Circumferential gap between conical and cylindrical shroud

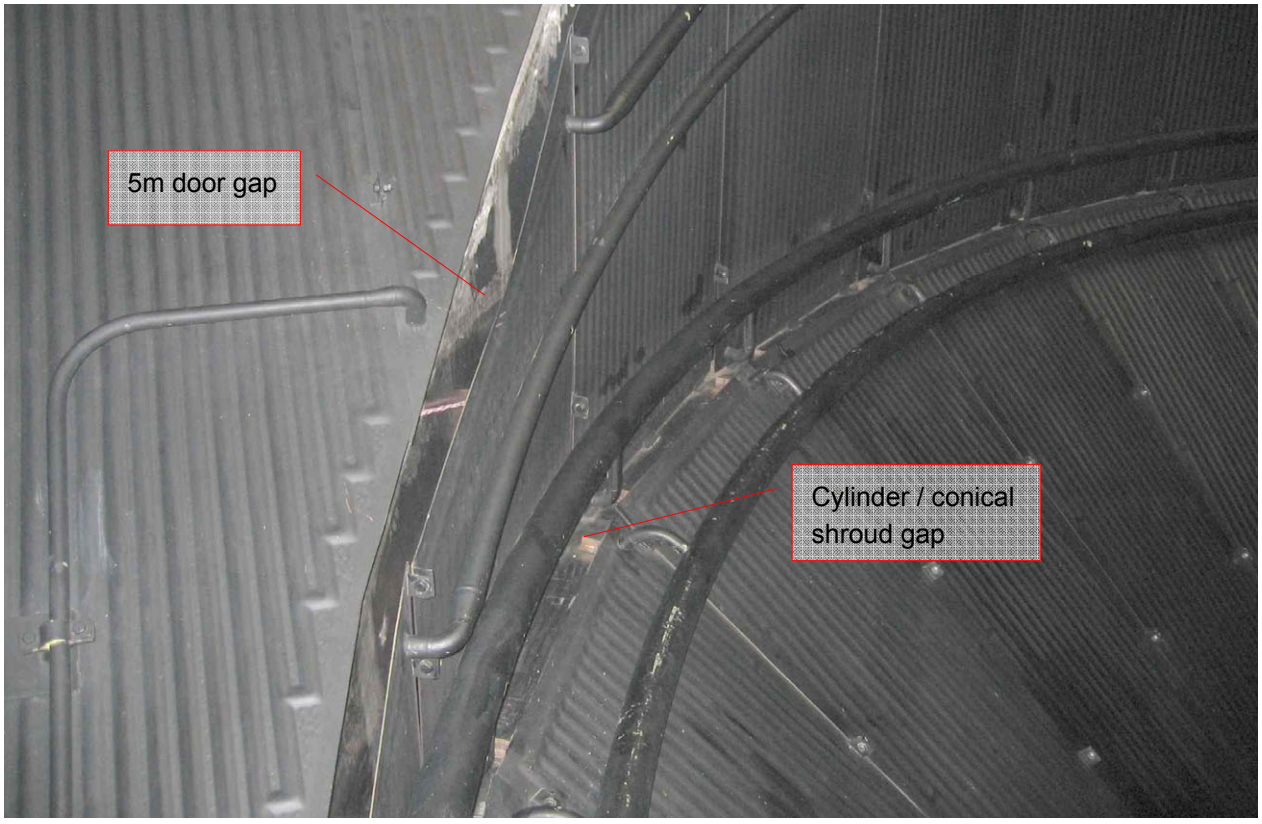

Figure 6.4-9: Circumf. gaps around 5m door connection and between conical and cylindrical shroud

Figure 6.4-10: Circumferential gap around 5m door shroud

Figure 6.4-11: Typical placement of shroud temperature sensor

Description	Location	Size	Number	Optical
Open circular holes in shroud for LSS ports access	Cylinder shroud	Diam 300mm	13	black hole
Open circular holes in shroud with SS armatures	Cylinder shroud	Diam 300mm	3	SS
Closed circular holes in shroud for LSS ports access, not cooled	Cylinder shroud	Diam 300mm	8	Z306
Basic Scaffolding supports	bottom shroud	160x160mm	12	SS
Sunburn on LSS back wall (around 5m door), changed surface	5m door and surrounding	Diam ~8m	1	black
LSS control harness	lower ports	diam ~150mm, length	1	white
Circumferential gap between bottom and conical shroud	below SB shroud	Ring width ~200mm	1	SS / trapping
Circumferential gap between nozzle and cylinder shroud		Ring width 160mm	1	SS / trapping
Triangular gap between nozzle and cylinder shroud	vertical mid of SUSI beam	triangle 500mm x 1m	2	SS / trapping
Mechanical supporting structure mounted to LSS wall	top of cylinder shroud, West and 2* displaced by 120°	300x300mm²	3	SS / trapping
Circumferential gap between conical and cylinder shroud	lower end of cylinder	ring width 80mm	1	SS / trapping
Circumferential vertical gap between top (cover) and cylinder shroud	upper end of cylinder	ring height 50mm	1	SS / trapping
Circumferential gap in shrouds between main cylinder and cylinder leading to 5m door	at cylinder to 5m door	ring width 80mm	1	SS / trapping
Circumferential gap in shrouds between 5m door and cylinder leading to 5m door	at 5m door	ring width ~40mm (from photo)	1	SS / trapping
Temperature sensors located directly on flushing line	all over the shrouds	n/a	n/a	Temperature impact negligible

Table 6.4-1: Summary of LSS inspection findings

- Open hole ➔ T = T_vessel = 293 K, ideal black, $\varepsilon = 1$
- Closed by black plate bolted to the shroud, $\varepsilon = \varepsilon$_Z306. From thermal analysis ➔ T < 1K above shroud temperature
- SS armatures protruding from open hole ➔ T = T_vessel = 293 K, steel, $\varepsilon = 0.2$
- Mechanical Supports ➔ T = T_vessel = 293 K, steel, $\varepsilon = 0.2$

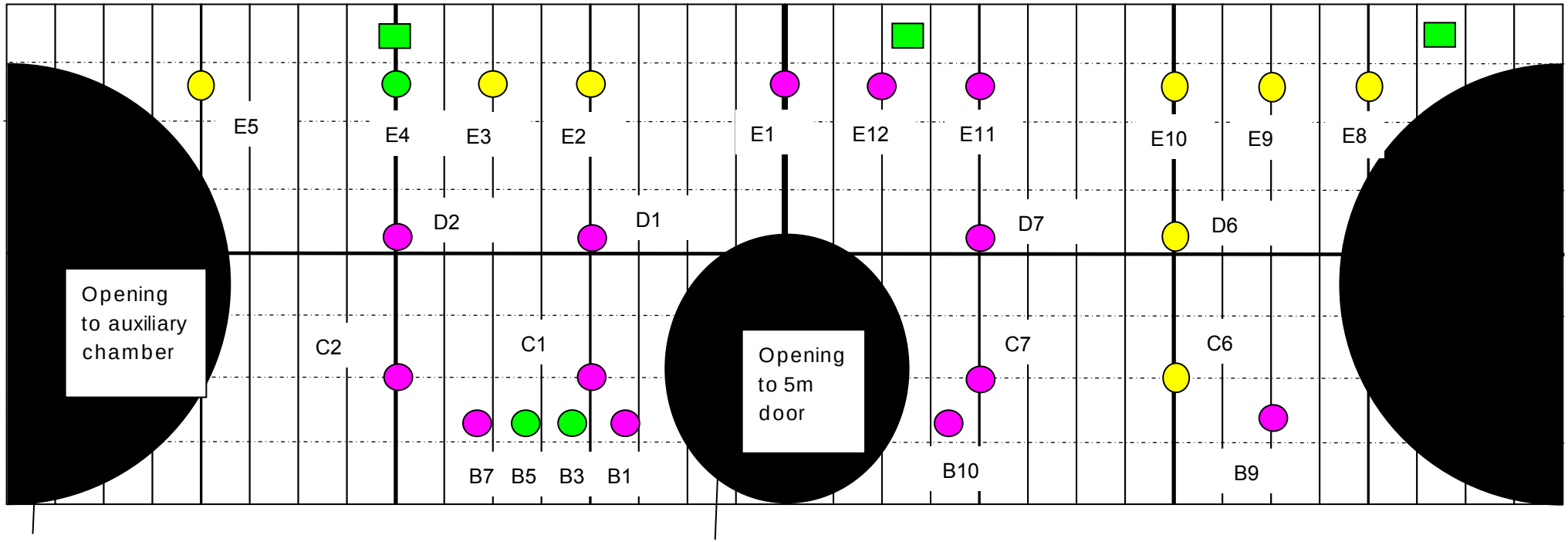

Figure 6.4-12: Positions of holes in LSS main cylinder shroud

6.5 Proposed Refinement of LSS TMM /GMM

Based on the findings described in the previous section a refined TMM/GMM of the LSS has been established. The details are described in the following:

A circumferential gap of 0.150 m width between Nozzle Shroud and Main Chamber Cylinder Shroud has been introduced, see **Figure 6.5-1** and **Figure 6.5-2**. This circumferential gap results in an absolute gap that varies between 0.150 m and 0.255 m. Since the vessel completely covers this gap the artificial gap is set to vessel temperature of 293 K with an assumed emissivity of 0.2 (steel).

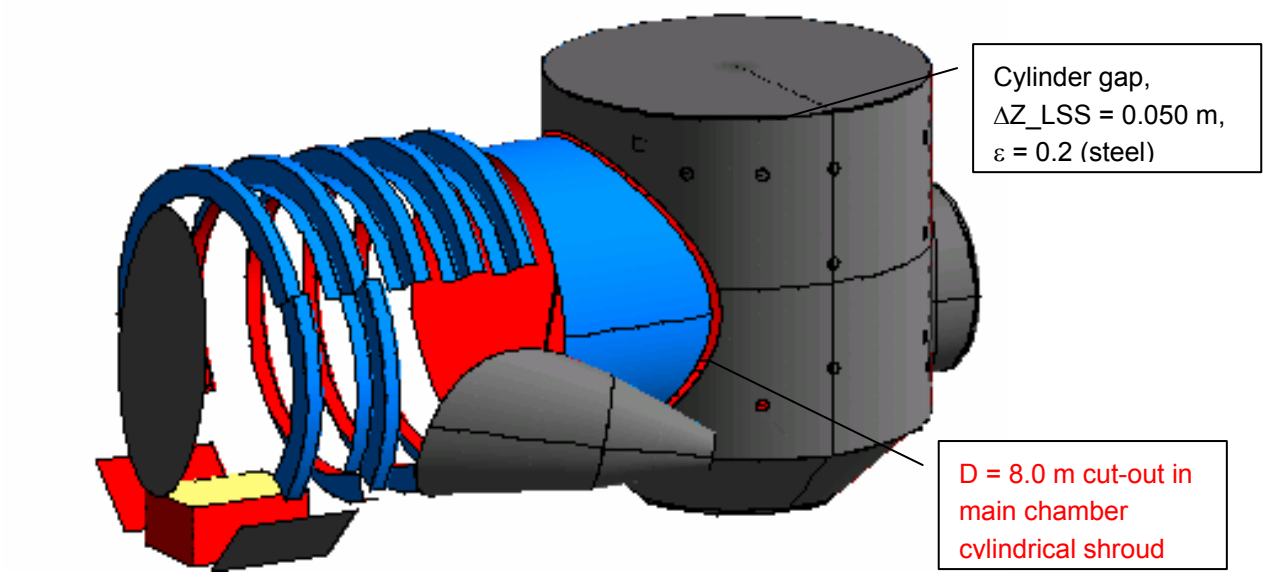

Figure 6.5-1: Refined GMM of LSS: View on 8m-Nozzle and Baffles (Vessel is removed)

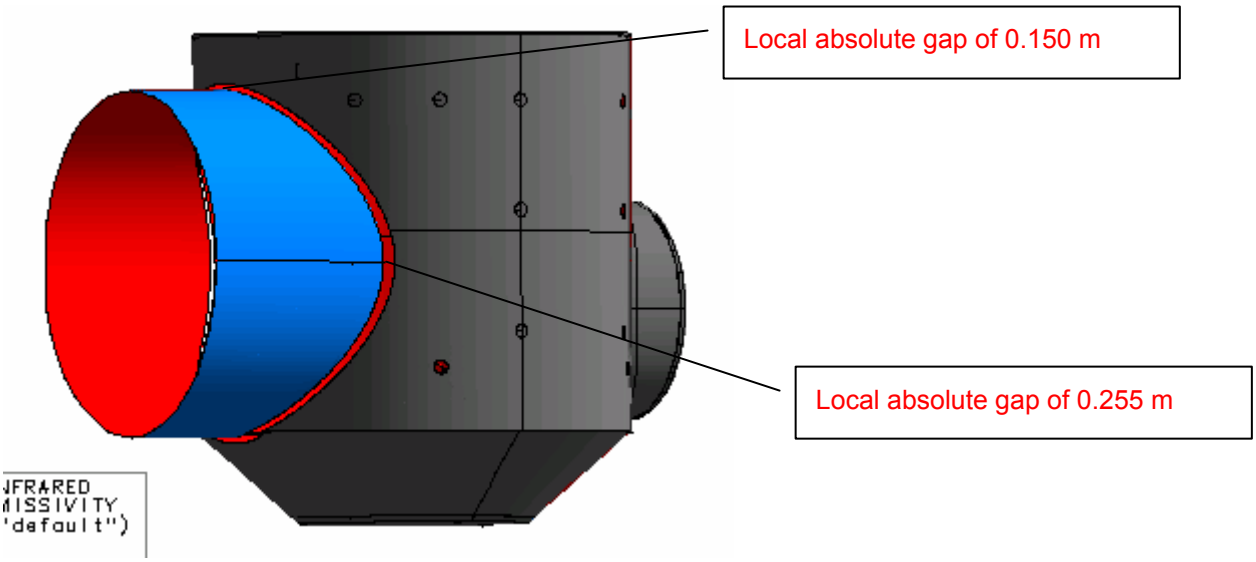

Figure 6.5-2: Refined GMM of LSS: View on “8m-Nozzle” (Baffles and Cone Spout removed)

The test harness inside the LSS has been introduced in the GMM, see **Figure 6.5-3**. Gaps between the bottom shrouds are also introduced in the GMM as shown in **Figure 6.5-4**. The vertical gap between Main

Chamber Top Shroud and Cylinder Shroud has been measured inside the LSS with 0.05 m and is also introduced in the LSS GMM.

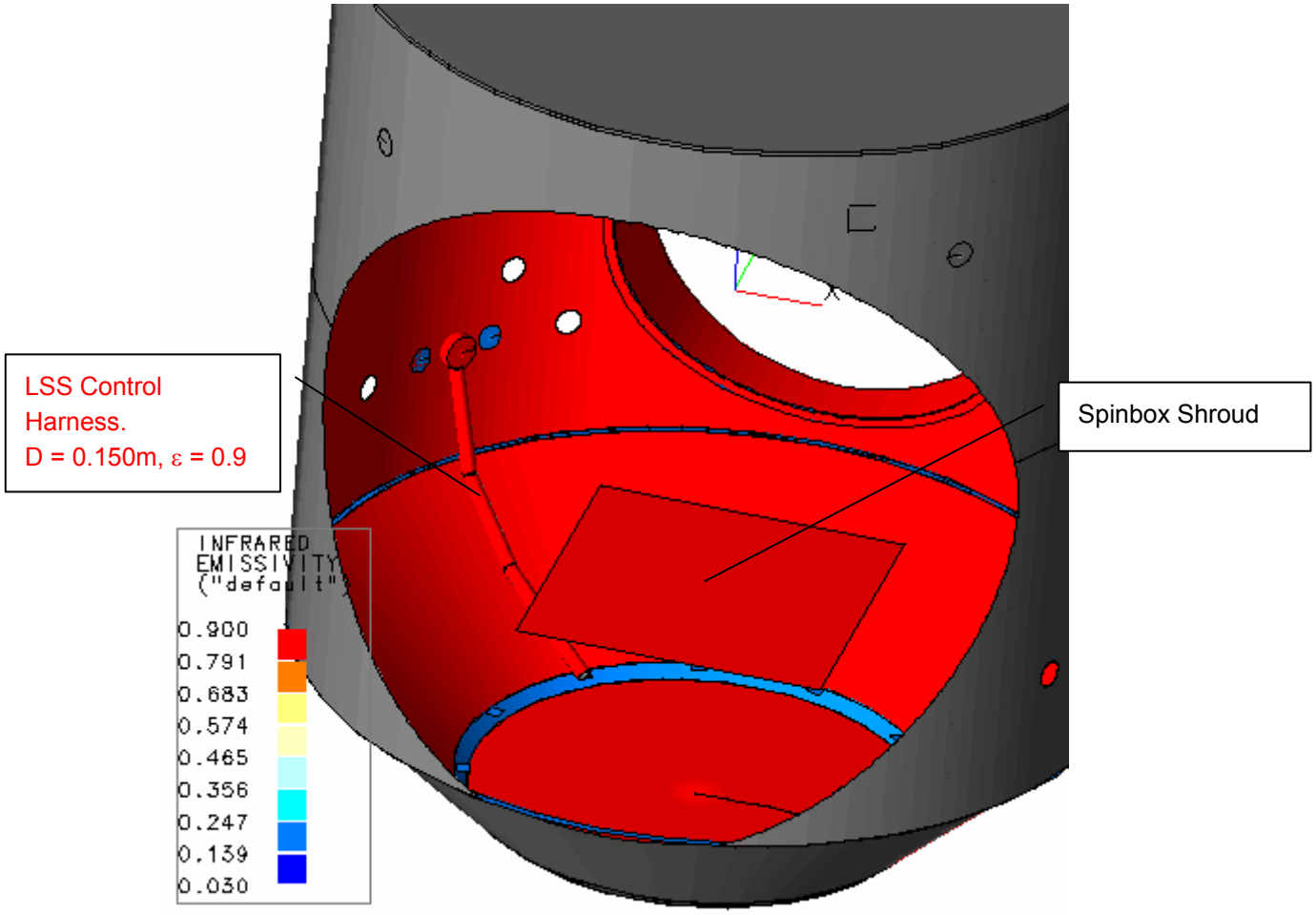

Figure 6.5-3: Refined GMM of LSS: View into the Main Chamber (Auxiliary Chamber removed)

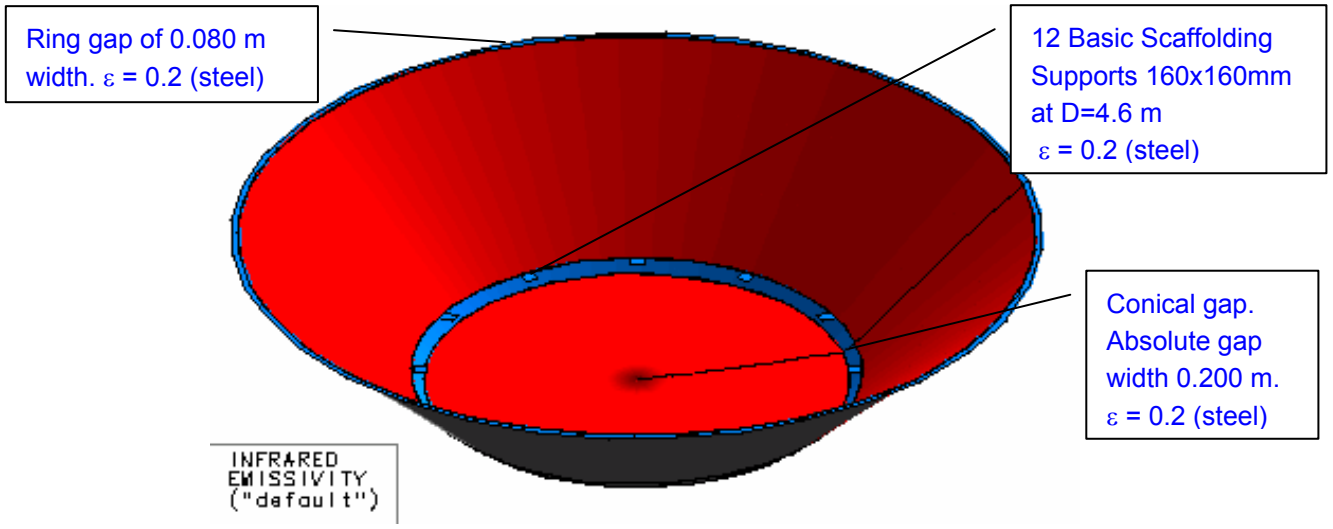

Figure 6.5-4: Refined GMM of LSS: 12 Scaffolding Supports on the Bottom Shroud.

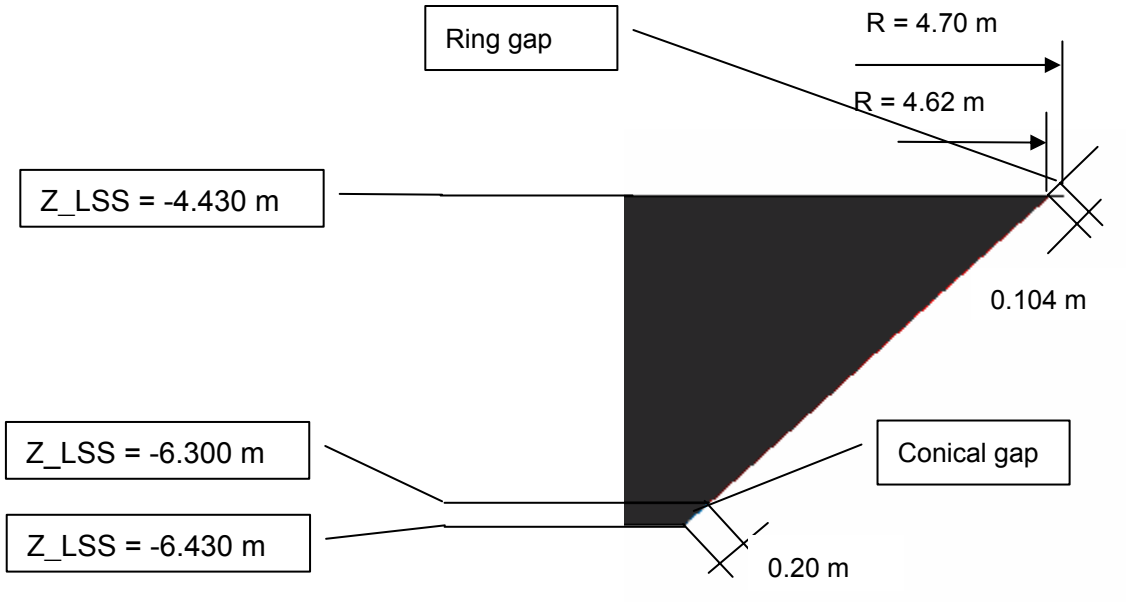

Figure 6.5-5: Refined GMM of LSS: Details of Implemented Gap Dimensions

The conical gap (**Figure 6.5-4** and **Figure 6.5-5**) of 0.20 m width is an approximation of the comprehensive as-built geometry of the bottom shroud. Cross check with the LSS CAD-model revealed a gap that varies between 0.10 m and 0.30 m.

Finally gaps between Main Chamber cylinder shroud and 5m door nozzle shroud as well as between 5m door nozzle shroud and 5m door disc shroud are introduced as shown in **Figure 6.5-6**.

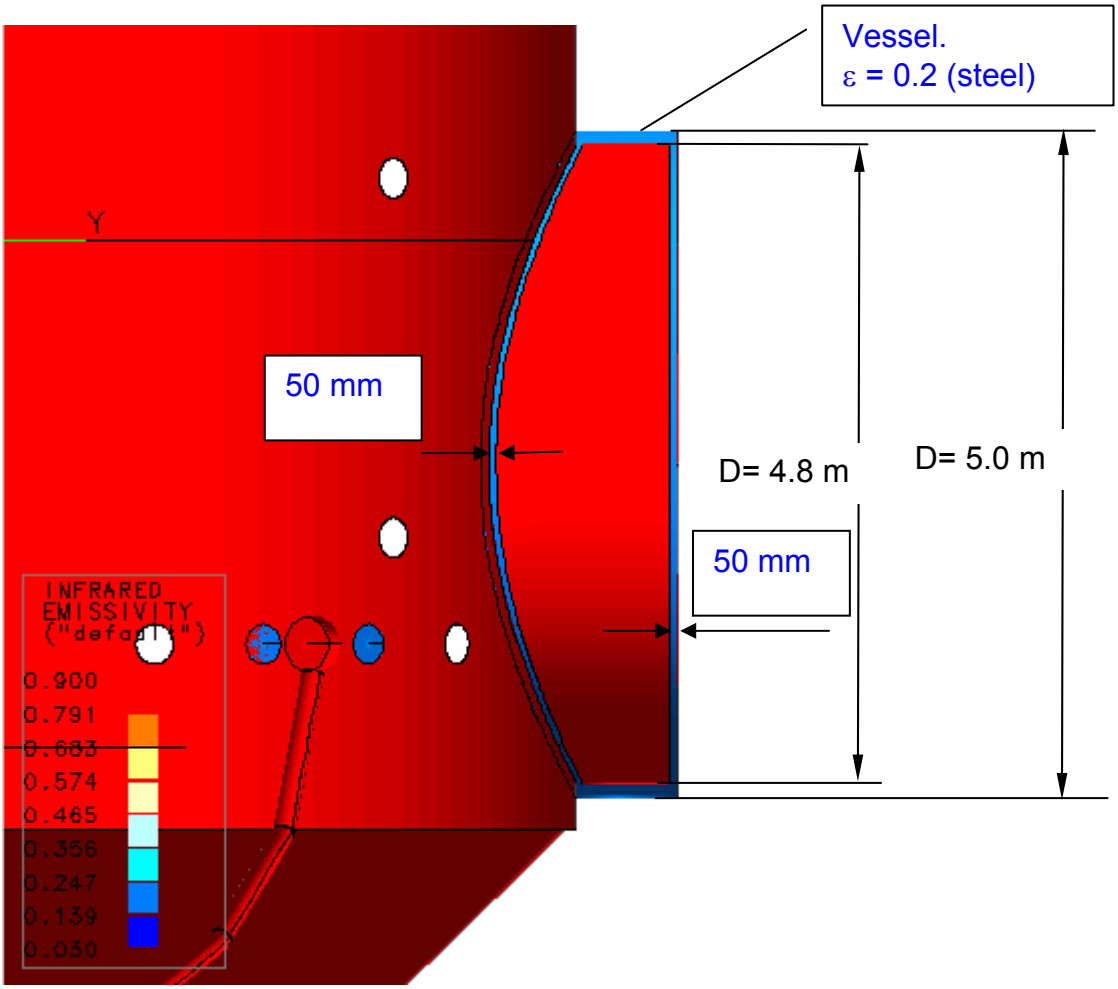

Figure 6.5-6: Refined GMM of LSS: Sectional view into Main Chamber and 5 m door nozzle

Summary and Conclusions:

- Assumptions used in LSS TMM/GMM significantly affects the calculated CVV temperature
- Emissivity of LSS walls at operational temperature is not known. Rough assessment reveals that the emissivity is not 0.9, but rather 0.8 or even lower
- Detailed modelling of gaps between the LSS shroud elements, cavities, test harness, etc. is mandatory for proper H-EPLM TMM correlation. A comprehensive refinement of the LSS TMM/GMM has been established in this matter.
- As far as practical “warm” gaps and cavities inside the LSS shall be covered with MLI for the next test
- Emissivity of LSS walls and effective heat sink temperature shall be measured at operational temperature

7 Gas Dynamics

7.1 PPS Performance

The Passive Phase Separator (PPS) was operated during the TB/TV test in test phases TP2 (LEOP), at the end of TP3 (Rapid Cool-down), during TP4 (TV1) and during TP7 (TB2). Dedicated PPS verification activities were executed at the end of TP3 (PVS 10). In addition, a dedicated PPS performance test was performed before the TB/TV test (see RD16).

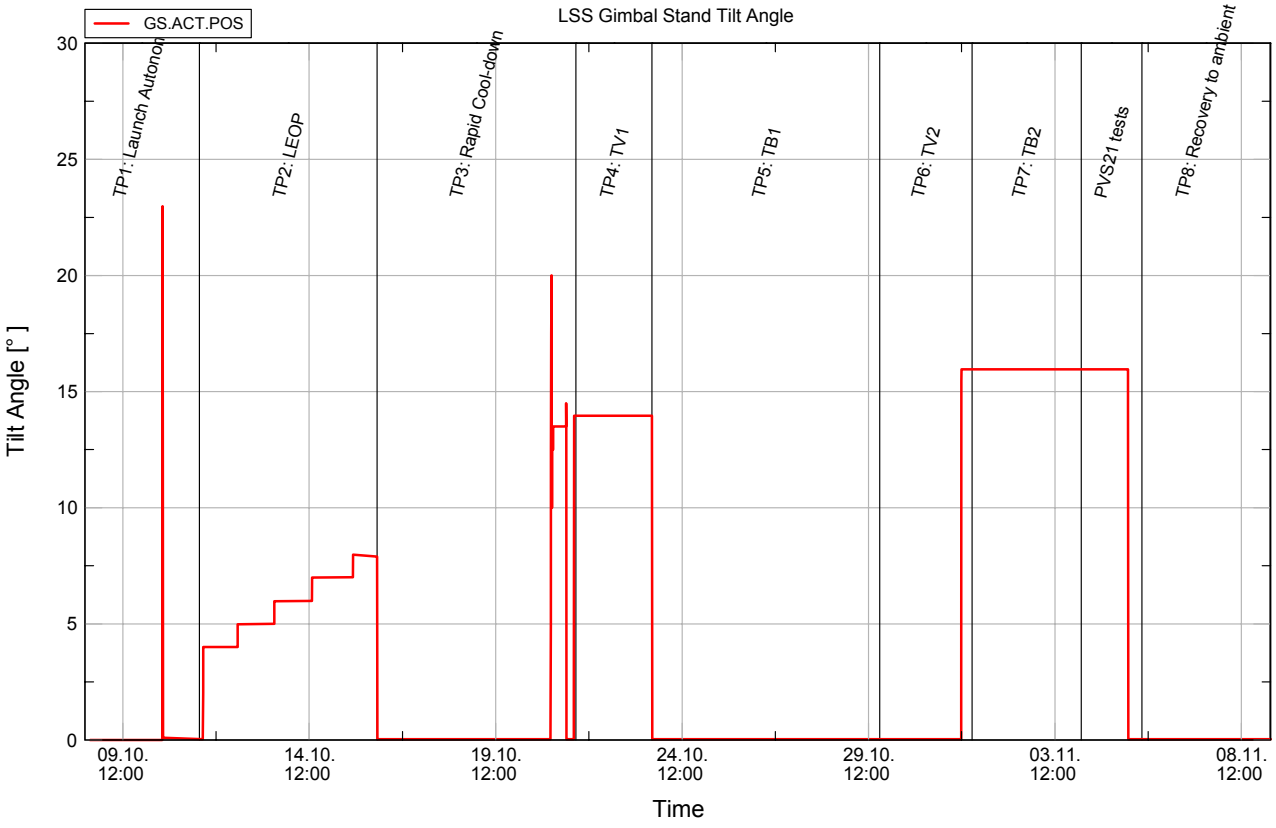

Figure 7.1-1: S/C tilt angle throughout TB/TV test

When the large nozzle was closed at the end of the LEOP simulation (TP2), the temperature difference measured across the PPS became positive which was interpreted as a liquid break-through at the time. However, a close look at the PPS outlet temperatures as shown in **Figure 7.1-3** reveals a slight temperature increase exactly at the time of opening the PPS bypass valve V104 on 16.10.05 at 06:30.

The PPS measurements performed at the end of TP3 in the frame of PVS 10 show that the upper bulkhead of the HTT was completely covered by a (internal) superfluid He film as indicated by the very low temperature reading of T107 located on the upper bulkhead. This can be explained by the very cold environment caused by the rapid HTT cool-down performed with high (up to 100 mg/s) mass flow rates. It was surprising to see that the PPS can be fully operated in this cold environment without tilting the spacecraft as shown in **Figure 7.1-4**, where the S/C tilt angle is shown together with the HTT and PPS temperatures. Valve states during this phase are shown in **Figure 7.1-5**. The HTT filling level at this time was about 90.1%, i.e. the PPS should be immersed in the liquid surface at a tilt angle of 14°.

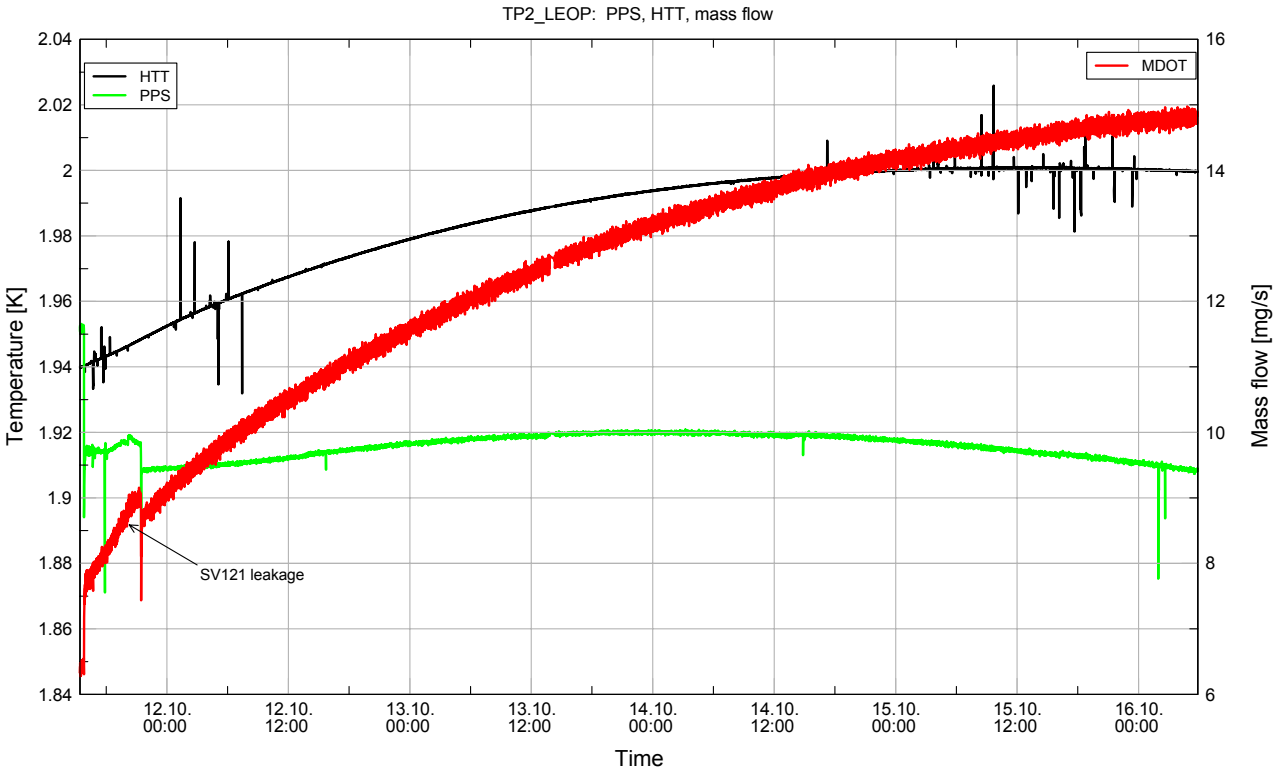

Figure 7.1-2: PPS temperature difference and mass flow during LEOP simulation

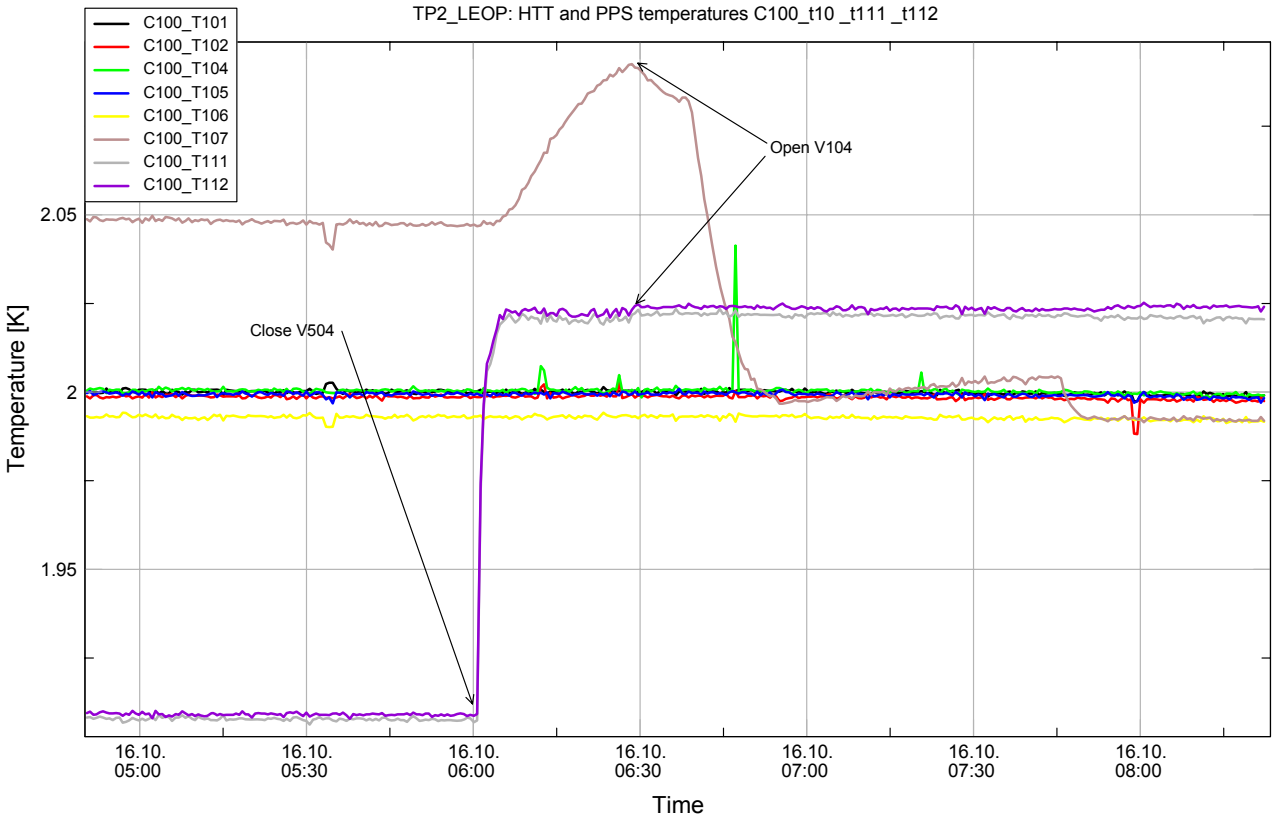

Figure 7.1-3: HTT and PPS temperature during large nozzle switch-off at end of TP2

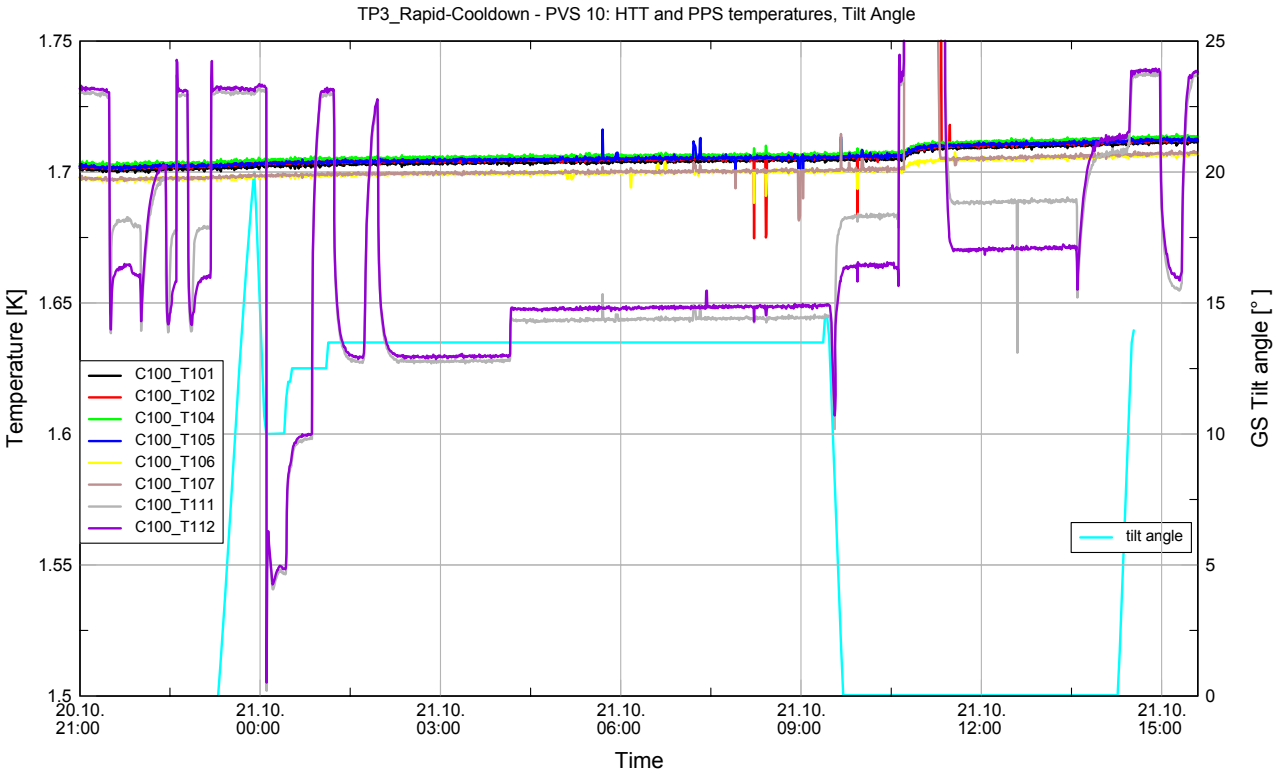

Figure 7.1-4: PPS operation on superfluid He film at end of TP3 (PVS 10)

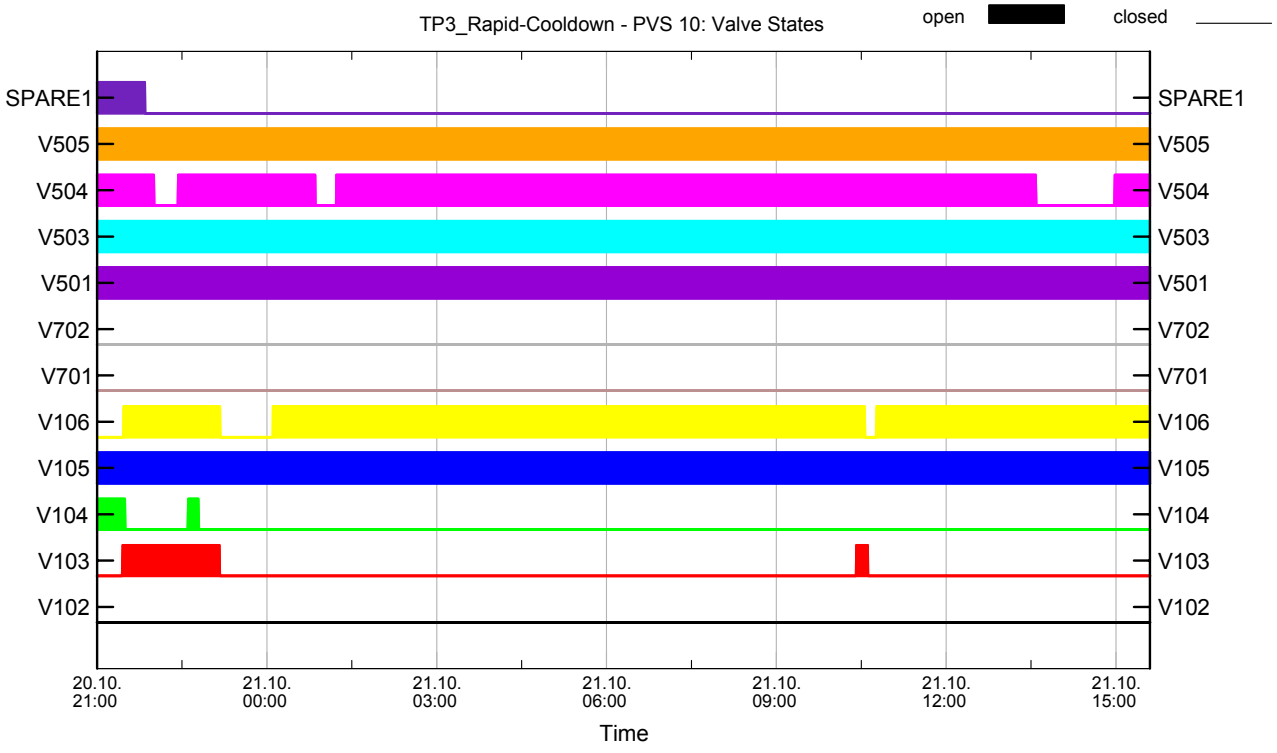

Figure 7.1-5: Valve states at end of TP3 (PVS 10)

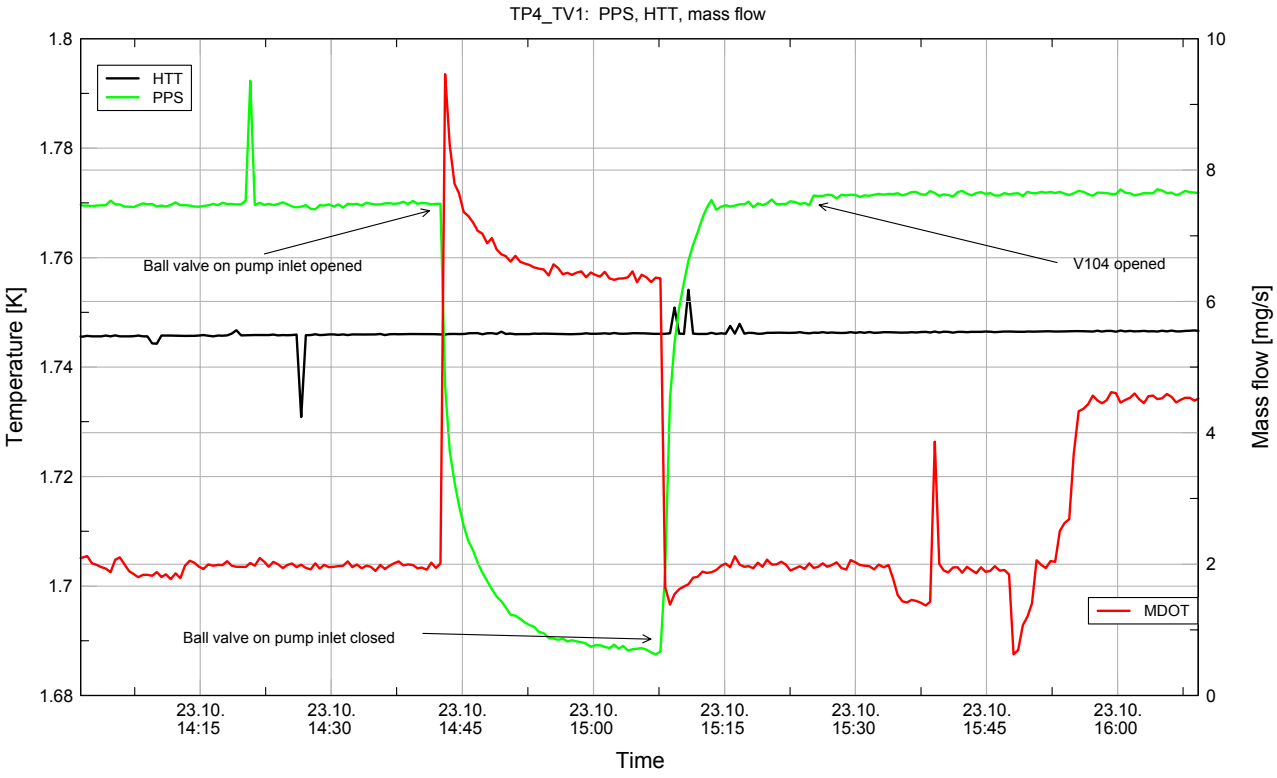

Figure 7.1-6: PPS temperature difference and mass flow at end of TP4

During TP4, the PPS valve V106 was opened and the mass flow rate was controlled by manipulation of the needle valve at the pump inlet. Throughout the phase, the PPS outlet sensors showed a temperature ~23 mK above the bath temperature. At the end of TP4, the large ball inlet valve on the pump was opened to achieve the largest possible mass flow rate at the given bath temperature, see **Figure 7.1-6**. The mass flow increased as expected, and a negative temperature difference of ~-58 mK was established. From these conditions, the ball inlet valve was closed again to simulate the steepest possible mass flow change when switching from the large to the small nozzles. After this closure, the same 23 mK temperature difference as before was established again. When the HTT outlet valve V104 (bypassing the PPS) was opened, a slight but unambiguous temperature increase was observed by the PPS outlet sensors, giving proof that the PPS was operating before with a mass flow of ~2 mg/s at 1.74 K HTT temperature.

The reproducible measurements of a PPS temperature increase when opening the PPS bypass valve lead to the conclusion that the PPS outlet temperature as measured by the C100 sensors T111 and T112 has a calibration offset against the HTT bath sensors (DLCM) T101, T102, T104 and T105, which is explained by different calibration batches of the sensors and self heating of the PPS sensors which are not in close contact to the liquid (superfluid) He bath as are the DLCM sensors.

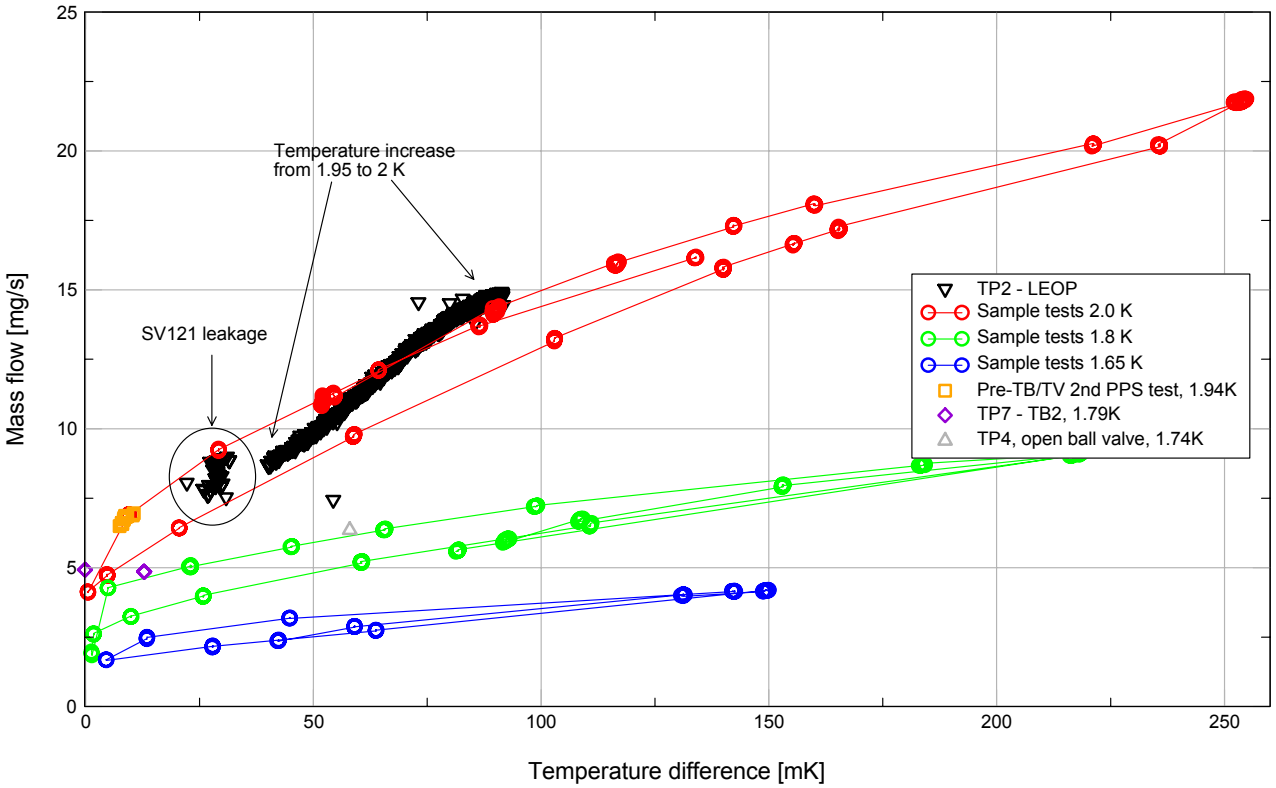

Figure 7.1-7: PPS temperature difference versus mass flow and comparison to sample tests

The PPS performance measurements are summarised in **Figure 7.1-7**, where the measurements achieved during the system level tests are compared to unit level test results gained by Linde. This comparison shows that the PPS operation on system level is as expected from the unit level measurements. Furthermore, the mass flow capability of the PPS is not fully exploited by the current set-up, and a further increase of the large nozzle diameter is possible while still fulfilling the PPS requirements.

7.2 Pressure Drop Evaluation

Dedicated pressure drop measurements of the helium system tubing have been performed during the TB/TV test as listed in rows 1 to 7 of **Table 7.2-1**. In addition, pressure drop measurements with external tubing at ambient temperature were performed before the TB/TV test as reported in rows 8 to 11. The measured pressure of P502 is the value from the original calibration without corrections, the pressure in the HTT is the saturated vapour pressure as calculated from the average of the DLCM temperature sensors.

Ref	Time stamp	Phase	Vent path		Temperatures [K]								Pressure [hPa]		mass flow
			HTT	Nozzle	HTT	L1	L2	L3	TS1	TS2	TS3	Nozzle	HTT svp	P502	[mg/s]
1	16.10.05 05:55	TP2	V106	big	2.000	2.3	8	8.5	38	89	116	116	31.3	14.4	14.8
2	23.10.05 15:04	TP4	V106	big	1.745	2	3	4	38	48	63	99	13.4	7.4	6.3
3	16.10.05 06:24	TP2	V106	small	2.000	4	6	6.2	38	89	116	116	31.3	26.9	4.6
4	04.11.05 11:50	TP7	V103/ V106	small	1.799	2.8	8	8	32	51	72	102	16.3	14.0	2.3
5	16.10.05 07:40	TP2	V104	big	1.999	4.5	7	7	38	89	116	116	31.2	21.5	24.4
6	16.10.05 06:37	TP2	V104	small	2.000	5	8.8	9.2	38	89	116	116	31.3	26.9	4.7
7	23.10.05 15:47	TP4	V104	small	1.745	2	3	4	38	48	63	99	13.4	12.6	1.9
8	07.10.05 16:40	pre	V103/ V106	big	1.942	5	10	10	26	82	152	293	26.2	15.2	6.6
9	07.10.05 13:17	pre	V104	big	1.862	5	10.4	10.4	25.7	79.5	151	293	20.3	15.4	7.4
10	07.10.05 16:50	pre	V103/ V106	small	1.942	5.8	12	12	28	82	152	293	26.2	23.1	1.6
11	07.10.05 13:26	pre	V104	small	1.862	6.9	12.4	12.4	29	79.5	152	293	20.3	19.6	1.3

Table 7.2-1: Pressure drop measurements overview

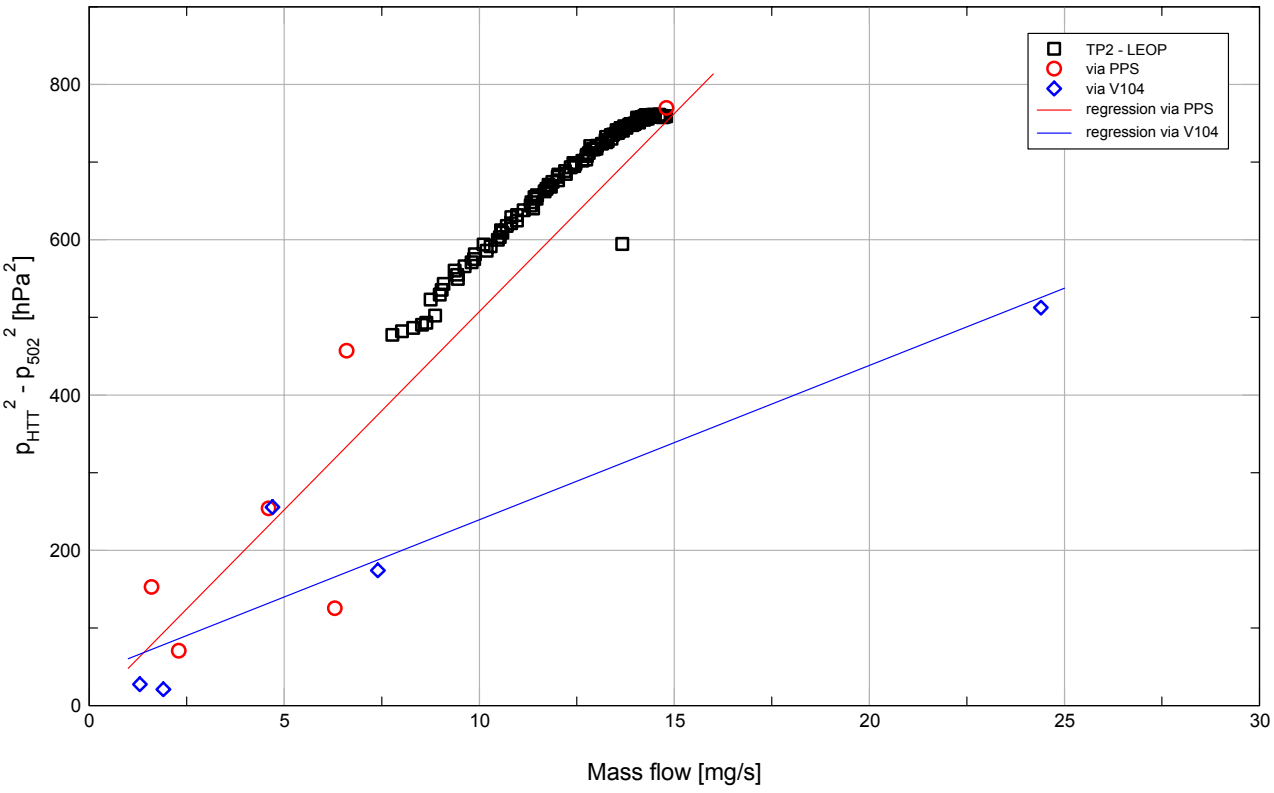

Figure 7.2-1: Pressure drop measured values

The pressure drop measurements listed above are shown in **Figure 7.2-1** in the squared pressure difference form, together with measurements taken during the LEOP phase while venting through the PPS and the large nozzle. It is obvious that significant deviations exist wrt the linear behaviour as indicated by the stroked lines which were calculated as linear trends of the measurement data for venting via the PPS or via V104, respectively.

The measured data are compared to analytical results in **Table 7.2-2**, where the mass flow and pressure drop is calculated for the measured HTT temperature (and thus the pressure in the HTT as defined by the saturated vapour pressure) and the temperature distribution along the vent line.

The analysis results for the original predictions with nozzle flow factor α_N set to 0.5 (as determined before the TB/TV test, see RD 16) are compared to results obtained with α_N set to 0.65. While mass flow measurements with warm external tubing are represented closer by α_N=0.5, significantly better correlation with the measured values is achieved by setting α_N to 0.65 for cold external tubing. Under these conditions, the measured mass flow deviates from the analysis results by no more than 6% with flow through the PPS (maximum deviation of 13% or 0.2 mg/s for flow through V104).

				α_N = 0.5 (original prediction)						α_N = 0.65 (after model update)					
	Vent path		Temp.	Pressure P502 [hPa]			mass flow [mg/s]			Pressure P502 [hPa]			mass flow [mg/s]		
Ref	HTT	Nozzle	HTT [K]	meas.	anal.	dev	meas.	anal.	dev	meas.	anal.	dev	meas.	anal.	dev
1	V106	big	2.000	14.4	18.8	30%	14.8	14.0	-5%	14.4	15.9	11%	14.8	15.5	5%
2	V106	big	1.745	7.4	6.8	-8%	6.3	5.5	-12%	7.4	5.6	-24%	6.3	5.9	-6%
3	V106	small	2.000	26.9	29.8	11%	4.6	3.5	-25%	26.9	29.2	9%	4.6	4.4	-4%
4	V103/ V106	small	1.799	14.0	15.2	9%	2.3	1.9	-19%	14.0	14.9	6%	2.3	2.4	3%
5	V104	big	1.999	21.5	26.9	25%	24.4	20.2	-17%	21.5	25.3	18%	24.4	24.7	1%
6	V104	small	2.000	26.9	30.6	14%	4.7	3.6	-24%	26.9	30.5	14%	4.7	4.6	-2%
7	V104	small	1.745	12.6	13.1	4%	1.9	1.7	-13%	12.6	13.1	4%	1.9	2.1	13%
8	V103/ V106	big	1.942	15.2	16.7	10%	6.6	7.9	19%	15.2	14.7	-3%	6.6	9.0	36%
9	V104	big	1.862	15.4	14.6	-5%	7.4	6.9	-7%	15.4	13.6	-12%	7.4	8.3	13%
10	V103/ V106	small	1.942	23.1	24.9	7%	1.6	1.8	14%	23.1	24.4	6%	1.6	2.3	46%
11	V104	small	1.862	19.6	19.2	-2%	1.3	1.4	11%	19.6	18.9	-3%	1.3	1.8	42%

Table 7.2-2: Pressure drop measurements in comparison to analysis

For the HOT evacuation measurements, a "re-calibration" of the high pressure sensors P701 and P501 has been performed which provides additional information on the pressure distribution along the vent line. Since the pressure sensors show a significant drift (related to the sensor temperature), reference values had to be used which were measured immediately after or before the respective test. The measurements of P501 and P701 would yield valuable information also for the pressure drop measurements described above, but no

reference data have been acquired in the setup of the pressure drop measurements listed in **Table 7.2-1**. A recalibration with the reference data used for the HOT evacuation did not lead to usable results.

For future pressure drop measurements, the following measurements will be performed in order to get more detailed information on the pressure drop distribution along the vent line.

- Measure the pressure at the Filling Port (i.e. downstream of the PPS valves V103/V106 or the HTT outlet valve V104, respectively)
- Attach a low pressure sensor to the V506 I/F to determine the pressure downstream of the external vent line heater with high resolution
- Use additional precision analogue manometers to check the calibration
- Implement calibration reference measurements before and after dedicated pressure drop measurements, using the HTT saturated vapour pressure and analogue manometers for reference.

7.3 HOT Evacuation Test Evaluation

7.3.1 Background information

In order to avoid potentially catastrophic flooding of the PPS during the initial mission phase, pumping on the PPS has to be started before it is immersed in liquid, which happens at the final engine cut-off during the launcher ascent. According to the baseline scenario, the HOT outlet valve V105 will be open throughout the mission. The HOT contains gaseous helium at ambient pressure before launch which has therefore to be evacuated during the launcher ascent to achieve a pressure below the HTT (saturated vapour) pressure before opening of the PPS shut-off valves V103/V106.

7.3.1.1 Available time span

Following lift-off at t=7 s, the pressure under the Ariane fairing decreases rapidly and has reached a level of < 500 mbar after approx. 50 s, followed by fairing jettison at 183 s. According to the Ariane A5-ECA DCI, the engine cut-off command is sent at t=1494 s. For ISO, the external valves were opened only 53 s after fairing jettison, and the PPS shut-off valves were opened 254 s before engine cut-off in order to allow safe PPS start-up.
As soon as the pressure under the fairing has decreased below ~500 mbar, the safety valve SV521 (opening pressure difference <460 mbar) opens and releases gaseous He to the environment under the fairing. For Herschel, the external vent line valves V501 / V503 will be opened already at this point. Considering the PPS start-up time as used in ISO and the external valves opening at 50 s, the available time span for evacuation of the HOT is thus 1190 s.

7.3.1.2 Final HOT pressure and measurement criterion

Since a (gaseous) helium mass flow from the HTT to the outside shall be enforced before the PPS is immersed in liquid, the pressure that has to be reached at the PPS valves before these are opened depends on the pressure in the HTT, which is directly linked to the HTT bath temperature by the saturated vapour pressure, see **Figure 7.3-1**. The baseline for the POC operation is to provide an initial HTT temperature of

1.8 K for the launch autonomy, which results in a minimum HTT temperature of 1.827 K (CDR analysis) at nominal launch, relating to 18 mbar in the HTT. The **pressure to be reached in the HOT** before opening of the PPS valves is therefore selected to **15 mbar** to guarantee a positive pressure drop across the PPS.

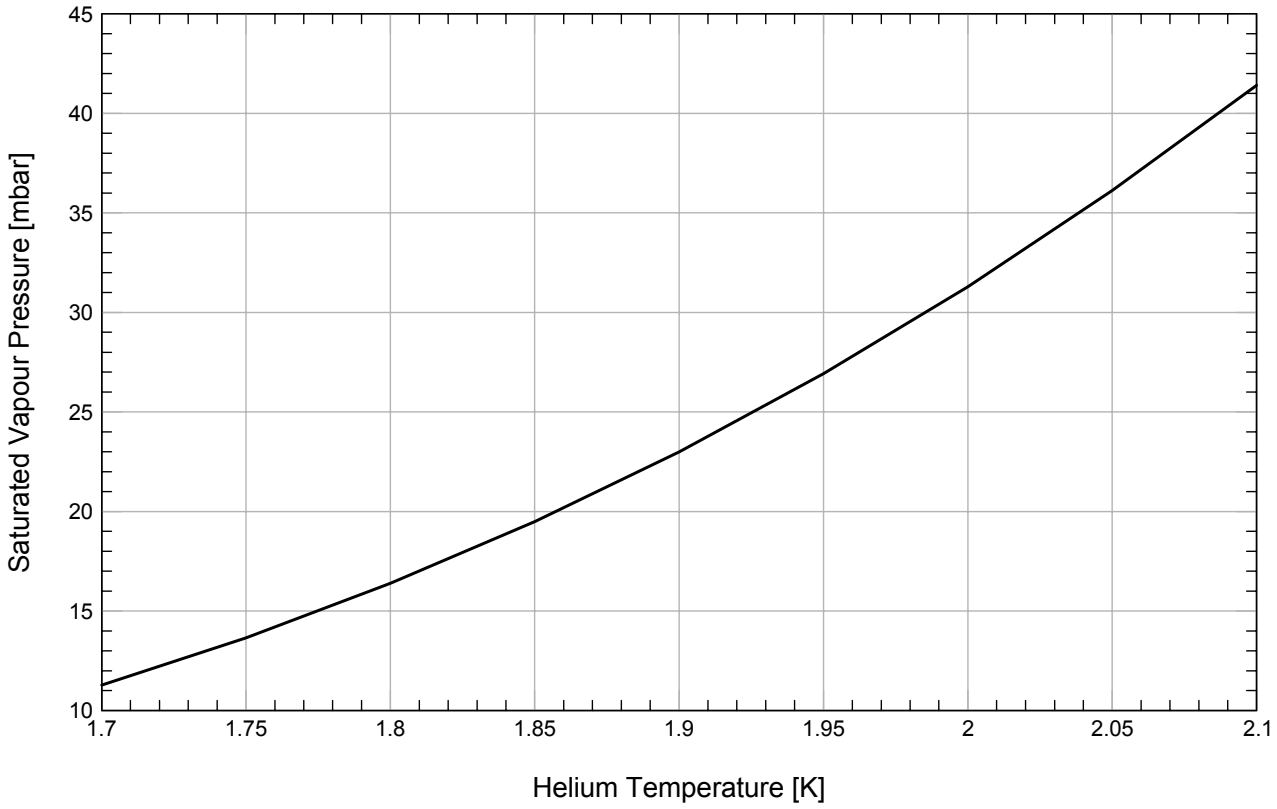

Figure 7.3-1: Helium saturated vapour pressure

The pressure sensor P701 located directly on the HOT is a high pressure sensor, mainly used for nominal He I operations and does not provide a high resolution for measurement of low pressures around 15 mbar. The original calibration curve for this sensor led to out-of range values before the target pressure in the HOT was reached. Therefore the pressure measured at the external vent line was used as reference for the HOT pressure during the tests. The pressure drop between the HOT and the pressure measurement pick-up point has to be considered. During the first HOT evacuation test, the evacuation was performed until an external vent line pressure of 9.5 mbar was measured before the external vent line valves were closed. After closure of the valves, the external vent line pressure rose by 2.3 mbar to 11.8 mbar. Considering the relative volumes of the HOT and the tubing, it is assumed that the pressure in the HOT was ~11.8 mbar when the external vent line valves were closed, see **Figure 7.3-2**. The difference of 2.3 mbar therefore has to be considered, resulting in a **pressure of 12.7 mbar that has to be achieved at the nozzle inlet of the external vent line** which was considered sufficient to guarantee a maximum pressure of 15 mbar in the HOT.

Figure 7.3-2 also shows P701 measurement data as achieved after the test by adjustment of the original calibration curve to the reference value measured in the external vent line after closure of the pump inlet.

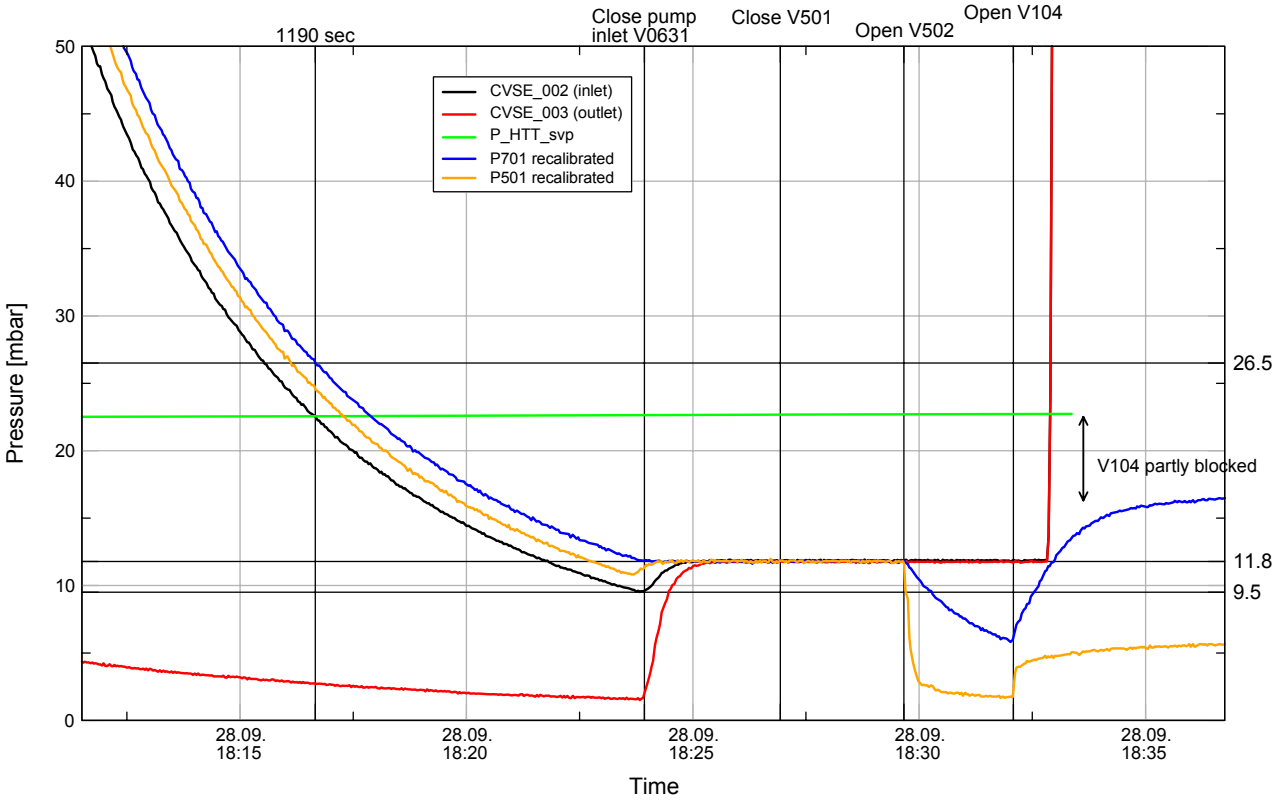

Figure 7.3-2: Pressure relaxation after closure of pump inlet valves during HOT evacuation 1

7.3.1.3 Pressure sensors setup

The first calibration curves used for the CVSE sensors during the HOT evacuation test 1 was a simple linear equation. The detailed calibration curve as determined at the ASED calibration facility was implemented before the HOT evacuation test 2 (on 02.10.05 14:30).

The set-up of the cryo vacuum service equipment (CVSE) including its sensors had to be modified before starting the TB/TV test with TP1, implementing 10 m long capillary tubes (4 mm diameter) to connect the measurement points to the CVSE sensors located in the LSS basement outside the chamber. The set-up used throughout the test is shown in **Figure 7.3-3**.

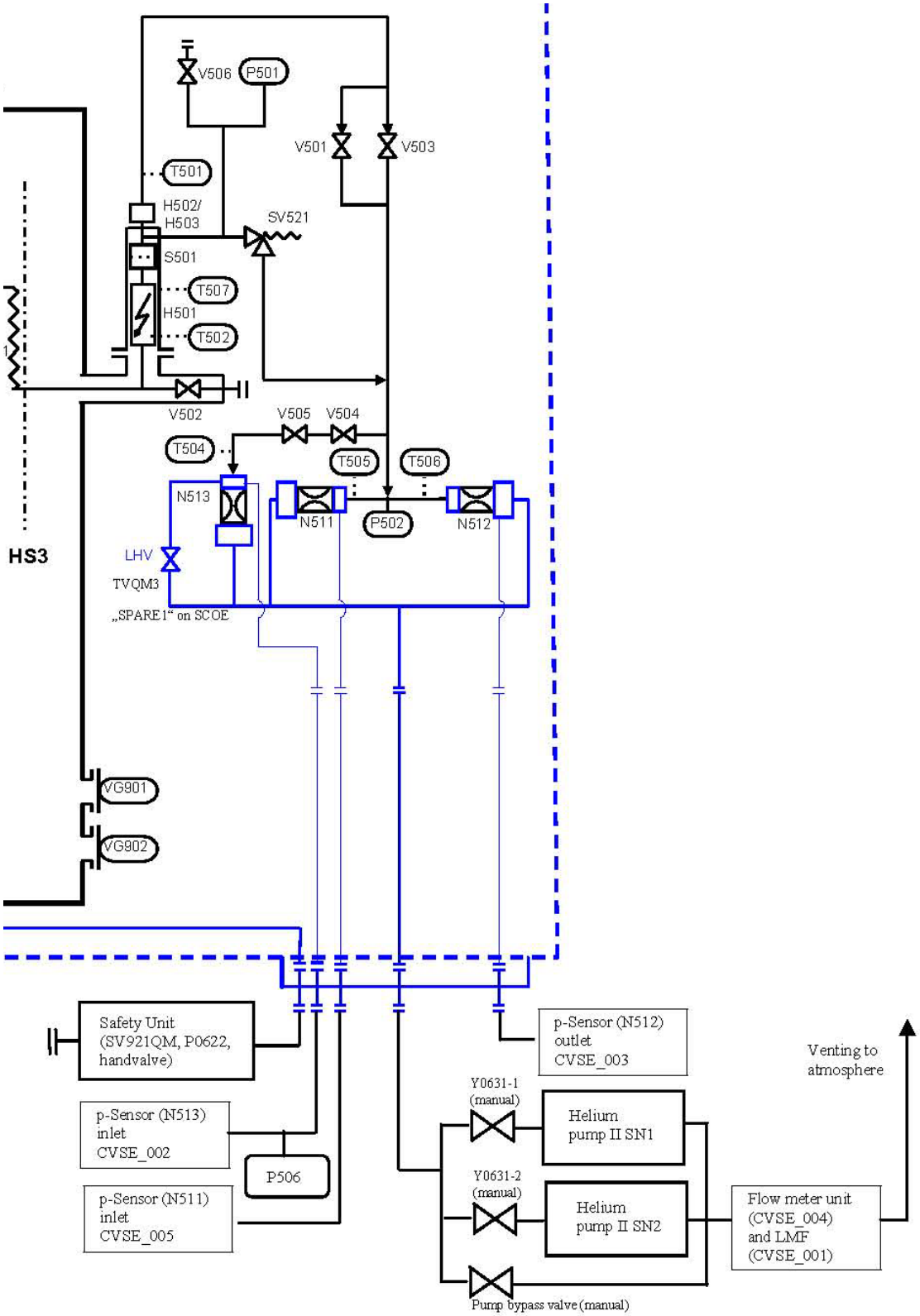

Figure 7.3-3: CVSE setup during TB/TV test

The flight pressure sensor **P502** which measures the pressure in the external vent line near the inlet to the small nozzles was not available during the HOT evacuation tests 1 and 2 due to a problem with the electrical connections, which was resolved before the start of the TB/TV test and the HOT evacuation performed during TP1. At the end of the TB/TV test, an additional reference measurement was performed where the P502 reading was compared to the HTT saturated vapour pressure by closing the pump inlet valves with open V104 and external vent line valves. In this configuration, no pressure drop has to be considered between HTT and external vent line since no mass flow is possible (after an initial relaxation). **Figure 7.3-4** shows the readings of the CVSE pressure sensors together with the saturated vapour pressure in the HTT (calculated from average DLCM temperature measurements) and the original P502 reading. It was found that the P502 calibration resulted in a pressure reading which is 2.97 mbar too low. At the same time, an additional reference point for the high pressure sensor P501 was taken. Note also the difference between the HTT saturated vapour pressure and the pressure readings of the CVSE sensors, which indicates a disagreement of ~5 mK or 0.3 mbar between the pressure and temperature measurements.

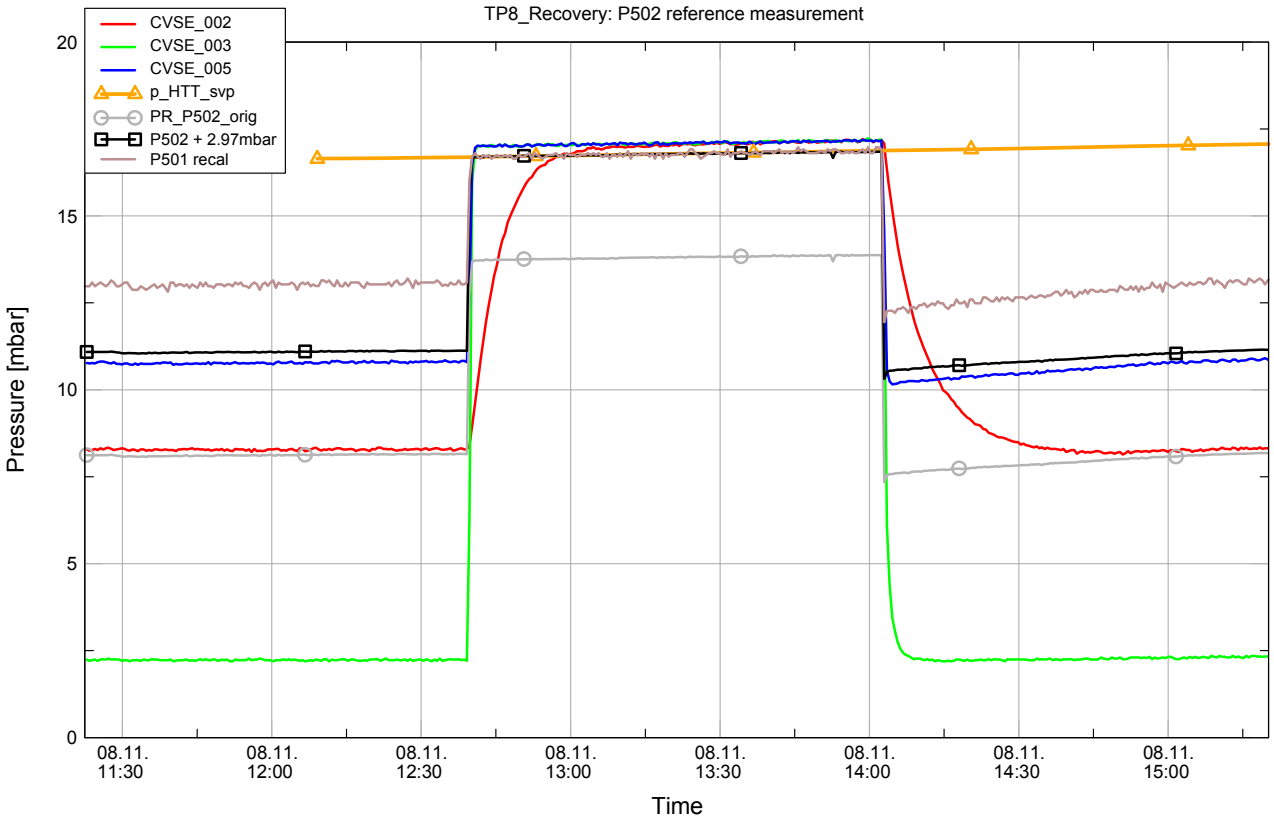

Figure 7.3-4: Reference measurement for P502 calibration with HTT saturated vapour pressure

In the detailed test evaluation, the **P701** raw data acquired during all three tests have been re-analysed and recalibrated with reference measurements gained after these tests. Although the calibration data are not consistent for all three tests due to a small drift (probably caused by temperature dependency), they can be used to achieve additional information for the individual test if only the reference data at the end of this test are used for the calibration. The resulting direct measurements of the HOT are considered to be reliable enough for a detailed evaluation. The recalibrated P701 measurements indicate a higher HOT pressure near the end of the evacuation sequence than extrapolated from the external vent line pressure measurements. Based on these measurements, the **evacuation of the HOT to 15 mbar is not possible** with the current baseline set-up.

7.3.1.4 Tests overview

The evacuation of gaseous helium at 1 bar initially from the HOT, which will be performed during the launcher ascent phase, has been tested in total three times during the STM campaign.

In the first test, the evacuation duration was 1441 s to reach a value of less than 12.7 mbar in the external tubing, indicating a pressure of less than 15 mbar in the HOT. It was decided to increase the target temperature for the HOT heating phase from 50 K as performed during the first test to 55 K in order to accelerate the evacuation.

The second test performed with this initial HOT temperature resulted in an evacuation duration of 1326 s.

Before the third test, the diameter of the large nozzle was increased from 2.2 mm to 3.3 mm. In addition, the measurement set-up had to be changed as described above. The third test was then performed during the initial phase of the TB/TV test (TP1 - Launch Autonomy) with a HOT heating target temperature of 55 K.

These tests are described in detail in the following sections.

7.3.2 HOT Evacuation Test 1

This test was performed before the TB/TV test to assess the feasibility of the HOT evacuation with the planned timeline in order to reproduce the planned launch autonomy scenario in the TB/TV test as closely as possible, see RD08, RD10, RD13. The target pressure to be reached at the PPS outlet prior to opening of the PPS valves is 15mbar, which is below the expected HTT pressure.

Table 7.3-1 shows the detailed sequence of events including operation of manual valves as recorded during the test.

For a detailed evaluation of the test, the data measured with the high pressure sensors P701 and P501 in the HOT and at the exit of the vent line heater unit, respectively, have been compared to the measurements of the CVSE sensors after closure of the pump inlet valve (time stamp 28.09.2005 18:28), and the conversion law was adjusted to yield the same pressure. In addition, the P501 conversion law has been adjusted to give the same P501 pressure reading as measured by P701 before opening of the pump inlet valve (time stamp 28.09.2005 17:54). While this adjustment of the calibration curve is valid only for the HOT evacuation test 1, and the absolute value of P701/P501 around 1 bar is not confirmed by other measurements, it gives valuable information on the pressure drop between the HOT, the outlet of the vent line heater unit and the nozzles inlet. **Figure 7.3-9** shows the pressure histories measured with the high pressure sensors in the HOT and on the external tubing (P701 and P501, after re-"calibration" as described above) and with the ground support low pressure sensors. A detailed view of the pressures near the end of the HOT evacuation test 1 is given in **Figure 7.3-2**.

As can be seen at the end of the test, the pressure in the HOT stays significantly below the HTT saturated vapour pressure after opening of the HTT outlet valve V104, with pumping on the opened V502. This indicates a partial blockage of V104 at that time.

A total time of 1477 sec for evacuation of the HOT to the required pressure was measured during this test. During the launcher ascent phase, only a time span of ~1190 sec is available for the evacuation of the HOT; the HOT pressure reached after this time is 26.5 mbar.

Time	Event	Time since opening of pump inlet
15:23:00	Initial conditions, HOT at 18K, evacuated, pumps connected and valved off Valve states: all HTT valves closed V105 and V102 closed, V701 open All external ventline valves open, nozzle bypass valve closed	
15:24:00	Start of HOT pressurization from supply dewar, warm GHe heats HOT	
17:20:00	Start heating HOT (from 43K)	
17:28:40	50 K reached by T704, H701 switched off. T701 reads 45K	
17:32:30	T704 dropped to 46.5 K, H701 switched on again	
17:47:00	pressure ratio of P701 (current/at V501 closure) reaches 50/45, H701 switched off	
17:47:06	End of HOT heating (logbook)	
17:47:06	End of HOT heating (SCOE)	
17:55:00	short mass flow peak (pump start-up)	
17:57:06	open pump inlet	
17:57:00	first response of P501 and P701	
17:57:13	beginning of continuous mass flow (via SV512)	
18:01:02	open V501	
18:01:00	bend in P501 and P701 curve	
18:03:51	switch to 500mg/s mass flow meter	
18:19:43	15 mbar at CVSE_002 (updated correlation)	00:22:37
18:21:07	12.7 mbar at CVSE_002 (updated correlation)	00:24:01
18:23:46	9.5 mbar at CVSE_002 (updated correlation)	
18:26:06	V0631 closed	
18:27:06	V501 closed	
18:27:00	11.8 mbar at CVSE_002 (updated correlation)	
18:32:06	V104 opened	

Table 7.3-1: HOT Evacuation Test 1 sequence of events

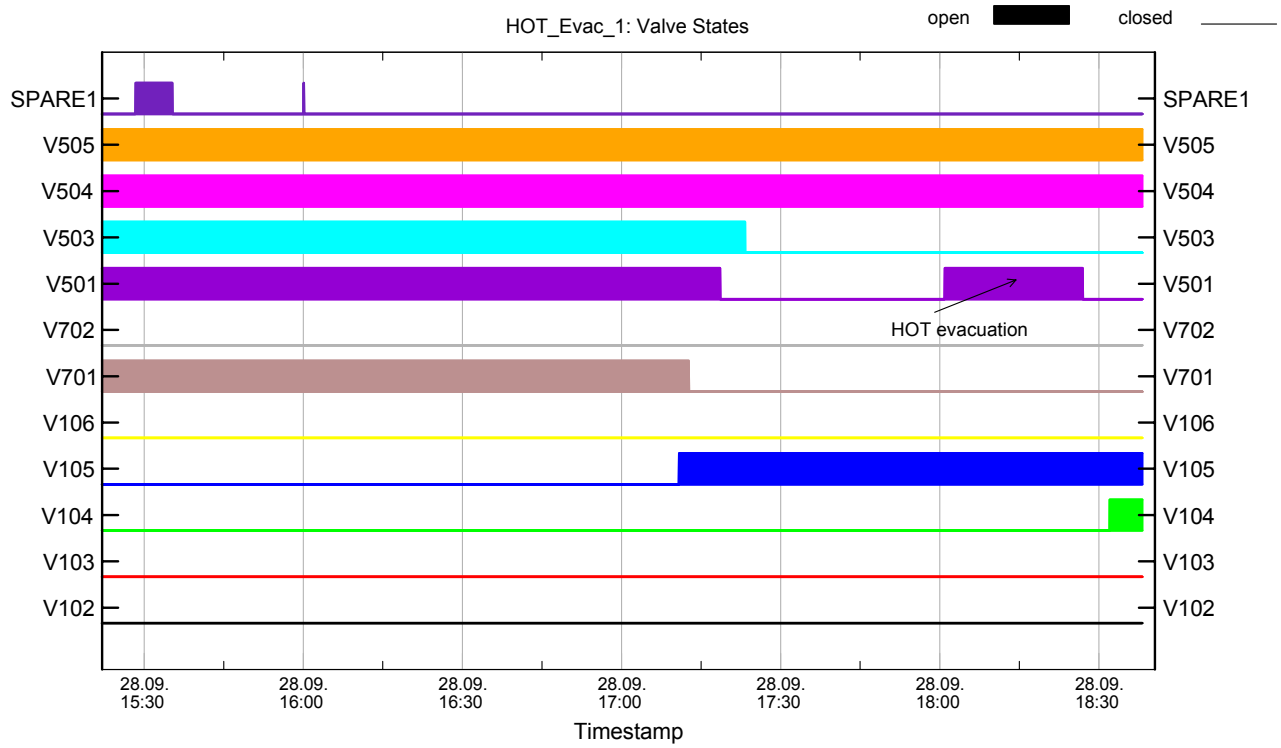

Figure 7.3-5: LHV states during HOT evacuation test 1

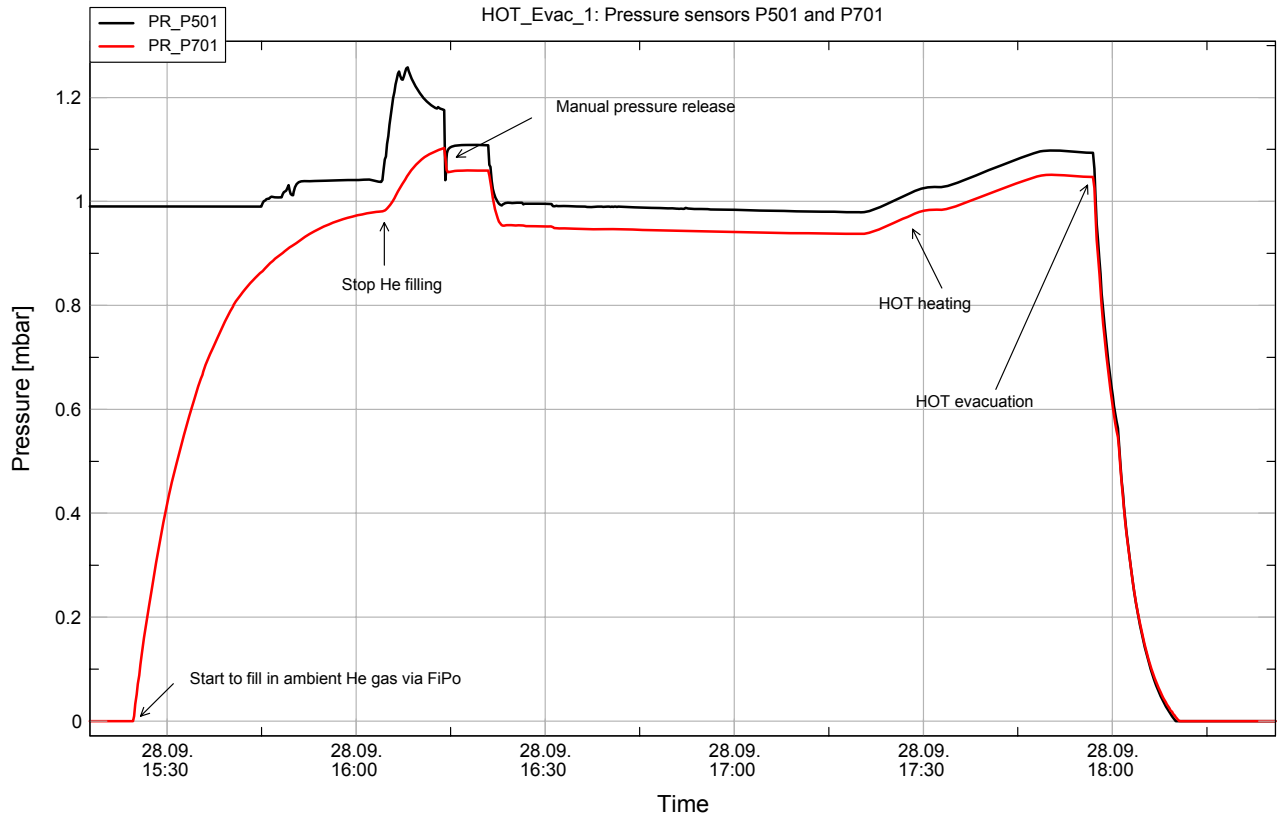

Figure 7.3-6: HOT and external vent line pressure during HOT evacuation test 1 (1bar sensors)

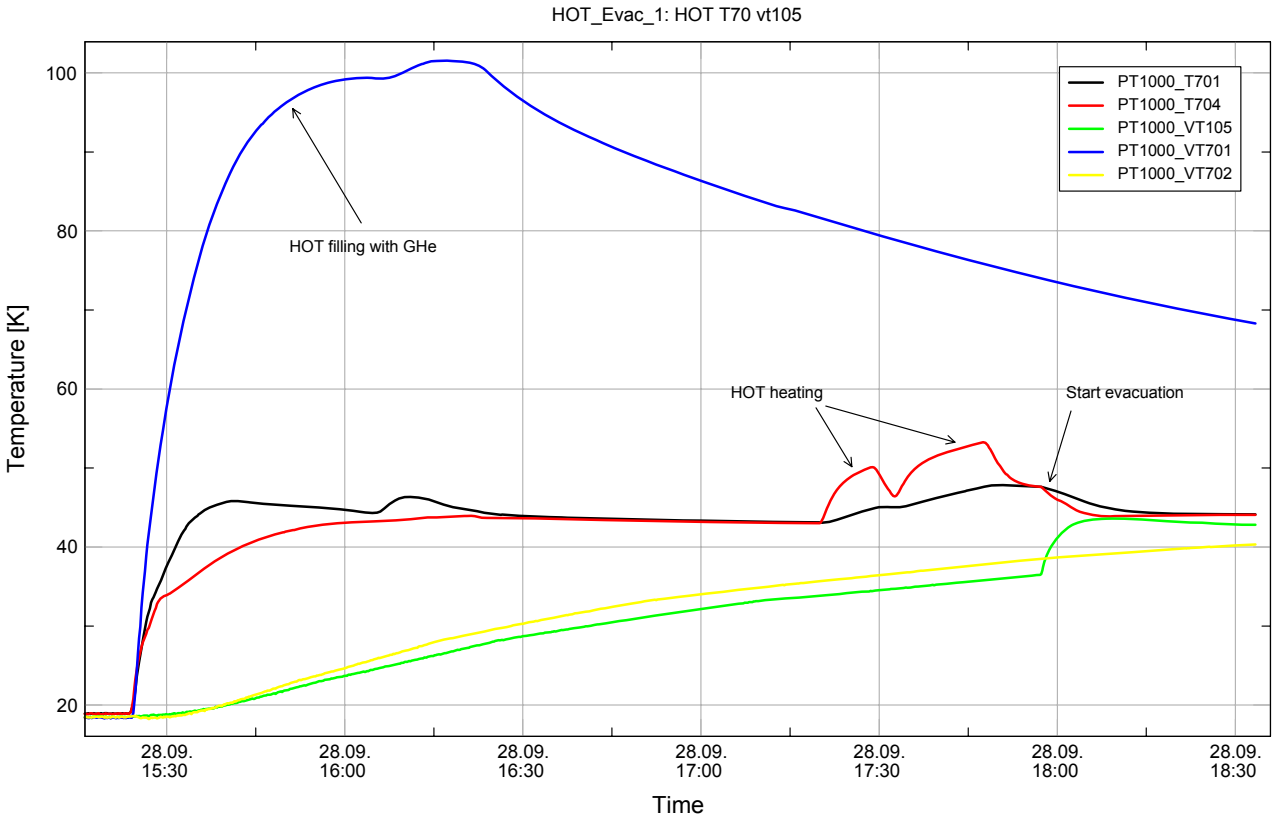

Figure 7.3-7: HOT temperatures during HOT evacuation test 1

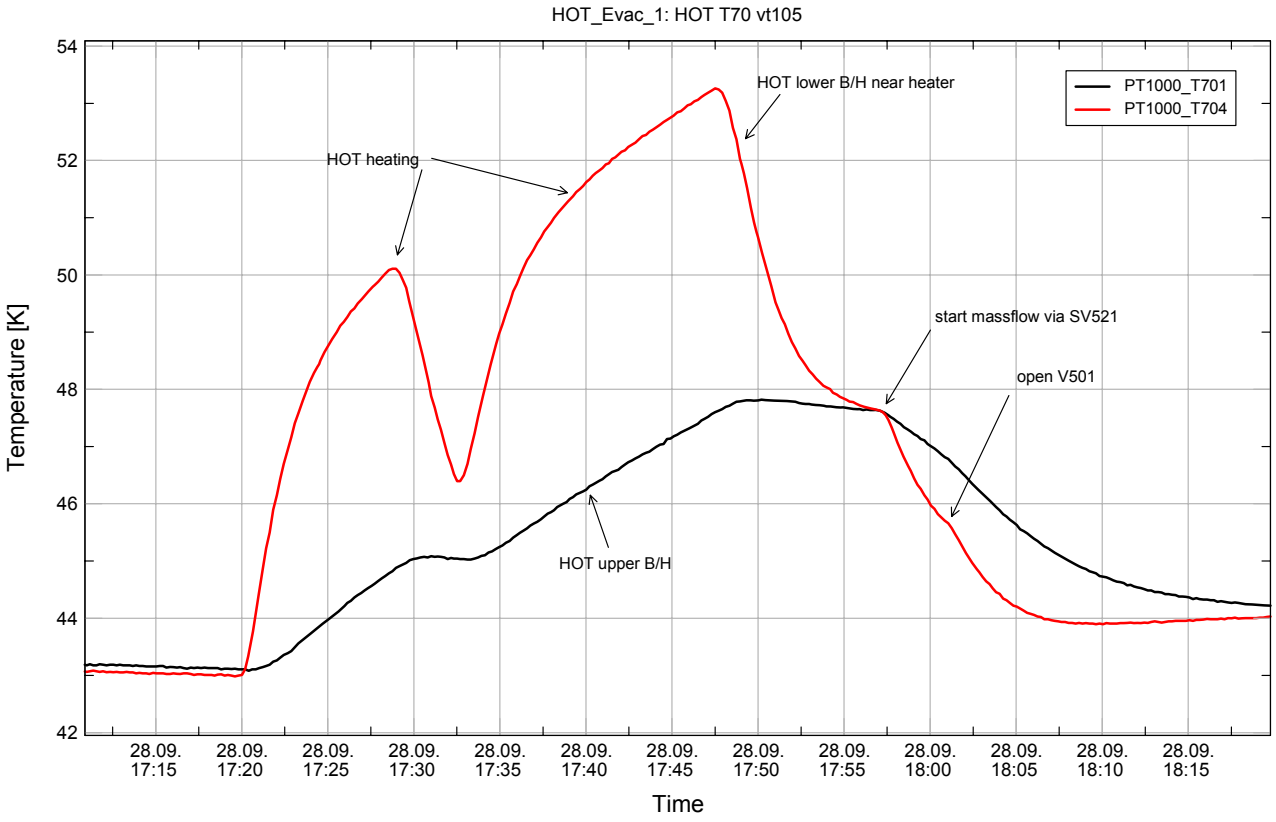

Figure 7.3-8: Detailed HOT temperatures during evacuation test 1

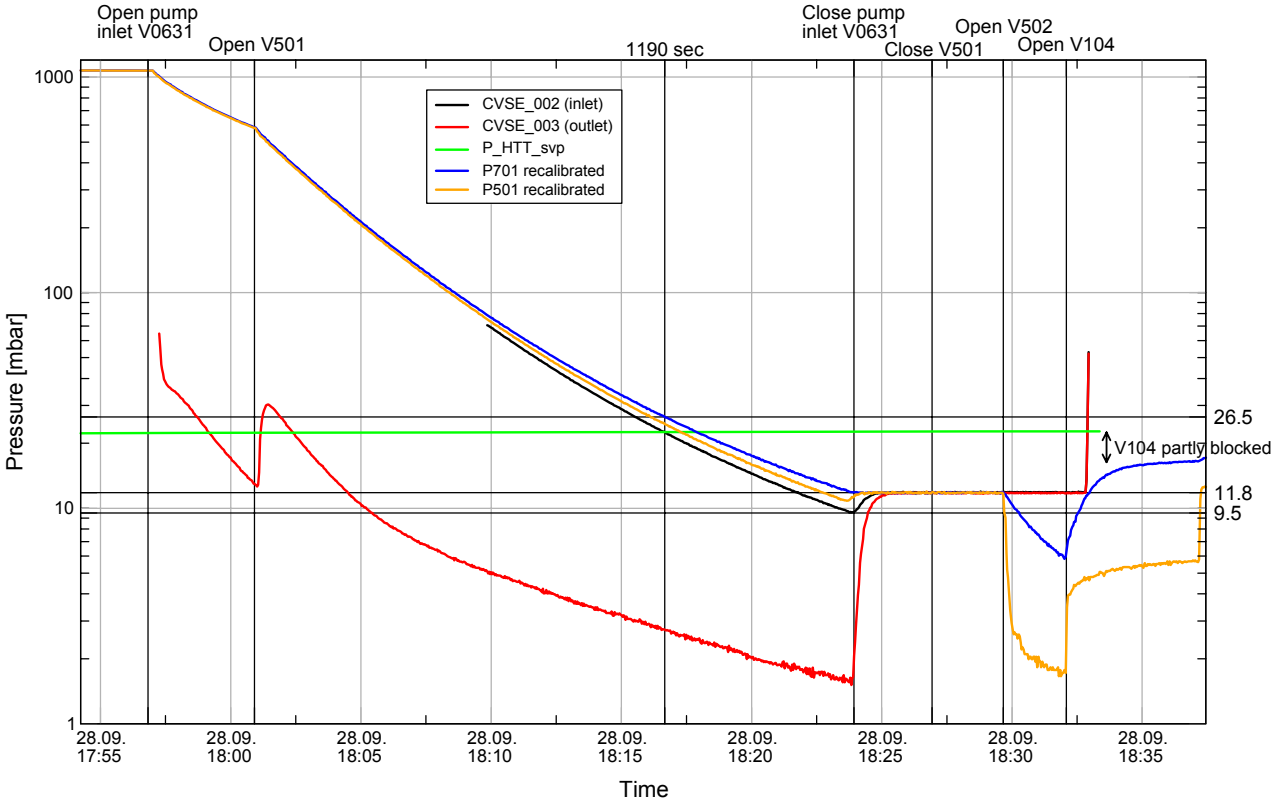

Figure 7.3-9: Pressure during HOT evacuation test 1

7.3.3 HOT Evacuation Test 2

The 2nd HOT evacuation test was performed with higher initial HOT temperature with the goal to reach the allowable pressure within the time frame that will be available during launch, see RD12, RD14.

The HOT was heated up to 55 K and the external vent line valves were closed. From these initial conditions, the pump inlet valve was opened, followed after 15 sec by the external vent line valves. Only 1326 sec after pump inlet opening, a nozzle inlet pressure of 12.3 mbar was reached, which was the criterion defined before the test. Detailed test evaluation and re-"calibration" of the P701 pressure sensors reveals that the pressure in the HOT reaches a value of 15 mbar after 1375 sec evacuation time, as shown in **Figure 7.3-14** and **Figure 7.3-15**.

The integrated helium mass flow meter readings indicate that a total helium mass of 85.5 g was vented during the HOT evacuation, whereas the 80 ltr HOT at 55 K and 1 bar only accounts for 70 g of gaseous helium. The remaining He mass of 15.5 g is located in the tubing, mainly in the cold HTT tubing, where a temperature of 4.22 K has to be assumed to account for the measured He mass.

The sequence of events is described in the following **Table 7.3-2**:

Time	Event
Mon, 03.10.05:	
13:52	V105 heating started
14:06	V105 heating stopped, VT105 is 75.2 K
Tue, 04.10.05:	
07:30:00	995 mbar on analogue manometer
07:34:00	H701 switched on
07:55:00	continuous manual venting until closure of V501
09:06:00	V501 closed
09:17:00	H501 heated with 20W to raise T507 to 288K
09:33:00	H701 switched off
09:30:00	Pump inlet valve is closed, outlet connected to mdot meter, mdot reads 18mg/s air ballast (corrected after this test).
09:46:00	open pump inlet valve (wrist watch, ~2min offset against SCOE)
09:46:15	open V501 (15 sec after pump inlet on stop watch)
10:06:00	1200 sec after pump inlet opening: CVSE_002 reads 14.8mbar, CVSE_005 reads 15.4 mbar
10:07:21	1281 sec after pump inlet opening: CVSE_002 reads 12.7 mbar
10:07:39	**1299 sec** after pump inlet opening: CVSE_002 reads 12.3 mbar
10:07:46	1306 sec after pump inlet opening: CVSE_005 reads 12.7 mbar
10:08:06	**1326 sec** after pump inlet opening: CVSE_005 reads 12.3 mbar
10:16:00	CVSE_002 & CVSE_005 read 8.3 mbar, end of evacuation, pump inlet closed
10:20:00	CVSE_002 & CVSE_003 read 11 mbar, analogue manometer reads 10.9 mbar (relaxation by 2.7 mbar)
10:22:00	V501 closed

Table 7.3-2: HOT Evacuation Test 2 sequence of events

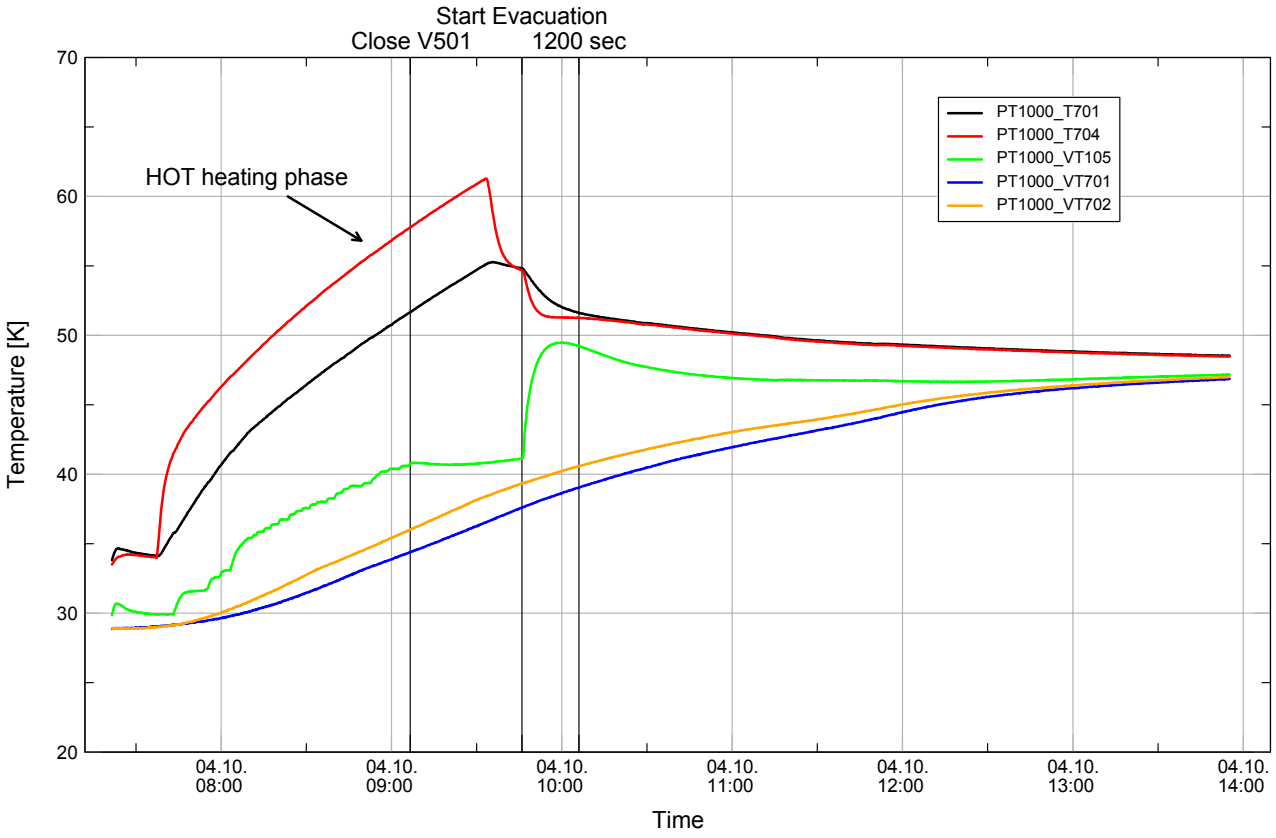

Figure 7.3-10: HOT temperatures during HOT evacuation test 2

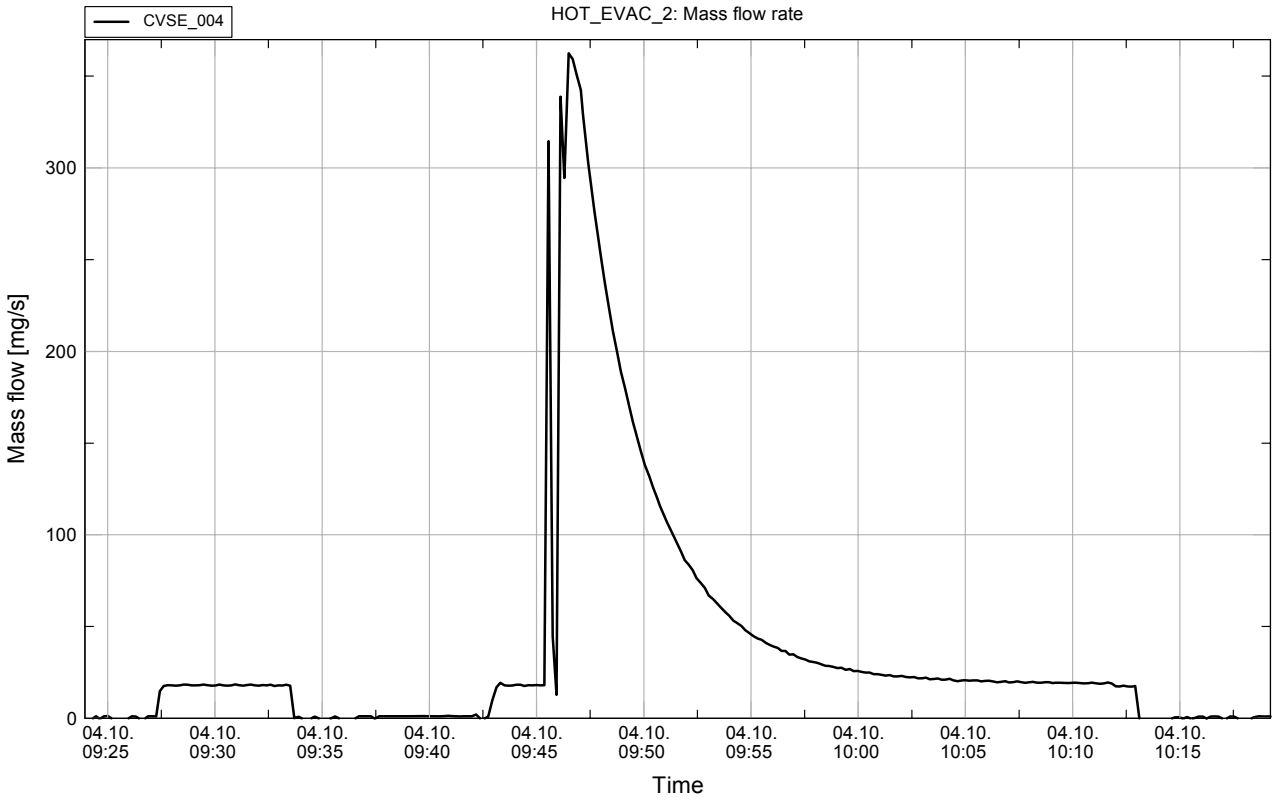

Figure 7.3-11: Mass flow rate during HOT evacuation test 2

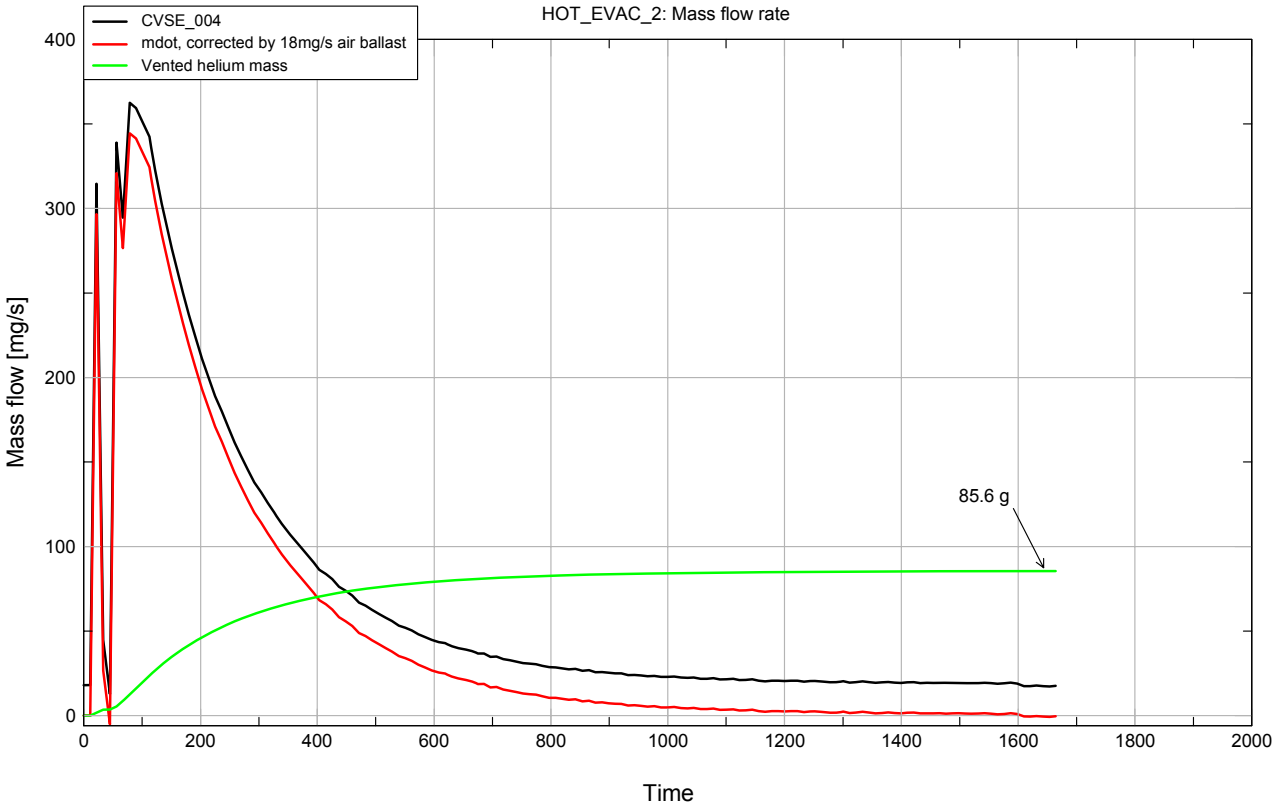

Figure 7.3-12: Vented helium mass during HOT evacuation test 2

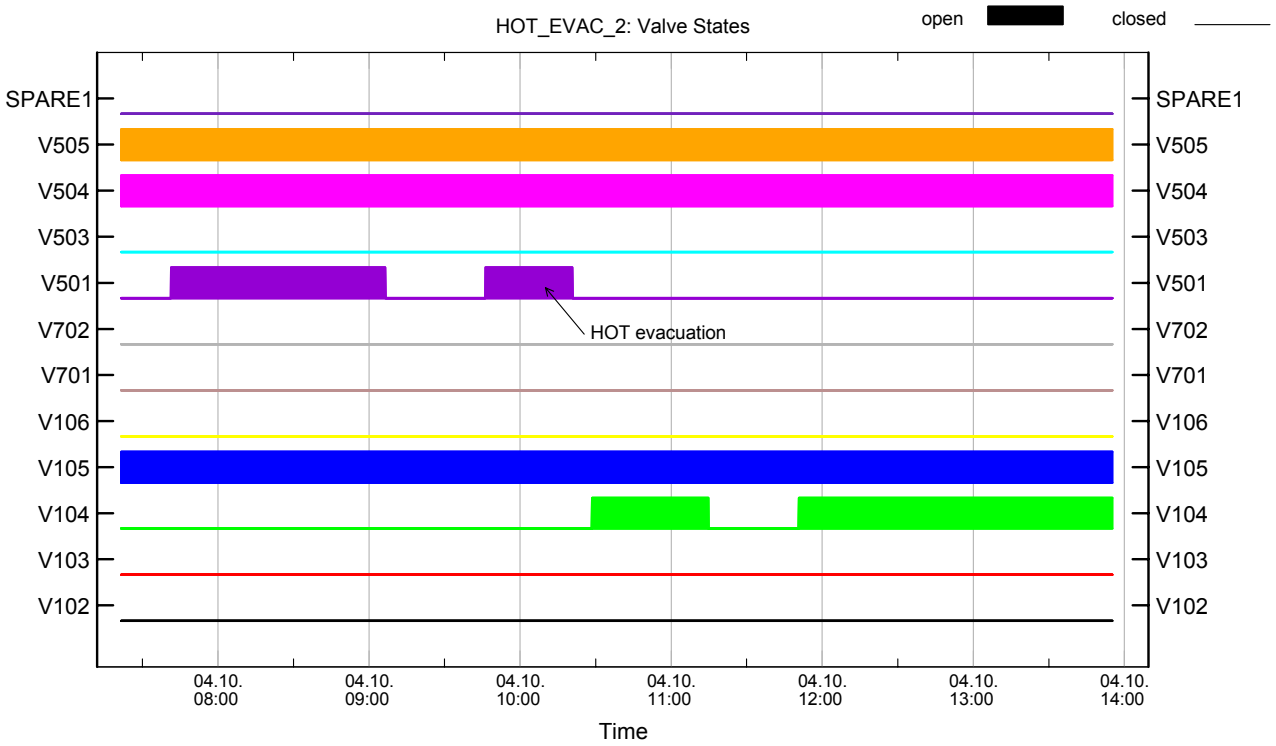

Figure 7.3-13: Electromagnetic valve states for HOT evacuation test 2

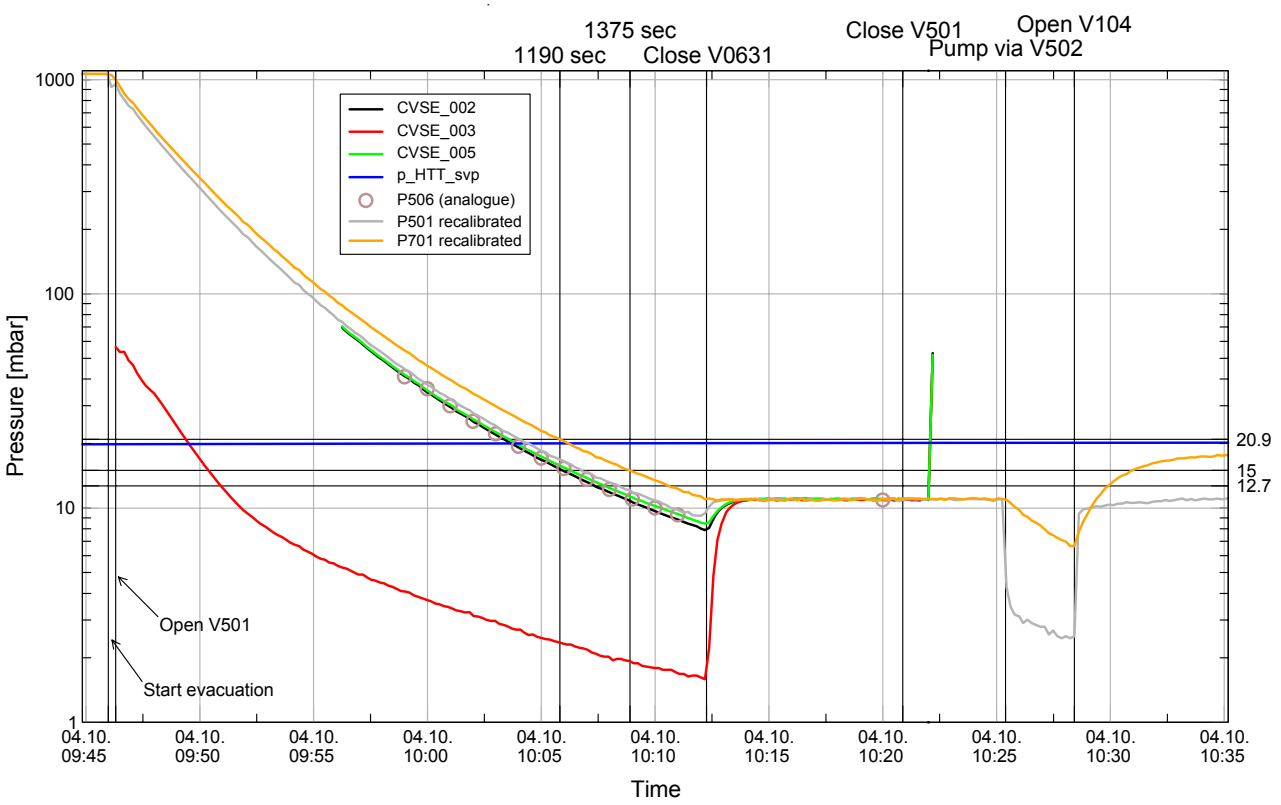

Figure 7.3-14: Pressure evolution during HOT evacuation test 2

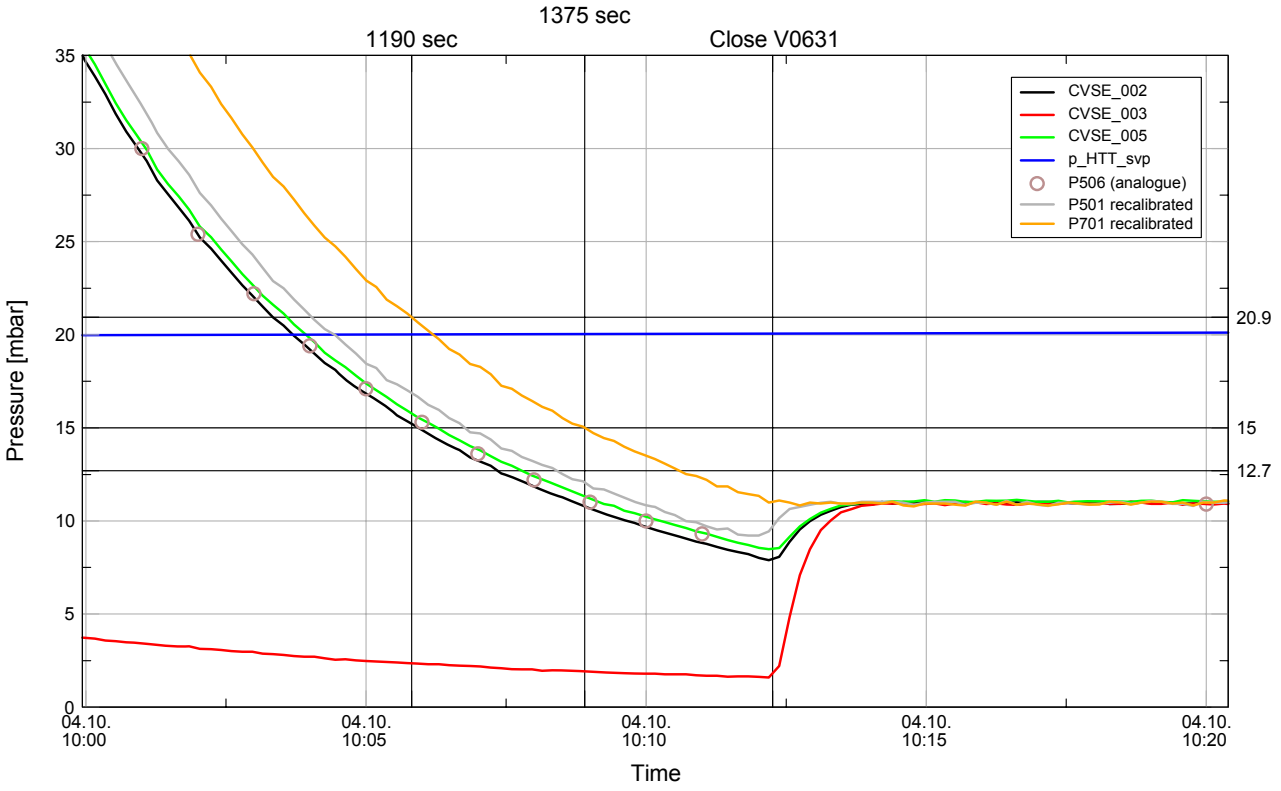

Figure 7.3-15: Pressures at end of HOT evacuation test 2

7.3.4 HOT Evacuation Test 3 during TB/TV Test Phase TP1

Due to the increased HTT heat load detected during the initial phase of the TB/TV test, the originally planned test sequence had to be modified and the HOT evacuation was performed significantly before the end of the Launch Autonomy simulation, i.e. the PPS was not started immediately after the HOT evacuation (covered by PVS 2, see RD01)

Due to the measurements taken in the first and second HOT evacuation tests, the diameter of the large nozzle was increased from 2.2 mm to 3.3 mm before the third test. The diameter of the small nozzles was not changed.

During this test, the integrated mass flow measurement indicates a He mass of ~17 mg which is stored in the He tubing at the beginning of the test (i.e. ~20% of the total He mass to be vented during the evacuation). The measurement does not indicate that significant amounts of liquid He could be stored in the tubing at the beginning of the evacuation sequence.

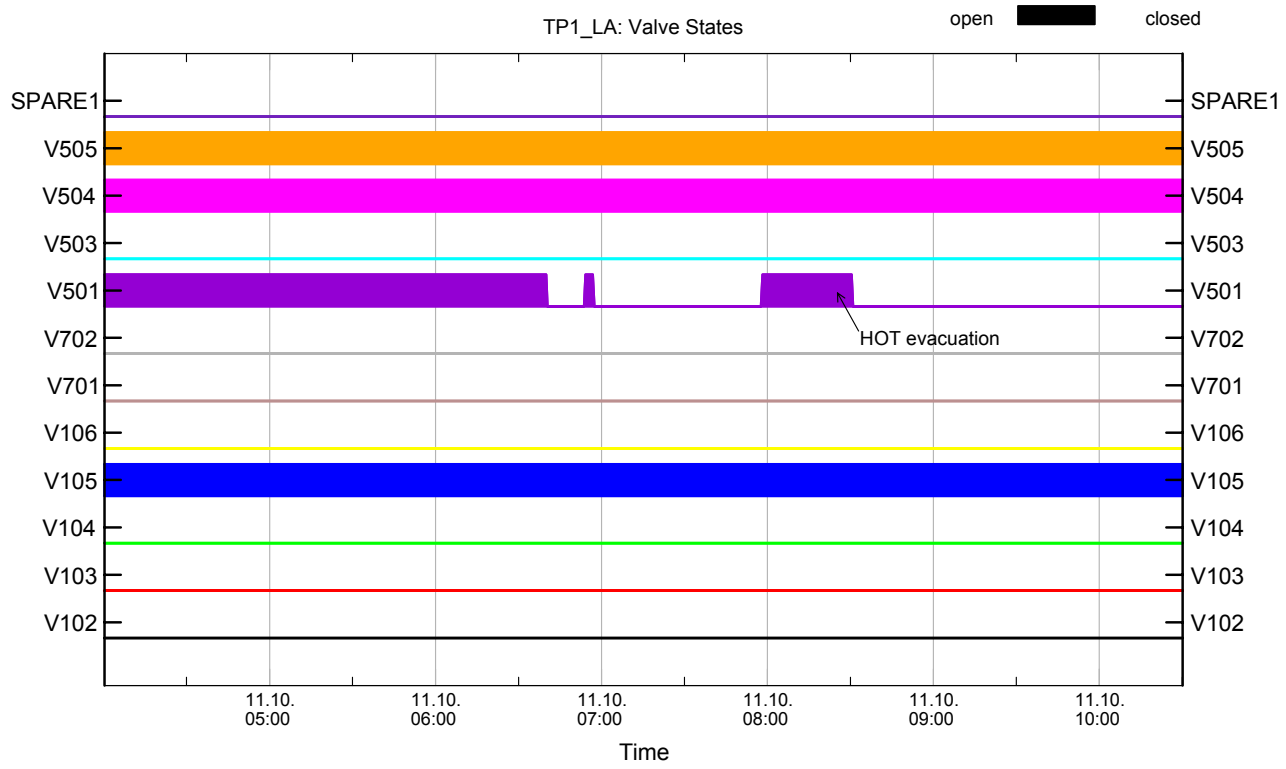

Figure 7.3-16: Valve states during HOT evacuation test 3

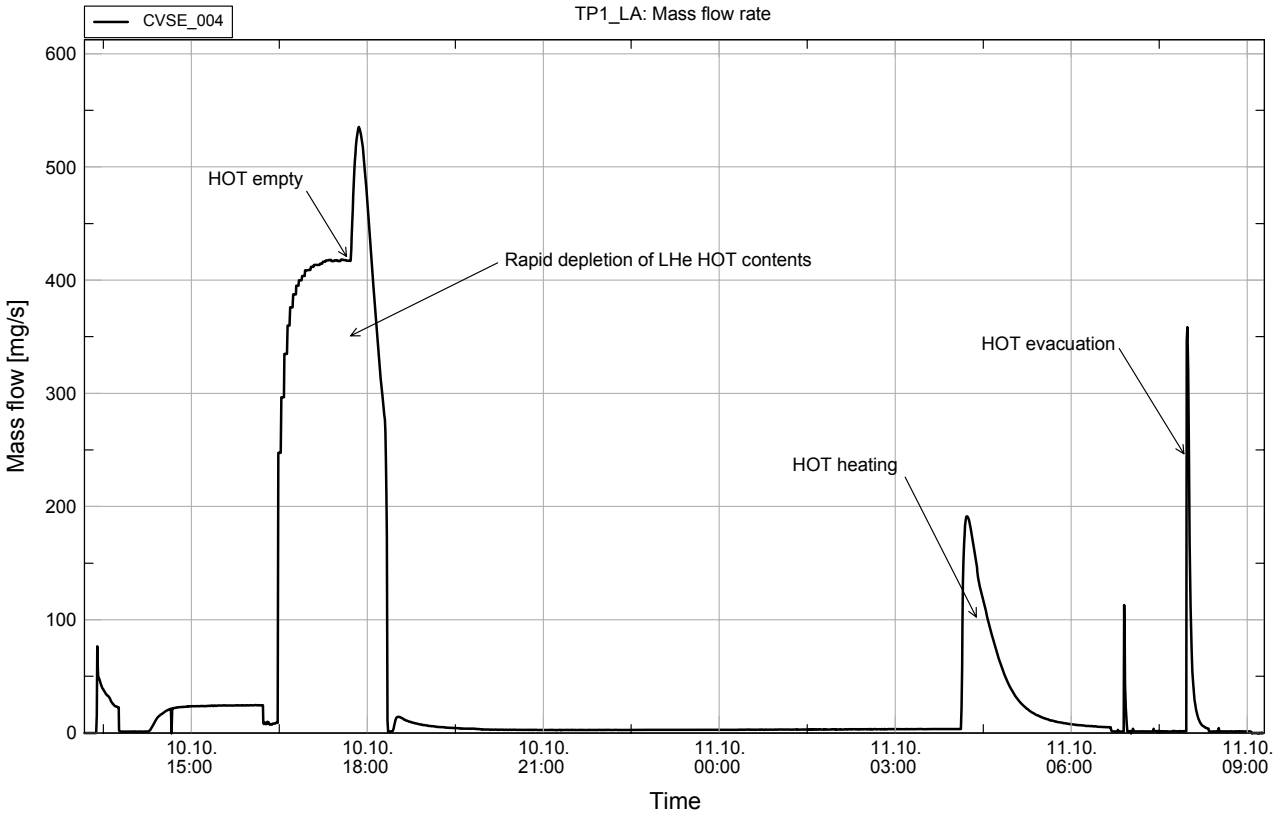

Figure 7.3-17: Mass flow rate during HOT evacuation test 3

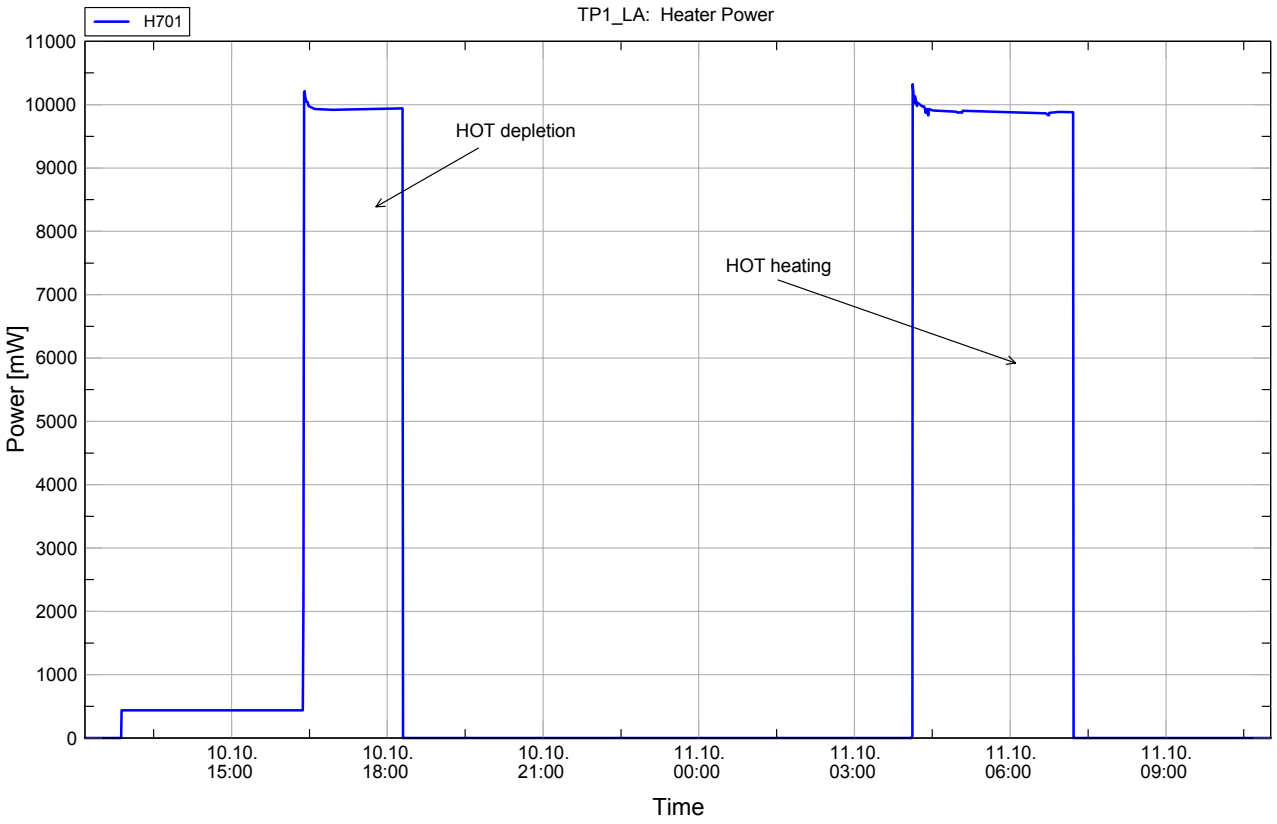

Figure 7.3-18: HOT heater power during HOT evacuation test 3

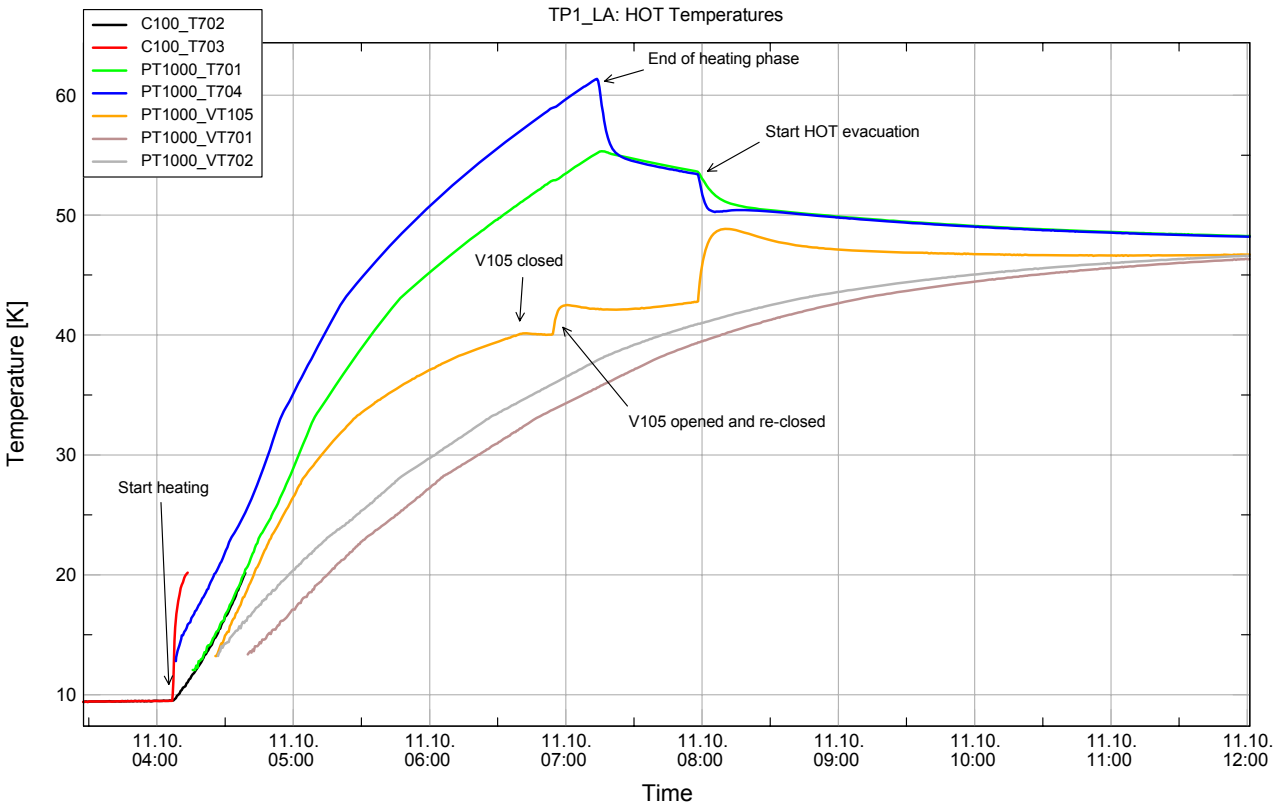

Figure 7.3-19: HOT and valves temperatures during HOT evacuation test 3

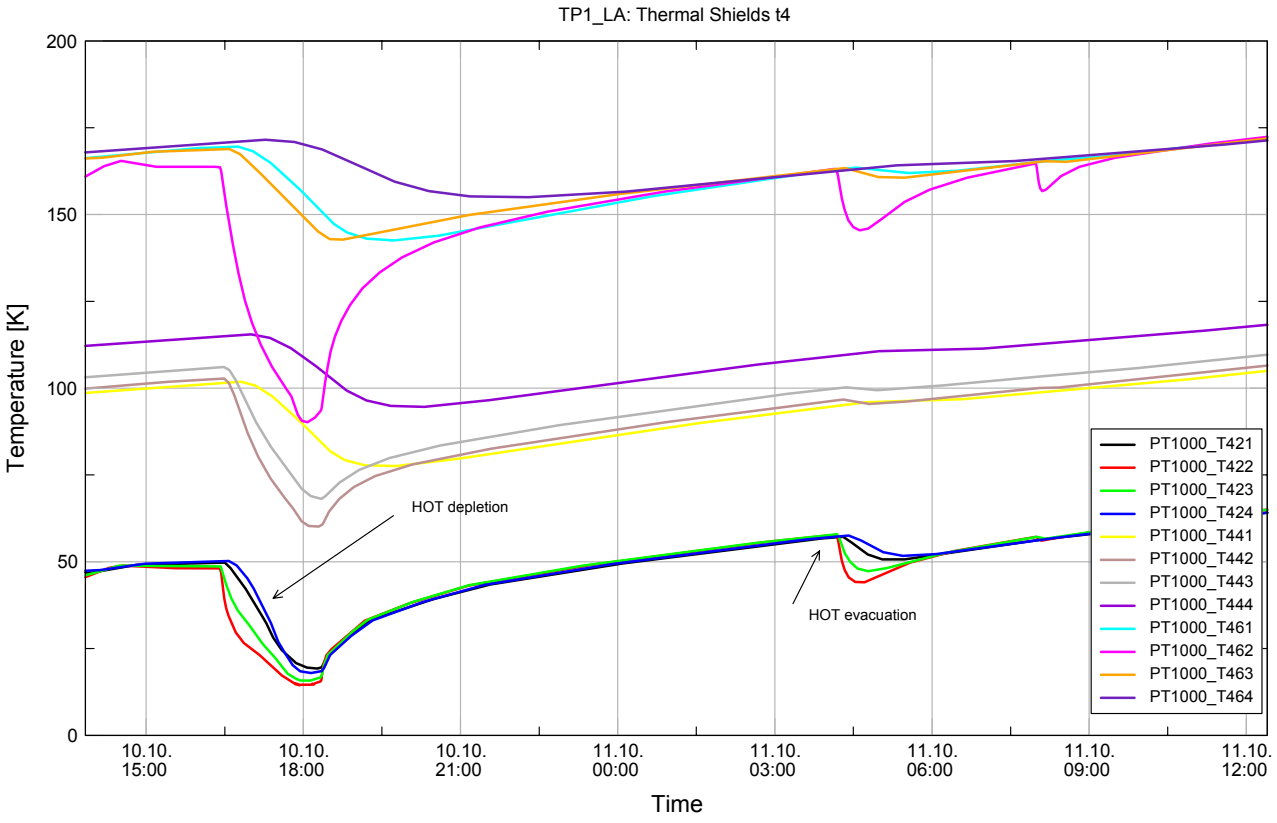

Figure 7.3-20: Thermal shields temperatures during HOT evacuation test 3

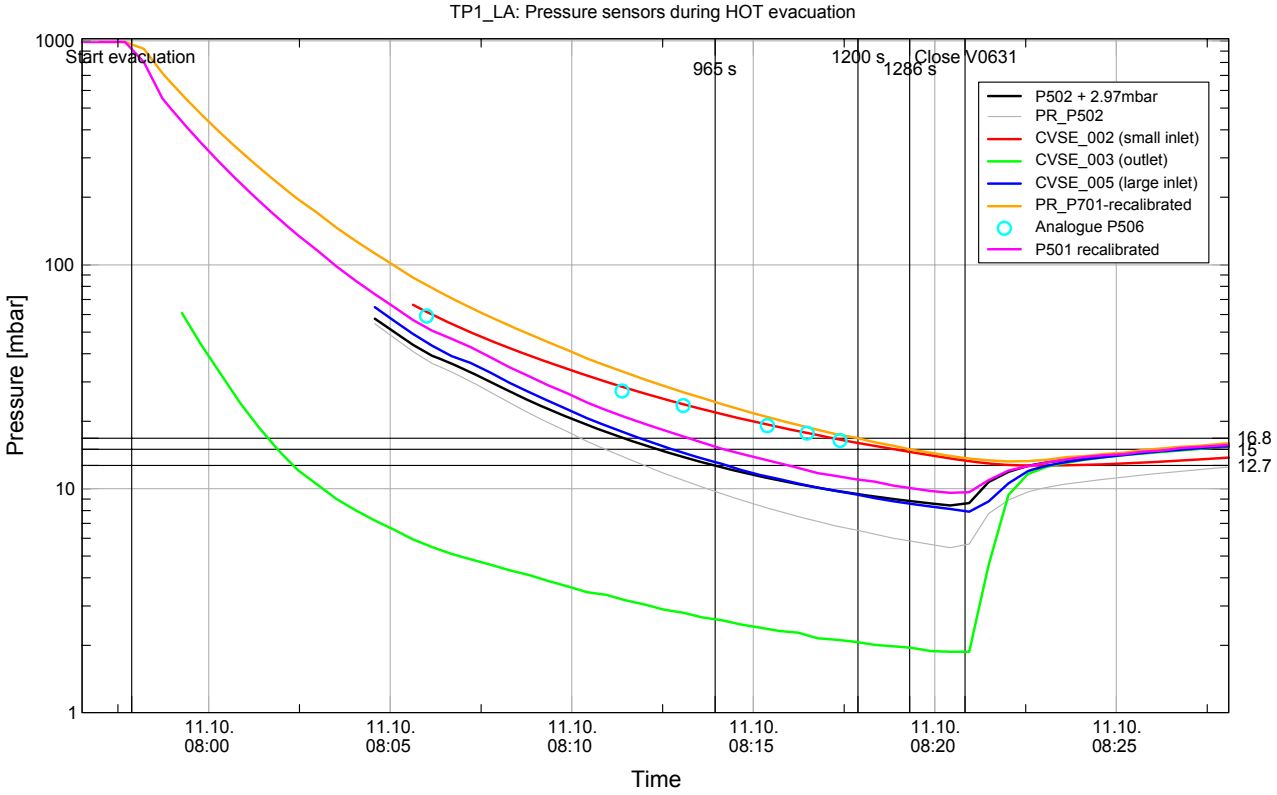

Figure 7.3-21: Pressure evolution during HOT evacuation test 3

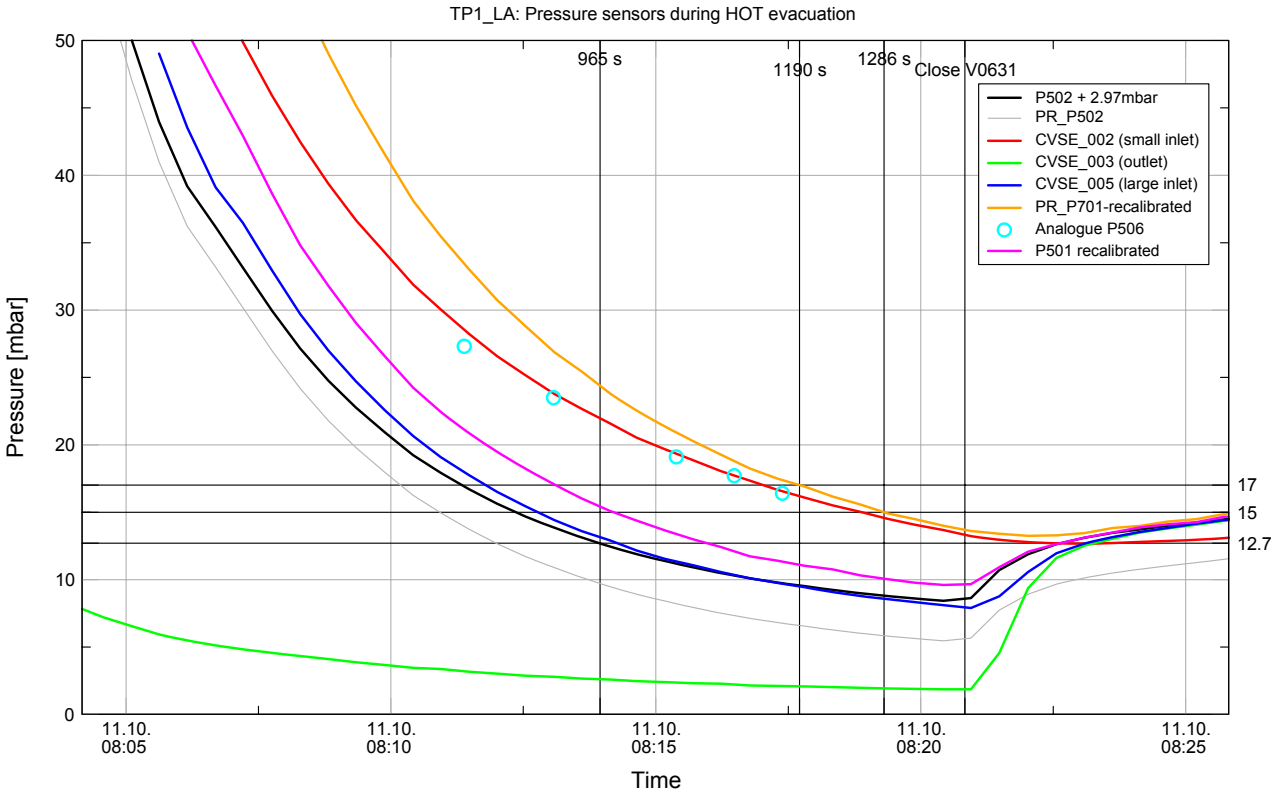

Figure 7.3-22: Pressures at end of HOT evacuation test 3

For the detailed evaluation, the same P501 and P701 calibration curves as for the 2nd HOT evacuation test have been used. As shown in **Figure 7.3-21** and **Figure 7.3-22**, the P701 and P501 measurements are in good agreement with the CVSE_003 and CVSE_005 data after closure of the pump inlet at the end of the evacuation sequence. The pressure increase during this phase is caused by the increase in the thermal shields temperatures as shown in **Figure 7.3-20**

The analogue manometer was installed in parallel to the CVSE_002 sensor measuring the small nozzle inlet pressure. As can be seen in **Figure 7.3-21** at the slow reaction of CVSE_002 to the closure of the pump inlet valve V0631, the measurement volume of the analogue manometer P506, together with the ~10 m long 4 mm diameter pressure pickup line, leads to a significant time delay of the signal.

The re-"calibrated" P701 measurements shown in **Figure 7.3-21** reveal that the pressure difference between the nozzle inlet and the P701 near the end of the evacuation was significantly higher than expected from the first evacuation tests. The criterion of 12.7 mbar at the nozzle inlet, which was used during the test, is therefore not sufficient to guarantee a pressure below 15 mbar in the HOT. The P701 measurements show that after 1190 s evacuation time, the pressure in the HOT was still at 17 mbar, while the threshold of 15 mbar was reached only after 1286 s evacuation.

As mentioned before, the PPS requirements allow a further increase of the large nozzle diameter to enable higher mass flow rates and evacuate the HOT and the helium tubing in a shorter time. In addition, the HOT valves V702 and V701 can be opened before the HOT heating phase, which will also lead to a slight reduction in the required time for evacuation.

8 Sensor Discrepancies

During the evaluation of the test data, following sensor anomalies are detected in addition to the already known anomalies (see section 4 of /RD01/):

- Accuracy of the sensors T246 and/or T252 is questionable (T246 in the range 15-18K about 0.3-0.5 K too high temperature)
- The PPS temperature sensors have an offset wrt the DLCM sensors
- Comparison of DLCM temperature sensors and calibrated CVSE pressure sensors indicates a disagreement between them of ~5mK or 0.3 mbar (by comparison to saturated vapour pressure).
- PT1000 sensors at CVV show about 1.2 K lower temperatures compared to PT100 test sensors
- The pressure sensor P502 shows an offset of -2.97 mbar wrt the CVSE pressure sensors at ambient temperature and 17 mbar absolute pressure.
- P501 and P701 raw data can be used for low pressure (>15 mbar) measurements when reference values at similar conditions (sensor temperature, pressure range) are provided.

9 Lessons Learnt

The following sections give an overview of the lessons learnt during H-EPLM STM TB/TV test campaign. These inputs will be considered in the preparation for the next TB/TV test.

9.1 ITP

- Test harness gets too hot ➔ check whether MLI wrapping is necessary, especially for TTAP/SVM and dedicated PLM heater harness bundles, sensor harness with MLI. Check possible drawbacks!
- Rig support (at least upper bars, heater!) to be wrapped in MLI, additional heater tbc
- Harness thermal anchoring not very efficient.
- Telescope heater to be implemented (n/a for PFM)
- Close circumferential gap between IR rig and HSS
- Burnt foil heaters on CVV, to be checked
- Telescope cover is necessary to protect from particle contamination; check possibility to remove cover with closed LSS lid (or to leave it in during test)
- Tilting: remove bracket on IR rig to increase possible tilt angle. 23° seems hardly achievable with STM experience; rotation of tilt axis might be required. Check tilting requirements from instruments.
- PVS form sheets are not useful, fields are not filled in. In each PVS the step number of the ITP shall be defined after which the PVS shall be executed and those steps which shall be replaced by the PVS shall be defined in the PVS.
- Red-mark position in ITP where a PVS is inserted.
- CVV temperature is highly sensitive to gaps in LSS shrouds. Cover (as far as possible) all gaps in LSS shrouds with MLI, especially where direct view to radiators exists.

9.2 Data Handling

- Assign correctly calibrated channels to all sensors (e.g. mass flow unit with 3 measurement ranges was switched and reconnected)
- Provide colour printer on test floor for SCOE data
- SCOE data handling on Linux workstations needs (more) training for operators before test. Avoid single source skills!
- Use UTC for all equipment clocks (incl. HACS)
- Use common temperature scale for all sensors including LSS shrouds ➔ possibility to show payload temperatures (e.g. CVV minimum temperature) and shroud temperature in one common chart.
- Prepare an excel sheet with all sensor acronyms (TDH + SCOE) in one column followed by the sensor description in the second column. PA/test staff shall fill-in any strange behaviour including date of observation as a remark. For each remark a separate excel cell shall be used on the right hand side of the sensor number.

9.3 Management / Organisation / Infrastructure

- 3 persons per position is not sufficient during long test. Plan 4 persons per position and allow for free days.
- Test director should not be on shift and must have a deputy.
- Three persons on test floor (shift leader, thermal/cryo, EGSE) are considered sufficient for initial and/or busy phases, reduction to two persons (shift leader, EGSE) seems possible during “lazy” phases, e.g. TB
- Necessity of PA presence on test floor throughout the test might be discussed
- Instrument cognizant presence on test floor or availability to be discussed
- Organize snack for late and night shift (and day shift during week-ends) in advance

- Prepare plan of EGSE / DH setup in check-out and test floor, check availability and size of furniture (chairs, desks, pin boards)
- Plan pre-test briefing with complete test staff, covering
  - data handling introduction
  - test setup incl. sensor/heater locations (lists and drawings, handout!)
  - activities to be performed at begin and end of phases

9.4 IT / Network

- LAN connection to home base: ISDN is very slow. Possible solutions include DSL link or (better) VPN, both have been frequently used on ETS side. Contact person is Jacob van der Meulen. Start discussions 6 months before planned campaign.
- Remote access via service remote login was ok (but requires fully equipped PC in FN)
- Router reassigns IP addresses every 1hr (tbc)

10 Summary and Conclusions

10.1 CVV Internal Performance

The instrument I/F thermal performance evaluation is described in a separate report [RD 02].

The He masses determined with the DLCM operation compare very well with the level probe measurements; the deviation is below 4% for all four cases. Note that the correlation between DLCM measurement and level probe read-out is excellent even for a very short heating time of only 20 s.

The PPS measurements have shown that the PPS operates on system level as expected from the unit level tests. The mass flow capacity is not fully exploited by the current pressure drop set-up, and a further increase of the large nozzle is possible. The PPS outlet temperature sensors show a significant calibration offset wrt the DLCM temperature sensors.

In the pressure drop measurements performed during the TB/TV test, the actual mass flow was by 5 to 25% lower than expected from the predictions. A better correlation of measurements and numerical results can be achieved by adjustment of the nozzle flow factor.

The HOT evacuation could not be completed within the required time frame of 1190 s. A total time of 1286 s was measured until the end pressure of 15 mbar was reached in the HOT. A further reduction of the evacuation time can be achieved by increasing the diameter of the large nozzle and by opening of two additional electromagnetic valves on the HOT (V701 and V702).

The temperature gradients within the Optical Bench are less than 0.65 K including the optical Bench Shield and the gradients within the Thermal Shields are less than less than 1 K. The relevant conclusions are compiled at the end of each sub-section. An overview of the measured CVV internal thermal performance is given in following **Figure 10.1-1** (TB1) and **Figure 10.1-2** (TB2) as heat flow charts.

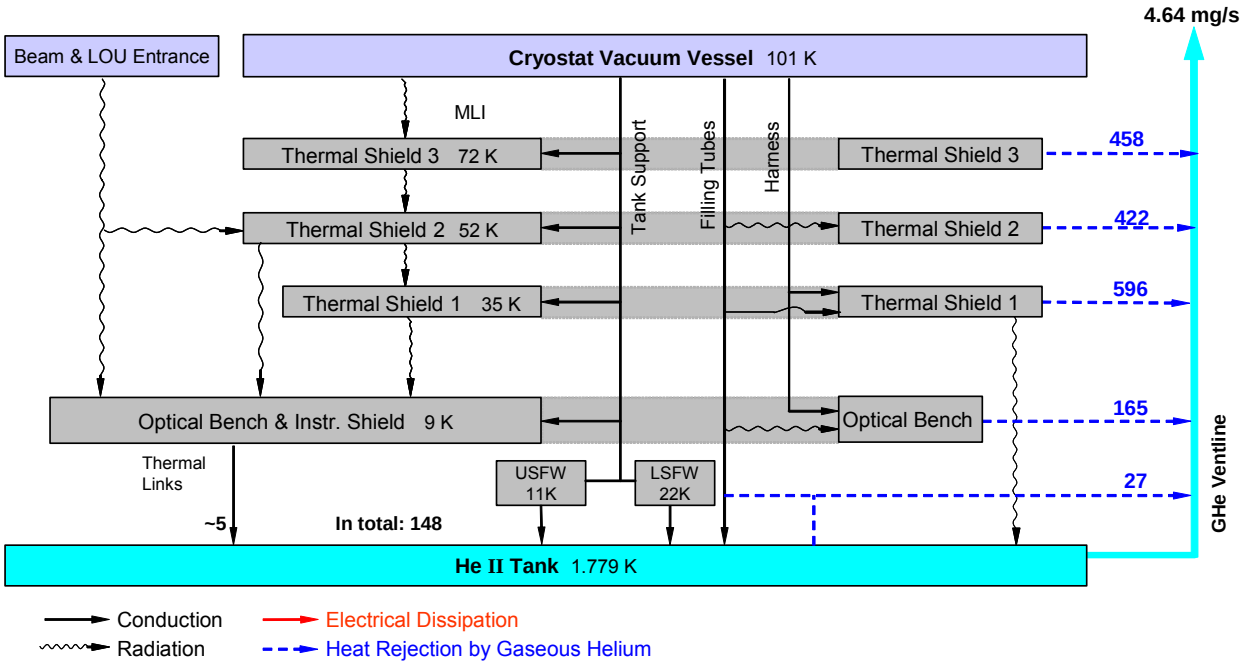

Figure 10.1-1: CVV Internal Heat Flow Chart in mW for TB1

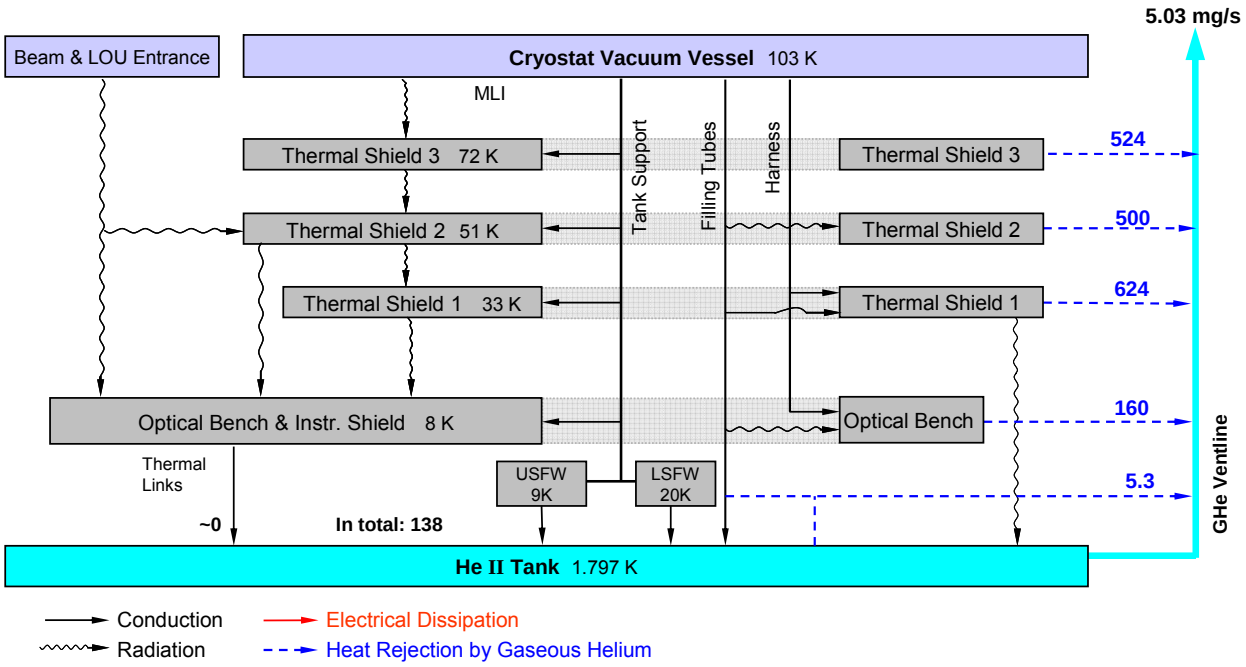

Figure 10.1-2: CVV Internal Heat Flow Chart in mW for TB2

10.2 CVV External Performance

A CVV temperature of 102 K has been reached in TB1. The SCOE sensors show even about 1.2 K lower temperatures. The gradient within the CVV main structure is about 5 K and the gradients to the external CVV radiators are less than 2 K. The CVV temperature is strongly dominated by the LSS thermal environment. A proposal for a refined LSS TMM is proposed; emissivity measurement of the LSS walls at operational temperature is needed.

The relevant conclusions are compiled at the end of each sub-section. An overview of the measured CVV external conditions is given in **Figure 10.2-1** (TB1) and **Figure 10.2-2** (TB2). The heat towards the CVV internal is the heat absorbed by the helium (gas and evaporation) and by the temperature drift of the liquid helium inside the HTT. The heat via the test harness is calculated by the harness cross section and temperature gradients along the harness bundles measured with dedicated sensors inside the bundles.

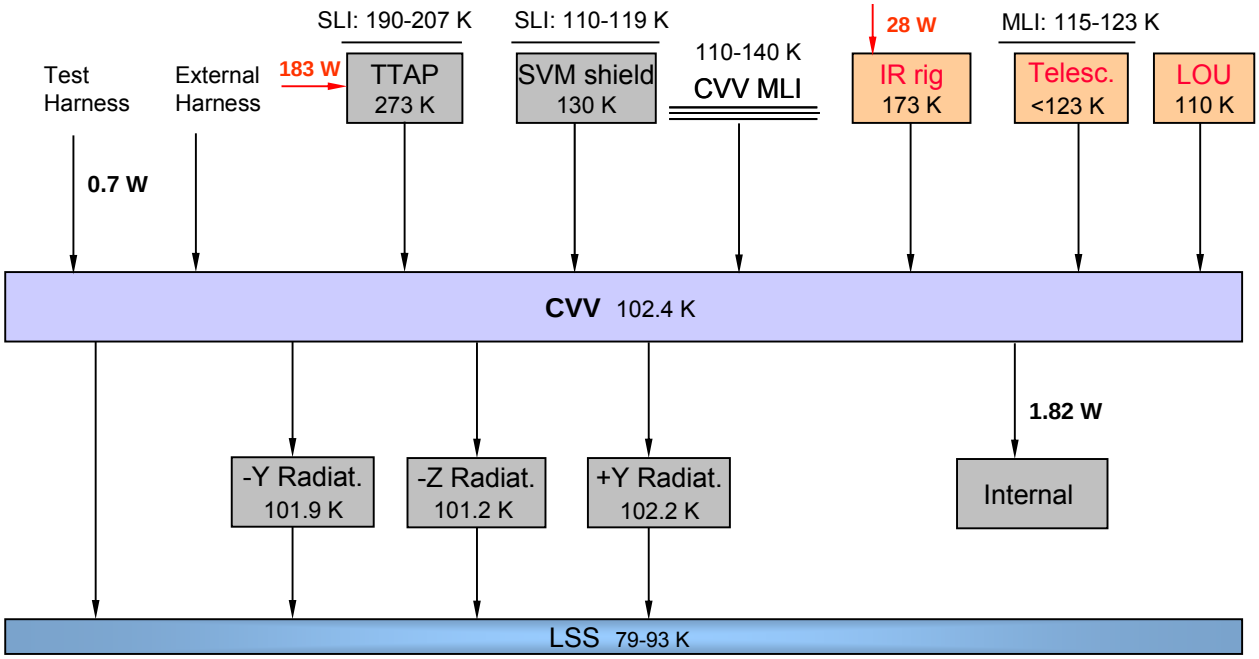

Figure 10.2-1: CVV External Thermal Conditions during TB1

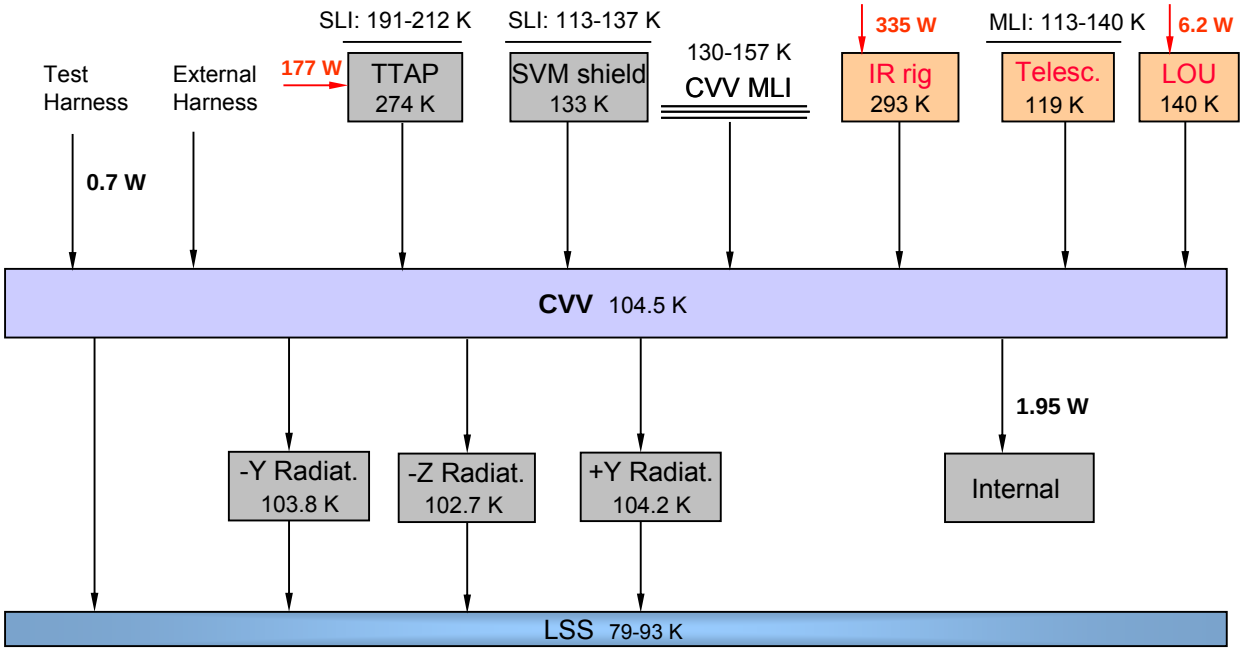

Figure 10.2-2: CVV External Thermal Conditions during TB2

ANNEX 1: Thermal Balance Steady State Temperatures

Sensor acronym	Sensor Location	Type	Range	Sensor ID	Sensor Status	TB1 (K)	TB2 (K)	TB2-TB1 (K)
MT101	TH-HIFI-1, on L0 IF	C100		MT101	ok	1.8113	1.8277 *	
MT102	TH-HIFI-2, on L0 IF	C100		MT102	ok	1.8107	1.8269 *	
MT103	TH-HIFI-3, on L1 IF	C100		MT103	ok	3.6826	2.5702 *	
MT104	TH-HIFI-4, on L1 IF	C100		MT104	ok	3.6646	2.5599 *	
MT105	TH-HIFI-5, on FPU	C100		MT105	ok	9.4008	7.7375 *	
MT106	TH-HIFI-6, on FPU	C100		MT106	ok	9.398	7.7279 *	
MT107	TH-HIFI-7, on FPU	Pt1000		MT107	ok	*n.a.*	*n.a.*	
MT108	TH-LOU-1, on LOU baseplate	Pt1000		MT108	ok	109.08	138.38	29.30
MT109	TH-LOU-2, on LOU baseplate	Pt1000		MT109	ok	109.15	138.84	29.69
MT110	TH-LOU-3, on LOU baseplate	Pt1000		MT110	ok	109.11	139.69	30.58
MT201	TH-SPIRE-1, on detector L0 rigid pod	C100		MT201	ok	1.8167	1.8293 *	
MT202	TH-SPIRE-2, on detector L0 rigid pod	C100		MT202	ok	1.8086	1.8238 *	
MT203	TH-SPIRE-3, on cooler evaporator L0 rigid/open tank pod	C100		MT203	offset	*1.8509*	*1.8555* *	
MT204	TH-SPIRE-4, on cooler evaporator L0 rigid/open tank pod	C100		MT204	ok	1.8032	1.8194 *	
MT205	TH-SPIRE-5, on cooler pump L0 rigid pod	C100		MT205	ok	1.8244	1.8319 *	
MT206	TH-SPIRE-6, on cooler pump L0 rigid pod	C100		MT206	ok	1.8058	1.8202 *	
MT207	TH-SPIRE-7, on SPIRE optical bench	C100		MT207	ok	3.9189	2.8413 *	
MT208	TH-SPIRE-8, on SPIRE optical bench	C100		MT208	ok	3.9285	2.8487 *	
MT213	TH-SPIRE-9, on SPIRE optical bench	Pt1000		MT213	ok	*n.a.*	*n.a.*	
MT250	TH-S-JFET-1, on S-J-FET baseplate	C100		MT250	ok	9.9412	8.2631 *	
MT251	TH-S-JFET-2, on S-J-FET baseplate	C100		MT251	ok	9.7023	8.1030 *	
MT252	TH-S-JFET-3, on S-J-FET baseplate	Pt1000		MT252	ok	*n.a.*	*n.a.*	
MT253	TH-P-JFET-1, on P-J-FET baseplate	C100		MT253	ok	9.7310	8.1652 *	
MT254	TH-P-JFET-2, on P-J-FET baseplate	C100		MT254	ok	9.9061	8.2813 *	
MT255	TH-P-JFET-3, on P-J-FET baseplate	Pt1000		MT255	ok	*n.a.*	*n.a.*	
MT301	TH-PACS-1, on Red Detector Assy (FPFPU.DET)	C100		MT301	ok	1.8060	1.8227 *	
MT302	TH-PACS-2, on Red Detector Assy (FPFPU.DET)	C100		MT302	ok	1.8062	1.8227 *	
MT303	TH-PACS-3, on Blue Detector Assy (FPFPU.BOL)	C100		MT303	ok	1.8078	1.9676 *	
MT304	TH-PACS-4, on Blue Detector Assy (FPFPU.BOL)	C100		MT304	ok	1.8041	1.9628 *	
MT305	TH-PACS-5, on cooler pump (FPFPU.COOL)	C100		MT305	ok	1.8070	1.8258 *	
MT306	TH-PACS-6, on cooler pump (FPFPU.COOL)	C100		MT306	ok	1.8057	1.8225 *	
MT307	TH-PACS-7, on cooler evaporator (FPFPU.COOL)	C100		MT307	ok	1.8009	1.8208 *	
MT308	TH-PACS-8, on cooler evaporator (FPFPU.COOL)	C100		MT308	ok	1.8004	1.8179 *	
MT309	TH-PACS-9, on L1-interface of Photometer optics	C100		MT309	ok	3.2498	*n.a.*	

Sensor acronym	Sensor Location	Type	Range	Sensor ID	Sensor Status	TB1 (K)	TB2 (K)	TB2-TB1 (K)
MT310	TH-PACS-10, on L1-interface of Photometer optics	C100		MT310	ok	3.2441	*n.a.*	
MT311	TH-PACS-11, on L1-interface of collimator	C100		MT311	ok	3.2489	*n.a.*	
MT312	TH-PACS-12, on L1-interface of collimator	C100		MT312	ok	3.2500	*n.a.*	
MT313	TH-PACS-13, on L1-interface of Spectrometer housing	C100		MT313	ok	3.2731	*n.a.*	
MT314	TH-PACS-14, on L1-interface of Spectrometer housing	C100		MT314	ok	3.2746	*n.a.*	
MT315	TH-PACS-15, on FPU	Pt1000		MT315	ok	*n.a.*	*n.a.*	
T101	DLCM-1, tank lower side; -x-y; in DLCM housing	C100	1.5K–15.0K	T101	ok	1.7785	1.7970 *	
T102	DLCM-2, tank lower side; -x+y; in DLCM housing	C100	1.5K–15.0K	T102	ok	1.7784	1.7967 *	
T103	HTT lower side; -x+z-y; nearby outside	Pt1000	13K - 370K	T103	ok	*n.a.*	*n.a.*	
T104	DLCM-2, tank lower side; -x+y; in DLCM housing	C100	1.5K - 15.0K	T104	ok	1.7796	1.7979 *	
T105	DLCM-1, tank lower side; -x-y; in DLCM housing	C100	1.5K–15.0K	T105	ok	1.7790	1.7973 *	
T106	HTT lower side; -x-z+y; nearby outside	C100	1.5K - 2.2K	T106	ok	1.7718	1.7906 *	
T107	HTT upper side; +x-z+y; nearby outside	C100	1.5K–15.0K	T107	ok	1.7726	1.7914 *	
T111	HTT upper side; +x-y-z; integrated into PPS housing	C100	1.5K–15.0K	T111	ok	1.8022	1.7949 *	
T112	HTT upper side; +x-y-z; integrated into PPS housing	C100	1.5K - 2.2K	T112	ok	1.8037	1.7983 *	
T113	Filling port end piece	C100	1.5K–15.0K	T113	ok	*n.a.*	*n.a.*	
T114	Filling port end piece	C100	1.5K–15.0K	T114	ok	*n.a.*	*n.a.*	
T202	OB Plate near PACS mounting foot (+z)	C100	3K - 20K	T202	ok	9.306	7.5984 *	
T207	OB Plate near HIFI mounting foot (+z/-y)	Pt1000	13K - 370K	T207	ok	*n.a.*	*n.a.*	
T208	OB Plate near HIFI mounting foot (+z/-y)	C100	3K - 20K	T208	ok	9.207	7.5109 *	
T211	Instrument Shield, close to HIFI	Pt1000	13K - 370K	T211	ok	*n.a.*	*n.a.*	
T212	Instrument Shield, close to PACS	C100	3K - 20K	T212	ok	9.310	7.6974 *	
T213	Instrument Shield, close to SPIRE	C100	3K - 20K	T213	ok	9.546	7.8940 *	
T221	L0 Cooling Strap 1; to PACS RED Detector	C100	1.6K - 2.0K	T221	ok	1.7716	1.7899 *	
T222	L0 Cooling Strap 2; to PACS Sorption Cooler Evaporator	C100	1.5K - 2.2K	T222	ok	1.7718	1.7905 *	
T223	L0 Cooling Strap 3; to PACS Sorption Cooler Pump	C100	2K - 10K	T223	ok	1.7812	1.7987 *	
T224	L0 Cooling Strap 4; to PACS BLUE Detector	C100	1.6K - 2.0K	T224	ok	1.7799	1.9471 *	
T225	L0 Cooling Strap 5; to SPIRE SM Detector enclosure	C100	1.6K - 2.0K	T225	ok	1.7723	1.7902 *	
T226	L0 Cooling Strap 6; to SPIRE Cooler Pump	C100	2K - 10K	T226	ok	1.7726	1.7909 *	
T227	L0 Cooling Strap 7; to SPIRE Cooler Evaporator	C100	1.5K - 2.2K	T227	ok	1.7759	1.7943 *	
T228	L0 Cooling Strap 8; to HIFI L0	C100	1.5K - 2.2K	T228	ok	1.7813	1.7983 *	
T231	L1 Ventline upstream to PACS Phot.Optics (L1 Inlet)	C100	1.5K - 2.2K	T231	ok	2.874 * *	1.9922 *	
T232	L1 Ventline downstream strap 1 to PACS Phot.Optics	C100	1.5K - 2.2K	T232	ok	2.9971	2.0936 *	
T233	L1 Ventline downstream strap 2 to PACS Collimator	C100	2K - 10K	T233	ok	3.0895	2.1700 *	
T234	L1 Ventline downstream strap 3 to PACS Spect.Housing	C100	2K - 10K	T234	ok	3.1530	2.2227 *	
T235	L1 Ventline upstream strap 4 to SPIRE Optical Bench	C100	2K - 10K	T235	ok	3.4095	2.3833 *	
T236	L1 Ventline downstream strap 4 to SPIRE Optical Bench	C100	2K - 10K	T236	ok	3.6621	2.5601 *	

Sensor acronym	Sensor Location	Type	Range	Sensor ID	Sensor Status	TB1 (K)	TB2 (K)	TB2-TB1 (K)
T237	L1 Ventline downstream to HIFI interface (L1 outlet)	C100	2K - 10K	T237	ok	3.6573	2.5516 *	
T242	L1; on Strap 1 on PACS FPU Side	C100	2K - 10K	T242	ok	3.1029	2.2240 *	
T244	L1, on Strap 5 on HIFI FPU side	C100	2K - 10K	T244	ok	3.6572	2.5521 *	
T246	L3 Ventline to 6-JFET (JFET-Phot)	C100	3K - 20K	T246	ok	9.7965	8.1696 *	
T247	L3 Ventline to 2-JFET (JFET-Spec)	C100	3K - 20K	T247	ok	9.7039	8.1096 *	
T248	L1; on Strap 4 on SPIRE FPU side	C100	3K - 20K	T248	ok	3.7983	2.7134 *	
T249	On Spire 2-JFET (JFET-Spec)	Pt1000	13K - 370K	T249	ok	*n.a.*	*n.a.*	
T250	On Spire 2-JFET (JFET-Spec)	C100	3K - 20K	T250	ok	9.7962	8.1709 *	
T251	On Spire 6-JFET (JFET-Phot)	Pt1000	13K - 370K	T251	ok	*n.a.*	*n.a.*	
T252	On Spire 6-JFET (JFET-Phot)	C100	3K - 20K	T252	ok	9.7188	8.1254 *	
T253	OB Plate near SPIRE foot (center)	Pt1000	13K - 370K	T253	ok	*n.a.*	*n.a.*	
T254	OB Plate near SPIRE foot (center)	C100	3K - 20K	T254	ok	9.3530	7.7930 *	
T255	OB Plate near SPIRE foot (-z+y)	Pt1000	13K - 370K	T255	ok	*n.a.*	*n.a.*	
T256	OB Plate near SPIRE foot (-z+y)	C100	3K - 20K	T256	ok	9.7378	8.1439 *	
T258	OB Plate near SPIRE foot (-y-z)	C100	3K - 20K	T258	ok	9.5991	8.0244 *	
T321	SVM Thermal Shield; on top +Y	Pt1000	13K - 370K	T321	ok	133.27	140.56	7.29
T322	SVM Thermal Shield; on top +Y/-Z	Pt1000	13K - 370K	T322	ok	129.03	131.53	2.50
T323	SVM Thermal Shield; on top -Z/-Y	Pt1000	13K - 370K	T323	ok	128.40	130.90	2.50
T324	SVM Thermal Shield; on top -Y	Pt1000	13K - 370K	T324	ok	134.19	140.58	6.39
T331	Telescope	Pt1000		T331	ok	123.77	118.74	
T332	Telescope	Pt1000		T332	ok	123.32	118.44	
T333	Telescope	Pt1000		T333	ok	123.47	118.43	
T334	Telescope	Pt1000		T334	ok	123.16	118.27	
T335	Telescope	Pt1000		T335	ok	122.26	117.30	
T336	Telescope	Pt1000		T336	ok	123.77	119.12	
T337	Telescope	Pt1000		T337	ok	123.47	118.25	
T338	Telescope	Pt1000		T338	ok	123.86	119.11	
T339	Telescope	Pt1000		T339	not connected	******	******	
T340	Telescope	Pt1000		T340	ok	123.13	118.51	
T421	1st Shield, outside on lower bulkhead in +X+Y plane	Pt1000	13K - 370K	T421	ok	34.78	32.57 *	-2.21
T422	1st Shield, outside on cylinder near ventline	Pt1000	13K - 370K	T422	ok	34.41	31.93 *	-2.48
T423	1st Shield, outside on upper cone cylindrical part	Pt1000	13K - 370K	T423	ok	34.41	31.95 *	-2.46
T424	1st Shield, outside on upper cone close to beam entrance	Pt1000	13K - 370K	T424	ok	34.69	32.43 *	-2.26
T441	2nd Shield, outside on lower bulkhead	Pt1000	13K - 370K	T441	ok	51.87	51.03 *	-0.84
T442	2nd Shield, outside on cylinder near ventline	Pt1000	13K - 370K	T442	ok	51.91	51.08 *	-0.83
T443	2nd Shield, outside on upper cone cylindrical part	Pt1000	13K - 370K	T443	ok	51.89	51.06 *	-0.83
T444	2nd Shield outside on upper cone close to beam entrance	Pt1000	13K - 370K	T444	ok	52.00	51.18 *	-0.82

Sensor acronym	Sensor Location	Type	Range	Sensor ID	Sensor Status	TB1 (K)	TB2 (K)	TB2-TB1 (K)
T461	3rd Shield, outside on lower bulkhead	Pt1000	13K - 370K	T461	ok	71.36	71.64 *	0.28
T462	3rd Shield, outside on cylinder near ventline	Pt1000	13K - 370K	T462	ok	70.89	71.09 *	0.20
T463	3rd Shield, outside on upper cone cylindrical part	Pt1000	13K - 370K	T463	ok	71.32	71.59 *	0.27
T464	3rd Shield, outside on upper cone near beam entrance	Pt1000	13K - 370K	T464	ok	71.50	71.81 *	0.31
T501	GHe S/S external ventline, upstream	Pt1000		T501	ok	142.1	145.26 *	3.16
T502	GHe S/S external ventline outlet,	Pt1000		T502	ok	91.73	92.08 *	0.35
T504	GHe S/S external ventline, near P501	Pt1000		T504	ok	100.33	101.56 *	1.23
T505	GHe S/S external ventline	Pt1000		T505	ok	100.5	101.56 *	1.06
T506	GHe S/S external ventline, on nozzle	Pt1000		T506	ok	100.5	101.58 *	1.08
T507	GHe S/S external ventline outlet	Pt1000		T507	ok	91.35	91.70 *	0.35
SPARE1 (former T601)	Cover Heatshield	Pt1000		SPARE1	ok	89.08	90.91	1.83
SPARE2 (former T602)	Cover Heatshield	Pt1000		SPARE2	ok	89.04	90.86	1.82
T651	Cryostat baffle, Outer cylinder; -Z	Pt1000	13K - 370K	T651	ok	99.81	102.19	2.38
T652	Cryostat baffle, Inner baffle; +Z	Pt1000	13K - 370K	T652	not connected	******	******	
T701	HOT upper side; -y-z; nearby center	Pt1000	13K - 370K	T701	ok	21.66	20.08 *	
T702	HOT upper side; +y+z; nearby center	C100	1.5K - 15.0K	T702	ok	*n.a.*	20.11 *	
T703	HOT lower side; -z; nearby center	C100	3K - 20K	T703	ok	*n.a.*	19.53 *	
T704	HOT lower side; +z; nearby center	Pt1000	13K - 370K	T704	ok	21.58	20.03 *	0.32
T801	TS3 bracket on lower chain 18	Pt1000	13K - 370K	T801	ok	72.45	72.77 *	-0.76
T802	TS2 bracket on lower chain 18	Pt1000	13K - 370K	T802	ok	53.08	52.32 *	-2.03
T803	TS1 bracket on lower chain 18	Pt1000	13K - 370K	T803	ok	36.59	34.56 *	0.37
T804	TS3 bracket on lower chain 14	Pt1000	13K - 370K	T804	ok	72.55	72.92 *	-0.79
T805	TS2 bracket on lower chain 14	Pt1000	13K - 370K	T805	ok	52.54	51.75 *	-2.00
T806	TS1 bracket on lower chain 14	Pt1000	13K - 370K	T806	ok	36.23	34.23 *	0.27
T851	TS3 bracket on upper chain 08	Pt1000	13K - 370K	T851	ok	71.57	71.84 *	-0.85
T852	TS2 bracket on upper chain 08	Pt1000	13K - 370K	T852	ok	51.84	50.99 *	-2.05
T853	TS1 bracket on upper chain 08	Pt1000	13K - 370K	T853	ok	35.23	33.18 *	0.32
T861	Upper spatial framework	Pt1000	13K - 370K	T861	ok	----	*n.a.* *	
T862	Upper spatial framework	C100	3K - 20K	T862	ok	10.76	9.32 *	
T901	CVV; -Z side, top	Pt1000	13K - 370K	T901	ok	99.90	101.68	1.78
T902	CVV; -Z side, mid	Pt1000	13K - 370K	T902	ok	99.88	101.42	1.54
T903	CVV; -Z side, bottom	Pt1000	13K - 370K	T903	failed	******	******	
T904	CVV; +Z side, bottom	Pt1000	13K - 370K	T904	ok	103.36	105.69	2.33
T905	CVV; +Z side, mid	Pt1000	13K - 370K	T905	ok	101.77	104.16	2.39
T906	CVV; +Y side, mid	Pt1000	13K - 370K	T906	ok	101.00	102.99	1.99
T907	CVV +Y Radiator upper part	Pt1000	13K - 370K	T907	ok	100.57	102.55	1.98
T908	CVV +Y Radiator lower part	Pt1000	13K - 370K	T908	ok	101.69	103.56	1.87

Sensor acronym	Sensor Location	Type	Range	Sensor ID	Sensor Status	TB1 (K)	TB2 (K)	TB2-TB1 (K)
T909	CVV -Y Radiator lower part	Pt1000	13K - 370K	T909	ok	100.98	102.84	1.86
T910	CVV -Y Radiator upper part	Pt1000	13K - 370K	T910	ok	100.15	102.17	2.02
T911	CVV -Z Radiator upper part	Pt1000	13K - 370K	T911	ok	99.68	101.10	1.42
T912	CVV -Z Radiator lower part	Pt1000	13K - 370K	T912	ok	100.59	101.99	1.40
T931	LOU Support Plate +X,-Z; near Alignment Window	Pt1000	13K - 370K	T931	ok	109.30	138.58	29.28
T932	LOU Support Plate +X,+Z; near Alignment Window	Pt1000	13K - 370K	T932	ok	109.41	139.34	29.93
T933	LOU Radiator	Pt1000	13K - 370K	T933	ok	106.57	130.37	23.80
T934	LOU Waveguides near upper GFRP bracket (+X)	Pt1000	13K - 370K	T934	ok	119.76	143.34	23.58
T935	LOU Waveguides near lower GFRP bracket (-X)	Pt1000	13K - 370K	T935	ok	172.80	179.96	7.16
VT102	V102 Valve, mounted on HTT covered by MLI cap	Pt1000	13K - 370K	VT102	ok	*n.a.*	*n.a.*	
VT103	V103 Valve, mounted on HTT covered by MLI cap	Pt1000	13K - 370K	VT103	ok	*n.a.*	*n.a.*	
VT104	V104 Valve, mounted on HTT covered by MLI cap	Pt1000	13K - 370K	VT104	ok	*n.a.*	*n.a.*	
VT105	V105 Valve, mounted on lower spatial framework	Pt1000	13K - 370K	VT105	ok	21.22	19.44*	-1.78
VT106	V106 Valve, mounted on HTT covered by MLI cap	Pt1000	13K - 370K	VT106	ok	*n.a.*	*n.a.*	
VT701	V701 Valve, mounted on lower spatial framework	Pt1000		VT701	ok	22.19	19.42*	-2.77
VT702	V702 Valve, mounted on lower spatial framework	Pt1000		VT702	ok	21.19	19.42*	-1.77
P101	HTT	p		P101	ok	17.8 mbar	18.6 mbar*	
P502	GHe S/S external Ventline	p		P502	ok	13.5 mbar	12.7 mbar*	
Mdot	He Mass flow rate	mdot		CVSE 004	ok	4.64 mg/s	5.03 mg/s*	0.39 mg/s
PLM_CVV_Pt_upper-BH-pYpZ	CVV upper BH +Y+Z	Pt100		1000	ok	102.13	104.60	2.47
PLM_CVV_Pt_upper-BH-mYpZ	CVV upper BH -Y+Z	Pt100		1001	noise	102.1	104.55	2.45
PLM_CVV_Pt_LOU-strut	CVV upper BH -Y near LOU strut	Pt100		1002	ok	101.8	104.15	2.35
PLM_CVV_Pt_upper-cyl-pY	CVV upper Cyl +Y	Pt100		1003	noise	102.7	104.58	1.88
PLM_CVV_Pt_upper-cyl-pYpZ	CVV upper Cyl +Y+Z	Pt100		1004	ok	102.8	105.04	2.24
PLM_CVV_Pt_upper-cyl-pZ	CVV upper Cyl +Z	Pt100		1005	noise	104.0	106.2	2.23
PLM_CVV_Pt_upper-cyl-mYpZ	CVV upper Cyl -Y+Z	Pt100		1006	ok	102.68	105.02	2.34
PLM_CVV_Pt_upper-cyl-mY	CVV upper Cyl -Y	Pt100		1007	ok	102.1	104.23	2.13
PLM_CVV_Pt_cryobaffle-pYpZ	CVV cryostat baffle +Y+Z	Pt100		1008	ok	101.86	104.59	2.73
PLM_CVV_Pt_cryobaffle-mYpZ	CVV cryostat baffle -Y+Z	Pt100		1009	ok	101.78	104.52	2.74
PLM_CVV_Pt_upper-BH-mZ	CVV upper BH -Z	Pt100		1100	noise	101.45	103.56	2.11
PLM_CVV_Pt_upper-BH-mY-telescope-strut	CVV upper BH -Y near Telescope strut IF	Pt100		1101	ok	101.24	103.16	1.92
PLM_CVV_Pt_upper-BH-pY-HSS-strut-IF	CVV upper BH +Y near HSS strut IF	Pt100		1102	ok	101.52	103.91	2.39
PLM_CVV_Pt_upper-cyl-mYmZ	CVV upper Cyl -Y-Z	Pt100		1103	ok	101.15	102.84	1.69
PLM_CVV_Pt_upper-cyl-mZ	CVV upper Cyl -Z	Pt100		1104	ok	101.20	102.70	1.50
PLM_CVV_Pt_upper-cyl-pYmZ	CVV upper Cyl +Y-Z	Pt100		1105	ok	101.70	103.30	1.60
PLM_CVV_Pt_beneath-LOU	CVV upper BH -Y next to LOU window	Pt100		1106	ok	101.71	104.03	2.32
PLM_CVV_Pt_LOU-baffle	LOU Radiator mid -Z	Pt100		1107	noise	108.7	133.58	24.88

Sensor acronym	Sensor Location	Type	Range	Sensor ID	Sensor Status	TB1 (K)	TB2 (K)	TB2-TB1 (K)
PLM_CVV_Pt_cryobaffle-mYmZ-telescope-strut	CVV cryostat baffle -Y-Z near Telescope strut IF	Pt100		1108	ok	101.95	104.25	2.30
PLM_CVV_Pt_cryobaffle-pYmZ	CVV cryostat baffle +Y-Z	Pt100		1109	ok	101.54	104.11	2.57
PLM_CVV_Pt_lower-BH-mZ	CVV lower BH -Z	Pt100		1200	ok	102.88	104.57	1.69
PLM_CVV_Pt_lower-BH-mYmZ-SVM-strut	CVV lower BH at SMV strut IF -Y-Z	Pt100		1201	ok	103.13	104.80	1.67
PLM_CVV_Pt_lower-BH-mZ-SVM-strut	CVV lower BH at SMV strut IF -Z	Pt100		1202	ok	103.75	105.38	1.63
PLM_CVV_Pt_cyl-mYmZ	CVV Cyl -Y-Z	Pt100		1203	ok	101.70	103.34	1.64
PLM_CVV_Pt_cyl-pYmZ	CVV Cyl +Y-Z	Pt100		1204	ok	102.23	103.78	1.55
PLM_CVV_Pt_cyl-mZ-radiator-IF	CVV cyl -Z near Radiator interface	Pt100		1205	ok	101.70	103.11	1.41
PLM_CVV_Pt_lower-BH-pYpZ	CVV lower BH +Y+Z	Pt100		1300	ok	104.77	106.94	2.17
PLM_CVV_Pt_lower-BH-mYpZ	CVV lower BH -Y+Z	Pt100		1301	ok	104.22	106.42	2.20
PLM_CVV_Pt_lower-BH-pZ-SVM-strut	CVV lower BH at SMV strut IF +Z	Pt100		1302	ok	106.03	108.61	2.58
PLM_CVV_TC_MLI-upper-BH-pYpZ	CVV MLI upper BH +Y+Z	TC		1400	ok	110	137.8	27.80
PLM_CVV_TC_MLI-upper-BH-mYpZ	CVV MLI upper BH -Y+Z	TC		1401	ok	109.8	136.3	26.50
PLM_CVV_TC_MLI-upper-cyl-pY	CVV MLI upper Cyl +Y	TC		1403	ok	107.7	130.3	22.60
PLM_CVV_TC_MLI-upper-cyl-pYpZ	CVV MLI upper Cyl +Y+Z	TC		1404	ok	116.4	147.4	31.00
PLM_CVV_TC_MLI-upper-cyl-pZ	CVV MLI upper Cyl +Z	TC		1405	ok	121.8	156.0	34.20
PLM_CVV_TC_MLI-upper-cyl-mYpZ	CVV MLI upper Cyl -Y+Z	TC		1406	ok	115.5	146.9	31.40
PLM_CVV_TC_MLI-upper-cyl-mY	CVV MLI upper Cyl -Y	TC		1407	ok	111.5	134.8	23.30
PLM_CVV_TC_MLI-cryobaffle-pYpZ	CVV MLI cryostat baffle +Y+Z	TC		1408	ok	109.7	136.8	27.10
PLM_CVV_TC_MLI-cryobaffle-mYpZ	CVV MLI cryostat baffle -Y+Z	TC		1409	ok	109.8	136.2	26.40
PLM_CVV_TC_MLI-lower-BH-pYpZ	CVV MLI lower BH +Y+Z	TC		1700	ok	137.6	153.2	15.60
PLM_CVV_TC_MLI-lower-BH-mYpZ	CVV MLI lower BH -Y+Z	TC		1701	ok	140.2	156.5	16.30
PLM_CVV_TC_MLI-lower-BH-pZ-SVM-strut	CVV MLI lower BH at SMV strut IF +Z	TC		1702	ok	125.4	153.5	28.10
PLM_Rad_Pt_mYpX-radiator-top	upper -Y radiator	Pt100		2001	ok	101.5	103.65	2.15
PLM_Rad_Pt_mYpX-radiator-upper	upper -Y radiator	Pt100		2002	ok	101.25	103.35	2.10
PLM_Rad_Pt_mYpX-radiator-lower	upper -Y radiator	Pt100		2003	ok	101.41	103.38	1.97
PLM_Rad_Pt_mYpX-radiator-bottom	upper -Y radiator	Pt100		2004	noise	101.5	103.45	1.95
PLM_Rad_Pt_mYmX-radiator-top	lower -Y radiator	Pt100		2011	strong noise	*102.2*	*104.1*	1.90
PLM_Rad_Pt_mYmX-radiator-upper	lower -Y radiator	Pt100		2012	ok	102.7	103.87	1.17
PLM_Rad_Pt_mYmX-radiator-lower	lower -Y radiator	Pt100		2013	ok	102.55	104.4	1.85
PLM_Rad_Pt_mYmX-radiator-bottom	lower -Y radiator	Pt100		2014	ok	102.39	104.35	1.96
PLM_Rad_Pt_mZpX-radiator-top	upper -Z radiator	Pt100		2101	ok	101.01	102.65	1.64
PLM_Rad_Pt_mZpX-radiator-upper	upper -Z radiator	Pt100		2102	ok	100.49	101.96	1.47
PLM_Rad_Pt_mZpX-radiator-mid	upper -Z radiator	Pt100		2103	ok	100.78	102.20	1.42
PLM_Rad_Pt_mZpX-radiator-lower	upper -Z radiator	Pt100		2104	noise	101.1	102.5	1.40
PLM_Rad_Pt_mZpX-radiator-bottom	upper -Z radiator	Pt100		2105	ok	101.18	102.56	1.38
PLM_Rad_Pt_mZmX-radiator-top	lower -Z radiator	Pt100		2111	noise	102.0	103.5	1.50

Sensor acronym	Sensor Location	Type	Range	Sensor ID	Sensor Status	TB1 (K)	TB2 (K)	TB2-TB1 (K)
PLM_Rad_Pt_mZmX-radiator-mid	lower -Z radiator	Pt100		2112	ok	101.78	103.21	1.43
PLM_Rad_Pt_mZmX-radiator-bottom	lower +Y radiator	Pt100		2113	small noise	101.7	103.07	1.37
PLM_Rad_Pt_pYpX-radiator-top	upper +Y radiator	Pt100		2201	small noise	101.54	103.7	2.16
PLM_Rad_Pt_pYpX-radiator-upper	upper +Y radiator	Pt100		2202	small noise	101.78	103.85	2.07
PLM_Rad_Pt_pYpX-radiator-lower	upper +Y radiator	Pt100		2203	small noise	101.45	103.40	1.95
PLM_Rad_Pt_pYpX-radiator-bottom	upper +Y radiator	Pt100		2204	small noise	102.2	104.05	1.85
PLM_Rad_Pt_pYmX-radiator-top	lower +Y radiator	Pt100		2211	ok	102.80	105.60	2.80
PLM_Rad_Pt_pYmX-radiator-upper	lower +Y radiator	Pt100		2212	ok	102.80	105.60	2.80
PLM_Rad_Pt_pYmX-radiator-lower	lower -Z mX radiator bottom	Pt100		2213	strong noise	*103.1*	*105.1*	2.00
PLM_Rad_Pt_pYmX-radiator-bottom	lower +Y radiator	Pt100		2214	ok	102.99	105.0	2.01
LOU_RAD_TC_upper-mZ	LOU Radiator upper -Z	TC		2300	ok	110.30	135.0	24.70
LOU_RAD_TC_upper-pZ	LOU Radiator upper +Z	TC		2301	ok	110.0	134.8	24.80
LOU_RAD_TC_mid	LOU Radiator mid +Z	TC		2302	ok	109.81	134.9	25.09
LOU_RAD_TC_lower-mZ	LOU Radiator lower -Z	TC		2303	ok	108.1	128.6	20.50
LOU_RAD_TC_lower-pZ	LOU Radiator lower +Z	TC		2304	ok	108.27	129.6	21.33
LOU_HSG_TC_rad-heater-control	LOU Baseplate Center	TC		2310	ok	111.62	140.9	29.28
LOU_SUP_TC_CVV-side	LOU support strut on CVV side	TC		2320	ok	103.24	105.5	2.26
LOU_SUP_TC_LOU-side	LOU support strut on LOU side	TC		2321	ok	111.66	140.8	29.14
PLM_LOWG_TC_LOU-waveguide-pZ-SVMIF	LOU Waveguide +Z near SVM I/F	TC		2401	ok	261.42	262.4	0.98
PLM_LOWG_TC_LOU-waveguide-pZ-lower	LOU Waveguide +Z near lower bracket	TC		2402	ok	255.91	257.3	1.39
PLM_LOWG_TC_LOU-waveguide-pZ-mid	LOU Waveguide +Z near mid bracket	TC		2403	ok	147.38	159.5	12.12
PLM_LOWG_TC_LOU-waveguide-pZ-upper	LOU Waveguide +Z near LOU I/F	TC		2404	ok	112.44	141.7	29.26
PLM_LOWG_TC_LOU-waveguide-mZ-SVMIF	LOU Waveguide -Z near SVM I/F	TC		2411	ok	261.27	262.3	1.03
PLM_LOWG_TC_LOU-waveguide-mZ-lower	LOU Waveguide -Z near lower bracket	TC		2412	ok	254.39	255.8	1.41
PLM_LOWG_TC_LOU-waveguide-mZ-mid	LOU Waveguide -Z near mid bracket	TC		2413	ok	149.62	161.4	11.78
PLM_LOWG_TC_LOU-waveguide-mZ-upper	LOU Waveguide -Z near LOU I/F	TC		2414	ok	112.49	141.5	29.01
PLM_LHV_Pt_V501-support	V501 support plate	Pt100		2501	ok	101.68	103.35	1.67
PLM_LHV_Pt_V504-support	V504 support plate	Pt100		2502	ok	101.4	102.9	1.50
PLM_LHV_Pt_SV521-support	SV521 support plate	Pt100		2503	ok	101.7	103.21	1.51
PLM_Harn_Pt_Harness-profile-3800-mZ-top	Harness profile 3800 -Z top	Pt100		2600	ok	101.85	103.23	1.38
PLM_Harn_Pt_Harness-profile-3800-mZ-mid	Harness profile 3800 -Z mid	Pt100		2601	ok	102.05	103.5	1.45
PLM_Harn_Pt_Harness-profile-3800-mZ-bottom	Harness profile 3800 -Z bottom	Pt100		2602	noise	102.7	104.1	1.40
PLM_Harn_Pt_Harness-profile-4041-pYmZ-top	Harness profile 4041 +Y-Z top	Pt100		2610	ok	102.1	103.7	1.60
PLM_Harn_Pt_Harness-profile-4041-pYmZ-mid	Harness profile 4041 +Y-Z mid	Pt100		2611	ok	102.29	103.7	1.41
PLM_Harn_Pt_Harness-profile-4041-pYmZ-bot	Harness profile 4041 +Y-Z bottom	Pt100		2612	not working	******	******	******
PLM_Harn_Pt_Harness-profile-2300-pYpZ-top	Harness profile 2300 +Y-Z top	Pt100		2620	ok	104.62	106.99	2.37
PLM_Harn_Pt_Harness-profile-2300-pYpZ-mid	Harness profile 2300 +Y-Z mid	Pt100		2621	ok	106.35	108.75	2.40

Sensor acronym	Sensor Location	Type	Range	Sensor ID	Sensor Status	TB1 (K)	TB2 (K)	TB2-TB1 (K)
PLM_Harn_Pt_Harness-profile-2300-pYpZ-bott	Harness profile 2300 +Y-Z bottom	Pt100		2622	ok	106.9	109.39	2.49
PLM_Harn_Pt_Harness-profile-2900-mYpZ-top	Harness profile 2900 -Y-Z top	Pt100		2630	ok	104	106.54	2.54
PLM_Harn_Pt_Harness-profile-2900-mYpZ-mid	Harness profile 2900 -Y-Z mid	Pt100		2631	ok	104.8	107.32	2.52
PLM_Harn_Pt_Harness-profile-2900-mYpZ-bot	Harness profile 2900 -Y-Z bottom	Pt100		2632	noise	104.7	107.5	2.80
PLM_Harn_Pt_Harness-profile-3334-mY-top	Harness profile 3334 -Y top, LOU harness	Pt100		2640	ok	102.48	104.57	2.09
PLM_Harn_Pt_Harness-profile-3334-mY-mid	Harness profile 3334 -Y mid, LOU harness	Pt100		2641	ok	102.47	104.60	2.13
PLM_Harn_Pt_Harness-profile-3334-mY-botto	Harness profile 3334 -Y bottom, LOU harness	Pt100		2642	ok	102.64	104.75	2.11
PLM_HST_Pt_Ext-ubing-V503-outlet	External tubing at V503 outlet	Pt100		2701	ok	101.22	102.56	1.34
PLM_HST_Pt_Ext-ubing-V505-inlet	External tubing at V505 inlet	Pt100		2702	ok	101.45	102.96	1.51
PLM_Strut_TC_PLMSVM-24-pYpZ-top	PLM/SVM strut 24 (TMM 21) +Y+Z top	TC		3240	ok	118.40	121.23	2.83
PLM_Strut_TC_PLMSVM-24-pYpZ-upper	PLM/SVM strut 24 (TMM 21) +Y+Z upper	TC		3241	ok	197.1	200.31	3.21
PLM_Strut_TC_PLMSVM-24-pYpZ-lower	PLM/SVM strut 24 (TMM 21) +Y+Z lower	TC		3242	ok	207.55	210.3	2.75
PLM_Strut_TC_PLMSVM-24-pYpZ-bottom	PLM/SVM strut 24 (TMM 21) +Y+Z bottom	TC		3243	ok	247.18	248.29	1.11
PLM_Strut_TC_PLMSVM-26-pZ-top	PLM/SVM strut 26 (TMM 23) +Z top	TC		3260	ok	110.61	113.8	3.19
PLM_Strut_TC_PLMSVM-26-pZ-upper	PLM/SVM strut 26 (TMM 23) +Z upper	TC		3261	ok	178.8	184.53	5.73
PLM_Strut_TC_PLMSVM-26-pZ-lower	PLM/SVM strut 26 (TMM 23) +Z lower	TC		3262	ok	209.09	213.26	4.17
PLM_Strut_TC_PLMSVM-26-pZ-bottom	PLM/SVM strut 26 (TMM 23) +Z bottom	TC		3263	ok	259.23	260.46	1.23
PLM_Strut_TC_PLMSVM-33-mY-top	PLM/SVM strut 33 (TMM 6) -Y top	TC		3330	ok	109.12	111.6	2.48
PLM_Strut_TC_PLMSVM-33-mY-upper	PLM/SVM strut 33 (TMM 6) -Y upper	TC		3331	ok	155.03	159.98	4.95
PLM_Strut_TC_PLMSVM-33-mY-lower	PLM/SVM strut 33 (TMM 6) -Y lower	TC		3332	ok	203.12	206.11	2.99
PLM_Strut_TC_PLMSVM-33-mY-bottom	PLM/SVM strut 33 (TMM 6) -Y bottom	TC		3333	ok	260.05	260.90	0.85
PLM_Strut_TC_PLMSVM-36-mYmZ-top	PLM/SVM strut 36 (TMM 9) -Y-Z top	TC		3360	ok	104.92	106.62	1.70
PLM_Strut_TC_PLMSVM-36-mYmZ-upper	PLM/SVM strut 36 (TMM 9) -Y-Z upper	TC		3361	ok	132.28	134.47	2.19
PLM_Strut_TC_PLMSVM-36-mYmZ-lower	PLM/SVM strut 36 (TMM 9) -Y-Z lower	TC		3362	ok	163.64	165.14	1.50
PLM_Strut_TC_PLMSVM-36-mYmZ-bottom	PLM/SVM strut 36 (TMM 9) -Y-Z bottom	TC		3363	ok	252.50	253.04	0.54
PLM_Strut_TC_PLMSVM-38-mZ-top	PLM/SVM strut 38 (TMM 11) -Z top	TC		3380	ok	106.0	107.6	1.61
PLM_Strut_TC_PLMSVM-38-mZ-upper	PLM/SVM strut 38 (TMM 11) -Z upper	TC		3381	ok	140.71	142.13	1.42
PLM_Strut_TC_PLMSVM-38-mZ-lower	PLM/SVM strut 38 (TMM 11) -Z lower	TC		3382	ok	178.99	179.90	0.91
PLM_Strut_TC_PLMSVM-38-mZ-bottom	PLM/SVM strut 38 (TMM 11) -Z bottom	TC		3383	ok	248.73	249.20	0.47
PLM_Strut_TC_PLMSVM-41-mYmZ-top	PLM/SVM strut 41 (TMM 14) +Y-Z top	TC		3410	ok	105.10	106.77	1.67
PLM_Strut_TC_PLMSVM-41-mYmZ-upper	PLM/SVM strut 41 (TMM 14) +Y-Z upper	TC		3411	ok	131.68	133.71	2.03
PLM_Strut_TC_PLMSVM-41-mYmZ-lower	PLM/SVM strut 41 (TMM 14) +Y-Z lower	TC		3412	ok	163.65	165.3	1.65
PLM_Strut_TC_PLMSVM-41-mYmZ-bottom	PLM/SVM strut 41 (TMM 14) +Y-Z bottom	TC		3413	ok	251.78	252.33	0.55
PLM_Strut_TC_PLMSVM-44-pY-top	PLM/SVM strut 44 (TMM 17) +Y top	TC		3440	ok	106.04	108.73	2.69
PLM_Strut_TC_PLMSVM-44-pY-upper	PLM/SVM strut 44 (TMM 17) +Y upper	TC		3441	ok	124.38	132.98	8.60
PLM_Strut_TC_PLMSVM-44-pY-lower	PLM/SVM strut 44 (TMM 17) +Y lower	TC		3442	ok	168.92	172.57	3.65
PLM_Strut_TC_PLMSVM-44-pY-bottom	PLM/SVM strut 44 (TMM 17) +Y bottom	TC		3443	ok	255.23	255.92	0.69

Sensor acronym	Sensor Location	Type	Range	Sensor ID	Sensor Status	TB1 (K)	TB2 (K)	TB2-TB1 (K)
PLM_SVTS_TC_SVM-TS-Face-pY	SVM TS +X face sheet +Y side	TC		4001	ok	125.72	128.73	3.01
PLM_SVTS_TC_SVM-TS-Face-mY	SVM TS +X face sheet -Y side	TC		4002	ok	124.69	127.66	2.97
PLM_SVTS_TC_SVM-TS-Strut-pY-lower	SVM TS strut +Y near SVM I/F	TC		4010	ok	273.12	273.47	0.35
PLM_SVTS_TC_SVM-TS-Strut-pY-upper	SVM TS strut +Y near shield I/F	TC		4011	ok	126.83	128.67	1.84
PLM_SVTS_TC_SVM-TS-Strut-pY-face	SVM TS face sheet +Y strut I/F	TC		4012	ok	127.08	129.02	1.94
PLM_SVTS_TC_SVM-TS-Strut-mZ-lower	SVM TS strut -Z near SVM I/F	TC		4020	ok	272.90	273.26	0.36
PLM_SVTS_TC_SVM-TS-Strut-mZ-upper	SVM TS strut -Z near shield I/F	TC		4021	ok	136.20	138.15	1.95
PLM_SVTS_TC_SVM-TS-Strut-mZ-face	SVM TS face sheet -Z strut I/F	TC		4022	ok	134.88	136.8	1.92
PLM_SVTS_TC_SVM-TS-MLI-pY	SVM TS MLI +Y	TC		4501	ok	114.7	130.0	15.30
PLM_SVTS_TC_SVM-TS-MLI-pYmZ	SVM TS MLI +Y-Z	TC		4502	ok	111.75	115.8	4.05
PLM_SVTS_TC_SVM-TS-MLI-mYmZ	SVM TS MLI -Y-Z	TC		4503	ok	110.5	113.2	2.70
PLM_SVTS_TC_SVM-TS-MLI-mY	SVM TS MLI -Y	TC		4504	ok	118.75	137.2	18.45
TEL_MTD_TC_Structure-IF-pYpZ-upper	Telescope TD IF +Y+Z upper	TC		6000	ok	125.0, -1.8 K/day	120.7	
TEL_MTD_TC_Structure-IF-pYpZ-lower	Telescope TD IF +Y+Z lower	TC		6001	ok	123.8, -1.7 K/day	121.2	
TEL_MTD_TC_Structure-IF-mZ-upper	Telescope TD IF -Z upper	TC		6200	ok	124.3, -1.9 K/day	119.6	
TEL_MTD_TC_Structure-IF-mZ-lower	Telescope TD IF -Z lower	TC		6201	ok	120.0, -1.4 K/day	116.6	
TEL_MTD_TC_Structure-IF-mYpZ-upper	Telescope TD IF -Y+Z upper	TC		6300	ok	125.0, -1.7 K/day	120.8	
TEL_MTD_TC_Structure-IF-mYpZ-lower	Telescope TD IF -Y+Z lower	TC		6301	ok	123.4, -1.6 K/day	121.1	
TEL_MLI_TC_pZ_outer	Telescope TD MLI +Z outer	TC		6400	ok	123.1, -0.9 K/day	140	
TEL_MLI_TC_pZ_inner	Telescope TD MLI +Z inner	TC		6401	ok	120.5, -1.0 K/day	133.7	
TEL_MLI_TC_pYpZ_outer	Telescope TD MLI +Y+Z outer	TC		6410	ok	120.5, -1.0 K/day	135.4	
TEL_MLI_TC_pYpZ_inner	Telescope TD MLI +Y+Z inner	TC		6411	ok	117.5, -1.0 K/day	128.6	
TEL_MLI_TC_pYmZ_outer	Telescope TD MLI +Y-Z outer	TC		6500	ok	115.5, -1.1 K/day	117.9	
TEL_MLI_TC_pYmZ_inner	Telescope TD MLI +Y-Z inner	TC		6501	ok	115.2, -1.0 K/day	119.3	
TEL_MLI_TC_mYmZ_outer	Telescope TD MLI -Y-Z outer	TC		6600	ok	116.4, -1.1 K/day	117.7	
TEL_MLI_TC_mYmZ_inner	Telescope TD MLI -Y-Z inner	TC		6601	ok	115.4, -1.0 K/day	120.2	
TEL_MLI_TC_mZ_outer	Telescope TD MLI -Z outer	TC		6610	ok	115.3, -1.1 K/day	113.3	
TEL_MLI_TC_mZ_inner	Telescope TD MLI -Z inner	TC		6611	ok	112.0, -1.4 K/day	113.7	
TEL_MLI_TC_mYpZ_outer	Telescope TD MLI -Y+Z outer	TC		6700	ok	121.6, -1.1 K/day	134.1	
TEL_MLI_TC_mYpZ_inner	Telescope TD MLI -Y+Z inner	TC		6701	ok	119.3, -1.1 K/day	127.6	
PLM_TMS_TC_Telescope-MS-pYpZ-upper	Telescope mounting structure +Y+Z upper	TC		6800	ok	124.1, -1.7 K/day	121.1	
PLM_TMS_TC_Telescope-MS-pYpZ-lower	Telescope mounting structure +Y+Z lower	TC		6801	ok	105.0, -0.1 K/day	107.3	
PLM_TMS_TC_Telescope-MS-mZ-upper	Telescope mounting structure -Z upper	TC		6820	ok	120.4, -1.3K/day	117.2	
PLM_TMS_TC_Telescope-MS-mZ-lower	Telescope mounting structure -Z lower	TC		6821	ok	104.0, -0.1 K/day	105.1	
PLM_TMS_TC_Telescope-MS-mYpZ-upper	Telescope mounting structure -Y+Z upper	TC		6830	ok	124.4, -1.6 K/day	122.4	
PLM_TMS_TC_Telescope-MS-mYpZ-lower	Telescope mounting structure -Y+Z lower	TC		6831	ok	103.8, 0.0 K/day	106.3	
EQU_RIG_TC_HSS-Rig-lower-py-l1	HSS Thermal Control rig lower +Y	TC		8001	ok	175.2	290.2	115

Sensor acronym	Sensor Location	Type	Range	Sensor ID	Sensor Status	TB1 (K)	TB2 (K)	TB2-TB1 (K)
EQU_RIG_TC_HSS-Rig-lower-py-l2	HSS Thermal Control rig lower +Y	TC		8002	ok	173.1	293.2	120.1
EQU_RIG_TC_HSS-Rig-lower-py-l3	HSS Thermal Control rig lower +Y	TC		8003	ok	173.1	293.0	119.9
EQU_RIG_TC_HSS-Rig-lower-py-l4	HSS Thermal Control rig lower +Y	TC		8004	ok	173.1	293.2	120.1
EQU_RIG_TC_HSS-Rig-lower-py-r1	HSS Thermal Control rig lower +Y	TC		8011	ok	172.7	291.6	118.9
EQU_RIG_TC_HSS-Rig-lower-py-r2	HSS Thermal Control rig lower +Y	TC		8012	ok	172.9	294.2	121.3
EQU_RIG_TC_HSS-Rig-lower-py-r3	HSS Thermal Control rig lower +Y	TC		8013	ok	172.9	293.8	120.9
EQU_RIG_TC_HSS-Rig-lower-py-r4	HSS Thermal Control rig lower +Y	TC		8014	ok	172.4	293.8	121.4
EQU_RIG_TC_HSS-Rig-lower-mid-l1	HSS Thermal Control rig lower mid	TC		8101	ok	173.1	291.5	118.4
EQU_RIG_TC_HSS-Rig-lower-mid-l2	HSS Thermal Control rig lower mid	TC		8102	ok	173.1	293.2	120.1
EQU_RIG_TC_HSS-Rig-lower-mid-l3	HSS Thermal Control rig lower mid	TC		8103	ok	172.5	294.0	121.5
EQU_RIG_TC_HSS-Rig-lower-mid-l4	HSS Thermal Control rig lower mid	TC		8104	ok	173.1	293.2	120.1
EQU_RIG_TC_HSS-Rig-lower-mid-r1	HSS Thermal Control rig lower mid	TC		8111	ok	173.0	292.2	119.2
EQU_RIG_TC_HSS-Rig-lower-mid-r2	HSS Thermal Control rig lower mid	TC		8112	ok	172.4	294.0	121.6
EQU_RIG_TC_HSS-Rig-lower-mid-r3	HSS Thermal Control rig lower mid	TC		8113	ok	172.5	294.4	121.9
EQU_RIG_TC_HSS-Rig-lower-mid-r4	HSS Thermal Control rig lower mid	TC		8114	ok	172.4	293.3	120.9
EQU_RIG_TC_HSS-Rig-lower-my-l1	HSS Thermal Control rig lower -Y	TC		8201	ok	172.2	293.0	120.8
EQU_RIG_TC_HSS-Rig-lower-my-l2	HSS Thermal Control rig lower -Y	TC		8202	ok	172.2	294.9	122.7
EQU_RIG_TC_HSS-Rig-lower-my-l3	HSS Thermal Control rig lower -Y	TC		8203	ok	172.7	295.3	122.6
EQU_RIG_TC_HSS-Rig-lower-my-l4	HSS Thermal Control rig lower -Y	TC		8204	ok	173.5	294.6	121.1
EQU_RIG_TC_HSS-Rig-lower-my-r1	HSS Thermal Control rig lower -Y	TC		8211	ok	174.4	290.0	115.6
EQU_RIG_TC_HSS-Rig-lower-my-r2	HSS Thermal Control rig lower -Y	TC		8212	ok	173.1	293.2	120.1
EQU_RIG_TC_HSS-Rig-lower-my-r3	HSS Thermal Control rig lower -Y	TC		8213	ok	173.2	293.9	120.7
EQU_RIG_TC_HSS-Rig-lower-my-r4	HSS Thermal Control rig lower -Y	TC		8214	ok	173.1	293.2	120.1
EQU_RIG_TC_HSS-Rig-upper-py-l1	HSS Thermal Control rig upper +Y	TC		8301	offset	172.8	*291.1*	118.3
EQU_RIG_TC_HSS-Rig-upper-py-l2	HSS Thermal Control rig upper +Y	TC		8302	ok	173.1	293.2	120.1
EQU_RIG_TC_HSS-Rig-upper-py-l3	HSS Thermal Control rig upper +Y	TC		8303	ok	173.0	293.2	120.2
EQU_RIG_TC_HSS-Rig-upper-py-l4	HSS Thermal Control rig upper +Y	TC		8304	ok	172.7	291.0	118.3
EQU_RIG_TC_HSS-Rig-upper-py-r1	HSS Thermal Control rig upper +Y	TC		8311	ok	172.8	294.7	121.9
EQU_RIG_TC_HSS-Rig-upper-py-r2	HSS Thermal Control rig upper +Y	TC		8312	offset	172.8	*282.4*	109.6
EQU_RIG_TC_HSS-Rig-upper-py-r3	HSS Thermal Control rig upper +Y	TC		8313	ok	173.1	293.2	120.1
EQU_RIG_TC_HSS-Rig-upper-py-r4	HSS Thermal Control rig upper +Y	TC		8314	ok	172.9	291.8	118.9
EQU_RIG_TC_HSS-Rig-upper-mid-l1	HSS Thermal Control rig upper mid	TC		8401	ok	173.2	292.7	119.5
EQU_RIG_TC_HSS-Rig-upper-mid-l2	HSS Thermal Control rig upper mid	TC		8402	ok	173.1	293.1	120
EQU_RIG_TC_HSS-Rig-upper-mid-l3	HSS Thermal Control rig upper mid	TC		8403	ok	173.4	295.0	121.6
EQU_RIG_TC_HSS-Rig-upper-mid-l4	HSS Thermal Control rig upper mid	TC		8404	ok	173.1	293.2	120.1
EQU_RIG_TC_HSS-Rig-upper-mid-r1	HSS Thermal Control rig upper mid	TC		8411	ok	173.7	292.5	118.8
EQU_RIG_TC_HSS-Rig-upper-mid-r2	HSS Thermal Control rig upper mid	TC		8412	ok	173.8	292.7	118.9

Sensor acronym	Sensor Location	Type	Range	Sensor ID	Sensor Status	TB1 (K)	TB2 (K)	TB2-TB1 (K)
EQU_RIG_TC_HSS-Rig-upper-mid-r3	HSS Thermal Control rig upper mid	TC		8413	ok	173.1	293.7	120.6
EQU_RIG_TC_HSS-Rig-upper-mid-r4	HSS Thermal Control rig upper mid	TC		8414	ok	172.7	291.1	118.4
EQU_RIG_TC_HSS-Rig-upper-my-l1	HSS Thermal Control rig upper -Y	TC		8501	ok	172.7	293.9	121.2
EQU_RIG_TC_HSS-Rig-upper-my-l2	HSS Thermal Control rig upper -Y	TC		8502	ok	173.2	293.8	120.6
EQU_RIG_TC_HSS-Rig-upper-my-l3	HSS Thermal Control rig upper -Y	TC		8503	ok	173.4	294.2	120.8
EQU_RIG_TC_HSS-Rig-upper-my-l4	HSS Thermal Control rig upper -Y	TC		8504	ok	173.1	292.5	119.4
EQU_RIG_TC_HSS-Rig-upper-my-r1	HSS Thermal Control rig upper -Y	TC		8511	offset	*172.6*	*290.3*	117.7
EQU_RIG_TC_HSS-Rig-upper-my-r2	HSS Thermal Control rig upper -Y	TC		8512	ok	173.1	293.2	120.1
EQU_RIG_TC_HSS-Rig-upper-my-r3	HSS Thermal Control rig upper -Y	TC		8513	ok	173.1	293.1	120
EQU_RIG_TC_HSS-Rig-upper-my-r4	HSS Thermal Control rig upper -Y	TC		8514	ok	172.5	289.5	117
EQU_RIG_TC_HSS-Rig-MLI-1	HSS Thermal Control rig MLI 1, bottom -Y	TC		8601	ok	138.3	172.6	34.3
EQU_RIG_TC_HSS-Rig-MLI-2	HSS Thermal Control rig MLI 2, bottom mid	TC		8602	ok	143.1	175.7	32.6
EQU_RIG_TC_HSS-Rig-MLI-3	HSS Thermal Control rig MLI 3, bottom +Y	TC		8603	ok	137.9	174.2	36.3
EQU_RIG_TC_HSS-Rig-MLI-4	HSS Thermal Control rig MLI 4, lower -Y	TC		8604	ok	136.7	170.2	33.5
EQU_RIG_TC_HSS-Rig-MLI-5	HSS Thermal Control rig MLI 5, lower mid	TC		8605	ok	143.3	173.9	30.6
EQU_RIG_TC_HSS-Rig-MLI-6	HSS Thermal Control rig MLI 6, lower +Y	TC		8606	ok	143.4	179.2	35.8
EQU_RIG_TC_HSS-Rig-MLI-7	HSS Thermal Control rig MLI 7, upper -Y	TC		8607	ok	139.5	168.1	28.6
EQU_RIG_TC_HSS-Rig-MLI-8	HSS Thermal Control rig MLI 8, upper mid	TC		8608	ok	143.4	178.7	35.3
EQU_RIG_TC_HSS-Rig-MLI-9	HSS Thermal Control rig MLI 9, upper +Y	TC		8609	ok	140.9	176.3	35.4
EQU_RIG_TC_HSS-Rig-MLI-10	HSS Thermal Control rig MLI 10, top -Y	TC		8610	ok	136.7	174.0	37.3
EQU_RIG_TC_HSS-Rig-support-1	HSS Thermal Control rig support +Y	TC		8701	ok	199.6	275.3	75.7
EQU_RIG_TC_HSS-Rig-support-2	HSS Thermal Control rig support mid +y	TC		8702	ok	203.2	269.8	66.6
EQU_RIG_TC_HSS-Rig-support-3	HSS Thermal Control rig support mid -Y	TC		8703	ok	203.2	272.4	69.2
EQU_RIG_TC_HSS-Rig-support-4	HSS Thermal Control rig support -Y	TC		8704	ok	197	273.0	76
EQU_RIG_TC_HSS-Rig-mZpY	HSS Thermal Control rig MLI 11, top mid	TC		8801	ok	141.7	172.5	30.8
EQU_RIG_TC_HSS-Rig-mZmY	HSS Thermal Control rig MLI 12, top +Y	TC		8802	ok	141.3	181.2	39.9
EQU_HACS_TC_mZ-radiator	HACS -Z camera radiator	TC		9000	ok	241	241	0
EQU_HACS_TC_mZ-electronics	HACS -Z camera electronics module	TC		9001	ok	241	241	0
EQU_HACS_TC_mZ-support	HACS -Z camera support module	TC		9002	ok	112.4	140.8	28.4
EQU_HACS_TC_mZ-optics	HACS -Z camera optics module	TC		9003	ok	112.62	136.9	24.28
EQU_HACS_TC_pZ-radiator	HACS +Z camera radiator	TC		9010	ok	241	241	0
EQU_HACS_TC_pZ-electronics	HACS +Z camera electronics module	TC		9011	ok	241	241	0
EQU_HACS_TC_pZ-support	HACS +Z camera support module	TC		9012	ok	112.55	141.7	29.15
EQU_HACS_TC_pZ-optics	HACS +Z camera optics module	TC		9013	ok	113.9	142.1	28.2
EQU_TTAS_TC_Structure-pZ	TTAS structure on +Z side	TC		9100	ok	263.25	264.8	1.55
EQU_TTAS_TC_Structure-mZ	TTAS structure on -Z side	TC		9101	ok	266.68	267.3	0.62
EQU_TTAS_TC_Structure-center	TTAS structure on top plate center	TC		9102	ok	267.82	268.9	1.08

Sensor acronym	Sensor Location	Type	Range	Sensor ID	Sensor Status	TB1 (K)	TB2 (K)	TB2-TB1 (K)
EQU_IAD_TC_Structure-pZ	IAD structure on +Z side	TC		9200	ok	272.14	272.7	0.56
EQU_IAD_TC_Structure-mZ	IAD structure on -Z side	TC		9201	ok	272.0	272.4	0.4
EQU_IAD_TC_MLI-pYpZ	IAD MLI on +Y+Z side	TC		9210	ok	154.0	158.4	4.4
EQU_IAD_TC_MLI-mYpZ	IAD MLI on -Y+Z side	TC		9211	ok	149.65	151.5	1.85
EQU_IAD_TC_MLI-mYmZ	IAD MLI on -Y-Z side	TC		9212	ok	153.9	154.3	0.4
EQU_IAD_TC_MLI-pYmZ	IAD MLI on +Y-Z side	TC		9213	ok	149.15	149.3	0.15
EQU_TTAP_TC_Structure	TTAP SVM/CVV strut I/F, close to struts 25, 26	TC		9301	ok	273.90	274.40	0.5
EQU_TTAP_TC_Structure	TTAP SVM/CVV strut I/F, close to struts 23, 24	TC		9302	ok	273.11	273.6	0.49
EQU_TTAP_TC_Structure	TTAP SVM/CVV strut I/F, close to struts 43, 44	TC		9303	ok	273.41	273.8	0.39
EQU_TTAP_TC_Structure	TTAP SVM/CVV strut I/F, close to struts 41, 42	TC		9304	ok	273.72	274.1	0.38
EQU_TTAP_TC_Structure	TTAP SVM/CVV strut I/F, close to struts 37, 38	TC		9305	ok	273.21	273.6	0.39
EQU_TTAP_TC_Structure	TTAP SVM/CVV strut I/F, close to struts 35, 36	TC		9306	ok	272.74	273.1	0.36
EQU_TTAP_TC_Structure	TTAP SVM/CVV strut I/F, close to struts 33, 34	TC		9307	ok	273.04	273.5	0.46
EQU_TTAP_TC_Structure	TTAP SVM/CVV strut I/F, close to struts 29, 30	TC		9308	ok	273.19	273.7	0.51
EQU_TTAP_TC_Str-outer-pYpZ	TTAP Structure outer +Y+Z	TC		9310	ok	274.30	274.7	0.4
EQU_TTAP_TC_Str-outer-pYmZ	TTAP Structure outer +Y-Z	TC		9311	ok	273.50	273.8	0.3
EQU_TTAP_TC_Str-outer-mYmZ	TTAP Structure outer -Y-Z	TC		9312	ok	272.62	273.0	0.38
EQU_TTAP_TC_Str-outer-mYpZ	TTAP Structure outer Y+Z	TC		9313	ok	273.00	273.5	0.5
EQU_TTAP_TC_SLI-pYpZ	TTAP SLI +Y+Z	TC		9601	ok	207.0	212.3	5.3
EQU_TTAP_TC_SLI-pZ	TTAP SLI +Z	TC		9602	ok	198.00	205.1	7.1
EQU_TTAP_TC_SLI-mYpZ	TTAP SLI -Y+Z	TC		9603	ok	197.55	203.5	5.95
EQU_TTAP_TC_SLI-mYmZ	TTAP SLI -Y-Z	TC		9604	ok	204.1	203.5	-0.6
EQU_TTAP_TC_SLI-mZ	TTAP SLI -Z	TC		9605	ok	190.37	191.4	1.03
EQU_TTAP_TC_SLI-pYmZ	TTAP SLI +Y-Z	TC		9606	ok	202.8	204.5	1.7
EQU_TTAP_TC_SLI-center	TTAP SLI center	TC		9607	ok	190.18	196.6	6.42
EQU_THA_TC_Test-harness-upper-pY	Test Harness upper +Y	TC		9800	ok	134	136.5	2.5
EQU_THA_TC_Test-harness-upper-pZ	Test Harness Telescope upper -Y	TC		9801	ok	160.05	169.5	9.45
EQU_THA_TC_Test-harness-upper-mY	Test Harness upper -Y	TC		9802	ok	295.5	294.9	-0.6
EQU_THA_TC_Test-harness-upper-mZ	Harness Profile 3900 upper -Z	TC		9803	ok	102.57	103.9	1.33
EQU_THA_TC_Test-harness-lower-pY	Test Harness lower +Y	TC		9810	ok	148.85	151.2	2.35
EQU_THA_TC_Test-harness-lower-pZ	Test Harness Telescope lower -Y	TC		9811	ok	248	250	2
EQU_THA_TC_Test-harness-lower-mY	Test Harness lower -Y	TC		9812	ok	303.5	302.7	-0.8
EQU_THA_TC_Test-harness-lower-mZ	Harness Profile 3900 lower -Z	TC		9813	ok	102.94	104.3	1.36

*) Average taken from 09:09 until 11:09 on 03.11.2005, because valve switching at the end of TB2

**) taken from begin of TP6, because T231 were not available during TP5 (TB1), see NCR 1649

ANNEX 2: HACS Power Dissipation during TV Testing

-----Ursprüngliche Nachricht-----
Von: Peter Hoffmeyer [mailto:peh@terma.com]
Gesendet: Montag, 15. Mai 2006 12:29
An: Dietmar.Schink@astrium.eads.net
Cc: Keld Schmidt Schultz
Betreff: FW: HACS Power Dissipation during TV Testing

Dear Dietmar,
Keld has found the information from the Acceptance Test Report, please see below.
Best regards,
Peter H.

From: Keld Schmidt Schultz
Sent: 11. maj 2006 13:24
To: Peter Hoffmeyer
Subject: RE: HACS Power Dissipation during TV Testing

Hej Peter,

From the Acceptance Test Report:

Heater power dissipation: 2.56 W
Camera power dissipation (average): 1.40 W

For camera power dissipation variations, see the HK data files. Notice however that the HK data files contain the camera power consumption on the primary side of the DC/DC converters. Secondary power (= power dissipation) can be estimated using this empiric formula:

Ps = Pp * ((a + b*Pp) /(1 + c*Pp + d*Pp*Pp))/100

where

Ps is Secondary power
Pp is Primary power from file

a = -325350
b = 870781.9
c = 9163.448
d = 55.26521

See also the Software Design Specification page 27.

Mvh,
-Keld.

END OF DOCUMENT

	Name	Dep./Comp.		Name	Dep./Comp.
X	Alberti von Mathias Dr.	ASG22		Schweickert Gunn	ASG22
	Barlage Bernhard	AED13		Steininger Eric	AED32
	Bayer Thomas	ASA42	X	Stritter Rene	AED11
	Brune Holger	ASA45		Suess Rudi	OTN/ASA44
	Edelhoff Dirk	AED2		Thörmer Klaus-Horst Dr.	OTN/AED65
	Fehringer Alexander	ASG13	X	Wagner Klaus	ASG22
X	Fricke Wolfgang Dr.	AED 65	X	Wietbrock Walter	AET12
	Geiger Hermann	ASA42		Wöhler Hans	ASG22
	Grasl Andreas	OTN/ASA44			
	Grasshoff Brigitte	AET12			
	Hartmann Hans	AED32	X	Alcatel Alenia Space Cannes	ASP
X	Hauser Armin	ASG22	X	ESA/ESTEC	ESA
	Hendry David	Terma			
	Hengstler Reinhold	ASA42		**Instruments:**	
X	Hinger Jürgen	ASG22		MPE (PACS)	MPE
X	Hohn Rüdiger	AED65		RAL (SPIRE)	RAL
	Hölzle Edgar Dr.	AED32		SRON (HIFI)	SRON
	Huber Johann	ASA42		**Subcontractors:**	
	Hund Walter	ASE442		Air Liquide, Space Department	AIR
X	Idler Siegmund	AED312		Air Liquide, Space Department	AIRS
	Ilsen Stijn	Terma		Air Liquide, Orbital System	AIRT
	Ivády von András	FAE12		Alcatel Alenia Space Antwerp	ABSP
X	Jahn Gerd Dr.	ASG22		Austrian Aerospace	AAE
	Kalde Clemens	ASM2		Austrian Aerospace	AAEM
	Kameter Rudolf	OTN/ASA42		APCO Technologies S. A.	APCO
	Kettner Bernhard	AET42		Bieri Engineering B. V.	BIER
	Knoblauch August	AET32		BOC Edwards	BOCE
	Koelle Markus	ASA43		Dutch Space Solar Arrays	DSSA
	Koppe Axel	AED312		EADS Astrium Sub-Subsyst. &	ASSE
X	Kroeker Jürgen	AED65		EADS CASA Espacio	CASA
	La Gioia Valentina	Terma		EADS CASA Espacio	ECAS
	Lamprecht Ernst	OTN/ASQ22		EADS Space Transportation	ASIP
	Lang Jürgen	ASE442		Eurocopter	ECD
	Langenstein Rolf	AED15		European Test Services	ETS
X	Langfermann Michael	ASA41		HTS AG Zürich	HTSZ
	Much Christoph	ASA43		Linde	LIND
	Müller Jörg	ASA42		Patria New Technologies Oy	PANT
	Müller Martin	ASA43		Phoenix, Volkmarsen	PHOE
	Peltz Heinz-Willi	ASG13		Prototech AS	PROT
	Pietroboni Karin	AED65		QMC Instruments Ltd.	QMC
	Platzer Wilhelm	AED2		Rembe, Brilon	REMB
	Reichle Konrad	ASA42		Rosemount Aerospace GmbH	ROSE
	Runge Axel	OTN/ASA44		RYMSA, Radiación y Microondas	RYM
X	Schink Dietmar	AED32		SENER Ingenieria SA	SEN
X	Schlosser Christian	OTN/ASA44		Stöhr, Königsbrunn	STOE
	Schmidt Rudolf	FAE12		Terma A/S, Herlev	TER